USING OPTICAL IMAGING METHODS TO ASSESS LASER-TISSUE INTERACTIONS

By

Gerald Joseph Wilmink

Dissertation

Submitted to the Faculty of the

Graduate School of Vanderbilt University

in partial fulfillment of the requirements

for the degree of

DOCTOR OF PHILOSOPHY

in

Biomedical Engineering

December, 2007

Nashville, Tennessee

Approved:

Professor Eric Duco Jansen

Professor Anita Mahadevan-Jansen

Professor Jeffrey M. Davidson

Professor Lillian B. Nanney

Professor Susan R. Opalenik

Professor Frederick R. Haselton

ACKNOWLEDGEMENTS

I thank God for the gift of life and for all of the wonderful service opportunities that He has made available to me. I am very grateful for my supportive mother, my dad, Joe Gambino, my grandparents, and my lovely wife Kimberly. Without such a wonderful support system this dissertation would not have been possible. I am also grateful for my wonderful adviser, Dr. Eric Duco Jansen. For without his patience and support I would not be where I am today. I will never forget the trips we took together to ASLMS and the Jansen summer lab parties. I am also grateful for Dr. Jansen and Anita Mahadevan-Jansen for paving the way for my next research opportunity down in San Antonio. I feel honored to have the chance to work with Dr. Pat Roach, and I look forward to having the opportunity to use my laser skills in the area of Terahertz radiation research.

I am also very grateful for each member of my Ph.D. committee. I doubt I will ever meet anyone quite like Dr. Susan Opalenik. Dr. Opalenik was always there for me with an encouraging word and an open ear. During my most difficult times she was like a stream in the desert. I feel blessed for the opportunity to work with Dr. Jeff Davidson. He is one of the most brilliant scientists that I have ever met and I feel honored that I had the chance to work with him. I will never forget the many fruitful discussions that Dr. Davidson, Dr. Jansen, and I shared together in the BME conference room. I also really enjoyed working with Dr. Lillian Nanney. She taught me so much about immunohistochemistry, and she always made time available for me to use her microscope (at any hour of the day!!!). For without that microscope I would not have the beautiful histological images that are in this dissertation, and I would also have a healthy set of working retinas. I am also very grateful for time that I shared with Dr. Frederick Haselton.

TABLE OF CONTENTS

LIST OF TABLES

LIST OF FIGURES

LIST OF SYMBOLS

Symbol	Definition	Units
Q	Energy	J
E_o	Irradiance at surface	W/m^2
φ	Fluence Rate	W/m^2
H	Radiant exposure	J/m^2
W	Radiant energy density	J/m^3
S	Rate of heat generation	W/m^3
δ	Penetration depth	M
δ_{eff}	Effective penetration depth	M
μ_a	Absorption coefficient	m^{-1}
μ_s	Scattering coefficient	m^{-1}
μ_s'	Reduced scattering coefficient	m^{-1}
μ_{eff}	Effective attenuation coefficient	m^{-1}
g	Anisotropy factor	-
n	Index of refraction	-
L_v	Latent heat of vaporization	J/g
ρ	Density	g/m^3
c	Heat capacity	J/g K
k	Thermal conductivity	W/mK
$\acute{\alpha}$	Thermal diffusivity	m^2/s
h	Convection coefficient	W/m^2 K
T	Temperature	°C or °K
τ_p	Laser pulse duration	S
τ_{th}	Thermal time constant	S
τ_s	Stress time constant	S
ω_L	Gaussian radius	M
R	Universal gas constant = 8.314	J/mole K
r	Radial position	M
z	Depth in tissue	M
Ω	Arrhenius damage integral	-
E_a	Activation energy	J/mole
A	Frequency factor	1/s
ε	Emissivity	-
h	Planck's constant	6.62×10^{-23} J s
c	Speed of light	m/s
σ	Speed of sound in tissue	m/s
λ	Wavelength	M

CHAPTER I

INTRODUCTION

Gerald Joseph Wilmink

Department of Biomedical Engineering

Vanderbilt University

Nashville, Tennessee 37235

1.1. Introduction

In 2007 over 300,000 lasers were purchased for use in therapeutic and diagnostic medical applications [1]. This represents an explosive increase of roughly 50% compared to the numbers reported in 2003 [1]. Lasers are used in many medical subspecialties, and are nearly ubiquitous in the fields of dermatology and ophthalmology. Dermatologists most commonly use cutaneous lasers to achieve aesthetic, surgical, and therapeutic clinical objectives.

Effective laser procedures are achieved by tailoring the laser's parameters to the physical and optical characteristics of the target tissue. Laser parameters are selected to optimize efficacy while minimizing unwanted side effects and tissue damage. From a phenomenological standpoint, it is known that laser-induced tissue injury occurs via oxidative, photothermal, photomechanical, and photochemical mechanisms. However, the specific cellular and molecular pathways which initiate and govern these mechanisms are poorly understood.

Current research in laser-induced tissue damage has focused on damage that is generated in the extracellular matrix or collateral tissue. Little data have been published on the damage that is occurring directly to the cells. Nonlethal disruption of cellular function at the laser target lies upstream to events in the adjacent tissue and provides a means for determining causative mechanisms in laser-induced tissue damage. Consider that structural proteins in the tissue matrix require temperature increases greater than 20 °C in order to denature [2]. In contrast, a minor temperature increase of 5-6 °C causes the denaturation of labile intracellular proteins and the activation of cellular response mechanisms [3]. Therefore, the activation of these intracellular pathways can be used as a more sensitive metric of tissue damage [3-6].

The most widely investigated group of chaperone proteins activated in response to thermal stress is the heat shock protein (HSP) family. Members of the HSP family

have been proven to be the among the most sensitive indicators of cellular stress. The best characterized and most sensitively inducible member of the heat shock family is heat shock protein 70 (*hsp70*) [7]. This research utilizes the transcriptional activation of the heat shock protein gene (*hsp70*) as a sensitive indicator for intracellular protein damage.

Advances in optoelectronic imaging detectors and genomic manipulation methods have converged to spawn the unique field of bio-optical imaging. Optical imaging methods provide the highest sensitivity of any imaging modality, with bioluminescence imaging (BLI) and fluorescent imaging (FLI) being the most compelling [8]. Both of these methods use highly sensitive charge-coupled devices (CCD) to track the light emitted from cells within transgenic animals. From a functional standpoint, FLI and BLI are similar in that both enable the study of ongoing biological processes *in vivo*. They both use reporter gene systems in which the promoter sequence for a gene of interest functions as an “on-off” switch for transcription of the light emitting luciferase or green fluorescent protein (GFP). They are different in that FLI uses excitation light to activate GFP which then emits light, while BLI uses the expression of an enzyme (luciferase) to catalyze a chemiluminescent reaction which emits light. In FLI, GFP-tagged cells can be followed but are difficult to quantify due to surface weighting, issues with uniform excitation, and modest background owing to auto-fluorescence [9]. In contrast, BLI is based on the sensitive detection of visible light produced by a luciferase mediated oxidation reaction, and can be used to detect very low signals with little background. Since BLI methods are more accurate for signal quantification, the bulk of this work is conducted using this modality.

Molecular imaging is an ideal tool for investigating the biological processes involved in laser-tissue interactions. Using these noninvasive imaging methods, the magnitude of cellular damage following laser-skin procedures can be tracked both

spatially and temporally. The relationship between laser operating parameters and the biomolecular effects that they induce can be carefully defined, leading to the rational selection of laser parameters for improved outcomes in medical procedures. Ultimately, these research techniques may improve current aesthetic and surgical laser protocols, and may guide the development of novel applications for the therapeutic laser.

1.2. Specific Aims

The general goal for this research project was to assess the cellular processes that are associated with laser-tissue damage using novel skin models and optical imaging techniques. Laser-induced cellular damage was investigated using *in vitro* and *in vivo* models. Each of these skin models consisted of cells that are equipped with the reporter gene system where the promoter sequence of heat shock protein 70 (*hsp70*) drives expression of luciferase (luc) and green fluorescent protein (GFP). The reporter light emission was measured using bioluminescent and fluorescent imaging methods. For this study there are two working hypotheses: 1. *hsp70* expression can be used as a surrogate marker for sublethal laser tissue damage; 2. *hsp70* expression can be used as a biomarker in the design of laser preconditioning protocols. In pursuit of our goal, the following specific aims were sought:

Specific Aim #1: To evaluate sublethal tissue damage associated with an aesthetic laser skin resurfacing procedure using a skin equivalent model and bioluminescent imaging strategies.

Approximately 250,000 patients undergo elective aesthetic laser procedures every year and the numbers are on the rise. Traditionally, human subjects, animals, and cell cultures have all been used as model systems in the study of laser skin resurfacing procedures. Each of these models has significant limitations. Briefly, research with

human subjects has stringent ethical and practical limits, animal skin does not repair like human skin, and cells in culture do not behave akin to intact tissues. Consequently a novel skin model is needed. To this end a highly reproducible skin equivalent model (organotypic raft model) that enables noninvasive and longitudinal studies of gene expression was developed. The raft model consists of human cells incorporated into an extracellular matrix. Cells in this tissue model were transfected with the *hsp70-luc* transgene allowing for quantitative analysis using BLI techniques. Raft cultures were treated using a carbon dioxide (CO_2) laser, which is a commonly used clinical resurfacing laser. Quantitative BLI techniques were used to evaluate the spatio-temporal expression of *hsp70* promoter activity, and these data were compared to traditional damage markers using histological methods. This report indicates that quantitative BLI in engineered tissue equivalents provides a powerful model to assess laser-tissue damage.

*Specific Aim #2. To investigate the role that laser wavelength and energy have on surgical ablative performance using a transgenic mouse model (*hsp70-luc-GFP*) and optical imaging methods.*

Various cutaneous pathologies require the removal of unwanted biological tissue while causing minimal damage to adjacent tissue. Laser sources in the infrared (IR) spectra are strongly absorbed by tissue and are commonly used for this purpose. Using a transgenic mouse strain with the *hsp70* promoter driving luciferase and GFP expression, we sought to evaluate laser-induced cellular damage in laser ablated tissues; with added emphasis on the role that laser wavelength and radiant exposure have on surgical laser performance. *Hsp70* was used to compare the characteristics of excisional wound repair after surgery with the free electron laser (FEL) using various mid-IR wavelengths. Luciferase activity was recorded using bioluminescent imaging

(BLI), GFP was imaged with confocal fluorescent imaging (FLI), and the depth of tissue damage was measured using histological methods. BLI data indicate that peak *hsp70* expression occurred 5-12 hours after laser ablation. Compared to the other mid-IR wavelengths tested, a wavelength of 6.10 μm induced the lowest magnitude of *hsp70* expression, damaged the shallowest volume of collateral tissue, and caused the least robust wound repair response. The data suggest that 6.10 μm is the superior ablative wavelength.

Specific Aim #3: Develop a therapeutic laser preconditioning protocol, using thermal infrared and optical imaging methods, to enhance cutaneous wound repair.

In the United States approximately 100,000 surgeries are performed daily, and worldwide millions of surgical procedures are performed annually [10]. The rise in incidence of diabetes has correlated with an increase in the frequency of chronic wounds. Chronic wounds reportedly affect 4 million people annually, and these increased medical needs have increased the demand for dermatological surgical interventions to decrease healing times [11]. Surgical patients at risk for impaired healing could benefit from therapeutic prophylactic measures aimed at improving wound repair. We hypothesized that eliciting mild stress responses could serve to protect tissue when subsequent stresses are applied. We aimed to develop a laser-delivered preconditioning protocol that favorably modifies cutaneous wound repair. Laser protocols were optimized *in vivo* on a transgenic murine model using *hsp70* expression and temperature measurements as benchmarks. Reparative responses were assessed by measuring biomechanical properties and histological parameters of wound healing. *In vivo* BLI data indicate that the optimized laser protocol increased *hsp70* expression by 15-fold. Tensiometric data show that preconditioning improves the final strength of wounds. This work suggests that a mild laser-induced heat shock acting through an

expression of *hsp70* may show promise as a preconditioning therapeutic intervention prior to surgery.

1.3. Dissertation Outline

This work has been organized in the following manner:

Chapter I provides a brief introduction to the problem addressed in this research, establishing the significance of the work. The specific aims of the project are also outlined and summarized.

Chapter II provides background information regarding laser-tissue interactions, heat shock proteins, wound repair, tissue preconditioning, and optical imaging methods.

Chapter III reports on the development of an organotypic raft model (engineered skin) consisting of cells equipped with the *hsp70-luc* transgene. Quantitative BLI in these engineered skin equivalents enables sequential *hsp70* gene expression measurements and can be used as a high throughput screening platform for future laser-tissue interaction studies. This work was published in the 2006 special issue of the *Journal of Biomedical Optics*.

Chapter IV reports on the use of a transgenic mouse model expressing luciferase and GFP under control of the heat shock protein 70 promoter. Experiments employing this transgenic animal were used to understand sublethal damage and wound repair using the Free Electron Laser. This work has been submitted for publication to *Journal of Biomedical Optics* and is currently under review.

Chapter V describes a set of experiments using thermal infrared and optical imaging tools to optimize a laser preconditioning protocol for wound enhancement. This manuscript has been submitted for publication to the *Journal of Investigative Dermatology* and is currently under review.

Chapter VI summarizes the results of Chapters III through V and the overall objectives of this dissertation. The societal implications and potential for future studies are also discussed.

1.4. Works Cited

1. Steele, R., *Laser Marketplace 2007: Diode-laser market*, in *Laser Focus World*. 2007.
2. le Lous, M., et al., *Influence of collagen denaturation on the chemorheological properties of skin, assessed by differential scanning calorimetry and hydrothermal isometric tension measurement.* Biochim Biophys Acta, 1982. **717**(2): p. 295-300.
3. Morimoto, R.I., P.E. Kroeger, and J.J. Cotto, *The transcriptional regulation of heat shock genes: a plethora of heat shock factors and regulatory conditions.* Exs, 1996. **77**: p. 139-63.
4. Beckham, J.T., et al., *Assessment of cellular response to thermal laser injury through bioluminescence imaging of heat shock protein 70.* Photochem Photobiol, 2004. **79**(1): p. 76-85.
5. O'Connell-Rodwell, C.E., et al., *A genetic reporter of thermal stress defines physiologic zones over a defined temperature range.* Faseb J, 2004. **18**(2): p. 264-71.
6. Wilmink, G.J., et al., *Assessing laser-tissue damage with bioluminescent imaging.* Journal of Biomedical Optics, 2006. **11**(4): p. 041114.
7. Dinh, H.K., et al., *Gene expression profiling of the response to thermal injury in human cells.* Physiol Genomics, 2001. **7**(1): p. 3-13.
8. Massoud, T.F. and S.S. Gambhir, *Molecular imaging in living subjects: seeing fundamental biological processes in a new light.* Genes Dev, 2003. **17**(5): p. 545-80.
9. Weissleder, R., *A clearer vision for in vivo imaging.* Nat Biotechnol, 2001. **19**(4): p. 316-7.
10. Information, K., *Wound Care, 3rd Edition, Vol. III: Surgical and Trauma Wounds*. 2007: Rockville, Maryland. p. 219.
11. Sullivan, F., *U.S. Advanced Wound Management Product Markets*. 2001.

CHAPTER II

BACKGROUND AND SIGNIFICANCE

Gerald Joseph Wilmink

Department of Biomedical Engineering

Vanderbilt University

Nashville, Tennessee 37235

2.1. Introduction

Skin models and techniques capable of imaging laser-induced biological effects would be of great utility to the medical laser community. Understanding the cellular and molecular pathways that govern laser-tissue damage will aid in improving current medical procedures. Considering that the eventual goal of this research is to improve clinical laser procedures it is appropriate to investigate laser-tissue damage on human tissues. Histological and biochemical analysis can be conducted on human skin, but these methods require invasive biopsies. Furthermore, multiple biopsies are required to fully capture and understand the time course of these biological effects. Engineered skin models and animal models that use non-invasive imagining techniques are appropriate for this work because they can be used to report these temporal biological effects and do not require tissue harvesting. However, since animal and human skin are different, and these differences may influence our results, these variations must be considered.

This chapter begins with an introduction to the biomolecules that make up skin, and how these biomolecules affect the transport and deposition of laser light. Particular emphasis is placed on heat transfer mechanisms and photothermal effects. Intracellular photothermal effects are then discussed in a section on Heat Shock Proteins (HSP). This is followed by a section documenting current tissue preconditioning methods that are used to upregulate HSP expression. The chapter concludes with a section on how molecular imaging techniques can be harnessed to quantify HSP expression.

2.2. Properties of skin

2.2.1. Skin composition and morphology

Skin covers the entire body and is therefore its largest organ. At the most basic level, skin's vital function is to provide an efficient barrier to the outside world. Chemical, mechanical, and thermal mechanisms can breach this barrier. Regardless of the mechanism, once skin is invaded it will elicit a dynamic wound healing response to combat the insult.

Skin consists of an outer epidermis, an underlying dermis, and a hypodermis. The epidermis is a self-renewing epithelium. The epidermis consists primarily of water, but does have resident keratinocytes which stratify resulting in epidermis thickness varying across the human body between 50 to 1000 μm [1, 3]. The epithelium varies in thickness in order to achieve varying levels of protection. The epidermis is composed primarily of epithelial keratinocytes, but also contains langerhans and melanocyte cell types. Keratinocytes are genetically programmed to undergo differentiation, and the five stages of differentiation are shown in **Figure 2.1**. From the outside moving inward, the layers of the epithelium are the following: stratum corneum, stratum lucidum, stratum granulosum, stratum spinosum, and the stratum basale . The inner stratum basale layer consists of a single layer of cells that are highly concentrated with melanin pigment granules. These melanin pigment granules are produced by melanocytes and are transferred to keratinocytes by cytocrine secretion [4]. Melanocytes determine skin color and melanin broadly absorbs from λ = 200-1200 nm, with absorption decreasing with wavelength [4, 5]. Aside from providing skin its color, the stratum basale also has structural significance owing to its participation in the formation of the basement membrane at the dermal-epidermal interface. The basement membrane provides

structural support for cells, anchorage for neighboring cells, and stimuli for cell growth and migration [6]. The basement membrane consists of non-fibrillar type IV collagen, laminin, entactin/nidogen, and sulfated proteoglycans [6]. These components interact with epithelial and mesenchymal cells and provide a structural division between the epidermis and the dermis.

The dermis is 300-4000 μm thick and functions to provide skin with strength, shape, and overall structural integrity. The dermis consists of resident fibroblasts that attach to an extracellular matrix (ECM) [1]. The ECM provides the microenvironment necessary for maintaining normal epidermal-mesenchymal interactions [1]. The ECM consists of fibrillar collagen embedded within a ground substance. The ground substance consists of water, collagen, elastin, gylcosaminoglycans (GAGs), and proteoglycans. GAGs are very hydrophilic and commonly sequester a volume of water 1000 times their own volume [2]. This feature causes most of the water that is present in skin to reside in the ground substance of the dermis.

Fibrillar collagen, most commonly type I (large diameter fibrils) and type III collagen (small diameter fibrils), consists of three α-chains which aggregate into a triple-helix forming a tropocollagen (TC) molecule [2]. TC molecules then aggregate to form microfibrils, which gather to form fibrils. In terms of the supramolecular structure, type I collagen monomers aggregate in larger diameter fibrils, while type III collagen aggregates in smaller diameter fibrils [7]. The staggered monomer fibrils then form sheets of lamellae [2]. Since normal fibrillar collagen exhibits a characteristic periodicity of ~67 nm, loss of this banding pattern is commonly used as an indication of thermal denaturation [2, 7]. Polarized microscopy, transmission electron microscopy (TEM), and low angle X-ray diffraction can be used to discern denaturation and the loss of this specific banding pattern. As the dermis is traversed from the papillary to reticular portion, the diameter of the collagen fibrils, bundle size, and the ratio of type I to type III collagen

increases progressively, see **Figure 2.1**. The number of fibroblasts, the "master" cells of the dermis, are also more numerous in the papillary dermis than in the reticular dermis [8]. Given that fibroblasts produce collagen in the ECM, their activity is directly responsible for the structural variation that is established within the dermis.

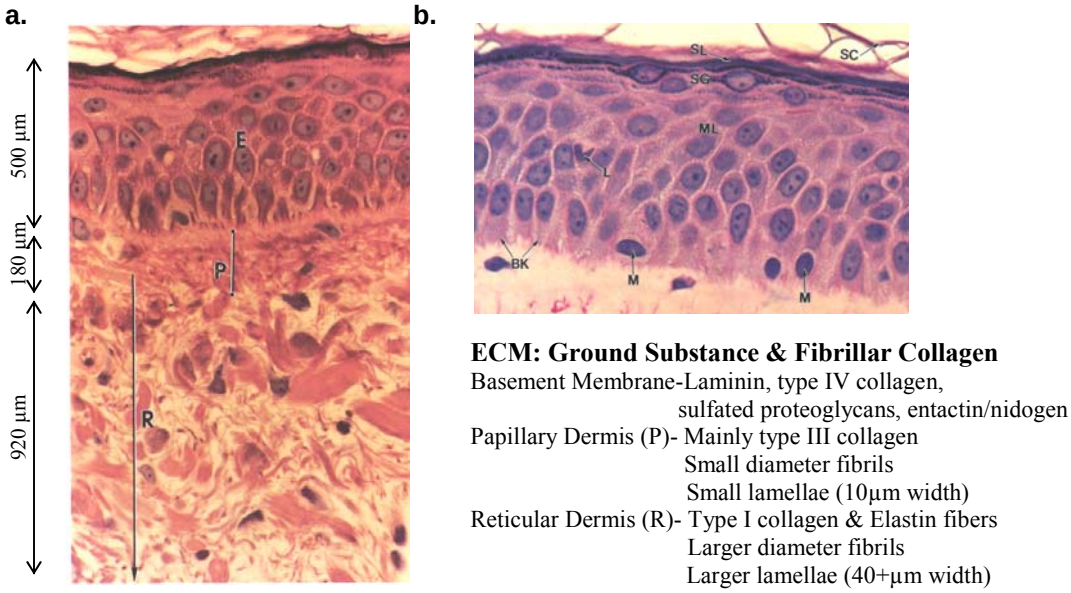

Figure 2.1. **Human skin composition [1]. (a)** Epidermis-dermis. H&E (630x). **(b)** Stratified squamous epithelium (630x). Legend: extracellular matrix (ECM), epidermis (E), papillary dermis (P), reticular dermis (R), langerhans (L), melanocyte (M), melanin pigment granule (ML), stratum corneum (SC), stratum lucidum (SL), stratum granulosum (SG), stratum spinosum (SS), stratum basale (BK).

2.2.2. Mechanical properties

The ECM has two main elements, namely, the insoluble fibers which resist tensile forces and fibrillar collagen polymers which provide the tensile strength of the ECM and inflate the network [7]. Synergistically these ECM elements provide resistance to compression and also allow diffusion of small molecules in and out of the tissue. Other mechanical properties of skin, such as stiffness, extensibility, and ultimate tensile strength, largely determine the desired biological affect that is achieved in a laser

procedure. When skin is loaded with tension it exhibits a nonlinear concave up stress-strain characteristic [2]. The ramification of this stress-strain curve is that under normal conditions skin behaves elastically, but becomes stiffer when loaded [2]. The mechanical properties of skin are commonly measured using suction cup techniques, ballistometry, and tensiometry [9]. In this work, we use an Instron 5542 tensiometer (Instron, Canton, MA) to measure the tensile strength of skin at different time points during wound repair.

2.3. Laser energy deposition and transport

2.3.1. Laser background

The concept of laser irradiation was initially proposed in 1917 by Albert Einstein. It came into practical fruition in 1958 when Townes developed a microwave precursor to the optical laser [10]. In the 1960's Maiman made the first optical solid state ruby crystal laser [11]. Lasers are now routinely used in a myriad of medical procedures for diagnosis and treatment. LASER stands for Light Amplification through Stimulated Emission of Radiation. The fundamental principle behind the laser process is that atoms which constitute the laser gain medium (e.g. CO_2 gas) are excited into higher energy states by energy pumped in through a source, such as an electric discharge, flashlamp or another laser. When these atoms return to their lower energy state, they release a photon which will then interact with another excited atom in the medium. This new atom is then stimulated to return to its ground state and subsequently releases its own photon. This released photon is similar in nature to the first photon in direction, energy, and phase. Eventually, the vast majority of the atoms violate thermal equilibrium and remain in an upper energy state, a process called population inversion. Population inversion allows stimulated emission to predominate over stimulated absorption making lasing

possible. The cascade of recruiting more atoms into the process is maintained by two reflecting mirrors that trap the majority of photons within the laser cavity. Only about 10-20% of photons escape through the one of these mirrors that is partially transmitting [12, 13].

The emitted light from the laser is unique compared to other forms of electromagnetic radiation. All of the laser's energy is of the same wavelength, collimated, coherent, and polarized. Of these characteristics, the first two are particularly important for thermal-tissue interactions. The energy is of the same wavelength (monochromatic) because the energy band gap from which each photon is derived is the same. Lasers are designed for the Ultra-violet (100-380nm), Visible (380-700nm) and Infra-red (700nm – 1mm) portions of the electromagnetic spectrum. Examples of commonly used lasers include the argon fluoride (ArF, λ=193 nm) in the UV, the helium neon (HeNe λ=632 nm) in the visible, and the Erbium Yttrium Aluminum Garnett (Er-YAG λ= 2.94 μm) in the infra-red. A photon's energy determines its wavelength through the relationship:

$$E = \frac{hc}{\lambda} \tag{1}$$

where h is Planck's constant (6.62 x 10^{-23} [Js]), c is the speed of light in [m/s], λ is the wavelength in [m], and E is the energy in [J]. Consequently, a tissue's response to a given laser is a result of only one wavelength. Most medical laser applications derive most of their benefit due to wavelength specificity. Tissue components that absorb light are called chromophores. Tissue components can be chromatically targeted instead of just physically targeted. Selective photothermolysis takes advantage of this, wherein one chromophore absorbs a given wavelength better than its surrounding tissue [5]. This absorption leads to the selective destruction of a desired target chromophore leaving other tissue relatively undamaged.

Laser light is collimated, which means that the directionality is the same for all of the photons in a laser beam due to the orientation of the laser cavity and mirrors. As a result, the light can more effectively be focused and intensified for use in medical procedures compared to other forms of light.

Most lasers exhibit a Gaussian profile of irradiation across the laser beam,

$$E(r) = E_0(r=0)\exp\left(\frac{-2r^2}{\omega_L^2}\right) \quad (2)$$

where the beam has a radius (r) and a Gaussian radius (ω_L) at which the initial irradiance (E_o in [W/m^2]) at the center of the beam has been reduced to 1/e^2 (13.5%). Within the area encircled by the Gaussian radius, there lies approximately 87% of the integrated power of the laser beam [12, 13]. Lasers deliver energy continuously or in a pulsed fashion. In general, the continuous delivery of energy results in the homogenous heating of tissue via thermal diffusion, while pulsed energy delivery strategies are more commonly employed because the pulsing regime gives the tissue time to properly diffuse the heat.

2.3.2. Laser optical properties: absorption and scattering

The amount of incident laser power delivered per area to a tissue is defined as the irradiance (E_o) [W/m^2]. As photons propagate into the tissue, the irradiance is attenuated and is governed by the tissue's reflection/transmission at boundaries, absorption, and scattering properties. Thus, in order to accurately represent the amount of energy that enters the tissue, the amount of reflected light that is lost at the surface must be taken into account. These specular loses are due to the mismatch in the index of refraction between the tissue and air.

For a 0^o angle of incidence, the fraction of specularly reflected light is shown by Fresnel's equation: (3)

$$R = \left(\frac{n_i - n_t}{n_i + n_t} \right)^2$$

Where n_i is refraction of the incident medium, air (n_i = 1.0) and n_t is the index of refraction for the sample, tissue (n_t = 1.33) The air – tissue interface leads to a 2.7 % reflection loss at the surface.

In an absorption dominated case where scattering is minimal, the remaining 97.3% of light is now governed by Beer's Law to determine its penetration into tissue,

$$E(z) = E_o e^{(-\mu_a z)} \quad (4)$$

Where E_o is the irradiance at the surface [W/m^2] and E(z) is the fluence at depth z [m], μ_a is the absorption coefficient [1/m] for the tissue at a given wavelength. The penetration depth (δ) is the inverse of the absorption coefficient. Its value represents the depth to which light will penetrate to an intensity of 1/e (37%) of the original surface intensity, less reflective losses. The tissue and the wavelength selected for irradiation determines the penetration depth.

When scattering is dominant over absorption, light transport becomes complicated and cannot be solved analytically. Analogous to the absorption coefficient, the scattering probability is wavelength dependant and is represented as μ_s (m^{-1}), the scattering coefficient. In addition to the probability that scattering occurs, it is necessary to know the direction of scattering. When scattered photons come in contact with structures or particles which exhibit spatial variations, particularly in regards to spacing and orientation, they are redirected in different directions. The direction angle at which the photons scatter is called the anisotropy (g):

$$g = \text{average}(\cos\theta) \tag{5}$$

where θ is the angle of scattering. This value can range from -1 to 1 as θ varies from 0^o (direct forward scatter) to 180^o (direct backward scatter). When light is scattered isotropically then g = 0. For most tissues, g falls between 0.7-0.99 representing a predominantly forward scattering situation.

In order to account for the direction of scattering, a reduced scattering coefficient is calculated:

$$\mu_s' = (1-g)\mu_s \tag{6}$$

Using this value, an effective attenuation coefficient is obtained that is combined with the absorption coefficient to give a more complete picture of photon interaction in tissue. The μ_{eff} accounts for the absorption of photons, the scattering of photons, and the direction of scattering:

$$\mu_{eff} = \sqrt{3\mu_a\left(\mu_a + \mu_s'\right)} \tag{7}$$

As aforementioned, in absorption dominated interactions the penetration depth is inversely proportional to the absorption coefficient. Likewise for absorptive and scattering conditions, the effective penetration depth is calculated by taking the inverse of μ_{eff} :

$$\delta_{eff} = \frac{1}{\sqrt{3\mu_a\left(\mu_a + \mu_s'\right)}} \tag{8}$$

Like other lasers in the infrared, the interaction of the CO_2 laser in tissue is an absorption dominated case, and scattering can be disregarded [12]. The absorption is largely due to the significant portion of tissue that is water. At a λ of 10.6 μm water absorbs strongly (μ_a = 800 cm^{-1}), and has a shallow penetration depth of 12.5 μm [14]. Most of skin is composed of water, the stratum corneum is anatomically designed to protect the body from dessication and water loss. This layer also causes the optical properties of tissue to deviate from tissue consisting of *only* water. The presence of these dehydrated

regions of tissue that do not absorb this wavelength as strongly, causes the penetration depth to increase to ~ 20 μm [15]. In fact, the success of the CO_2 laser can largely be attributed to its ability to control epidermal vaporization depth with minimal damage being done to the papillary dermis [16]. Damage to the papillary dermis occurs by the residual thermal effects of the laser, which is discussed in further detail in the later sections. In previous studies using the CO_2 laser, the residual thermal damage can be minimized to depths of 60-120 μm [15].

2.3.3. Photothermal effects

Once light penetrates tissue, the optical energy is absorbed by target chromophores and converted into heat, causing photothermal effects to occur. The rate and amount of energy that is deposited into the tissue per unit volume per unit time is given by the rate of heat generation, S[W/m^3]:

$$S(r,z) = \mu_a(r,z)E_o(r,z) \tag{9}$$

Where μ_a is the absorption coefficient [m^{-1}], and E_o (r,z) is the irradiance at some point (r,z) in the tissue [W/m^2]. Heat absorption induces a temperature rise described by:

$$\Delta T = \frac{S\Delta t}{\rho c} \tag{10}$$

where ΔT is the temperature rise in [°C or °K], Δt is the duration of the heat exposure in [seconds], ρ is the density of the tissue that is heated in [g/m^3], and c is the specific heat of the tissue in [J/g K].

Depending on the duration of the exposure, heat transfer occurs via the classic paths of heat transfer: conduction, convection, radiation, and evaporation. Conduction is the primary mode of heat transport in tissue and is driven by a temperature gradient. Fourier's law describes how heat is conducted across tissue,

$$q''_{cond} = -kA\frac{\Delta T}{\Delta X} \quad (11)$$

where q_{cond} = the heat flux [W], k is the thermal conductivity [W/m K], A is the area in [m^2] and the last term is the temperature gradient in the direction of heat flow. When the rate of heat generation and the heat conduction are put together, the general heat transfer equation is:

$$k\nabla^2 T + S = \rho c\frac{\partial T}{\partial t} \quad (12)$$

where, the first term is the temperature gradient in all directions, S is the heat generation, and the right hand side is the change in temperature over time with ρ as density [g/m^3] and c [J/g K] as the heat capacity. The equation describes the build up of heat within the tissue and its distribution over time.

Convection plays a role in heat transfer when a fluid is present that can circulate the heat away from an area. Consequently, convection is a concern at the surfaces of tissue where heat can be lost to the surrounding air. Convection is described by the equation,

$$q''_{conv} = h\left(T_S - T_a\right) \quad (13)$$

where $q"_{conv}$ = the heat flux [W/m^2], h is the convection coefficient [W/m^2K], and T_s is the temperature of the tissue and T_a is the surrounding temperature.

Radiation only plays a minor role in the heat transfer in these experiments, but for completeness it is provided here:

$$q = \sigma\varepsilon\left(T_S^4 - T_a^4\right) \quad (14)$$

where, q = the heat flux [W], σ is Bolzman's constant = 5.67x 10^{-8} [W/m^4 K], ε is the emissivity that is unitless and is a measure of how well a surface radiates energy, T_s is the temperature of the tissue and T_a is the surrounding temperature. Radiation is not prominent for transfer of heat to surrounding tissue.

Although not a classic path of heat transfer, evaporation plays an important role in the transfer of heat in this study. As aforementioned, the organotypic raft cultures

consist primarily of water. Since water can hold thermal energy, the higher the water content of the tissue, the more capable it is of holding thermal energy. Water's ability to hold thermal energy is due to its high specific heat. However, when the thermal buildup exceeds the water's ability to hold heat, vaporization can occur as the liquid changes state into a gas. For water to make this change of phase, called the latent heat of vaporization (L_v), it takes ~2260 mJ/mm^3 of volumetric energy.

Applying this concept within a thermal ablation model, for instance the simple steady state model, tissue vaporization is defined as the point when enough energy is provided to overcome the energy of vaporization [17]. Treating tissue as pure water, the energy needed to obtain vaporization is described by:

$$W_{abl} = \rho c\left(T_v - T_i\right) + \rho L_v \tag{15}$$

where, W_{abl} is the total heat of ablation [J/m^3], ρ is the density of water [g/m^3], c is the heat capacity [J/kg K], T_v is the temperature of vaporization, T_i is the initial temperature, and L_v is the latent heat of vaporization [J/kg]. The threshold radiant exposure needed at the surface to bring about vaporization is:

$$H_{Th} = \frac{W_{abl}}{\mu_a} \tag{16}$$

where, H_{Th} is in units of [J/m^3], W_{abl} is the total heat of ablation, and μ_a is the absorption coefficient of the tissue in [m]. Overall, this model reveals that the vaporization of tissue depends on the energy needed to heat the tissue from its initial temperature to the boiling temperature of water, and not on the energy required for uniformly vaporizing the water layer on the surface [18]. In this study we use long irradiation exposures, in which a significant amount of energy is deposited into the rafts. This energy can then be lost via evaporation heat loss mechanisms. In summary, the significant amount of energy

which is deposited into these rafts makes the process of evaporation an important heat loss pathway.

2.3.4. Measuring tissue temperatures

All objects emit radiation in proportion to their surface temperature. Infrared (IR) cameras measure an object's emitted infrared radiation and convert it to temperature. In recent years, many advances have been made in infrared technologies. Device development coupled with a better understanding of the theory governing thermography has improved the measurement and sensitivity of IR cameras. These advances make IR cameras very attractive to researchers interested in closely monitoring temperatures. In particular, in this work, the IR camera is used to ensure accurate dosimetry, as is required for the optimized preconditioning protocols using a laser source.

In 1800 Sir William Herschel was searching for a new optical material and accidentally discovered the 'infrared' band [19]. Herschel referred to this radiation as dark heat or invisible rays [20]. After its discovery many devices, such as the thermocouple and thermopile, were developed which improved detection of heat radiation and temperature sensitivity. The infared detector then was revolutionized in by Langley in 1878 with the invention of bolometer. Up to that time, most systems used bolometers [21]. The image converter and the photon detector then revolutionized IR detection. The military used these devices for enemy intrusion and detection, and prevented disclosure of infrared imaging [22]. The classified nature of infrared imaging was removed in 1950, and since then thermal-imaging systems have become readily available to researchers.

In order to understand the power and sensitivity limits of thermography, a brief section on theory will be discussed. As described previously, the electromagnetic

spectrum is divided into spectral bands according to wavelength. Thermography makes use of the infrared band, which contains wavelengths ranging from 0.75 μm to 100 μm. The basis of thermography involves the idea of a blackbody. A blackbody is an object that absorbs all radiation that is delivered to it, and the color that is emitted is related to its radiation. Plank described the distribution of radiation from a blackbody using the following formula:

$$W_{\lambda b} = \frac{2\Pi hc^3}{\lambda^5\left(e^{hc/\lambda\kappa T} - 1\right)} X10^{-6} < Watt/m^2\mu m > \quad (17)$$

where $W_{\lambda b}$ is the radiant emittance, c is the speed of light, h is Plank's constant, κ is Boltzmann's constant, and T is the absolute temperature of the blackbody. Wien differentiated Plank's formula in respect to wavelength resulting in:

$$\lambda_{\max} = \frac{2898}{T} < \mu m > \quad (18)$$

This mathematically expresses the observation that colors (wavelengths) vary as temperature increases.

Real objects do not behave like blackbodies due to the attenuation processes of absorption, reflection, and transmission. Therefore, to examine the properties of real objects, referred to as graybodies, are commonly compared to that of a blackbody. Graybodies, such as human tissues, have a constant spectral emissivity (ε). Applying this variable, a slight modification of equation (14), Plank's formula can be integrated yielding Stefan-Boltzmann's law which is the following:

$$W_{gb} = \sigma\varepsilon T^4 < Watt/m^2 > \quad (19)$$

This formula states that the total emissive power of a gray is proportional to the fourth power of its absolute temperature times the Stefan-Boltzmann constant (σ) being equal to 5.67 X 10^{-8} $Js^{-1}m^{-2}K^{-4}$ and the ε of the tissue (human skin = 0.98).

The above theory provides the basis for thermography and IR camera measurements. The Thermovision A20M IR camera from FLIR systems is used in this study and it incorporates the following variables into its calculations: the emission of the object, reflected emission of ambient sources, and atmospheric emissions. The camera then records a voltage and converts it to an actual tissue temperature. The camera's detector uses a focal plane array and a microbolometer, covers the spectral range of 7.5 to 13 μm, and is accurate within 2% of the actual reading. A picture of the IR camera and setup used to measure real time temperatures in this work is provided in **Figure 2.2**.

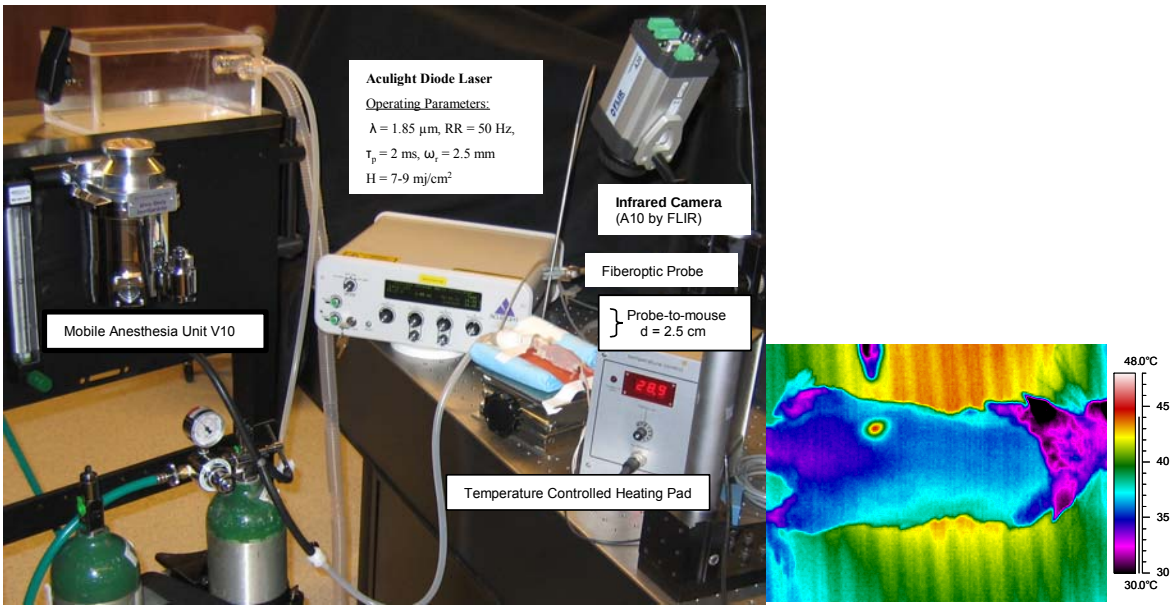

Figure 2.2. Thermal infrared (IR) imaging setup and sample image of laser treated mouse.

2.3.5. Thermal history

When laser light is delivered to tissue, chromophores absorb the photons and heating occurs. Heating triggers a temperature rise which increases the kinetic energy of the molecules. Once the kinetic energy is greater than the intramolecular bonds that hold the molecules together, the molecules denature. Thermal history is defined as the temperature profile and time at which the tissue is subjected to elevated temperatures. This history can be categorized as low temperature (43-100 ^{o}C), middle temperature (100-300 ^{o}C), and high temperature (300-1000 ^{o}C) [23]. The biological effects of thermal denaturation of tissues, membranes, cells, and molecules is summarized in **Figure 2.3**.

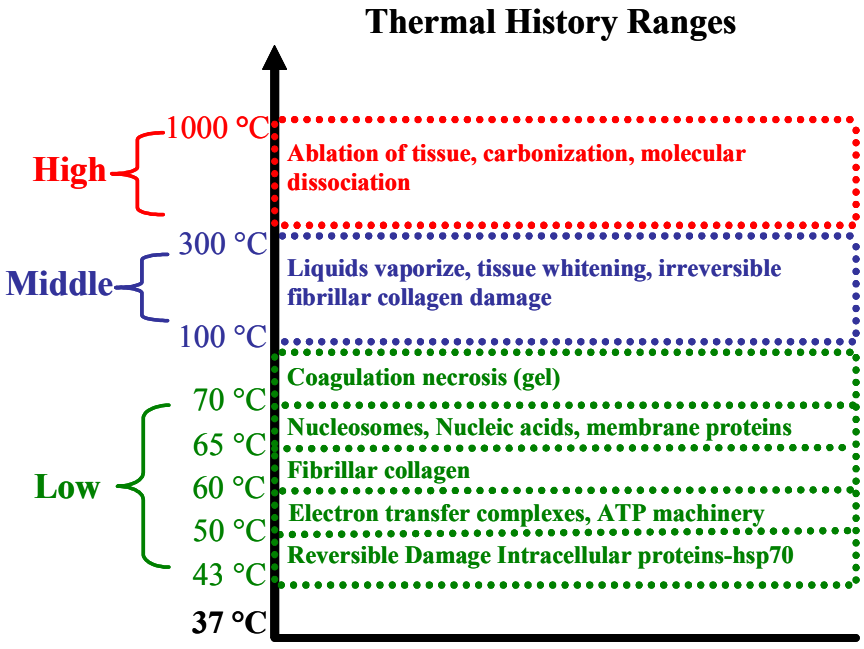

Figure 2.3. **Thermal history ranges for laser-treated tissues.** The biological effects of heat denaturation occurring in tissues, membranes, cells, and molecules.

The low temperature region is most relevant to this study and is characterized by deactivation of enzymes, protein unfolding (denaturation), acceleration of metabolism, cell death, cell shrinkage, biřefringence loss, membrane rupture, and hyalinization of collagen [23]. These effects are less outwardly visible and the cellular response can be delayed in time as different response proteins are transcribed and translated into their active forms. As a result of the cellular repair mechanisms, some low temperature damage can be reversible. Damaged proteins can be repaired or degraded and replaced with new ones. When tissue is heated to 40-50 °C, the tertiary structure of intracellular proteins and enzymes, stabilized by hydrogen and disulfide bonds, become sacrificed. Temperatures exceeding 50 °C inactivate electron transfer complexes and ATP machinery, functions which are critical to the cell. Once the tissue temperature reaches 60 °C for ~1 minute, structural proteins such as fibrillar collagen are noted to denature [2]. As the temperature climbs to 65 °C, nucleosomes and membrane proteins are compromised [5, 24]. Temperatures greater than 70 °C cause dramatic membrane protein denaturation and thereafter result in coagulation necrosis. The middle temperatures, where temperatures rise above 100°C, exhibit water dominated effects as the liquid begins to vaporize. At these elevated temperatures, structural proteins, such as fibrillar collagen, begin to damage irreversibly causing further coagulation and visible whitening. Structural proteins are more thermally stable than the intracellular proteins involved in reversible heat damage, and consequently coagulation signifies a lethal endpoint for the tissue [23]. Another irreversible change is the biřefringence loss that comes about when the regular arrangement of collagen molecules is disrupted. Biřefringence is a rotation in the angle of polarization of the tissue. Alterations in collagen microstructure can be detected by transmission polarizing microscopy (TPM), transmission electron microscopy (TEM), and high resolution multiphoton microscopy (MPM) using second-harmonic generation [23]. The high temperature region is

characterized by ablation of tissue, tissue vaporization, carbonization and molecular dissociation. In pulsed laser ablation, where temperatures climb to 340 °C, material is vaporized and ejected exposing collateral tissue to high temperatures.

The Arrhenius integral is a rate process for characterizing tissue damage, such as coagulation or birefringence loss, as a function of temperature and time at that temperature. Thermal damage is exponentially dependent on temperature and linearly dependent on the time of exposure [25]. The equation for the integral is:

$$\Omega = \ln\left(\frac{C_0}{C(t)}\right) = \int_0^{t_p} A\exp(-E_a / RT)dt \tag{20}$$

where Ω is the tissue damage, A is the frequency factor - i.e. damage rate (1/sec), E_a is the activation energy in [J/mole], T is the temperature of exposure [^oK], R is the gas constant at 8.32 [J/mol K], and the integral is over the time of the heat exposure. The Arrhenius integral essentially expresses the idea that denaturation occurs slowly at low temperatures and quickly at high temperatures, where comparable levels of denaturation can be achieved by decreasing the magnitude of exposure time for each 5 °C increase in temperature. The Arrhenius integral takes into account temperature-time history of the sample to predict tissue damage based on the damage threshold. The threshold for tissue damage is usually determined by pathological analysis and is a ratio of the concentration of native (undamaged) tissue before irradiation exposure (C_0) to the concentration of native tissue at the end of the exposure time (C_t). The threshold for determination of damaged to undamaged tissue is arbitrarily selected. In this report, the Arrhenius relationship is also shown to accurately describe intracellular processes.

2.4. Dermatological laser applications

2.4.1. Aesthetic procedures

Lasers are an integral tool for a wide variety of dermatological applications because of their intrinsic properties that spawn from the notion that different chromophores absorb light differently at various wavelengths. Depending on the application, lasers are selected with a specific target chromophore in mind. Selectively matching a laser for a specific chromophore equips dermatologists with a versatile tool. Some of the applications that cutaneous lasers are currently being used for include: port wine stain removal, scar revision, wrinkle removal, and for the photorejuvenation of skin [15, 16, 26, 27]. Cutaneous laser skin resurfacing (LSR) is one of the most common surgical procedures, with more than 150,000 procedures being performed every year [3]. Resurfacing is governed by the principle of selective photothermolysis (SP), a technique used to conduct microsurgery using the selective absorption of pulses of radiation to confine heat to targets. SP requires that the absorption of the target be higher than surrounding tissue. The goal of LSR is to selectively ablate tissue, induce collagen shrinkage, induce the synthesis and remodeling of new collagen, and restrict residual thermal damage (RTD) [15]. LSR is successful when the following conditions are satisfied: 1. power density is sufficient that vaporization outpaces the speed of diffusion. 2. Energy delivered in less than thermal relaxation time (τ), $\tau = \delta^2/4\kappa$, thus $\tau \sim 1$ms 3. Fluence small enough to denature a thin layer of collagen [15]. The LSR platform exploits the absorption properties of water seen at infrared wavelengths. Tissue, consisting primarily of water, also absorbs highly in the infrared. The ablative and non-ablative infrared lasers that are currently being used for LSR include the following: CO_2,

Er:YAG, and the Nd:YAG [15, 16, 27]. Of this group, the CO_2 and the Er:YAG lasers have achieved the most cosmetic success [27].

2.4.2. Surgical ablation procedures

Various cutaneous pathologies require the removal or incision of unwanted biological tissue while causing minimal damage to adjacent tissue. Since laser light can be manipulated and delivered in a controlled and precise manner, it is particularly well suited for surgical ablation procedures. Laser wavelengths which have strong absorption in tissue, can confine energy in smaller volumes and are resultantly the most efficient at ablating tissue. Due to their strong absorption in biological tissues, laser sources in the ultraviolet and infrared spectra are naturally great candidates. However, ultraviolet lasers are strongly absorbed by DNA and have significant mutagenic potential. As a result, infrared laser sources are more attractive for clinical applications.

In the infrared (IR) spectrum, the principal dermal chromophores are water (~65 % by volume) and the protein collagen (~35%). The absorption coefficients of these chromophores are provided in **Figure 2.4**. Water exhibits maximal absorption at λ = 2.94 μm (μ_a= 12000 cm^{-1}) and λ = 6.10 μm (μ_a = 2740 cm^{-1}) [2]. Collagen exhibits absorption peaks at λ = 6.10 μm (amide I band) where the absorption of water is a factor of 6 lower than collagen, and at λ = 6.45 μm (amide II band) where the absorption of water is half that of collagen. Using these absorption properties and the relationship ($\delta=1/\mu_a$), the optical penetration depth (δ) for each FEL wavelength can be estimated: 6.45 μm (δ = 10.7 μm), 6.10 μm (δ = 2.79 μm), and 2.94 μm (δ = 1 μm). A requisite for investigating wavelength-dependence experiments is a tunable laser. The Vanderbilt free electron laser (FEL) is a pulsed infrared laser that is tunable between 2 and 10 μm. The FEL's tunability allows the examination of wavelength-dependent properties of tissue/matter independent of inter-laser variability. In the past, comparative studies have

investigated the relationship between laser wavelength and radiant exposure and their resultant thermal biological effects [28]. In these studies, surgical laser ablation will be explored using the FEL.

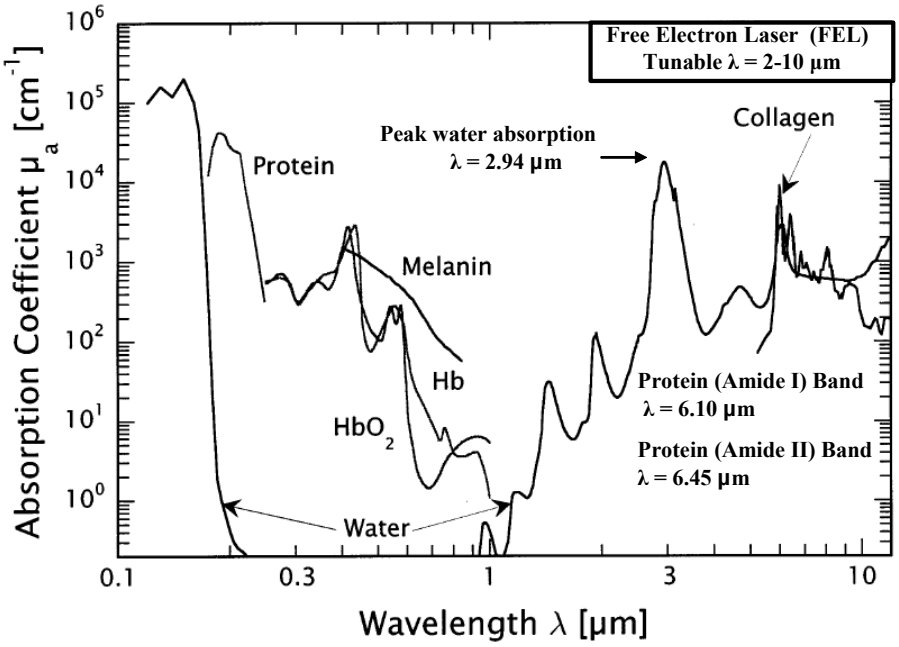

Figure 2.4. Optical absorption coefficients of principal tissue chromophores in the infrared spectra (modified from [2]).

2.5. Heat Shock Proteins

Molecular chaperones, including heat shock proteins (hsps), are examined in this study because they are highly characterized and have been used as surrogate markers for tissue damage [25, 29, 30]. At a cellular level, Hsps assist newly translated or improperly folded proteins to form into their most stable, native conformation. Hsps assist nascent translated proteins by protecting them from interactions with other cytosolic proteins. When a protein is translated, its N-terminus extends out from the ribosome leaving it exposed to the cytosol. As a result, proteins are vulnerable to binding with a multitude of other proteins, precluding proper folding. Hsps remedy this problem by using their substrate binding domains to find linear sections of nascent proteins that are rich in hydrophobic amino acids [31]. Once protected, the nascent proteins are shielded from potential cluster aggregation, and are able to fold properly.

The method for rescuing mature proteins that have been denatured by heat or chemicals is similar to the chaperones' role in helping form nascent polypeptides [31]. Whenever proteins are heated to temperatures above physiological levels, they begin to denature, and unfold from their tertiary and quaternary structures. Consequently, the domains of the heated proteins are no longer functional and the proteins are unable to perform their respective tasks of binding and interacting with other molecules. The presence of these malfolded proteins leads to the upregulation of chaperones which then intervene and allow the proteins to refold into their native state. Heat activated hsp induction depends on temperature, time of exposure, and cell type but the triggering factor is the presence of denatured proteins in the cell. Most mammalian cell lines respond to a temperature increase of at least 5-6^{o} C , which is at 42^{o} C if the ambient optimal growth temperature of the cells is at 37^{o} C [32].

The genes encoding Hsps are highly conserved and occur in every species. These genes and their products are assigned to families on the basis of sequence of homology and molecular weight [33]. Heat shock proteins vary in size, location, and function and a comprehensive overview is provided in **Table 2.1** [31, 33, 34].

Table 2.1. Heat shock protein family [31, 33, 34]

Members	Location	Cellular Function	Tissue Function	Organism Function
Hsp10	Mitochondria Chloroplast	Tolerance of ischemia	Present in maternal serum	Role in stress during pregnancy Development and cell growth
Hsp27	Cytosol/nucleus	Resistance to chemotherapeutic drugs, hydrogen peroxide, UV radiation, hyperthermia	Actin binding proteins	
Hsp40	Endoplasmic reticulum (ER)	Substrate binding of hsp70		
Hsp47	ER		Folding of type II & type III collagen	
Hsp60	Mitochondria	Tolerance hyperthermia, ischemia		
Hsp65	Mitochondria	Tumor regression	Regression malignant tumors	
Hsp70	Cytosol/nucleus	Tolerance of hypothermia, ischemia, hypoxia, regulation hsp response, reduced denaturation upon heat exposure, resistance to apoptosis, tolerance UV radiation	Recovery of contractility after ischemia, resistance to heart to ischemic injury, reduction of hyperthermic damage to midgut	Tolerance of hyperthermia, growth and development, regulation of HS response
Hsc70		Neurotransmitter release		Tolerance of hyperthermia
Grp78	Endoplasmic Reticulum	Protein secretion		
Hsp90	Cytosol/nucleus	Tolerance hyperthermia, ischemia, apoptosis, cell cycle control, cancer		
Hsp100	Cytosol/nucleus	Protein turnover	Tolerance to high temps	Host infection in Leishmania
Hsp101	Cytosol/nucleus	Tolerance of hyperthermia		
HSF1/2	Cytosol	Trimerizes and binds to HSE		Oogensis, development, thermotolerance
Crystallin		Tolerance hyperthermia, resistance to TNF	Skeletal muscle, and heart	Neuropathologic conditions

Hsp70 is structurally and functionally distinct from the other Hsps because they lack a cylindrical structure and are highly inducible [31]. Cylindrical proteins envelope misfolded proteins allowing denatured proteins to fold. In contrast, the hsp70 protein is considered a holding protein that binds small portions of amino acid chains and plays a

significant role in protecting newly translated proteins and rescuing mature denatured proteins. Hsp70 rescues mature denatured proteins by assisting in the renaturation process, in which the improperly folded proteins are refolded back into their native tertiary structures. Once the protein obtains its tertiary structure, it can then function properly.

The heat shock protein 70 system is a ubiquitous set of proteins that are found in all organisms. Interestingly, virtually all of the hsp70 proteins found in various species are relatively the same as evidenced by their high amino acid conservation (60-78% in eukaryotes) [35]. The widespread nature and high conservation show that hsp70s are crucial to survival since they have withstood evolutionary change through time. The hsp family of proteins is constitutively expressed (making up 5% to 10 % of total protein content in the cell) but some forms can also be upregulated (up to 15 % of total cellular content) in the presence of cellular insults [36]. These insults include heat stress, oxidative stress, anoxia, cytokines, viral infection and heavy metals [32, 36]. The hsps are thought to be involved in response to conditions such as inflammation, wound healing, cancer, atherosclerosis, and amyloid disease such as Alzheimer's [36-38]. Hsp70 has also been shown to block apoptosis by preventing translocation of *Bax*, an apoptotic signaling protein, to the mitochondria [39]. Hsp70 was examined for its part in impaired inflammatory wound healing response of diabetic mice [40]. The hsp70 response was delayed in cutaneous wounds of diabetic mice when compared to nondiabetic controls and was correlated to a delay in wound healing.

The hsp70s have a mass of approximately 70 kDa and contain two domains. The first one is the N-terminal ATP binding domain, and the second is the C-terminal substrate binding domain. As ATP attaches to the hsp70 molecule, the substrate binding domain will more rapidly bind and release the substrate [31]. There are three heat shock transcription factors (HSF) that drive the signaling for turning on hsp70. Of these, HSF1

is the only HSF that is stress-activated and is not implicated in constitutive activation of hsp70 [41]. Most HSF1 resides in clusters called stress granules with hsp70. Protein denaturation caused by stress, such as heat, causes hsp70 to release from the HSF1 and be recruited to repair denatured proteins [34]. This frees the HSF1 molecules to translocate to the nucleus, whereupon, they join as trimers and bind to the DNA sections that are called heat shock elements (HSE) to initiate hsp transcription [35, 41]. Newly synthesized hsps then bind to free HSF1s as a feedback inhibition signal to prevent the overproduction of hsp70, see **Figure 2.5**.

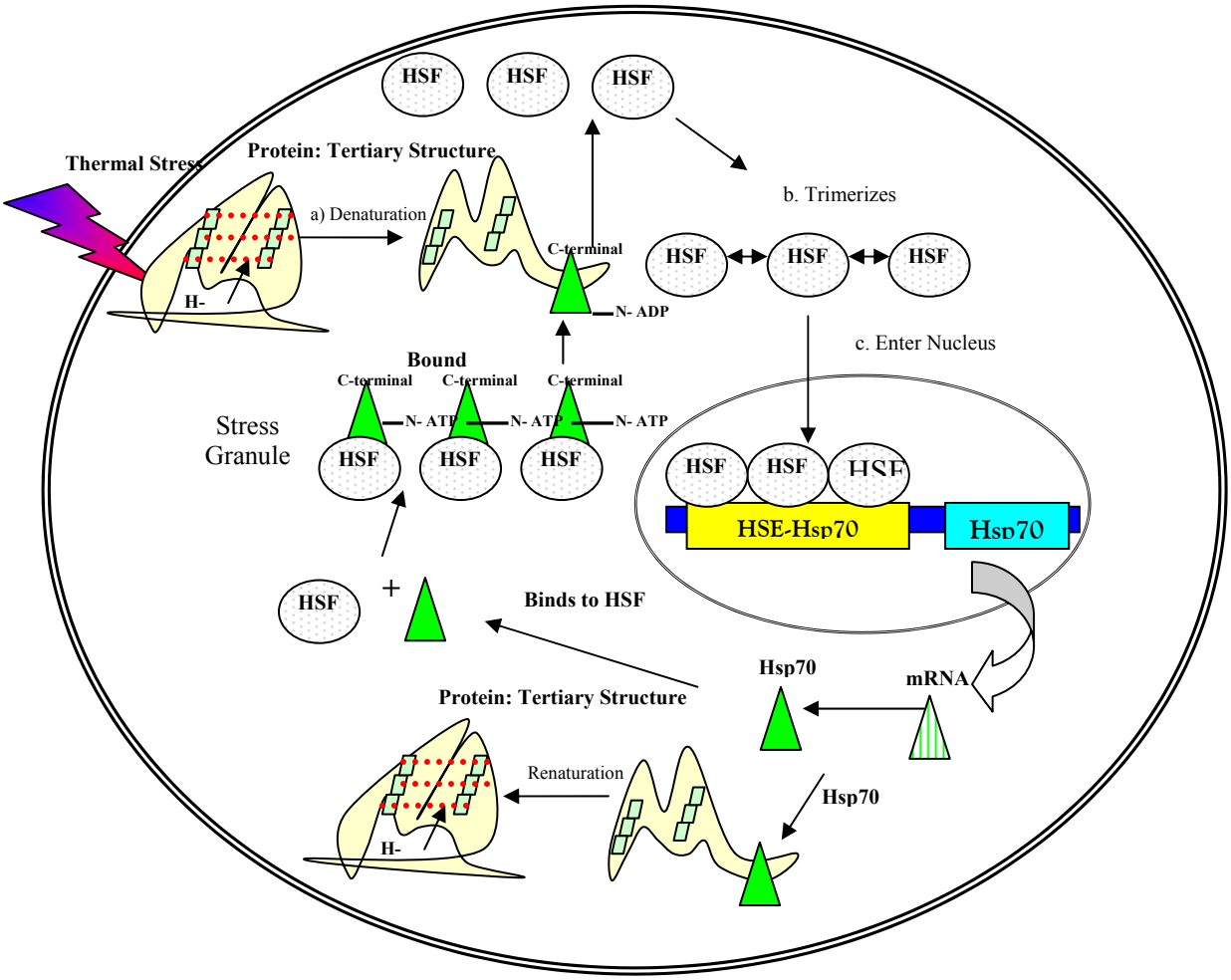

Figure 2.5. **Schematic of the intracellular hsp70 response** [32].

Traditionally, hsp70 levels in cells have been determined by methods such as Western blotting, enzyme linked immunosorbent sandwich assays (ELISA), and *in situ* hybridization [42] [25, 43]. However, all of these techniques require that the tissue be sacrificed, precluding longitudinal analysis. In contrast, the method used in this study to track hsp70 response uses a reporter gene. The key regulatory feature of reporter genes is accomplished by using the promoter sequence for the gene of interest, in our case hsp70, in conjunction with an optically active reporter, firefly luciferase. The luciferase protein is easier to monitor than hsp70 because of its light producing capabilities that can be detected with a CCD camera. So, as luciferase is monitored, by association hsp70 promoter activity is tracked, which ultimately means that the system tracks the signaling that turns on hsp70 in the cells. Monitoring of the hsp70 response in cell cultures and in raft cultures by means of a reporter gene provides an effective and convenient method of determining cellular response to heat stress after laser irradiation [25, 30].

2.6. Wound healing

2.6.1. Wound healing response

Immediately after injury, normal tissue elicits a wound healing response. The wound healing response is a complex coordinated sequence of overlapping biochemical and cellular events that result in the restoration of damaged tissue [44]. By and large, the wound healing process consists of four temporally overlapping phases, see **Figure 2.6**. Wound healing commences with hemostasis where platelets are activated and generate a fibrin clot. In addition to establishing hemostasis, platelets also function to broadcast the injury to adjacent tissue. Platelets employ the release of cytokines as the mechanism for communicating their signals [45]. The array of cytokines that are

distributed include the following: epidermal growth factor (EGF), insulin-like growth factor (IGF-1), platelet-derived growth factor (PDGF), and the transforming growth factor (TGF-β) [45-47].

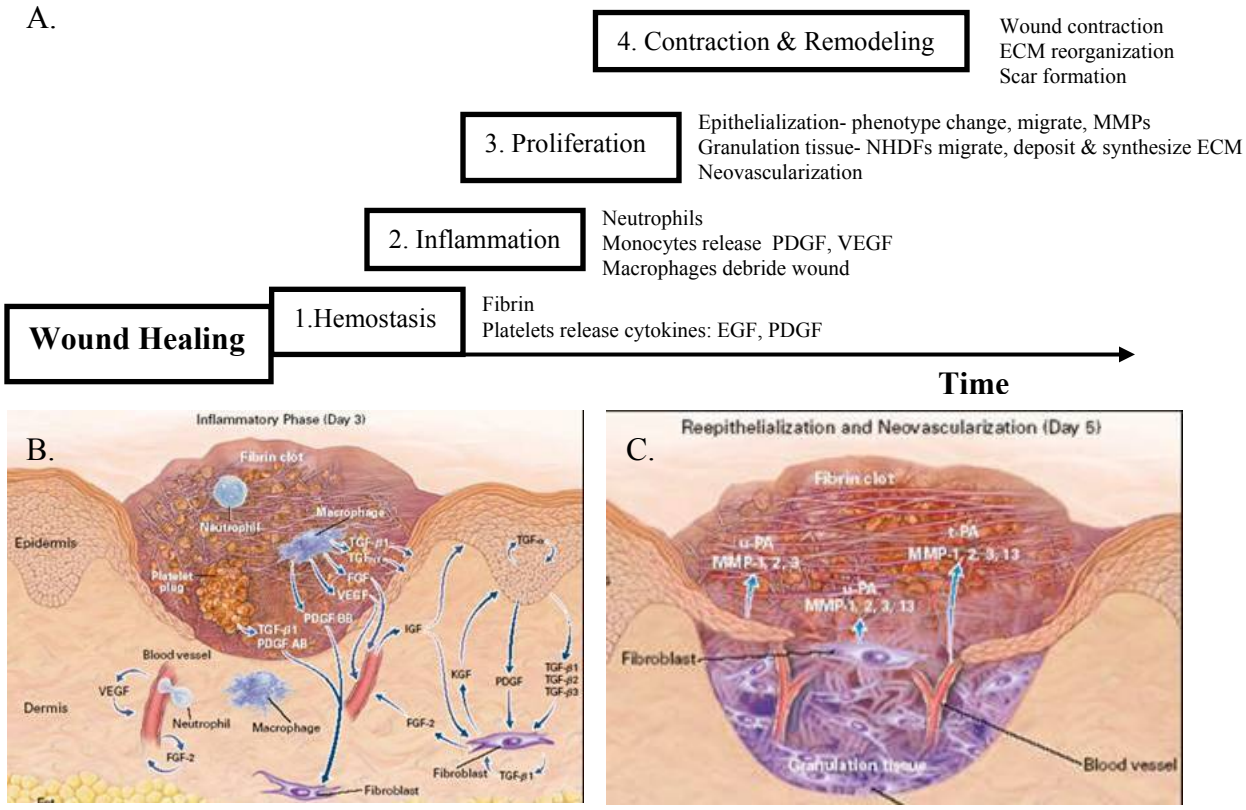

Figure 2.6. Wound healing (modified from [45]). **(a)**. The four temporally overlapping phases are provided in the boxes, with time as the axis. **(b)**. Inflammatory phase **(c)**. Proliferation phase [45, 47]

The dispersion of these cytokines establishes a chemotactic gradient that fosters the recruitment and migration of many inflammatory cells. The inflammatory cascade begins with the recruitment of polymorphonuclear leukocytes, which serve to cleanse the wounded area of bacteria and foreign particles [47]. Soon afterward, monocytes in transit to become macrophages, are recruited to the scene [45]. Once at the injured site,

macrophages begin phagocytizing debris and foreign microbes, and also assist in bridging the transition between inflammation and repair [47, 48].

The proliferation phase involves the re-epithelialization of the epidermis, the formation of granulation tissue, and the development of new blood vessels. Efficacious re-epithelialization requires the epithelial cells to undergo the following phenotypic alterations: 1. Retraction of intracellular tonofilaments 2. Dissolution of intracellular desmosomes 3. Formation of actin filaments 4. Dissolution of hemi-desmosomal links 5. Increased production of matrixmetalloproteinases (MMPs) [47, 49]. These alterations thereby allow the epithelial cells to separate from neighboring cells and nearby fibroblasts, and proceed to migrate laterally dissecting eschar from viable tissue (**Figure 2.6**). By 48 hours, macrophages, fibroblasts, and blood vessels invade the wound space and develop granulation tissue. Fibroblasts are signaled to the wound site by growth factors, such as PDGF and TGF-β1 [50]. Once they have migrated to the site, fibroblasts proliferate, express integrin receptors, and synthesize extracellular matrix macromolecules (ECM) [47]. The concomitant deposition of ECM and neo-vascularization by endothelial cells transforms the wound clot into granulation tissue [51]. In order to achieve optimal wound healing, a balance between matrix degradation and biosynthesis is established [51]. The specific ECM products that are synthesized and deposited in this phase are proteoglycans, collagens, and fibronectin [45, 51]. After fibroblasts deposit the granulation bed, keratinocytes advance and further epithelialize the wound. The contraction and remodeling phase, the final phase of wound healing, is characterized by matrix reorganization and collagen fibrillogenesis resulting in the formation of a scar [48]. Although scars do protect the skin from future invasion, mechanically they are only 70 percent as strong as normal uninjured skin [47].

2.6.2. Perfusion

Blood flow during the inflammatory and neovascularization phases of wound repair can be measured using a variety of techniques. The most common systems used to measure blood flow are laser perfusion and ultrasound systems [52]. Both of these methods take advantage of the Doppler effect. The Doppler effect is defined as the change in the frequency of waves (sound or light) reflected by a moving object. By measuring this change in frequency, the blood velocity can be estimated. In this study, both methods were used to assess wound repair, but the laser perfusion method proved to be superior due to some limitations in ultrasound imaging (minimal visible anatomical markers). Laser Doppler Perfusion imaging was conducted in this study using a Periscan PIM II Imaging device, see **Figure 2.7**. The systems uses a solid state laser with a λ = 670 nm, which has an optical penetration depth of 200 to 300 μm in mouse tissue. The optical penetration depth is ideal for imaging mouse skin because the dermis is ~300 μm deep and therefore this system can measure the vasculature of the entire wound bed. In the vasculature, red blood cells flow at different velocities. When laser light interacts with moving red bood cells, the light is back-scattered and shifted in frequency, while the light from tissue does not get frequency shifted. A photodetector is used to measure the photocurrent and the velocities are calculated.

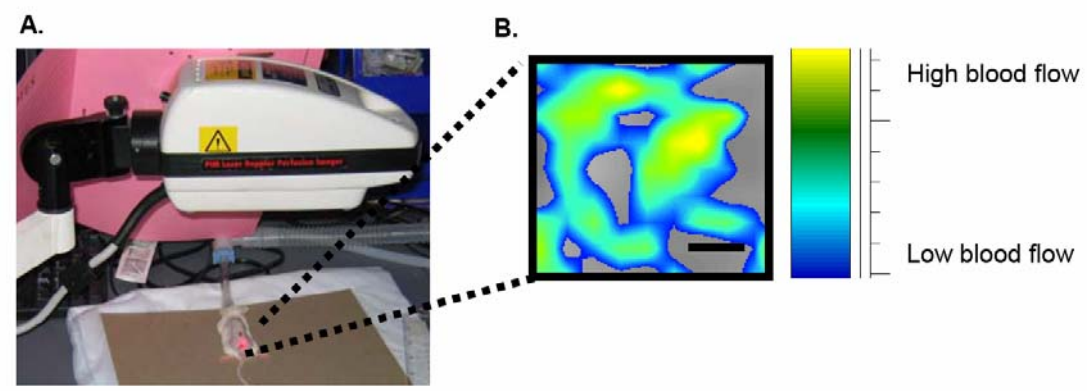

Figure 2.7 (A) Laser Doppler perfusion imaging device used to measure blood flow in mouse skin (B). Blood flow in laser treated tissue (bar = 5 mm).

2.6.3. Enhancing wound repair

Chronic nonhealing wounds are a costly problem in the United States reportedly costing our health care system an estimated $1 billion/year to manage [46]. The mere economics of this problem coupled with the complexity of the wound healing response has compelled scientists to identify agents to improve tissue repair. Recently, the identification of therapeutics which are integral to wound healing have renewed interest in developing new pharmacological agents. Some of these candidate therapies include using the following: inflammatory cell mediators, growth factors, cytokines, and extracellular derived agents [46, 53-55].

Factors affecting the inflammatory response, such as CM101, MRP8, and MRP14, have been implicated augmenting tissue repair. CM101, an anti-pathoangiogenic polysaccharide derived from group B streptococcus, functions to inhibit inflammation and accelerate repair through an angiogenic mechanism [55]. Migration inhibitory factor related-protein 8 (MRP8) and MRP14 belong to the S100 protein family and are found in activated macrophages [55-57]. MRP8 and MRP14 play roles in the activation and the infiltration of macrophages during inflammation, and it is suggested that their elevated expression may have a therapeutic effect [57].

Growth factors that are considered candidates for repair include the following: PDGF, EGF, TGF-β1-3, bFGF, and IGF-1 [46, 53, 58-60]. PDGF mediates chemotaxis and cell proliferation during wound repair, and as a result is considered a noteworthy mediator of repair [58, 59]. During the early phases of wound repair, studies suggest that the topical application of EGF can stimulate epthelialization in wounds [61]. The three isoforms of TGF-β have been shown to stimulate the synthesis and secretion of extracellar matrix constituents, processes that are integral for efficient wound repair [62-64] Of the three isoforms, the exogenous application of TGF- β1 has most effectively enhanced tissue remodeling [62, 63]. Recombinant bFGF has been shown to accelerate normal rat wound healing by intensifying the production of collagen and fibroblasts in wounds [53, 60]. IGF-1 is synthesized locally at the site of a wound, and topical application in combination other growth factors has been demonstrated to induce neovascularizaton [65, 66].

Cytokines capable of enhancing tissue repair include granulocyte-macrophage colony stimulating factor (GM-CSF), cardiac ankyrin repeat protein (CARP), interleukin-1 (IL-1), and interleukin-2 (IL-2) [46, 67]. GM-CSF stimulates monocyte activation and chemotaxis, and functions to increase the breaking strength of repaired tissue [68]. CARP increases the vascular component in granulation tissue during tissue repair, and it has been suggested as a potential strategy for initiating neovascularization [67].

Extracellular derived agents that participate in epithelial migration and matrix remodeling and include the matrix metalloproteinases (MMPs) and their tissue inhibitors of metalloproteinases (TIMPs). MMPs are a family of zinc-dependent endopeptidases that are produced by most cells and function to degrade ECM components. MMPs are not constitutively expressed in skin, but are up-regulated in response to exogenous signals. MMPs that play roles in wound repair include the following: colleganase-3 (MMP-13), MMP-1, MMP-10, MMP-3, and MMP-8 [58, 69-71].

2.7. Tissue preconditioning

2.7.1. Preconditioning mechanism

There is evidence that pre-treating cells or tissue with an initial mild thermal elevation elicits a stress response that can serve to protect the tissue from subsequent lethal stresses [72-74] or can indeed improve wound healing [29]. This process of pretreating tissue is commonly referred to as 'preconditioning.' Preconditioned cells exhibit greater survivability than untreated cells when exposed to subsequent stresses [75]. Preconditioning is believed to be due to increased production of HSPs, as first described by Ritossa in 1962 [76]. Since increased *hsp70* expression is induced by stressors such as heat, it is hypothesized that its increased expression conveys increased cellular protection [74]. After an initial thermal stress, Hsp70 stabilizes the cell by tending to the recently denatured proteins and by preventing the production of misfolded proteins [77]. Hsp70 also functions at key regulatory points in the control of apoptosis, thereby inhibiting cell death and promoting cell survival [39, 75, 78, 79]

Since cells respond to thermal stress by activating traditional heat shock protein (HSP) genes and non-HSP genes, the mechanism responsible for the survival advantage observed in preconditioned cells may also be explained by the elevation of non-HS genes. To generalize, the most active non-HSP genes function either in signal transduction or in cell growth pathways. The MAP kinase pathway plays a central role in signal transduction pathways and it has been suggested to contribute to the increased survivability of pretreated cells [80]. Since MAP kinases phosphorylate HSF-1, and sufficient levels of HSF-1 are required for maximal hsp70 transcription, their stimulated activity is coupled to hsp70 expression. Protein kinases and phosphatases alter protein activity by phosphorylating and dephosphorylating proteins. The phosphatases DUSP1 and DUSP2 are activated by thermal stress [81, 82]. It has been hypothesized that

subsequent expression of DUSP phosphatases allow the MAP kinase pathway to “reset” thus rendering the cells responsive to subsequent stressors after an initial thermal stress [82]. There are various growth factors and cytokines which are thermally modulated and may be responsible for increased cell survival, and include the following: bFGF, VEGF, TGF-β, IL-1β, IL-12, and IL-8. [75, 80, 83-87]. It has been reported that the bFGF gene is upregulated during thermal exposures, and VEGF and TGF-β levels are upregulated after thermal exposures [83-85]. The thermally modulated cytokines include the downregulation of IL-1β, and the upregulation of IL-12 (NKSF p40) and IL-8 [75, 80, 86, 87]. These genes are important for repair and may also contribute to the survival advantage of pretreated tissue.

2.7.2. Laser preconditioning & wound repair

Tissue preconditioning has been used successfully for myocardial protection, but limited studies have used preconditioning to improve cutaneous wound repair [88, 89]. Physical and pharmacological techniques are the main methods used to upregulate HSP expression and precondition tissues. Recent pharmacological agents, Bimoclomal and Geldanamycin, show clinical promise but due to their non-specific actions and multiplicity of biochemical effects, are still considered inferior to traditional physical methods [90, 91]. Various physical methods are used to preocondition tissues and these methods are summarized in **Table 2.2**.

Table 2.2 Physical methods used for cell and tissue preconditioning

Method	Contact vs. Non-contact	Whole body, local periphery or internal tissues, cell culture	Target Tissue	Advantages	Limitations	Laboratory vs. Clinical Use
1. Incubators	Non-contact	Cell culture, transplanted tissues	Cell culture or tissue transplants	Control O_2, CO_2, humidity level	Contamination, media evaporation	Mainly laboratory (ex –vivo) some transplant potential in clinic (in –vivo)
2. Thermocyclers	Contact	Cell culture	Cell culture	Excellent temperature control	Media evaporation	Laboratory (ex-vivo)
3. Water bath	Contact	Whole body (animal), cell culture, periphery organ submersion (local tissue)	Whole body (animal), cell culture, animal periphery tissues	Excellent cell cultures, difficult to locally heat only periphery tissues	Animal heating causes dehydration and collateral tissue damage. No homogenous heating of plates, elevated temperatures in middle wells	Laboratory (ex-vivo), moderate potential in clinic (in-vivo) on periphery tissues
4. Metal rods	Contact	Local heating of periphery tissues	Skin	Inexpensive, easy to use, heat localized to particular region	Diffusion heats collateral tissue	Both
5. Heated blanket	Contact	Local heating of periphery tissues	Skin	Inexpensive, temperature feedback, heat localized to skin	Diffusion heats collateral tissue	Both
6. X- Ray	Non-contact	Local tissue	Internal tissues	Energy deposited within the body	Ionizing radiation	Ionizing radiation limits clinical potential
7. Radiofrequency	Non-contact	Local tissue	Internal tissues	Energy deposited within the body	Difficult to focus into small defined areas, need RF electrode	Currently used in clinic
8. Microwave	Non-contact	Local tissue	Brain, internal tissues	Heterogeneously treat brain regions	Requires MW antenna	Currently used in clinic
9. Focused ultrasound	Non-contact	Local tissue	Internal tissues	Short wavelengths, temperature mapping with MRI	Best for deep tissues	Currently used in clinic
10. Lasers	Non-contact	Local tissue	Skin or internal organs using fiberoptics	Rapid focused induction, limited affects in deeper tissues, Potential for temperature mapping with MRI or Infrared mapping	Wavelength-dependent light penetration, requires fiberoptic for endoscopic	Currently used in clinic

Whole body hyperthermia, using a water bath, is the classical physical preconditioning method. Whole body hyperthermia elevates HSP expression in the entire organism and commonly causes excessive tissue dehydration [92]. Harder et. al. circumvented these complications by using a heated blanket to locally induce HSP expression in restricted skin, and this technique improved skin flap survival in pigs [93]. Heated blankets are attractive because they are simple and inexpensive, but they rely on the diffusion of heat and require lengthy preconditioning sessions which are not conducive to the time constraints of a clinical setting. Non-contact physical methods,

such as focused ultrasound, radiofrequency, and microwave sources, also show promise since they can induce rapid and focused HSP induction in deep tissues [94, 95]. However, in applications targeting superficial skin, lasers are ideal because they can achieve for rapid and focused induction without effecting deeper tissues [96]. Studies using preconditioning for wound repair used electroheating probes to homogenously heat tissue [91]. Since electroheating probes can not selectively target and penetrate tissue, laser heating may advance tissue preconditioning aimed at improving tissue repair. Wound healing conditions create a stressful environment for the cells involved in the regeneration process and are therefore postulated to influence the expression of hsps [97]. Hsp70 is rapidly induced at wound sites, and this induction has been shown to improve cutaneous wound healing [37, 91]. Studies indicate that isoforms of TGF-b and hsp70 may contribute to an improved wound healing response [29, 96, 98-100]. In fact, there is indication that these factors may not only improve wound healing, but could assist in tissue regeneration [98]. Tissue regeneration gives rise to the scarless healing of connective tissue, and is currently only observed in healing embryos [101]. When compared to adult wound healing, significant differences have been observed in embryos. Some of the most profound observed differences include: the lack of conversion of fibroblasts into myofibroblasts, low TGF-b1 levels during wound healing, and enhanced TGF-b3 levels [98, 102]. Furthermore, studies reveal that a critical balance between the TGF-b isoforms may account for the perceived scarless repair. Although the exact mechanism as to how TGF-b may contribute to scarless healing has not been elucidated, TGF-b clearly plays a role in this process.

A countless number of experiments have been conducted with the intention of harnessing the healing power of TGF-b. The large majority of the experiments were conducted using the exogenous application of TGF-b. Casting the traditional techniques aside, Capon and colleagues proposed the use of laser to augment the wound healing

process [29, 96, 99]. Capon's experiments revealed that the local application of laser energy following skin incisions induced an accelerated wound closure. Although the mechanism has not been fully elucidated, hsp70 and TGF-b play active roles in this process. Following laser irradiation hsp70 is over-expressed, and coordinates the expression of a plethora of growth factors including TGF-b. In conclusion, the analysis of the literature, and the fundamental considerations concerning the healing process when using thermal lasers, are in favor of a modification of the growth factors synthesis after laser irradiation, induced by a heat shock response. An extensive review of the different techniques and several clinical studies confirm that thermal lasers could effectively promote skin wound healing, if they are used in a controlled manner.

2.8. Wound repair skin models

In order to quantify hsp70 expression both temporally and spatially a reproducible skin model is needed. Traditionally, in comparable studies human subjects were used [42]. The inherent difficulties in using human subjects are twofold: 1) difficulty in comparing laser induced hsp70 expression on a single subject; and 2) the stringent medical regulations associated with using human subjects, in particular regarding the harvesting of samples for analysis. In light of these difficulties, animal models emerged as a satisfactory model to study skin and wound healing. Of the multitude of animals commonly available, the model most closely resembling human skin is the porcine model. The porcine model is widely used to study wound repair, but because of substantial differences in tissue architecture it does not accurately reflect the human repair response after laser treatment [103, 104]. In addition, animal models are costly and achieve minimal reproducibility [103]. An alternative to using human subjects and animal models, is the use of cell cultures. In the past, colleagues have successfully

assessed hsp70 levels in cell cultures [25]. Cell culture studies provide a valuable strategy to analyze cellular damage at a molecular level. One limitation of cell culture studies, lies in the fact that cells react differently when incorporated into tissue. The most striking difference between cells in culture and cells in tissue can largely be attributed to the presence of an extracellular matrix (ECM). When in contact with an ECM, the cells function differently than when in contact with the polymer surface of a tissue culture dish. The cells relationship with the ECM also provides skin with distinct mechanical, thermal, and optical properties. Consequently, models lacking an ECM do not accurately reflect human skin.

In 1956, Gey and Ehrmann conducted some of the first studies aimed at observing cells in the context of an extracellular matrix [105]. Then in 1979 Bell and colleagues observed that fibroblasts could condense a collagen lattice forming a tissue-like dermal equivalent [106-108]. In an attempt to further develop this skin model, efforts were made to grow keratinocytes on top of the dermal equivalent resulting in the formation of multilayered skin equivalents [107, 109, 110]. In the midst of these skin studies, Michalopoulos and Pitot observed that liver epithelial cells floated like a “raft” atop the stromal collagen matrix [26, 111]. In light of these observations, Michalopoulos and Pitot coined the term “raft” culture [111]. The raft name has remained, and the method has been modified for skin applications. Raft cultures are artificial skin equivalents comprised of stromal and epithelial layers. The stromal layer is composed of human fibroblasts intermixed in a collagen matrix. Human keratinocytes are grown atop the dermal equivalent, and once transferred to a liquid-air interface induce differentiation akin to that observed in *in vivo* human skin [109]. In recent times, raft cultures have emerged as a novel and useful tool for a multitude of tissue studies [26, 112-114]. A picture of a raft culture is shown in **Figure 2.8.,** with the boxed region providing a histologic cross-section of a raft. Overall, we selected raft cultures as one of

our skin models because they are more reproducible then samples acquired from human subjects and provide cell-matrix information which cells in culture can not provide.

However, skin equivalents have a variety of shortcomings, and the next step was to incorporate the hsp70A1-luc-eGFP cassette into a full transgenic mouse model [25, 30, 115-118]. The transgenic mice are of a FVB background and contain an *hsp70* cassette (FVB.*hsp70A1-luc*-2A-GFP). The cassette is as follows: the murine *hsp70*A1 promoter (Genbank accession number M76613) was attached to the luciferase coding sequence from the pGL3-Basic plasmid (Promega, Madison, WI) as described previously and fused, in frame, to the ORF of the enhanced green fluorescent protein (eGFP; Clontech, Palo Alto, CA) with 54 base pairs (bp) of the FMDV 2A sequence followed by 24 bp of polylinker [30]. The cDNA for (eGFP) and luciferase (luc) vector are located downstream from the *hsp70* promoter. Therefore, whenever the transcriptional factors are present which induce *hsp70* mRNA transcription, these bicistronic reporters are transcribed and translated. Resultantly, the GFP and luciferase gene products emit light which can be used as a surrogate marker for *hsp70* gene activity levels, as previously shown [119].

Since other wound healing promoter sequences have been studied in full rodent models, the idea of experimenting with an *hsp70* transgenic model was very attractive [58, 69, 101, 120]. In contrast to cell culture, intact mouse skin includes a complex tissue architecture, vasculature, and extracellular matrix that resemble the optical and thermal properties of human skin. Compared to raft skin equivalents which lack inflammatory cells, animal models have a full complement of immune system cells and can achieve actual wound repair. Lastly, a full thickness animal model enables us to spatially resolve hsp70 expression in three dimensions. This aspect permits a visualization of the extent and amplitude of laser-induced thermal effects in living tissues. A picture of untreated mouse skin is provided in **Figure 2.9**.

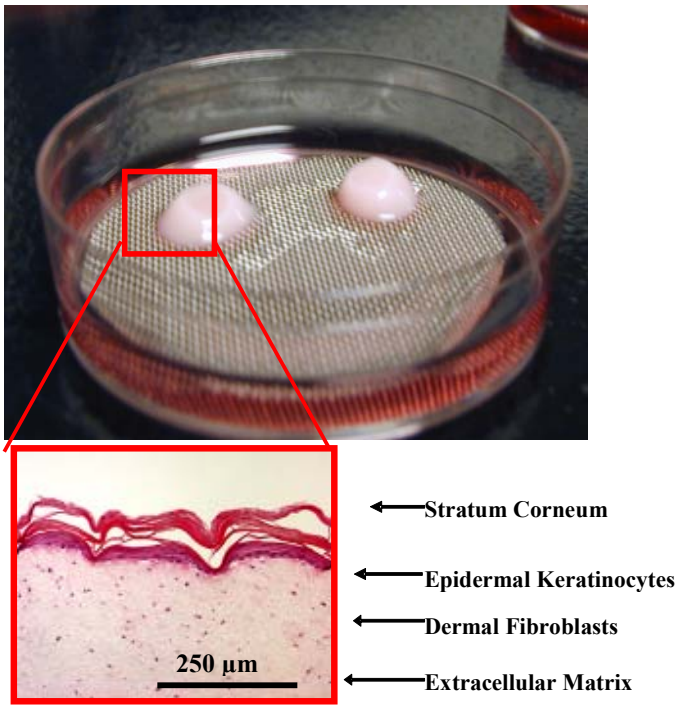

Figure 2.8. A picture of an organotypic raft culture skin equivalent. An hematoxlin and eosin stain (H &E) is also provided to illustrate tissue architecture (bar = 250 µm).

Epidermis:
-22 +/- 1 µm (n=16)
-Keratin

Dermis:
-Depth: 220 +/- 22 µm (n=16)
-Collagen/elastin (green)
-Hair follicle/stem cells

Subcutaneous Fat:
-Thickness: 68 +/- 10 µm (n=16)
-Blood vessels

Muscle (Pannicalus Carnosus):
-Depth: 320 +/- 30 µm (n=16)

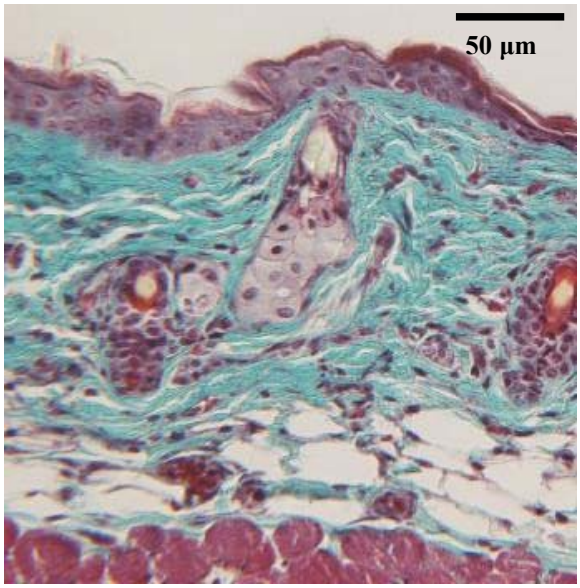

Figure 2.9. Transgenic (Hsp70-luc-GFP) Mouse Skin Composition .

2.9. Molecular and optical imaging

Molecular imaging is a discipline that is defined as the visual representation, characterization, and quantification of biologic processes at the cellular and subcellular level within living organisms. The following imaging techniques are considered molecular imaging approaches: Positron Emission Tomography, Single Photon Emission Computed Tomography, Magnetic Resonance Imaging, Computed Tomography, Ultrasound, and Optical Imaging. The two main optical imaging methods are Bioluminescent and Fluorescent imaging. The modalities are similar in that they both are concerned with how to detect light emitted from live animals, but they are different both in their origins and characteristics.

For millions of years, nature has used bioluminescence as a tool for signaling in such organisms as the jellyfish, firefly and bacteria [121]. The uses of the light signaling are as varied as the different animals from which they have come. Baiting, camouflage, and courtship are examples of the utility of bioluminescence in nature [121]. Recently, however, man has learned how to harness this phenomenon in a synthetic manner and use it for the purpose of scientific advancement as a reporter gene.

Bioluminescence is a unique reaction in which light is produced through a chemical reaction. The origin of this light emission differs from fluorescent and phosphorescent emissions due to the fact that a chemical reaction, rather than the absorption of light, supplies its excitation energy. In all bioluminescent reactions, the key chemical reaction occurs between a luciferase protein (Luc) and a substrate [122]. The Luc uses oxygen to oxidize a substrate resulting in the formation of a molecule in an excited state. Upon returning to its normal state, the excited molecule then emits light.

Although all bioluminescent reactions require a chemical reaction, the reporter gene systems themselves are far from identical. The luminous source (genera), the luciferase, the luciferin, as well as external biochemical factors are all strikingly different

in each bioluminescent reporter gene system [122]. Each system consequently emits a different wavelength of light. The most commonly used luciferases used in bioluminescent imaging include the bacterial luciferase (*lux*) from the marine genera *Vibrio*, the firefly luciferase from the *Photinus pyralis*, and the Renilla luciferase from the anthozoan sea pansy *Renilla reniformis* [121]. The systems differ not only by their emission wavelengths, but also by the biochemical cofactors that are required for reactivity. For instance, the *Renilla* luciferase requires the coelenterazine substrate and Ca^{+2} to emit at 460 nm, while the luciferase from *Photinus pyralis* requires d-luciferin as a substrate and ATP, O_2, and Mg^{+2} as cofactors to emit at ~560 nm [122].

The luciferase enzyme found in the common North American firefly, *Photinus pyralis* is the most frequently used luciferase for a number of reasons, including its high quantum yield efficiency (~90%) [121]. This luciferase enzyme catalyzes the oxidation reaction of the substrate luciferin in the presence of ATP, Mg^{2+}, and molecular oxygen [123].

$$\text{Luciferase + Luciferin + ATP + } O_2 \xrightarrow{Mg\,2+} \text{Luciferase-Luciferin + AMP + } PP_i \qquad (21)$$

$$\text{Luciferase-Luciferin + AMP + } O_2 \longrightarrow \text{Oxyluciferin}_{\text{excited state}} + CO_2 + \text{AMP} \qquad (22)$$

$$\text{Oxyluciferin}_{\text{excited state}} \longrightarrow \text{Oxyluciferin}_{\text{ground state}} + h\nu \qquad (23)$$

In this reaction, the oxidation of luciferin forms oxyluciferin in its electronically excited state [122]. Oxyluciferin returns to the ground state while emitting light of wavelength 563 nm, at pH equal to or greater than 7 [124]. For each molecule of luciferin oxidized, a single photon is emitted [125]. The quantum yield of this bioluminescent reaction is between 88-90%, which is the highest known efficiency of any chemiluminescent reaction [123]. Kinetic studies of the luciferase reaction *in vitro* indicate a peak-intensity reached within seconds following the addition of luciferin. In the

presence of excess luciferin, the light emitted is proportional to the concentration of luciferase protein [126].

The full luciferase gene (luc) that is derived from the firefly is 2387 base pairs long, which makes a 550 amino acid luciferase protein [121]. The various forms of luciferase are actually quite different from each other and they share very little sequence homology from organism to organism [121]. Because the luciferase is a monomer that does not require any post-translational modifications, it is available as a mature enzyme directly upon translation from its mRNA [122]. Once translated, the protein resides in the cytoplasm and peroxisomes of the cell where it can catalyze the bioluminescent reaction once the luciferin substrate has penetrated the cell membrane.

The luciferase-luciferin system is more advantageous than traditional methods of visualizing cellular response. This technology allows for non-invasive monitoring of biological phenomenon. The cells are left relatively unaffected except for the production of luciferase and addition of luciferin, both of which are not toxic to cells. Recently, it has been found that luciferase is not toxic to the cells, and in the contrary may play a physiological role in the protection of cells against oxidative stress [127]. Furthermore, multiple time points of data can be taken instead of one end point in which the sample is sacrificed, as is the case for Western blots, ELISAs, and immunohistochemical analysis. Therefore, the time course of expression can be tracked with one sample which is convenient and also more effective because biological variations that would be present in multiple samples are not a factor. In this system, there is inherently no background noise because cells do not naturally produce bioluminescence, except some very low levels of metabolic light [128]. Also, time is saved with the luciferase-luciferin system when compared to other more labor-intensive lab procedures that require many preparation steps before the actual assay is performed. Lastly, no hazardous reagents, such as radioactive isotopes, are required.

Fluorescent imaging uses the excitation light of one wavelength and a camera to measure the emitted light of shifted wavelengths. Both modalities have their inherent advantages and limitations and therefore it is valuable to use both modalities. The main advantage of fluorescence is that it doesn't require substrate for imaging, which allows for signal reporting in live and fixed cells. Compared to fluorescence, bioluminescence has many advantages for this study. Firstly, it is easier to quantify bioluminescent light than fluorescent light. The reason for this can be attributed to the fact that bioluminescent imaging does not require an excitation source. The benefit of not having an excitation source means that the number of cells that are detected is proportional only to the amount of light emitted, and not to the light which would be used for excitation [128]. Secondly, bioluminescent imaging can detect very low levels of light, and is more sensitive than fluorescent, MR, and CT imaging. Bioluminescent imaging is also more sensitive than fluorescence due to the fact that photo bleaching and autofluorescence play a major role in fluorescence measurements, but are non existent in bioluminescence. The disparity in penetration depths can also be attributed to sensitivity differences between the two modalities. Fluorescent imaging also has been shown to be surface weighted where cells closer to the surface appear brighter than deeper located cells [129]. Fluorescent imaging has been observed to image fluorophores that are a couple of millimeters below the surface, while bioluminescence can image light many centimeters below the surface [128]. In recent studies, bioluminescent imaging has been shown to detect as few as 100 cells in *in vitro* cell cultures, and as few as 200 cells could be detected at a depth of 2 cm in an *in vivo* mouse [130].

Both bioluminescence and fluorescence use charge coupled device (CCD) cameras to detect luciferase and green fluorescent protein emissions. CCD cameras have a high sensitivity to light in the visible and near infrared spectrums. CCD cameras

operate by converting light photons that strike the CCD pixel array with low energies (2-3 eV) into electrons. The electrical charge pattern then corresponds to the light pattern emitted by the source. Nitrogen cooled CCD cameras operate at a temperature of -105 ^{o}C, providing substantial reductions in dark current noise. Recently, Xenogen corporation (Alameda, CA) has emerged as the criterion standard for bioluminescent imaging. Xenogen's IVIS Models 100 and 200 have gained popularity due to their high resolution and sensitivity. The systems consist of a cooled integrating CCD camera mounted on a light-tight specimen chamber (dark box), anesthesia unit, a camera controller, a cooling system, all controlled by a computer.

In this study, as in most bioluminescent imaging studies, the tissue samples are placed in the system and imaged. Both black and white and bioluminescent images are acquired. The bioluminescent image is then superimposed on top of the black and white image. The bioluminescent data are represented with a color scheme reflecting the regions of maximal light output. The light output was quantified using LivingImage (v2.12,Xenogen) and Igor imaging analysis software (v.4.02A, Wavemetrics, Lake Oswego, OR). The light output from the specified regions of interest (ROIs) was quantified as a photon flux in units total number of photons emitted/second. The hallmark of the success of the IVIS systems is largely due to the fact that they are calibrated against a National Institute of Standards and Technology (NIST) traceable spectral radiance source [130]. This calibration converts the relative light units into radiance units. In doing so, the calibration normalizes for f-stop position, image time, and binning. Calibrating in this fashion is advantageous because it minimizes intersystem and intrasystem variability.

Bioluminescent and fluorescent imaging methods have been adapted for use in a multitude of applications, including the visualization of transgene expression in wound healing applications. In a recent study, the MMP-13 promoter, also known as

collagenase, fused to the luciferase gene was monitored after cutaneous wound repair to study the spatio-temporal characteristics of the MMP-13 promoter in wounds [69]. MMP-13 is a matrix metalloproteinase that plays a role in tissue remodeling in normal states. In this work, we use both bioluminescent and fluorescent imaging to study early wound repair in the context of laser-tissue interactions [see **Figure 2.10**.]

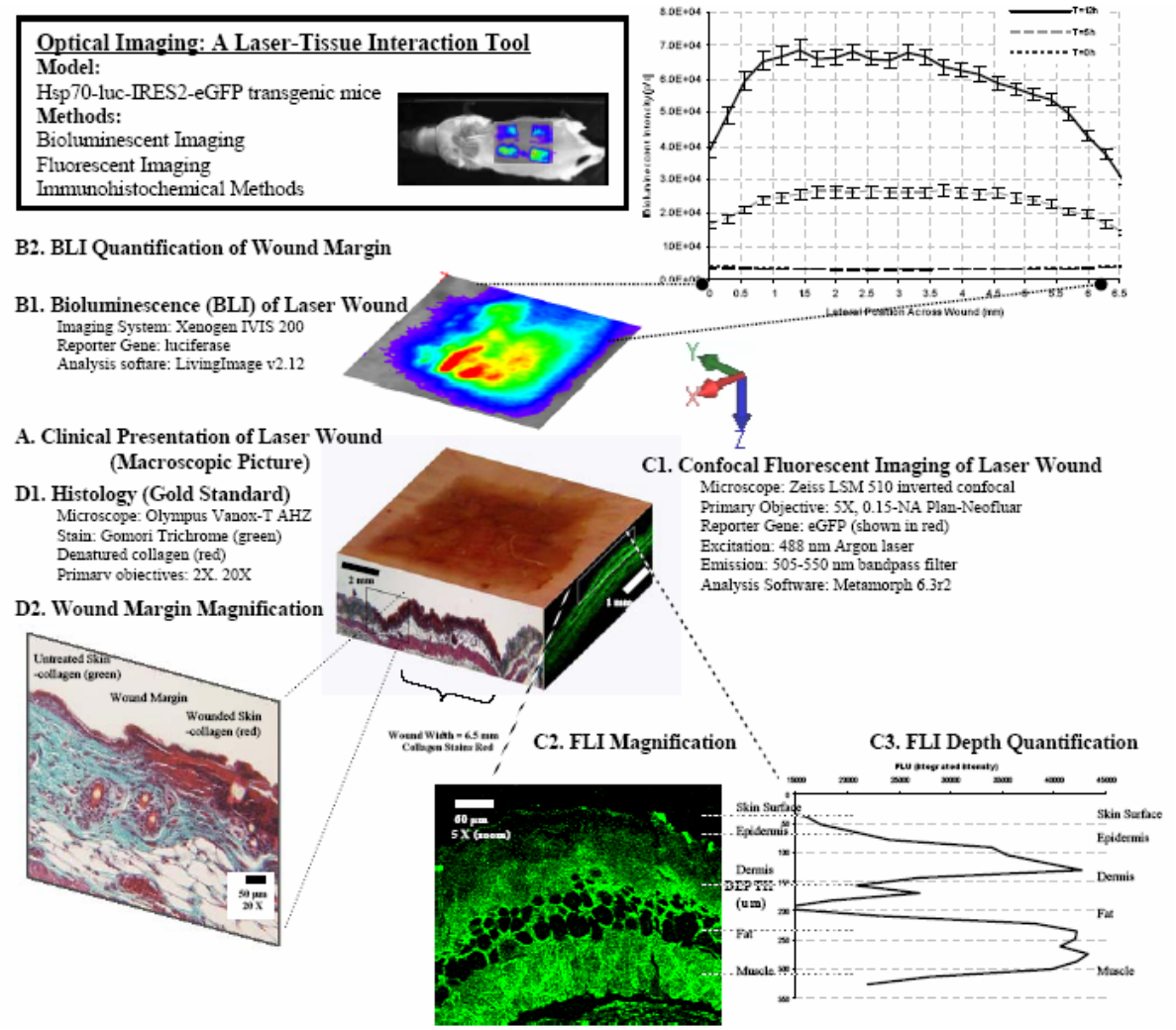

Figure 2.10. Optical Imaging: A Laser-Tissue Interaction Assessment Tool
(A) Macroscopic picture of FEL Wound (Clinical Presentation). (B1) Bioluminescence (BLI) of laser wounds. (B2) BLI Quantification: BLI versus lateral position across wound (mm). (C1) Fluorescent microscopy of hsp70-eGFP signal at 12 h (5X magnification, bar, 150 µm). 10 µm thick cross section slice of laser damaged dermis imaged with Zeiss Inverted LSM510 Confocal Microscope. Imaging mode: laser scanning fluorescence and DIC (Nomarski), 3-D "Z-series", and time-series. Fluorescent filter 488 nm. (C2) FLI Depth Quantification. The hsp70-eGFP signal can be measured in the z-direction using confocal fluorescent imaging. (D1) Immunohistochemistry of FEL wounded skin. Gomori trichrome (green) taken at 2X magnification, bar, 2 mm. Untreated collagen stains green and denatured collegen stains red.(D2) Wound Margin Magnification. 20X magnification of the wound margin in (D1). Untreated collagen stains green and denatured collegen stains red.

2.10. Works cited

1. Murphy, G.F. and A.J. Herzberg, *Atlas of dermatopathology*. 1996, Philadelphia: Saunders. x, 373 p.
2. Vogel, A. and V. Venugopalan, *Mechanisms of pulsed laser ablation of biological tissues.* Chem Rev, 2003. **103**(2): p. 577-644.
3. Alster, T.S. and J.R. Lupton, *Erbium:YAG cutaneous laser resurfacing.* Dermatol Clin, 2001. **19**(3): p. 453-66.
4. Thong, H.Y., et al., *The patterns of melanosome distribution in keratinocytes of human skin as one determining factor of skin colour.* Br J Dermatol, 2003. **149**(3): p. 498-505.
5. Anderson, R.R. and J.A. Parrish, *Selective photothermolysis: precise microsurgery by selective absorption of pulsed radiation.* Science, 1983. **220**(4596): p. 524-7.
6. Sundaramoorthy, M., et al., *Crystal structure of NC1 domains. Structural basis for type IV collagen assembly in basement membranes.* J Biol Chem, 2002. **277**(34): p. 31142-53.
7. Royce, P.M. and B.U. Steinmann, *Connective tissue and it heritable disorders : molecular, genetic, and medical aspects*. 2nd ed. 2002, New York: Wiley-Liss. xvii, 1201 p.
8. Montagna, W., A.M. Kligman, and K.S. Carlisle, *Atlas of normal human skin*. 1992, New York: Springer-Verlag. xvii, 384 p.
9. Jemec, G.B., et al., *Measurement of the mechanical properties of skin with ballistometer and suction cup.* Skin Res Technol, 2001. **7**(2): p. 122-6.
10. Graudenz, K. and C. Raulin, *[From Einstein's Quantum Theory to modern laser therapy. The history of lasers in dermatology and aesthetic medicine].* Hautarzt, 2003. **54**(7): p. 575-82.
11. Niemz, M.H., *Laser-tissue interactions : fundamentals and applications*. 1996, Berlin ; New York: Springer. xii, 297 p.
12. Welch, A.J., J.H. Torres, and W.F. Cheong, *Laser physics and laser-tissue interaction.* Tex Heart Inst J, 1989. **16**(3): p. 141-9.
13. Welch, A.J. and M.J.C.v. Gemert, *Optical-thermal response of laser-irradiated tissue*. Lasers, photonics, and electro-optics. 1995, New York: Plenum Press. xxvi, 925 p.
14. Hale, G.Q., MR, *Optical constants of water in 200nm to 200 um wavelength region.* Applied Optics, 1973. **12**(3): p. 555-563.
15. Ross, E.V., J.R. McKinlay, and R.R. Anderson, *Why does carbon dioxide resurfacing work? A review.* Arch Dermatol, 1999. **135**(4): p. 444-54.
16. Papadavid, E. and A. Katsambas, *Lasers for facial rejuvenation: a review.* Int J Dermatol, 2003. **42**(6): p. 480-7.
17. Jansen, E.D., *Partial vaporization model for pulsed mid-infrared laser ablation of water.* Journal of applied physics, 1995. **78**(1): p. 574.
18. Ton G. van Leeuwen, E.D.J., Massoud Motamedi, Ashley J. Welch, Cornelius Borst, *Excimer Laser Ablation of Soft Tissue: A Study of the content of Rapidly Expanding and Collapsing Bubbles.* IEEE Journal of Quantum Electronics, 1994. **30**(5): p. 1339-1345.
19. Herschel, W., *Experiments on the Refrangibility of the Invisible Rays of the Sun.* Philosophical Transactions of the Royal Society of London, 1800. **90**: p. 284-292.
20. Herschel, W., *Investigation of the Powers of the Prismatic Colours to Heat and Illuminate Objects.* Philosophical Transactions of the Royal Society of London, 1800. **90**: p. 255-283.

21. Daintith, J., *Biographical encyclapedia of scientists*, ed. C. Press. Vol. 2. 1994: CRC Press. 1075.
22. Systems, F., *Thermovision Manual*. 2004, FLIR Systems: Boston, MA. p. 1-228.
23. Thomsen, S., J.A. Pearce, and W.F. Cheong, *Changes in birefringence as markers of thermal damage in tissues.* IEEE Trans Biomed Eng, 1989. **36**(12): p. 1174-9.
24. Tsong, T.Y. and Z.D. Su, *Biological effects of electric shock and heat denaturation and oxidation of molecules, membranes, and cellular functions.* Ann N Y Acad Sci, 1999. **888**: p. 211-32.
25. Beckham, J.T., et al., *Assessment of cellular response to thermal laser injury through bioluminescence imaging of heat shock protein 70.* Photochem Photobiol, 2004. **79**(1): p. 76-85.
26. Kao, B., et al., *Novel model for evaluation of epidermal preservation and dermal collagen remodeling following photorejuvenation of human skin.* Lasers Surg Med, 2003. **32**(2): p. 115-9.
27. Khatri, K.A., et al., *Comparison of erbium:YAG and carbon dioxide lasers in resurfacing of facial rhytides.* Arch Dermatol, 1999. **135**(4): p. 391-7.
28. Xiao, Y., et al., *Wavelength-dependent collagen fragmentation during mid-IR laser ablation.* Biophys J, 2006. **91**(4): p. 1424-32.
29. Capon, A. and S. Mordon, *Can thermal lasers promote skin wound healing?* Am J Clin Dermatol, 2003. **4**(1): p. 1-12.
30. O'Connell-Rodwell, C.E., et al., *A genetic reporter of thermal stress defines physiologic zones over a defined temperature range.* Faseb J, 2004. **18**(2): p. 264-71.
31. Frydman, J., *Folding of newly translated proteins in vivo: the role of molecular chaperones.* Annu Rev Biochem, 2001. **70**: p. 603-47.
32. Morimoto, R.I., P.E. Kroeger, and J.J. Cotto, *The transcriptional regulation of heat shock genes: a plethora of heat shock factors and regulatory conditions.* Exs, 1996. **77**: p. 139-63.
33. Feder, M.E. and G.E. Hofmann, *Heat-shock proteins, molecular chaperones, and the stress response: evolutionary and ecological physiology.* Annu Rev Physiol, 1999. **61**: p. 243-82.
34. Morris, S.D., *Heat shock proteins and the skin.* Clin Exp Dermatol, 2002. **27**(3): p. 220-4.
35. Kiang, J.G. and G.C. Tsokos, *Heat shock protein 70 kDa: molecular biology, biochemistry, and physiology.* Pharmacol Ther, 1998. **80**(2): p. 183-201.
36. Pockley, A.G., *Heat shock proteins, inflammation, and cardiovascular disease.* Circulation, 2002. **105**(8): p. 1012-7.
37. Laplante, A.F., et al., *Expression of heat shock proteins in mouse skin during wound healing.* J Histochem Cytochem, 1998. **46**(11): p. 1291-301.
38. Steffensen, B., L. Hakkinen, and H. Larjava, *Proteolytic events of wound-healing--coordinated interactions among matrix metalloproteinases (MMPs), integrins, and extracellular matrix molecules.* Crit Rev Oral Biol Med, 2001. **12**(5): p. 373-98.
39. Mosser, D.D., et al., *Role of the human heat shock protein hsp70 in protection against stress-induced apoptosis.* Mol Cell Biol, 1997. **17**(9): p. 5317-27.
40. McMurtry, A.L., et al., *Expression of HSP70 in healing wounds of diabetic and nondiabetic mice.* J Surg Res, 1999. **86**(1): p. 36-41.
41. Huang, L., N.F. Mivechi, and D. Moskophidis, *Insights into regulation and function of the major stress-induced hsp70 molecular chaperone in vivo: analysis*

of mice with targeted gene disruption of the hsp70.1 or hsp70.3 gene. Mol Cell Biol, 2001. **21**(24): p. 8575-91.
42. Oberringer, M., et al., *Differential expression of heat shock protein 70 in well healing and chronic human wound tissue.* Biochem Biophys Res Commun, 1995. **214**(3): p. 1009-14.
43. Lakhotia, S.C., P. Srivastava, and K.V. Prasanth, *Regulation of heat shock proteins, Hsp70 and Hsp64, in heat-shocked Malpighian tubules of Drosophila melanogaster larvae.* Cell Stress Chaperones, 2002. **7**(4): p. 347-56.
44. Davidson, J.M. and S.I. Benn, *Biochemical and molecular regulation of angiogenesis and wound repair.* In: Cellular and Molecular Pathogenesis, A.E. Sirica (ed), Raven Press, New York, 1996: p. 79-108.
45. Tredget, E.E., *Pathophysiology and treatment of fibroproliferative disorders following thermal injury.* Ann N Y Acad Sci, 1999. **888**: p. 165-82.
46. Pierce, G.F. and T.A. Mustoe, *Pharmacologic enhancement of wound healing.* Annu Rev Med, 1995. **46**: p. 467-81.
47. Singer, A.J. and R.A. Clark, *Cutaneous wound healing.* N Engl J Med, 1999. **341**(10): p. 738-46.
48. Liaw, L., et al., *Altered wound healing in mice lacking a functional osteopontin gene (spp1).* J Clin Invest, 1998. **101**(7): p. 1468-78.
49. Goliger, J.A. and D.L. Paul, *Wounding alters epidermal connexin expression and gap junction-mediated intercellular communication.* Mol Biol Cell, 1995. **6**(11): p. 1491-501.
50. Takehara, K., *Growth regulation of skin fibroblasts.* J Dermatol Sci, 2000. **24 Suppl 1**: p. S70-7.
51. Tredget, E.E., et al., *Hypertrophic scars, keloids, and contractures. The cellular and molecular basis for therapy.* Surg Clin North Am, 1997. **77**(3): p. 701-30.
52. Hoskins, P.R., *A review of the measurement of blood velocity and related quantities using Doppler ultrasound.* Proc Inst Mech Eng [H], 1999. **213**(5): p. 391-400.
53. Davidson, J.M. and K.N. Broadley, *Manipulation of the wound-healing process with basic fibroblast growth factor.* Ann N Y Acad Sci, 1991. **638**: p. 306-15.
54. Deuel, T.F., et al., *Growth factors and wound healing: platelet-derived growth factor as a model cytokine.* Annu Rev Med, 1991. **42**: p. 567-84.
55. Nanney, L.B., et al., *CM101 stimulates cutaneous wound healing through an anti-angiogenic mechanism.* Angiogenesis, 2001. **4**(1): p. 61-70.
56. Odink, K., et al., *Two calcium-binding proteins in infiltrate macrophages of rheumatoid arthritis.* Nature, 1987. **330**(6143): p. 80-2.
57. Wu, N. and J.M. Davidson, *Migration inhibitory factor-related protein (MRP)8 and MRP14 are differentially expressed in free-electron laser and scalpel incisions.* Wound Repair Regen, 2004. **12**(3): p. 327-36.
58. Wu, N., E.D. Jansen, and J.M. Davidson, *Comparison of mouse matrix metalloproteinase 13 expression in free-electron laser and scalpel incisions during wound healing.* J Invest Dermatol, 2003. **121**(4): p. 926-32.
59. Bennett, N.T. and G.S. Schultz, *Growth factors and wound healing: biochemical properties of growth factors and their receptors.* Am J Surg, 1993. **165**(6): p. 728-37.
60. McGee, G.S., et al., *Recombinant basic fibroblast growth factor accelerates wound healing.* J Surg Res, 1988. **45**(1): p. 145-53.
61. Nanney, L.B., *Epidermal and dermal effects of epidermal growth factor during wound repair.* J Invest Dermatol, 1990. **94**(5): p. 624-9.

62. Quaglino, D., Jr., et al., *Transforming growth factor-beta stimulates wound healing and modulates extracellular matrix gene expression in pig skin: incisional wound model.* J Invest Dermatol, 1991. **97**(1): p. 34-42.
63. Quaglino, D., Jr., et al., *Transforming growth factor-beta stimulates wound healing and modulates extracellular matrix gene expression in pig skin. I. Excisional wound model.* Lab Invest, 1990. **63**(3): p. 307-19.
64. Levine, J.H., et al., *Spatial and temporal patterns of immunoreactive transforming growth factor beta 1, beta 2, and beta 3 during excisional wound repair.* Am J Pathol, 1993. **143**(2): p. 368-80.
65. Roesel, J.F. and L.B. Nanney, *Assessment of differential cytokine effects on angiogenesis using an in vivo model of cutaneous wound repair.* J Surg Res, 1995. **58**(5): p. 449-59.
66. Jyung, R.W., et al., *Increased wound-breaking strength induced by insulin-like growth factor I in combination with insulin-like growth factor binding protein-1.* Surgery, 1994. **115**(2): p. 233-9.
67. Shi, Y., et al., *CARP, a cardiac ankyrin repeat protein, is up-regulated during wound healing and induces angiogenesis in experimental granulation tissue.* Am J Pathol, 2005. **166**(1): p. 303-12.
68. Jyung, R.W., et al., *Granulocyte-macrophage colony-stimulating factor and granulocyte colony-stimulating factor: differential action on incisional wound healing.* Surgery, 1994. **115**(3): p. 325-34.
69. Wu, N., et al., *Real-time visualization of MMP-13 promoter activity in transgenic mice.* Matrix Biol, 2002. **21**(2): p. 149-61.
70. Wu, N.J., E.D. Jansen, and J.M. Davidson, *Comparison of MMP-13 Expression In Free-Electron Laser and Scalpel Incisions During Wound Healing.* J of Investigative Dermatology, (in press).
71. Draper, B.K., M.K. Davidson, and L.B. Nanney, *MMPs and TIMP-1 are differentially expressed between acute murine excisional and laser wounds.* Lasers Surg Med, 2002. **30**(2): p. 106-16.
72. Li, Y., et al., *Retinal preconditioning and the induction of heat-shock protein 27.* Invest Ophthalmol Vis Sci, 2003. **44**(3): p. 1299-304.
73. Kim, J.M., et al., *Effect of thermal preconditioning before excimer laser photoablation.* J Korean Med Sci, 2004. **19**(3): p. 437-46.
74. Topping, A., et al., *Successful reduction in skin damage resulting from exposure to the normal-mode ruby laser in an animal model.* British Journal of Plastic Surgery, 2001. **54**(2): p. 144-150.
75. Bowman, P.D., et al., *Survival of human epidermal keratinocytes after short-duration high temperature: synthesis of HSP70 and IL-8.* Am J Physiol, 1997. **272**(6 Pt 1): p. C1988-94.
76. Ritossa, F., *A new puffing pattern induced by temperature shock and DNP in Drosophila.* Experientia, 1962. **18**: p. 571-573.
77. Wynn, R.M., et al., *Molecular chaperones: heat-shock proteins, foldases, and matchmakers.* J Lab Clin Med, 1994. **124**(1): p. 31-6.
78. Samali, A. and T.G. Cotter, *Heat shock proteins increase resistance to apoptosis.* Exp Cell Res, 1996. **223**(1): p. 163-70.
79. Jaattela, M. and D. Wissing, *Emerging role of heat shock proteins in biology and medicine.* Ann Med, 1992. **24**(4): p. 249-58.
80. Dinh, H.K., et al., *Gene expression profiling of the response to thermal injury in human cells.* Physiol Genomics, 2001. **7**(1): p. 3-13.

81. Keyse, S.M. and E.A. Emslie, *Oxidative stress and heat shock induce a human gene encoding a protein-tyrosine phosphatase.* Nature, 1992. **359**(6396): p. 644-7.
82. Ishibashi, T., et al., *A novel dual specificity phosphatase induced by serum stimulation and heat shock.* J Biol Chem, 1994. **269**(47): p. 29897-902.
83. Erdos, G., et al., *Heat-induced bFGF gene expression in the absence of heat shock element correlates with enhanced AP-1 binding activity.* J Cell Physiol, 1995. **164**(2): p. 404-13.
84. Kanamori, S., et al., *Induction of vascular endothelial growth factor (VEGF) by hyperthermia and/or an angiogenesis inhibitor.* Int J Hyperthermia, 1999. **15**(4): p. 267-78.
85. Flanders, K.C., et al., *Hyperthermia induces expression of transforming growth factor-beta s in rat cardiac cells in vitro and in vivo.* J Clin Invest, 1993. **92**(1): p. 404-10.
86. Xie, Y., et al., *Heat shock factor 1 represses transcription of the IL-1beta gene through physical interaction with the nuclear factor of interleukin 6.* J Biol Chem, 2002. **277**(14): p. 11802-10.
87. Cahill, C.M., et al., *Transcriptional repression of the prointerleukin 1beta gene by heat shock factor 1.* J Biol Chem, 1996. **271**(40): p. 24874-9.
88. Plumier, J.C. and R.W. Currie, *Heat shock-induced myocardial protection against ischemic injury: a role for Hsp70?* Cell Stress Chaperones, 1996. **1**(1): p. 13-7.
89. Plumier, J.C., et al., *Transgenic mice expressing the human heat shock protein 70 have improved post-ischemic myocardial recovery.* J Clin Invest, 1995. **95**(4): p. 1854-60.
90. Kiang, J.G., et al., *Geldanamycin treatment inhibits hemorrhage-induced increases in KLF6 and iNOS expression in unresuscitated mouse organs: role of inducible HSP70.* J Appl Physiol, 2004. **97**(2): p. 564-9.
91. Vigh, L., et al., *Bimoclomol: a nontoxic, hydroxylamine derivative with stress protein-inducing activity and cytoprotective effects.* Nat Med, 1997. **3**(10): p. 1150-4.
92. Pespeni, M., M. Hodnett, and J.F. Pittet, *In vivo stress preconditioning.* Methods, 2005. **35**(2): p. 158-64.
93. Harder, Y., et al., *Improved skin flap survival after local heat preconditioning in pigs.* J Surg Res, 2004. **119**(1): p. 100-5.
94. Walters, T.J., et al., HSP70 expression in the CNS in response to exercise and heat stress in rats. J Appl Physiol, 1998. 84(4): p. 1269-77.
95. Madio, D.P., et al., On the feasibility of MRI-guided focused ultrasound for local induction of gene expression. J Magn Reson Imaging, 1998. 8(1): p. 101-4.
96. Souil, E., et al., Treatment with 815-nm diode laser induces long-lasting expression of 72-kDa heat shock protein in normal rat skin. Br J Dermatol, 2001. 144(2): p. 260-6.
97. Mehlen, P., K. Schulze-Osthoff, and A.P. Arrigo, Small stress proteins as novel regulators of apoptosis. Heat shock protein 27 blocks Fas/APO-1- and staurosporine-induced cell death. J Biol Chem, 1996. 271(28): p. 16510-4.
98. Martin, P., Wound healing--aiming for perfect skin regeneration. Science, 1997. 276(5309): p. 75-81.
99. Capon, A., et al., Laser assisted skin closure (LASC) by using a 815-nm diode-laser system accelerates and improves wound healing. Lasers Surg Med, 2001. 28(2): p. 168-75.

100. Cao, Y., et al., TGF-beta1 mediates 70-kDa heat shock protein induction due to ultraviolet irradiation in human skin fibroblasts. Pflugers Arch, 1999. 438(3): p. 239-44.
101. Bullard, K.M., M.T. Longaker, and H.P. Lorenz, Fetal wound healing: current biology. World J Surg, 2003. 27(1): p. 54-61.
102. Whitby, D.J. and M.W. Ferguson, Immunohistochemical localization of growth factors in fetal wound healing. Dev Biol, 1991. 147(1): p. 207-15.
103. Davidson, J.M., Animal models for wound repair. Arch Dermatol Res, 1998. 290 Suppl: p. S1-11.
104. Ross, E.V., et al., Nonablative skin remodeling: selective dermal heating with a mid-infrared laser and contact cooling combination. Lasers Surg Med, 2000. 26(2): p. 186-95.
105. Ehrmann, R.L. and G.O. Gey, The growth of cells on a transparent gel of reconstituted rat-tail collagen. J Natl Cancer Inst, 1956. 16(6): p. 1375-403.
106. Bell, E., B. Ivarsson, and C. Merrill, Production of a tissue-like structure by contraction of collagen lattices by human fibroblasts of different proliferative potential in vitro. Proc Natl Acad Sci U S A, 1979. 76(3): p. 1274-8.
107. Bell, E., et al., The reconstitution of living skin. J Invest Dermatol, 1983. 81(1 Suppl): p. 2s-10s.
108. Bell, E., et al., Recipes for reconstituting skin. J Biomech Eng, 1991. 113(2): p. 113-9.
109. Asselineau, D., et al., Human epidermis reconstructed by culture: is it "normal"? J Invest Dermatol, 1986. 86(2): p. 181-6.
110. Asselineau, D. and M. Prunieras, Reconstruction of 'simplified' skin: control of fabrication. Br J Dermatol, 1984. 111 Suppl 27: p. 219-22.
111. Michalopoulos, G. and H.C. Pitot, Primary culture of parenchymal liver cells on collagen membranes. Morphological and biochemical observations. Exp Cell Res, 1975. 94(1): p. 70-8.
112. Kao, B., et al., Evaluation of cryogen spray cooling exposure on in vitro model human skin. Lasers Surg Med, 2004. 34(2): p. 146-54.
113. Yeh, A.T., et al., Imaging wound healing using optical coherence tomography and multiphoton microscopy in an in vitro skin-equivalent tissue model. J Biomed Opt, 2004. 9(2): p. 248-53.
114. Viehoever, A.R., et al., Organotypic raft cultures as an effective in vitro tool for understanding Raman spectral analysis of tissue. Photochem Photobiol, 2003. 78(5): p. 517-24.
115. Wilmink, G.J., et al., Assessing laser-tissue damage with bioluminescent imaging. Journal of Biomedical Optics, 2006. 11(4): p. 041114.
116. Contag, C.H., et al., Visualizing gene expression in living mammals using a bioluminescent reporter. Photochem Photobiol, 1997. 66(4): p. 523-31.
117. Contag, P.R., et al., Bioluminescent indicators in living mammals. Nat Med, 1998. 4(2): p. 245-7.
118. Contag, C.H. and M.H. Bachmann, Advances in in vivo bioluminescence imaging of gene expression. Annu Rev Biomed Eng, 2002. 4: p. 235-60.
119. Wilmink, G.J., et al., Assessing laser-tissue damage with bioluminescent imaging. J Biomed Opt, 2006. 11(4): p. 041114.
120. Izzo, A.D., et al., In vivo optical imaging of expression of vascular endothelial growth factor following laser incision in skin. Lasers Surg Med, 2001. 29(4): p. 343-50.

121. Greer, L.F., 3rd and A.A. Szalay, Imaging of light emission from the expression of luciferases in living cells and organisms: a review. Luminescence, 2002. 17(1): p. 43-74.
122. Hastings, J.W., Chemistries and colors of bioluminescent reactions: a review. Gene, 1996. 173(1 Spec No): p. 5-11.
123. Gould, S.J. and S. Subramani, Firefly luciferase as a tool in molecular and cell biology. Anal Biochem, 1988. 175(1): p. 5-13.
124. Ugarova, N.N. and L.Y. Brovko, Protein structure and bioluminescent spectra for firefly bioluminescence. Luminescence, 2002. 17(5): p. 321-30.
125. Nguyen, V.T., M. Morange, and O. Bensaude, Firefly luciferase luminescence assays using scintillation counters for quantitation in transfected mammalian cells. Anal Biochem, 1988. 171(2): p. 404-8.
126. Brasier, A.R., J.E. Tate, and J.F. Habener, Optimized use of the firefly luciferase assay as a reporter gene in mammalian cell lines. Biotechniques, 1989. 7(10): p. 1116-22.
127. Szpilewska, H., A. Czyz, and G. Wegrzyn, Experimental evidence for the physiological role of bacterial luciferase in the protection of cells against oxidative stress. Curr Microbiol, 2003. 47(5): p. 379-82.
128. Rice, B.W., M.D. Cable, and M.B. Nelson, In vivo imaging of light-emitting probes. J Biomed Opt, 2001. 6(4): p. 432-40.
129. Massoud, T.F. and S.S. Gambhir, Molecular imaging in living subjects: seeing fundamental biological processes in a new light. Genes Dev, 2003. 17(5): p. 545-80.
130. Troy, T., et al., Quantitative comparison of the sensitivity of detection of fluorescent and bioluminescent reporters in animal models. Mol Imaging, 2004. 3(1): p. 9-23.

CHAPTER III

ASSESSING LASER-TISSUE DAMAGE WITH BIOLUMINESCENT IMAGING

Gerald J. Wilmink[1], Susan R. Opalenik[2], Joshua T. Beckham[1], Jeffrey M. Davidson[2,3], E. Duco Jansen[1]

[1] Department of Biomedical Engineering

[2] Department of Pathology

[3] Research Service, VA Tennessee Valley Health Care System

Vanderbilt University

Nashville, Tennessee 37235

Portions of this manuscript have been published in:

"Assessing Laser-Tissue Damage with Bioluminescent Imaging,"

Journal of Biomedical Optics. Vol. 11, Issue 4, page 041114 (2006).

3.1. Abstract

Effective medical laser procedures are achieved by selecting laser parameters that minimize undesirable tissue damage. Traditionally, human subjects, animal models, and monolayer cell cultures have been used to study wound healing, tissue damage, and cellular effects of laser radiation. Each of these models has significant limitations, and consequently a novel skin model is needed. To this end a highly reproducible human skin model that enables noninvasive and longitudinal studies of gene expression was sought. In this study, we present an organotypic raft model (engineered skin) used in combination with bioluminescent imaging (BLI) techniques. The efficacy of the raft model was validated and characterized by investigating the role of heat shock protein 70 (hsp70) as a sensitive marker of thermal damage. The raft model consists of human cells incorporated into an extracellular matrix. The raft cultures were transfected with an adenovirus containing a murine hsp70 promoter driving transcription of luciferase. The model enables quantitative analysis of spatio-temporal expression of proteins using BLI. Thermal stress was induced on the raft cultures by means of a constant temperature water bath or with a carbon dioxide (CO_2) laser: (λ= 10.6 μm, 0.679-2.262 W/cm^2, CW, unfocused Gaussian beam, ω_L = 4.5 mm, 1 min exposure). The bioluminescence was monitored non-invasively with an IVIS 100 Bioluminescent Imaging System. BLI indicated that peak hsp70 expression occurs 4-12 hours after exposure to thermal stress. A minimum irradiance of 0.679 W/cm^2 activated the hsp70 response, and a higher irradiance of 2.262 W/cm^2 was associated with a severe reduction in hsp70 response due to tissue ablation. RT-PCR demonstrated that hsp70 mRNA levels increased with prolonged heating exposures. ELISA protein assays confirmed that luciferase was an accurate surrogate for hsp70 intracellular protein levels. Hematoxylin & Eosin stains verified the presence of the thermally denatured tissue regions.

Immunohistochemical analyses confirmed that maximal hsp70 expression occurred at a depth of 150 μm. Bioluminescent microscopy was employed to corroborate these findings. These results indicate that quantitative BLI in engineered tissue equivalents provides a powerful model that enables sequential gene expression studies. Such a model can be used as a high throughput screening platform for laser-tissue interaction studies.

3.2. Introduction

Lasers play an increasing role in the medical field for diagnostic and therapeutic applications. Effective laser procedures are achieved by selectively tailoring the laser's parameters (wavelength, spotsize, pulse duration, radiant energy, beam profile) to the physical characteristics of the target tissue (anatomy, mechanical properties, heat capacity, thermal conductivity, absorption coefficient, scattering coefficient, anisotropy). Laser parameters are selected to optimize efficacy while minimizing unwanted side effects and tissue damage. From a phenomenological standpoint, it is known that laser-induced tissue injury occurs via oxidative, photothermal, photomechanical, and photochemical mechanisms [1]. Nevertheless, the specific cellular and molecular pathways which initiate and govern these mechanisms remain poorly understood [1, 2]. Traditional efforts aimed at assessing cellular tissue damage have used post-mortem strategies, such as histology, RT-PCR, *in situ* hybridization, and Western blots [3-6]. The major shortcoming of these methods is they all require sacrificing tissue, thereby precluding the ability to conduct sequential studies. Therefore, a strategy capable of reporting sub-lethal tissue damage in a non-invasive fashion was sought. Recent bioluminescent imaging (BLI) strategies have elucidated some of those signaling pathways which are activated during laser-induced tissue injury. The oxidative light emitting luciferase reaction of BLI can be harnessed for use as a surrogate marker for

promoter activity. BLI has been used to monitor a variety of biological processes in wound healing, transplantation, and apoptosis [3, 4, 7-10]. The key regulatory feature of BLI is accomplished by using the promoter sequence for the gene of interest, in our study heat shock protein 70 (hsp70), in conjunction with an optically active reporter, firefly luciferase (*luc*).

When tissue is thermally damaged, a cellular response mechanism consisting of heat shock proteins (hsp) is activated. Hsps are employed to repair cellular damage and protect the cell from further thermal injury [11]. This heat shock response is dependent on both temperature and time, and is induced by minimal temperature increases of at least 5-6^{o} C [11-13]. Of the heat shock family members, the most highly inducible is hsp70 [13]. In the presence of cellular insults, hsp70 can be dramatically up-regulated to make up to 15 % of total cellular protein content [14]. Due to its marked induction, hsp70 acts as a sensitive indicator of thermal damage to cells [6, 13]. Herein, the promoter sequence of the gene (murine hsp70a1) functions as an “on-off” switch for transcription of the light emitting luciferase. For this study, expression of the *luc* gene from the firefly (*Photinus pyralis*) was directed by the promoter of the hsp70 gene, as described previously [13]. Thus, measuring the light emitted from the luciferase reaction using BLI strategies, provides a noninvasive method to quantify hsp70 transcription.

Besides the method of assessing tissue damage at the cellular level, selecting an appropriate study model also poses a formidable challenge. In comparable studies, human subjects have been used, however using humans provides two intrinsic difficulties: 1) in measuring gene expression on a single subject over time and 2) in stringent medical limits (ethical and practical) of harvesting tissue samples at multiple times for histological and biochemical analysis [15, 16]. In light of these difficulties, animal models are used as a more viable model to study hsp70 expression and other laser-induced tissue effects [5, 17]. The porcine model is the closest non-primate

equivalent to human skin and is the most widely used dermal wound repair model, but because of differences in tissue architecture and immune responses, even it does not accurately reflect human wound healing [18, 19]. The use of cell cultures is an alternative to using human subjects and animal models, and we and others have successfully assessed hsp70 levels in cell culture [12, 13]. Cell culture studies provide valuable insights into the cellular response to thermal injury, but their utility is limited because cells, lacking an extracellular matrix (ECM), react differently than when incorporated in tissue. The ECM provides skin with distinct thermal and optical properties, but also functions at a biochemical level to actively engage with the cell. In the 1980s, Bissell found that the ECM is a key "signaling molecule" crucial for the normal functioning of cells [20]. Consequently, models lacking an ECM, while providing useful information, do not accurately exhibit the cell-matrix relationship present in *in vivo* human skin.

Starting in the mid 1970's, many research efforts were focused on making multilayered skin equivalents. These organotypic tissue cultures became known as 'raft' cultures and this method has been further modified for skin and other tissue applications [15, 16, 21]. Skin raft cultures are human skin equivalents comprised of stromal and epithelial layers. The stromal layer is composed of human fibroblasts in a collagen matrix. Human keratinocytes are grown atop the dermal equivalent, and once transferred to a liquid-air interface differentiate akin to that observed in *in vivo* human skin [22]. Herein, we employed raft cultures as our model because they are more easily available and more reproducible than samples derived from human subjects, consist of all human cells, and provide information regarding cell-matrix interactions.

In this study, we sought to develop a model that emulates human tissue while providing us with the capability of non-invasively, quantitatively, and sequentially assessing sub-lethal thermal damage. Our model employs a raft model that has been

equipped with a heat-inducible reporter gene system to assess the heat shock response using BLI. This model was developed, characterized, and validated using a heated water bath and a CO_2 laser using parameters similar to those used in laser skin resurfacing (LSR). The CO_2 laser is the criterion standard for (LSR) since it can be manipulated in such a fashion, to control the depth of epidermal vaporization while eliciting minimal damage to the papillary dermis [23]. The infrared wavelength is highly absorbed by tissue, which consists primarily of water and collagen, and minimizes residual thermal damage (RTD) [24, 25].

The overall goals of this study are: 1) develop an organotypic skin raft model, transfected with a hsp70-luc reporter gene construct to study spatio-temporal trends of hsp70 expression using BLI strategies; 2) validate the use of BLI as surrogate marker for hsp70 expression by correlating BLI with conventional methods of hsp70 analysis; and 3) demonstrate feasibility of this approach using heating in a water bath and with clinically relevant CO_2 laser parameters.

3.3. Materials and Methods

3.3.1 Cell culture conditions

Normal human neonatal dermal fibroblast (NHDF), normal human epithelial neonatal foreskin keratinocyte (NHEK), and normal human epithelial melanocyte (NHEM) (medium pigment) primary cell lines were obtained from the Vanderbilt University's Skin Diseases Research Tissue Culture Facility (SDRCC). The NHDFs were cultured in Dulbecco's Modified Eagle's Medium (DMEM), and supplemented with 10% Fetal Bovine Serum (FBS), (GIBCO BRL, Gaithersburg, MD). The NHEKs were cultured in Epilife Media, 1% Human Keratinocyte Growth Supplement - V2 (HKGS-V2), 1% Penicillin-Streptomycin-Amphotericin B (PSAB) (CASCADE BIOLOGICS, INC, Portland,

OR). The NHEMs were cultured in Medium 154 CF media, 1% Human Melanocyte Growth Supplement (HMGS), and 1% PSAB. (CASCADE BIOLOGICS, INC, Portland, OR). All cells were incubated at 37°C and 5% CO_2 under humidified conditions.

3.3.2 Recombinant adenovirus construction

Briefly, the Ad-hsp70a1-luc-IRES-eGFP was constructed as follows. The hsp70-luc construct was provided courtesy of Dr. Contag (Stanford University) and consisted of a mouse hsp70a1 promoter (95% homology to human hsp70A1A) with a truncated firefly luciferase gene (luc+) inserted downstream as described previously [12, 13, 26]. The hsp70-luc cassette was subcloned into a modified pShuttle vector (QBIOGENE) upstream of an IRES-eGFP cassette [10]. Generation of the final Adv construct was performed by co-transformation of the pShuttle-hsp70-luc-IRES-eGFP with the pAdEasy1 adenoviral vector by homologous recombination in *E.coli* as per manufacturer's instructions (AdEasy, QBIOGENE). Recombinants were selected for kanamycin resistance, and confirmed by restriction endonuclease analysis. The final linearized AdV construct was transiently transfected into 293 cells, to produce infectious virus particles (Superfect, Qiagen, Valencia, CA).

3.3.3 Virus propagation and purification

Following lysis and purification, the adenovirus had a titer of 1.3×10^7 Plaque forming units (PFU)/ml. The multiplicity of infection (MOI) is defined as the ratio of number of infectious virus units (PFU) to the number of cells. The transfection efficiency was optimized (data not shown), and the results demonstrated that an MOI of 1 generated the best response while minimizing virus use.

3.3.4 Construction of organotypic raft cultures

Organotypic raft cultures were constructed essentially as described [16, 21], with the concentration of NHDFs increased to 6 X 10^6 cells/ml. The raft cultures were incubated for 12–14 days in an atmosphere of 37°C, 5% CO_2, and media was changed every other day. Typical rafts were ~10 mm in diameter and ~2 mm thick. After this incubation period the rafts were transfected with the Adv-hsp70-luc at an MOI of 1 and incubated for 15 hours. Once transfected the rafts were washed with PBS, and then exposed to heat shock conditions. The heat shock conditions were provided by a constant temperature water bath or by a CO_2 laser.

3.3.5 Water bath and laser irradiation experiments

In order to understand the individual contribution that each cell type has to the raft model, cell culture experiments were conducted to characterize the heat shock responses of the cell lines utilized. On day 1, the cells were plated in 6 well (9.62 cm^2) tissue culture plates with 9.6 X 10^4 cells per well in 2 ml culture medium (Costar, Fisher Scientific, Sewanee, GA). For the ELISA experiments 2.5 x 10^5 cells per well were used to ensure adequate protein levels. After 24 hours, the cells were transfected with the adenovirus and returned to a 37 °C, 5% CO_2 incubator (Forma Scientific, Marietta, OH) for ~15 hours. After incubation, the transfection media was aspirated and the cells were washed with PBS. Fresh media was added to the cells, the culture plates were sealed with para-film to prevent contamination, and then heat shocked by floating them in a water bath at 43 °C or 44 °C for varying exposure times (0-40 minutes). The maximum exposure time of 40 minutes at 44°C was selected based on previous hsp70 studies [13]. Heat shocked cells were placed back in a 37 °C, 5% CO_2 incubator (Forma Scientific, Marietta, OH). Bioluminescent images were taken of the cells as described

below. Transfected raft cultures were exposed to a heated water bath or to CO_2 laser radiation. For each experiment, two negative controls were included to account for background luciferase activity (normally < 0.01 % of BL signal) and for constitutive hsp70 expression. The first negative control was a raft that was not transfected or heat shocked, and the second control was a raft that was transfected but not heated. Comparable water bath conditions were applied to the rafts as described for the cell culture experiments.

3.3.6 Laser radiation with Carbon Dioxide (CO_2) Laser

The ablating laser used in this study was a continuous wave CO_2 laser (λ = 10.6 μm, Laser Industries, Sharplan 1060). The laser beam profile was measured to be Gaussian by pinhole measurements. The laser beam radius was selected to ensure full raft radiation. A collimated beam with a radius (ω_L) of 4.5 mm was delivered to the raft cultures via an articulated arm. The laser parameters selected for this experiment ensured that the entire raft's area was radiated, but due to the inherent Gaussian beam profile the center of the raft experienced the highest irradiance. An external shutter (VMM-T1, Vincent Associates, Rochester, NY) was placed 2.5 cm below the fixed arm. The external shutter was used to control laser exposure time. **Figure 3.1(g)** is a schematic illustrating the laser setup.

Studies by Beckham et al. showed that the expression of hsp70 indeed follows an Arrhenius-type rate process, suggesting that hsp70 expression levels depend not just on temperature but on the temperature-time history [13]. Studies investigating hsp70's temperature-time history have observed that maximal hsp70 expression occurs in cells for minute exposures at temperatures ranging from 50 to 64.6 °C [12]. Using a thermocouple, the irradiances of 0.679-2.262 W/cm^2 for 1 minute exposures, as used in

our experiments, were confirmed to generate comparable temperatures 500 μm below the surface of each raft (data not shown).

3.3.7 Bioluminescent imaging (BLI)

Prior to BLI, the substrate for the bioluminescence reaction, D-luciferin potassium salt (Biosynth AG, Switzerland) in ddH_2O at a stock concentration of 0.94 mg/ml was administered to each sample. For the cell experiments, 100 μl of stock substrate was delivered to 2 ml of growth media per well, resulting in a final substrate concentration of 0.047 mg/ml. For raft experiments, 200 μl of substrate was delivered to each raft. After delivery of the substrate, the cells and raft cultures were incubated for one minute before imaging, to ensure maximal bioavailability of the substrate while accounting for the half life of luciferase [27].

3.3.8 Bioluminescent imaging system

The luciferase induced bioluminescent light emission activity was measured at various time points following heat shock using an IVIS 100 bioluminescent imaging system (Xenogen, Alameda, CA). Culture plates containing rafts or cell cultures were placed in the imaging chamber on a heated 37 °C stage and imaged. Both photographic and bioluminescent images were acquired. The bioluminescent image was then superimposed on top of the photographic image. The bioluminescent data is represented with a false color scheme representing the regions of varying light emission. The light emission was quantified using LivingImage analysis software (v2.12,Xenogen). The light emission from specified regions of interest (ROIs) was quantified as a photon flux in units of total number of photons emitted/second/ROI (p/s/ROI).

3.3.9 BLI of cell cultures

For all cell culture experiments, the bioluminescent signal was acquired for a seeding density of 9.6 X 10^4 cells/well in a 6 well plate. For each experiment, a negative control (transfected cells , no heat shock) was employed. The experimental group consisted of cells that were exposed to heat shock conditions. After the experimental cells were heat shocked, both sets of cells were imaged in the same manner. Substrate (100 µl) was re-administered to the cells one minute before each imaging point. Images were collected at 0, 2, 4, 6, 8, 12, 24, and 48 hours after the start of the heating protocol. Bioluminescence images were integrated over 3 minutes.

3.3.10 BLI of laser-treated rafts

To investigate the bioluminescent intensity of adenovirally transfected raft cultures in response to heating with a dermal laser (CO_2), 28 rafts were constructed and allowed to differentiate for 12 days. On day 12, the rafts were transfected with 100 µl of adenovirus (MOI= 1.0) and incubated for 15 hours. The 28 rafts were divided into 7 groups of 4 and included two negative control groups (n=4), with one group with no adenovirus and no heat shock and the other with adenovirus and no heat shock. The third group was a positive control (n=4), which consisted of samples that were heated in a water bath at 44°C for 20 minutes. The final four groups were exposed to laser radiation from a CW CO_2 laser (n=4 for each). These groups were irradiated with 0.43, 0.72, 1.0, and 1.43 Watts of power respectively, with corresponding irradiances of 0.679, 1.131, 1.584, and 2.262 W/cm^2 for 60 seconds. For each raft culture the bioluminescent images were acquired as described above. The ROI was defined as the area corresponding to one raft. Since more cells are present in a raft then in one well, more substrate was delivered to the rafts before imaging. Two hundred µl of substrate was delivered to each

raft before imaging by pipetting the substrate directly on to the rafts. Images were integrated over 1 minute.

3.3.11 ELISA assays

In order to correlate photon counts from imaging to actual hsp70 production in each of the cell types, an enzyme linked immunosorbent assay (ELISA) kit EKS-700 was used to quantify hsp70 protein levels in the samples (Stressgen, Victoria, BC, Canada).

For this experiment, the NHDF, NHEM, and NHEK cell lines were seeded in 6-well plates at a concentration of 2.5 x 10^5 cells per well, transfected (MOI=1) and incubated overnight. Fifteen hours later the transfection media was aspirated, and the cells were washed with PBS. Fresh media was added to the cells and the cells were heat shocked at 44°C for 20, 30, and 40 minutes. One hundred µl of substrate was added to the cells. The cells were imaged 12 hours after heat shock induction with the IVIS system. After imaging, the cells were lysed and the ELISA was conducted according to supplier's instructions (Stressgen, Victoria, BC, Canada).

3.3.12 RNA preparation and Real-Time RT-PCR analysis

To determine mRNA levels of hsp70, RNA was extracted from the cells that were exposed to water bath heating (44 °C for 10, 20, and 40 minutes) and assessed by real-time, RT-PCR. RNA was harvested from cell cultures with the RNeasy kit according to manufacturer's instructions (Qiagen, Valencia, CA). One µg of each sample was DNased and reverse transcribed into single stranded cDNA with a high capacity cDNA archive kit using random primers according to manufacturer's instructions (Qiagen and ABI, Foster City, CA). cDNAs were used as template in duplex PCR reactions, whereby amplification of the housekeeping gene, β-actin, is performed in the same reaction tube with that for hsp70. β-actin was selected as the endogenous control because under heat

shock conditions, β-actin had the smallest intra-sample variability (student-t test, p = 0.55) compared to GAPDH and 18S (data not provided). Each PCR reaction contained 5 µL of cDNA template (50 ng RNA equivalent), 10 µL 2X TaqMan PCR Master Mix (ABI), 1 µL of β-actin 20X Gene Expression Assay- VIC (ABI), 1 µL of HSPA1A 20X Gene Expression Assay- FAM (ABI) and 3µL of water. The cycling PCR reactions were performed in the iCycler, iQ machine (Bio-Rad) and consisted of a 10 min hot-start at 95 °C followed by 40 cycles of 95 °C denaturation for 15 sec and 60 °C annealing/elongation for 1 min. Relative quantitation of mRNA levels was assessed using the comparative C_T method (ABI User Bulletin #2). The hsp70 expression from each sample was normalized to β-actin, and calculated as a fold induction compared to control. The control for each cell type was a sample that was not heat shocked and was extracted at time = 0.

3.3.13 Flow cytometry

In order to provide information to supplement the ELISA data, cell viability and apoptosis assays were performed using flow cytometry. As described in the ELISA section, at 12 hours after thermal stress, medium was removed, then cells were trypsinized and re-suspended in PBS, and stained for 45 min for viability using Molecular Probes LIVE/DEAD viability and cytoxicity stain (L-3224) containing calcein AM (stains live cells green) and ethidium homodimer-1 (stains membrane compromised cells red). The cells were similarly analyzed for early signs of apoptosis using JC-1 stain from Molecular Probes, MitoProbe JC-1 Assay Kit (M34152). All cells were analyzed using a flow cytometer and counted with a Coulter counter (FACSCalibur, Becton Dickinson, Franklin Lakes, NJ, & Beckman Coulter Counter).

3.3.14 Histology and immunohistochemistry

A subset of raft cultures were harvested for immunohistochemical analysis in order to examine raft tissue architecture, to spatially correlate the hsp70 protein expression to luciferase expression, and to examine conventional histological markers of thermal damage. Twelve (12) hours after laser irradiation (which is the time point at which maximum hsp70 expression has been observed) the raft cultures were fixed in Tellyesniczky/Fekete solution (70% ETOH, Glacial Acetic Acid, 37-40% Formalin) or flash frozen in liquid nitrogen. The frozen samples were sectioned at 7 μm and stained. Histological analyses consisted of hematoxylin and eosin (H & E) and Gomori's trichrome (green) stains [30]. Immunohistochemical localization of hsp70 was conducted using mouse monoclonal hsp70 antibody (Santa Cruz Biotechnology, Santa Cruz, CA), diluted 1:200. The application of the Envision+HRP system (DakoCytomation, Carpinteria, CA) and DAB+ produced visible, interpretable results.

3.3.15 Bioluminescent microscopy

Bioluminescent microscopy was conducted to examine the spatial distribution of *in situ* adenoviral transfection, and to examine the hsp70-mediated luciferase expression throughout the raft. Samples were embedded in OCT, flash frozen in liquid nitrogen and sectioned with a microtome (96 μm thickness). Cross sections of the rafts were placed on a frozen microscope slide. Ten mM of ATP (500 μl) and 0.94 mg/ml of luciferin (100μl) was delivered to the slice, and imaged for 1 minute with the IVIS 200 imaging system (Xenogen). The IVIS 200, unlike the IVIS 100 that is used in all other experiments, is equipped with a custom made high magnification lens giving a distortion-free FOV of 3.9 cm. Combined with a binning of 1 and the enlarged chip size (2048 x 2048 pixels), this allows for imaging with a resolution of 20-60 μm, depending on the f-stop.

3.3.16 In situ raft transfections with Ad-CMV-luc

To address the question whether *in situ* transfection would indeed result in a spatially homogenous transfection in raft cultures, we used an adenovirus that expressed *luc* under control of a constitutive CMV promoter (Ad-CMV-Luc-IRES-GFP) [10]. Rafts were transfected with Ad-CMV with an MOI =1 for 15 hours and then washed with PBS. Forty-eight (48) hours after transfection (the time point corresponding to maximum expression for this construct), the rafts were imaged and then harvested for bioluminescence microscopy.

3.3.17 Co-localizing luciferase expression to hsp70 expression

In order to co-localize the hsp70 induced luciferase expression (i.e. bioluminescent light emission) to actual hsp70 protein, a transfected raft (Ad-hsp70-luc (MOI=1)) was irradiated with the CO_2 laser (1.584 W/cm^2 for 1 min). Twelve (12) hours after laser radiation, (the time point corresponding to maximum hsp70 expression), the rafts were imaged and then harvested for bioluminescence microscopy [12, 13].

3.4. Results

3.4.1 Schematic representation of experimental methodology

Figure 3.1 shows the experimental methodology used to construct the raft cultures, to laser treat the cultures, and to image the rafts with the bioluminescent imaging system.

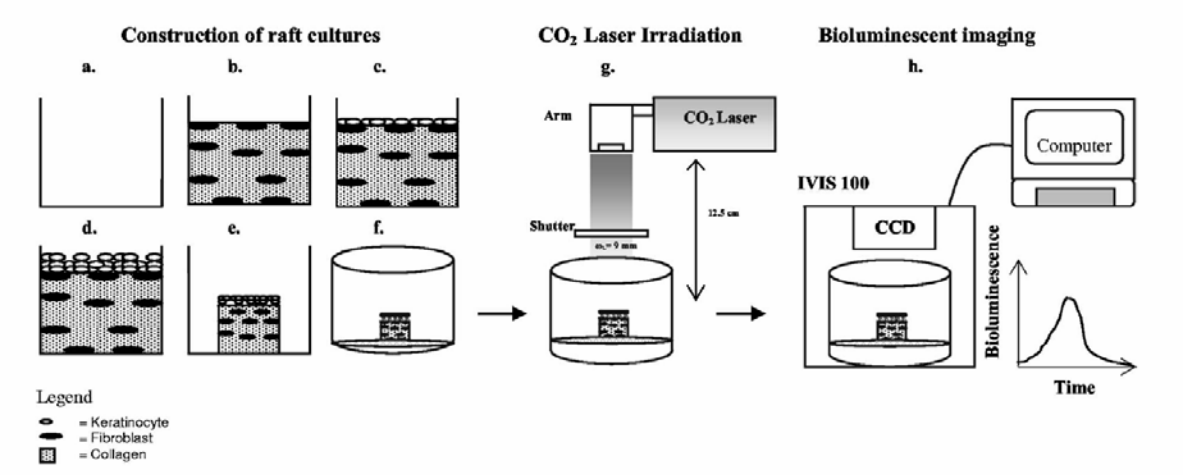

Figure 3.1. **Schematic representation of experimental methodology.**
(a-f) Construction of organotypic raft cultures: **(a)** In a 24 well plate. **(b)** NHDFs were mixed in a collagen matrix. **(c)** NHEKs were added on top of each raft. **(d)** NHEK's begin to differentiate. **(e)** The NHDFs induced contraction of rafts. **(f)** Rafts were lifted to air-liquid interface in petri dish and NHEKs fully differentiated after 10-14 days.
(g) Mature rafts were transfected with 100 µl (MOI= 1.0) of Ad-hsp70-luc and irradiated with CO_2 Laser with irradiances from 0.679-2.262 W/cm^2 for 1 minute.
(h) The bioluminescent signal was captured with an IVIS-100 or 200 BLI system.

3.4.2 Bioluminescence of Hsp70 driven luciferase in NHDFs

Figure 3.2 shows the results of transfected fibroblasts (MOI of 1) that were heat shocked 15 hours after transfection. Cells were exposed to a water-bath of 43 °C or 44 °C for 10, 20, or 40 minutes. Bioluminescent intensity was acquired 0, 2, 4, 6, 8, 10, 12, and 24 hours after heat shock. The results indicate that maximal hsp70 expression occurs 8-12 hours after heat shock. Moreover, relative to a non-heat shocked negative control, hsp70 driven luciferase is induced as much as 160-fold. Similar to previously published results in stably transfected cells, the trend suggests the severity of the heat shock is directly proportional to the magnitude of the heat shock response [13].

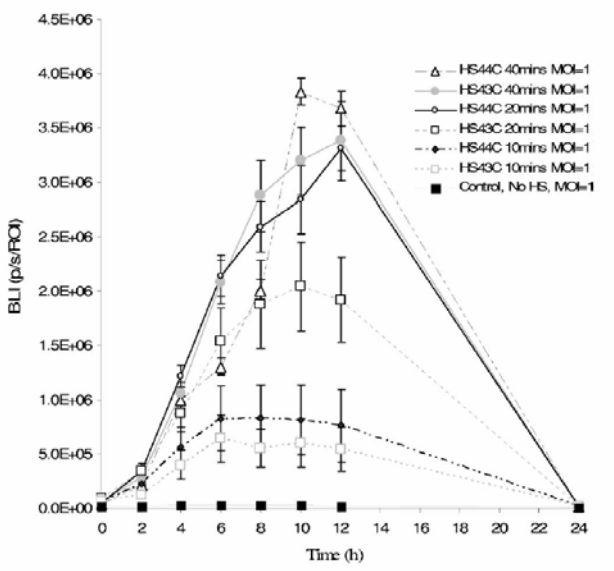

Figure 3.2. **Bioluminescent intensity for NHDFs transfected with Ad-hsp70-luc plotted over time.** Maximal hsp70 expression occurred 8-12 hours after heat shock. This experiment included seven groups conducted in triplicate: negative control, heat shocked at 43°C for 10 minutes (hereafter, HS43°C-10min), HS43°C-20min, HS43°C-40min, HS44°C-10min, HS44°C-20min, and HS44°C-40min. All samples were seeded with NHDFs at a concentration of 9.6 x 10^5 cells per well. At t= -15 hrs, the NHDF's were treated with an Ad-hsp70-luc with an MOI of 1. One hundred µl of D-luciferin (0.94 mg/ml) was added to each well 1 minute before the NHDF's were imaged. Error bars represent the standard deviation for each group.

3.4.3 Transcriptional and translational profiles for skin cells

The goal for this experiment was to examine the hsp70 response for 3 cell types (NHDFs, NHEKs, and NHEMs) at 5 conditions (10, 20, 30, and 40 minutes at 44 °C, and an unheated control) using the following assessment tools: bioluminescence, native hsp70 protein levels, cell viability, and real-time RT-PCR. **Figure 3.3(a-c)** shows the bioluminescence intensity plotted versus the heating protocols, **figure 3.3(d-f)** shows the bioluminescence plotted versus the native hsp70 protein levels (as quantified using ELISA), and **figure 3.3(g-h)** shows the percent of viable and apoptotic cells (as quantified using flow cytometry with JC-1 assay) on the 3 cell types. Data reported is 12 hours post heat shock. **Figures 3.4(a-c)** shows the relative hsp70 mRNA fold induction compared to control relative to β-actin versus time. For all cell types, statistically significant ($P<0.05$) increases in bioluminescent intensity are observed with increasing times of heat exposure [**Figure 3.3(a-c)**]**.** The peak bioluminescent intensities for the NHDFs and the NHEMs are comparable (both ~10^8 photons/second), while the NHEKs peak bioluminescent intensity is observed to be 10 times higher. In **figure 3.3(d-f)** it is observed that as the bioluminescent intensity is increased the native hsp70 protein levels are linearly increased ($R^2 > 0.96$), except for the NHEMs where no clear relationship exists. The data in **figure 3.3(g-h)** reveals for the NHDF and NHEK, at all heating exposures, less than 30 % of the cells demonstrate early signs of apoptosis. Apoptotic levels were not statistically significant different from unheated controls. Conversely, **Figure 3.3(i)** shows that the NHEMs, at all heating exposures, including the unheated controls, have greater than 60% of their cells being apoptotic. For all cell types, statistically significant ($P<0.05$) increases in hsp70 mRNA are observed with increasing times of heat exposure [**Figure 3.4(a-c)**]. Peak hsp70 mRNA expression occurred for all cells at 4-6 hours after heat shocking. Maximal mRNA levels occurred 4 hours after heat shocking for the NHDFs and the NHEMs, and at 6 hours for the NHEKs.

For all cell types, lower heating protocols (HS 44 °C 10 mins) resulted in a quicker mRNA response (~0-4 hrs), while higher heating protocols (HS 44 °C 40 mins) had maximal mRNA transcription at 6 hours. The maximal hsp70 mRNA fold induction of 725 times that of the control occurred in the NHDFs 4 hours after heat shocking.

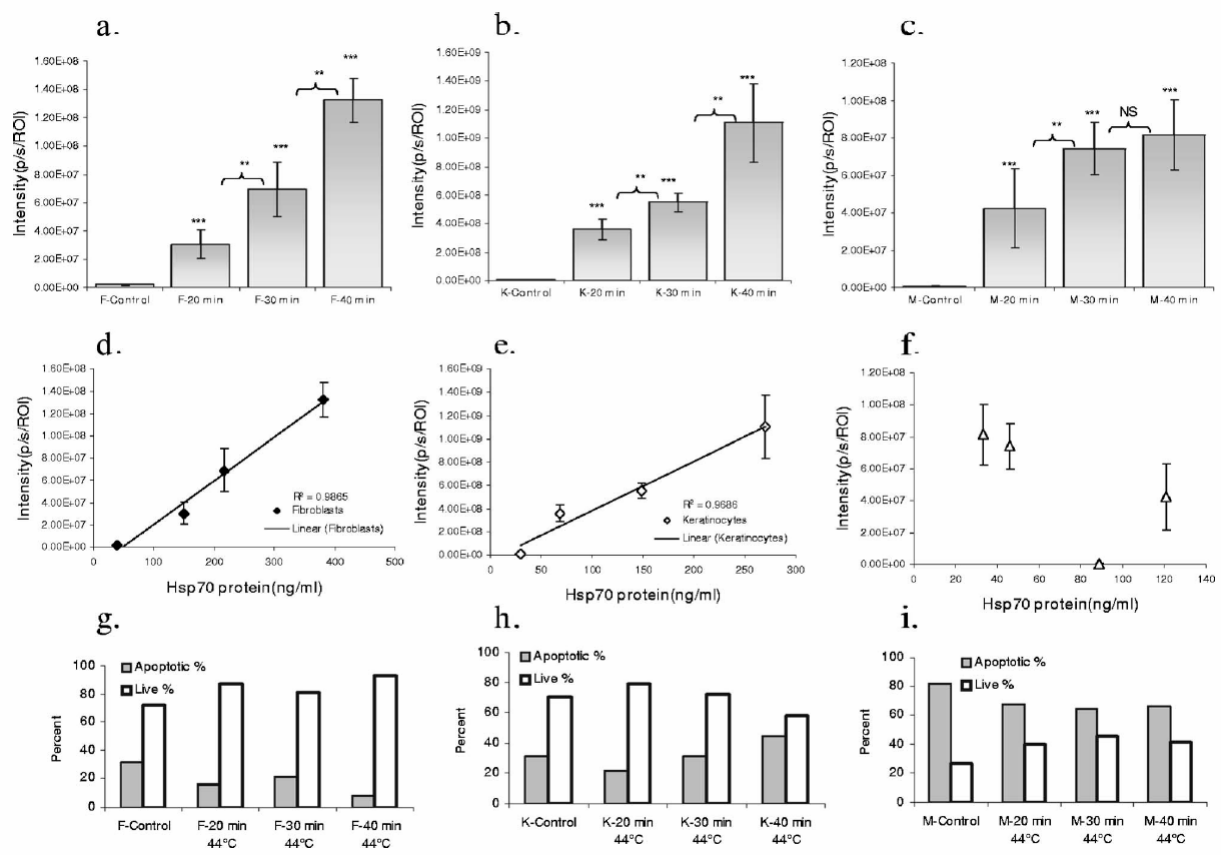

Figure 3.3. Characterizing the hsp70 response in NHDF, NHEK, and NHEM cell lines. Bioluminescence for NHDF **(a)**, NHEK **(b)**, and NHEM **(c)**; ELISA for NHDF **(d)**, NHEK **(e)**, and NHEM **(f)** and JC-1 apoptosis assay for NHDF **(g)**, NHEK **(h)**, and NHEM **(j)**. For all cell types, increasing the heating protocol results in increased bioluminescence. BL intensity and hsp70 protein levels are linearly correlated for the fibroblasts (R^2= 0.987) and keratinocytes (R^2= 0.969), but not for the NHEMs. More than 60% of the NHEMs showed early signs of apoptosis. For each cell type, 2.5 x 10^5 cells/well were plated in four 6-well plates. A control for each cell type consisted of cells that were transfected, but not heat shocked. All cells were transfected with Ad-hsp70 with an MOI of 1 for ~15 hrs and then heat shocked in a water bath at 44°C for 20, 30, and 40 minutes. Twelve hours after heat shock, 100 µl of D-luciferin (0.94 mg/ml) was added to each well 1 minute before the cells were imaged for bioluminescence. An ELISA for actual hsp70 protein levels was then conducted on each sample. The JC-1 expression (early apoptotic signal) for each sample group was analyzed using flow cytometry. The mean and standard deviations for bioluminescent intensities were statistically compared using a student's t-test (*** = P < 0.001, ** = P < 0.05, * = P < 0.01 and n=4).

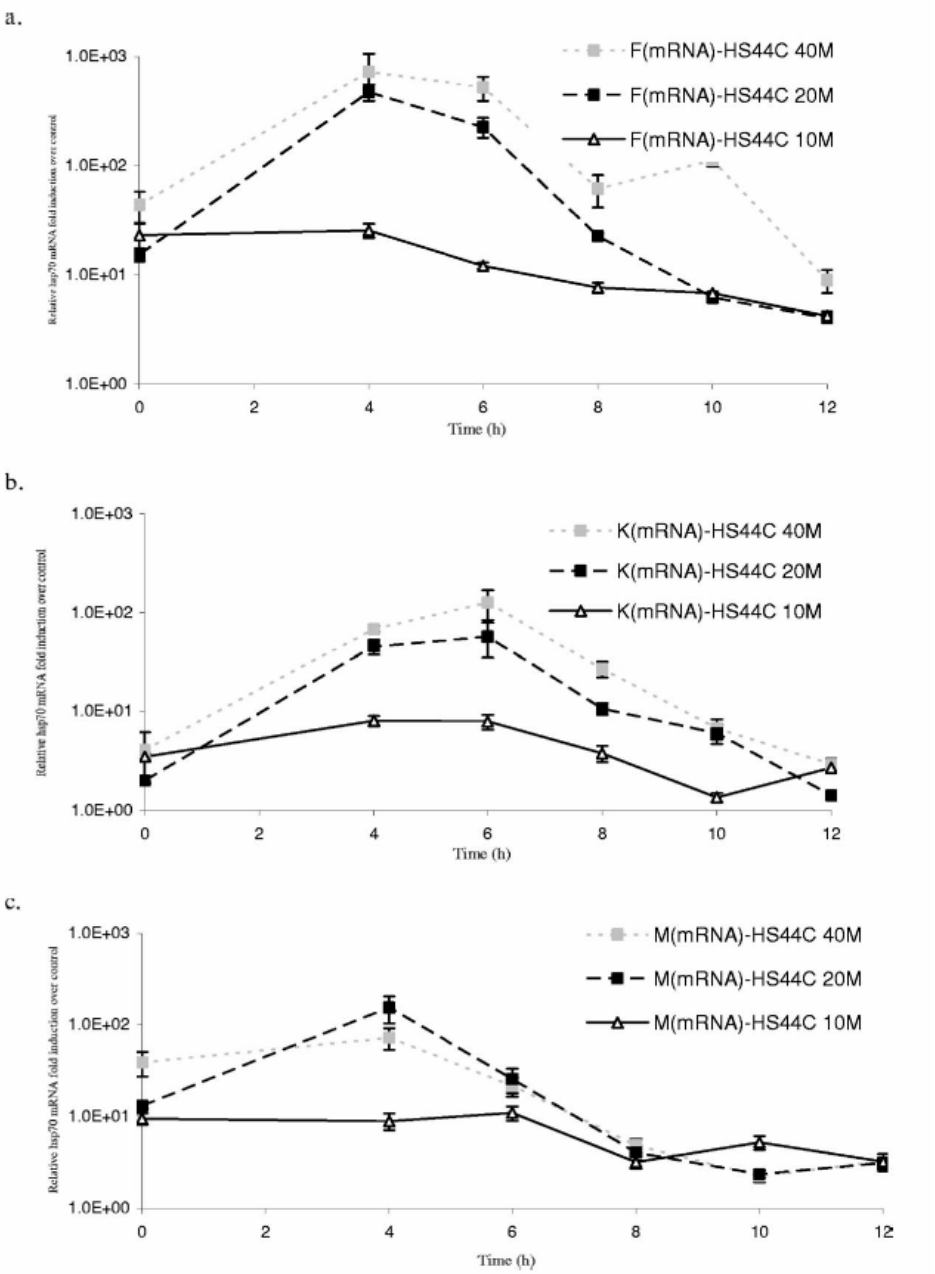

Figure 3.4. Measuring hsp70 mRNA expression with real-time RT-PCR in NHDFs (a), NHEKs **(b)**, and NHEMs **(c)**. 2.5 x 10^5 cells/well were plated in 6 well plates and transfected with Ad-hsp70-luc (MOI=1). The cells were then heat shocked in a water bath at 44°C for 10, 20, and 40 minutes. After heat shocking the total RNA was isolated, and 1 µg of RNA from each sample was reverse transcribed into single-stranded cDNA. Real-time, duplex PCR was performed to examine hsp70A1A (FAM), and the endogenous control, β-actin (VIC). Relative quantitation of mRNA levels was assessed using the comparative C_T method. The hsp70 mRNA expression from each sample was normalized to β-actin, and evaluated relative to controls. The final hsp70 mRNA expression was calculated as a fold induction compared to control.

3.4.4 Transfection is cell type dependent

To determine cell-type specific heat shock responses, the intracellular hsp70 protein levels and bioluminescent intensity were observed at various heating exposures. These tests were conducted to determine if the cell types exhibited different protein and luminescence levels for the same amount of delivered transgene. **Figure 3.5(a)** shows the measured protein levels (from ELISA assay) plotted versus increasing heat exposures. For all cell types, except the NHEMs, as the heating exposure is increased the hsp70 protein concentration increases. The NHDFs and NHEKs show similar hsp70 protein levels per given heating protocol, with the NHDF's expressing slightly higher, and statistically significant ($P<0.05$) more hsp70 than the NHEKs. In contrast, the NHEM's hsp70 protein concentration decreases as exposure to heat shock conditions increases.

For the three cell types, the bioluminescent intensity is plotted versus increasing heat exposures [**Figure 3.5(b)**]. Increasing the heating time increases the bioluminescent intensity for all cell types. However, the keratinocytes produce a factor of 9-10 times more bioluminescence for a given heating protocol compared to fibroblasts. For example, when comparing fibroblasts and keratinocytes heated for 30 minutes, the luminescent intensity of the keratinocytes is ~ 10 times higher than that produced by the fibroblasts, despite the fact that hsp70 protein levels, as well as the hsp70 mRNA levels in both cell types are similar.

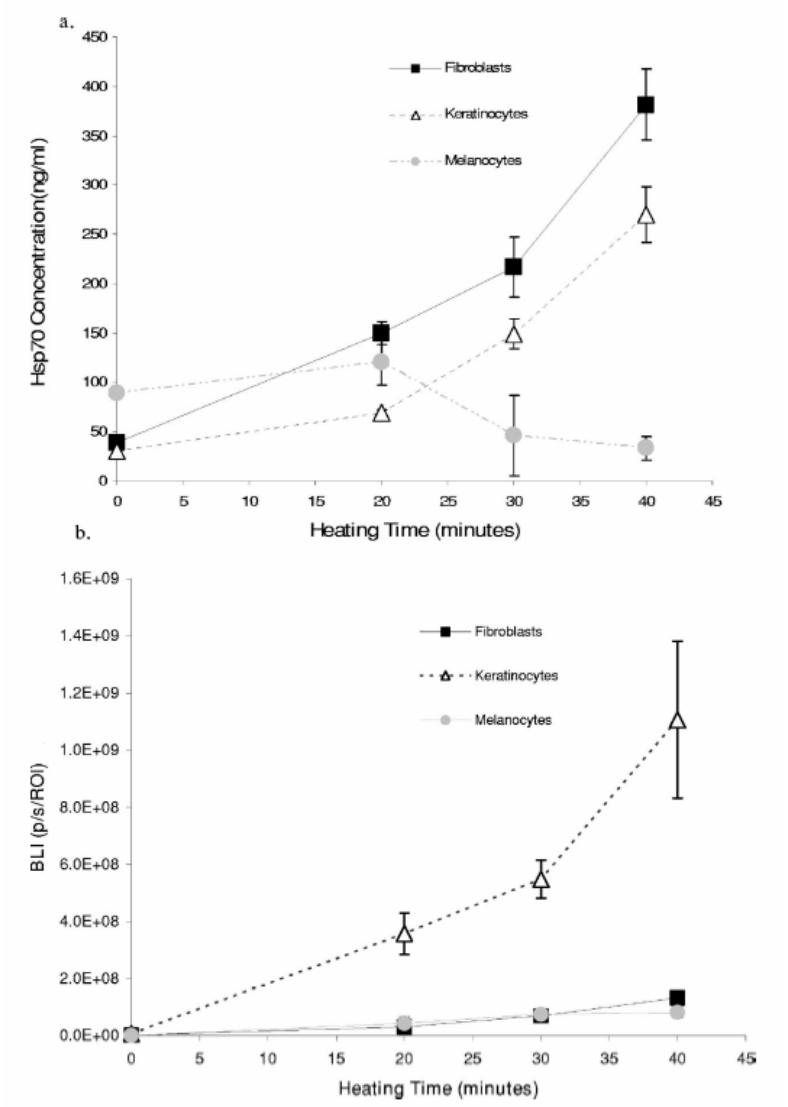

Figure 3.5. (a) Hsp70 protein concentration and (b) bioluminescent intensity plotted versus heating time. For all cell types, except the NHEMs, as the heating exposure is increased the hsp70 protein concentration increased. The NHEKs, produce one order of magnitude more bioluminescence for a given heating protocol compared to the NHDFs and NHEMs. For this experiment, each cell type was plated in four 6-well plates at a concentration of 2.5×10^5 cells/well. A control for each cell type consisted of cells that were transfected, but were not heat shocked. All cells were transfected with Ad-hsp70 with an MOI of 1 for ~15 hrs. The cells were then heat shocked in a water bath at 44°C for 20, 30, and 40 minutes. Twelve hours after heat shock, 0.94 mg/ml of D-luciferin (100 µl) was added to each well. The cells were then incubated for 1 minute prior to BLI. Immediately after the last imaging time point, an ELISA for the actual hsp70 protein levels was conducted on each sample.

3.4.5 Transient transfections

The expression of transgenes delivered by means of adenovirus has been reported to decrease over time due to extrusion of viral DNA and cell division, both of which lower the content of viral DNA per cell [28]. It should be noted that adenoviral transfection despite a number of advantages, including high transfection efficiency, is particularly vulnerable to this since the transgene remains episomal and does not integrate into the genomic DNA. In light of the fact that construction of a raft skin equivalent typically takes 10-14 days, we aimed to discern whether our system experiences a decrease in transgene expression, that would ultimately preclude us from transfecting our cells before constructing our raft cultures [21]. We seeded 9.6×10^4 NHDF cells/well in seven 6-well plates. At t = 0, all cells were transfected (Adv-hsp70-luc) and incubated for 15 hours. The media was changed for all plates, and at t = 15 hours the first plate was heated at 44°C for 40 minutes. Ten hours later (t = 25 hrs), the plate was imaged. The second plate was heated 24 hours after the first plate (t = 39 hrs) and imaged 10 hours later at (t = 49 hrs). This process was repeated for the remaining plates. The results are shown in **figure 3.6(a)** and demonstrate that transgene expression decreases over time. The bioluminescent intensity sharply increased from 0 to 49 hours and decreased from 49 to 145 hours. The third timepoint, 49 hours after transfection, had the highest bioluminescent intensity. From 49-72 hours, a 50 % decrease of bioluminescent signal was observed. At t =145 hours, the signal decreased to less than 17 % of the initial signal, 25 hours post infection.

From these results, we concluded that transfecting cells prior to construction of a raft (which take 10-14 days for maturation) is not feasible due to the fact that by the time the raft is fully stratified, very little transgene expression remains. For the remainder of the experiments we first constructed each raft (as described in the methods section) and

then ~15 hour prior to heat shock treatment, transfected the rafts *in situ* in the petri dish by applying 100 µl of adenovirus (MOI = 1) directly onto the rafts.

3.4.6 Homogeneously transfecting rafts in situ

In order to ensure that our *in situ* raft transfections were homogenous, rafts were assessed using standard BLI strategies and bioluminescent microscopy. For this study, a mature raft transfected with constitutively expressed Ad-CMV-luc (MOI=1) was imaged 48 hours after transfection, [**Figure 3.6(b)**]. The bioluminescent intensity is provided in **figures 3.6(c-d)**, and the homogeneity of the transfections was demonstrated laterally (X and Y) and in cross section (X and Z). The lateral image revealed that ~ 10^8 (p/s/cm^2/sr) was recorded across the entire raft. The bioluminescent microscopy image of the same raft showed that a constant ~ 2 x 10^6 (p/s/cm^2/sr) was emitted across the entire raft. The constant bioluminescent intensity across all directions in space indicated an effective homogenous transfection *in situ*.

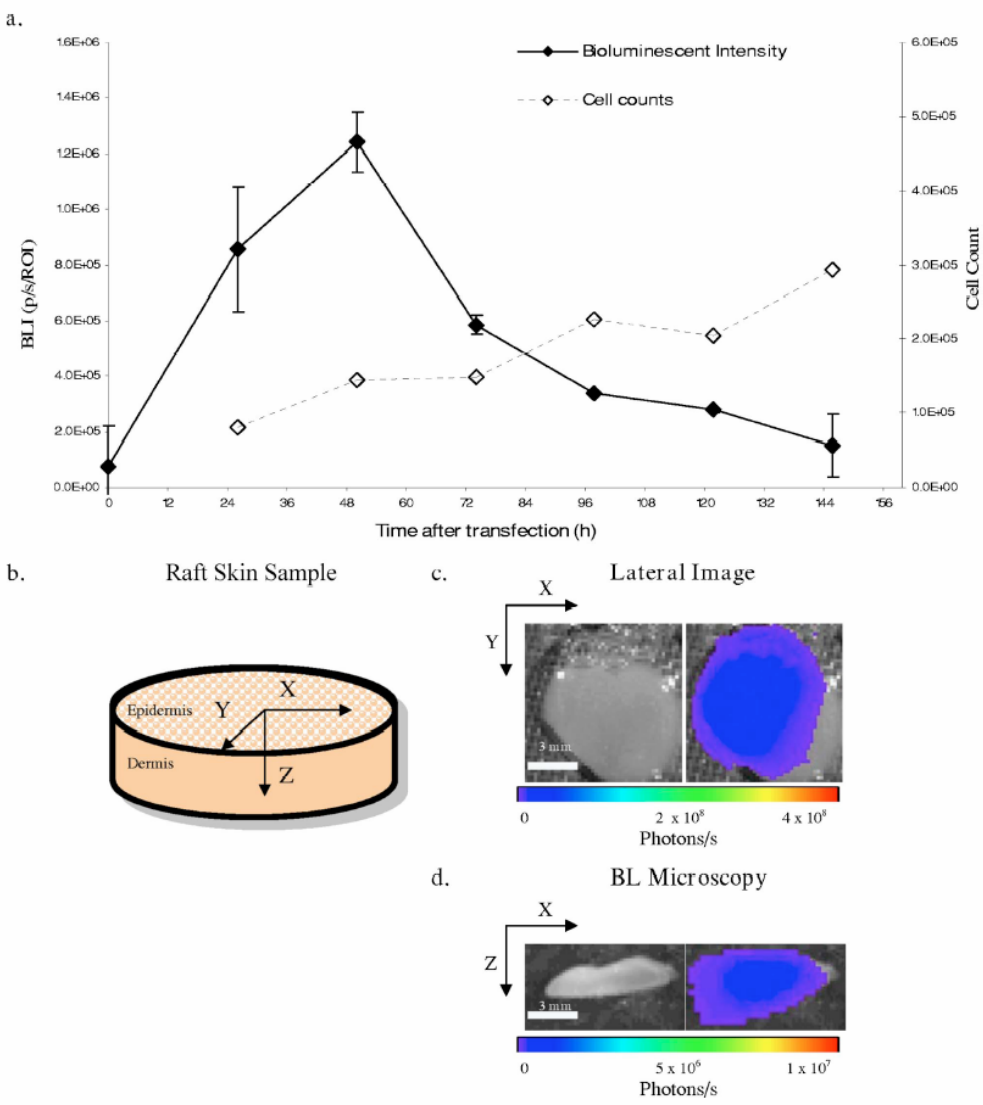

Figure 3.6. Transient transfection kinetics and the efficacy of *in situ* transfections. **(a)** Bioluminescent light intensity and cell counts for adenovirally (Ad-hsp70-luc) transfected normal human dermal fibroblasts are plotted versus time. The bioluminescence increased from 0 to 49 hours and plummeted from 49 to 145 hours. At time = -24 hrs, seven 6-well plates were seeded with NHDFs at a concentration of 9.6 x 10^4 cells per well. At time = 0, all 7 plates were then transfected with 20µl of adenovirus (titer = 1.3 X 10^7 PFU/ml, MOI = 1). After transfection at time=15 hrs, the first plate of NHDFs was heated in a water bath at 44°C for 40 minutes. At time=25 hrs, 100 µl of 0.94 mg/ml of luciferin was added 3 minutes prior to BLI. Plates 2, 3, 4, 5, 6, and 7 were heated at time=15, 39, 63, 87, 111, or 135 hrs respectively. The plates were then imaged at time=25, 49, 73, 97, 121, and 145 hours. Values are reported as mean +/-standard deviation; error bars smaller than symbol are not shown. **(b)**. Visual representation of raft imaging dimensions **(c)**. Lateral BL Image (IVIS 200) **(d)**. BL Microscopy Image (IVIS 200). In order to assess the transfection efficiency in three dimensions, independent on heating, the Ad-CMV-luc-IRES2-eGFP with a MOI of 1 was used to transfect the rafts.

3.4.7 Bioluminescence of laser irradiated rafts

The bioluminescent intensity is plotted versus time for the following raft samples: laser irradiated with 1.584 W/cm^2 for 60 seconds, water bath heated at 44°C for 20 minutes, and the negative control [**Figure 3.7(a)**]. **Figure 3.7(b)** shows the quantitative bioluminescence intensity plotted over time for all of the samples. The bioluminescence intensity is normalized by dividing the sample average bioluminescent intensity by the negative controls average bioluminescence intensity. This *fold-increase* value in bioluminescence illustrates the increase in bioluminescent signal that occurs due to heat inducing conditions. For all laser irradiated samples, the maximal expression occurred at t = 4-8 hours after exposure. Maximal expression occurred at t = 4 hours for the rafts heated in a water bath. The rafts exposed to a power of 1.0 Watt (1.584 W/cm^2) had the highest bioluminescent expression. Rafts irradiated with the highest irradiance (2.262 W/cm^2) were almost completely ablated, and hence had few viable cells left to contribute to the bioluminescence signal.

3.4.8 Co-localization of hsp70 on Laser Irradiated Raft Cultures

The immunohistochemistry of the raft cultures is shown in **Figure** 3.8(a-f). **Figure** 8(a) shows the hematoxylin and eosin stain (H & E) of a normal raft (20X), the epithelial and stromal layers can be clearly identified. **Figure 3.8(b)** shows the (H & E) of a raft that has been irradiated with the CO_2 laser (1.584 W/cm^2) at a 40X magnification. We observe that the epithelial layer is thermally damaged and appears to be coagulated. **Figure 3.8(c)** shows a Gomori trichrome stain, which stains for connective tissue, of the same raft as in 3.8(b), at a 20X magnification. The blank spot on the Gomori trichrome stain reveals that connective tissue is ablated due to the lasing process. **Figure** 3.8(d) shows the hsp70 antibody stain of a raft culture irradiated with the CO_2 laser for 1.584 W/cm^2 for 60 seconds (20X). A red dotted line drawn ~ 170 μm below the surface,

demarcates the region where maximal hsp70 expression is observed. The insert in **Figure 3.8(e)** shows **Figure 3.8(d)** at 100X magnification. **Figure** 3.8(f) shows the bioluminescent microscopy image. The laser irradiated rafts emit maximal bioluminescence 150-200 μm below the surface of the raft. This region of maximal expression corresponds to the same area denoted by the dotted red line in **Figure 3.8(d)** where maximum hsp70 protein levels were located.

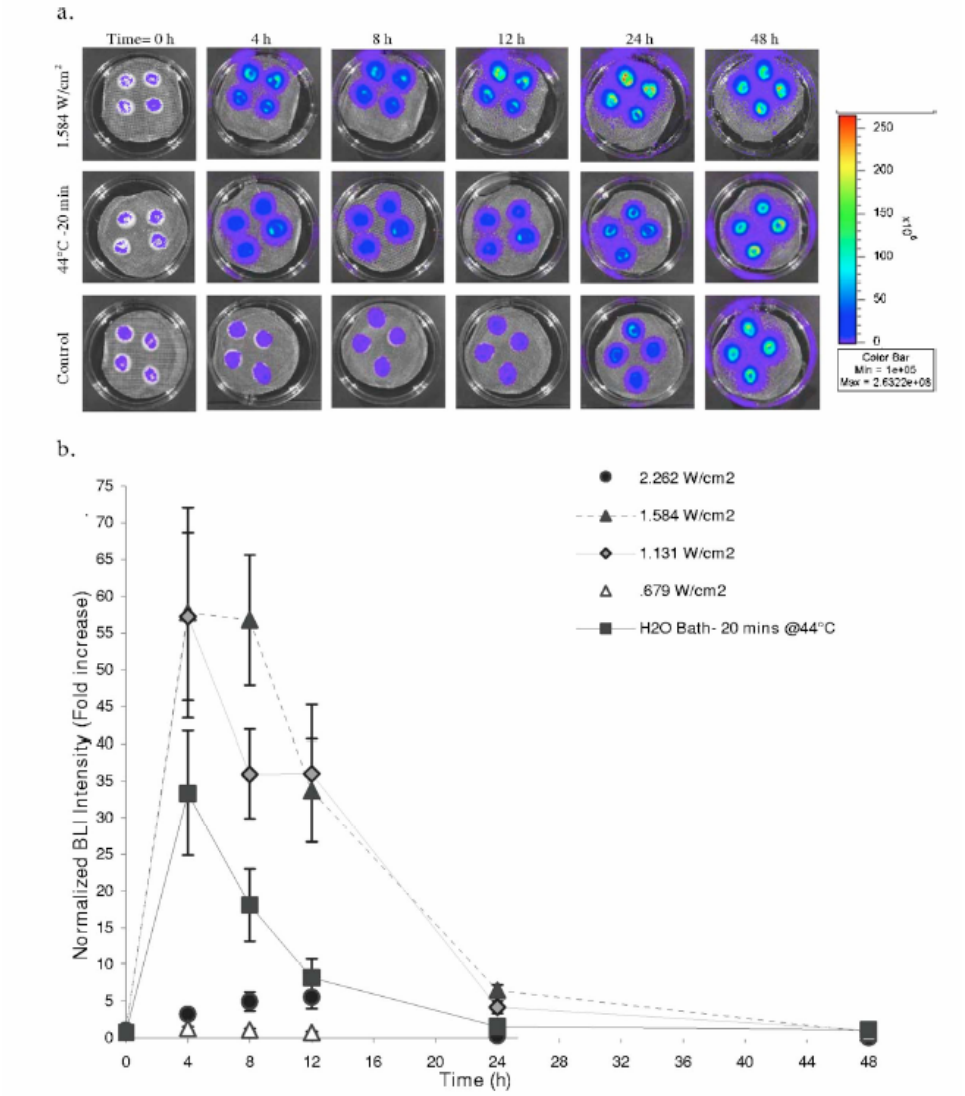

Figure. 3.7. **Visualizing the induction of hsp70 in organotypic raft cultures using BLI. (a).** The pseudocolor graphic of the bioluminescent signal of three samples of raft cultures: (1.584 W/cm^2, 0.7 W), 44 °C for 20 minutes, and unheated (negative) control is shown for visualization. The pseudocolor of the plot indicates where the highest light emission is present (red). At t= -15 hrs, 28 rafts were transfected with adenovirus (hsp70-luc) with MOI = 1. At t= 0 hrs, the rafts were exposed to heat shock inducing conditions via a water bath and CO_2 laser radiation. The 28 total rafts were treated in the following manner: two negative control groups (n=4), a positive control 44°C for 20 minutes (n=4), 0.679 W/cm^2 for 1 minute (n=4), 1.131 W/cm^2 for 1 minute (n=4), 1.584 W/cm^2 for 1 minute (n=4), and 2.262 W/cm^2 for 1 minute (n=4). After heat shock, 200 µl of 0.94 mg/ml of luciferin (Biosynth AG, Switzerland) was applied directly on top of each raft and allowed to diffuse within the raft for 1 minute before imaging. The samples were then imaged for 1 minute with the IVIS 100 system at t = 0, 4, 8, 12, 24, and 48 hrs. **(b)**. A plot of the intensity of the bioluminescent signal over time in adenovirally transfected raft cultures. For all samples, the maximal expression occurred at t = 4-8 hours after exposure. Maximal expression occurred at t = 4 hours for the rafts heated in a water bath. The rafts exposed to 0.72 Watts (1.584 W/cm^2) had the highest bioluminescence expression. The data normalized to the bioluminescent intensity of the control rafts (not heated), and the means and standard deviations were plotted. Values are reported as mean +/- SEM.

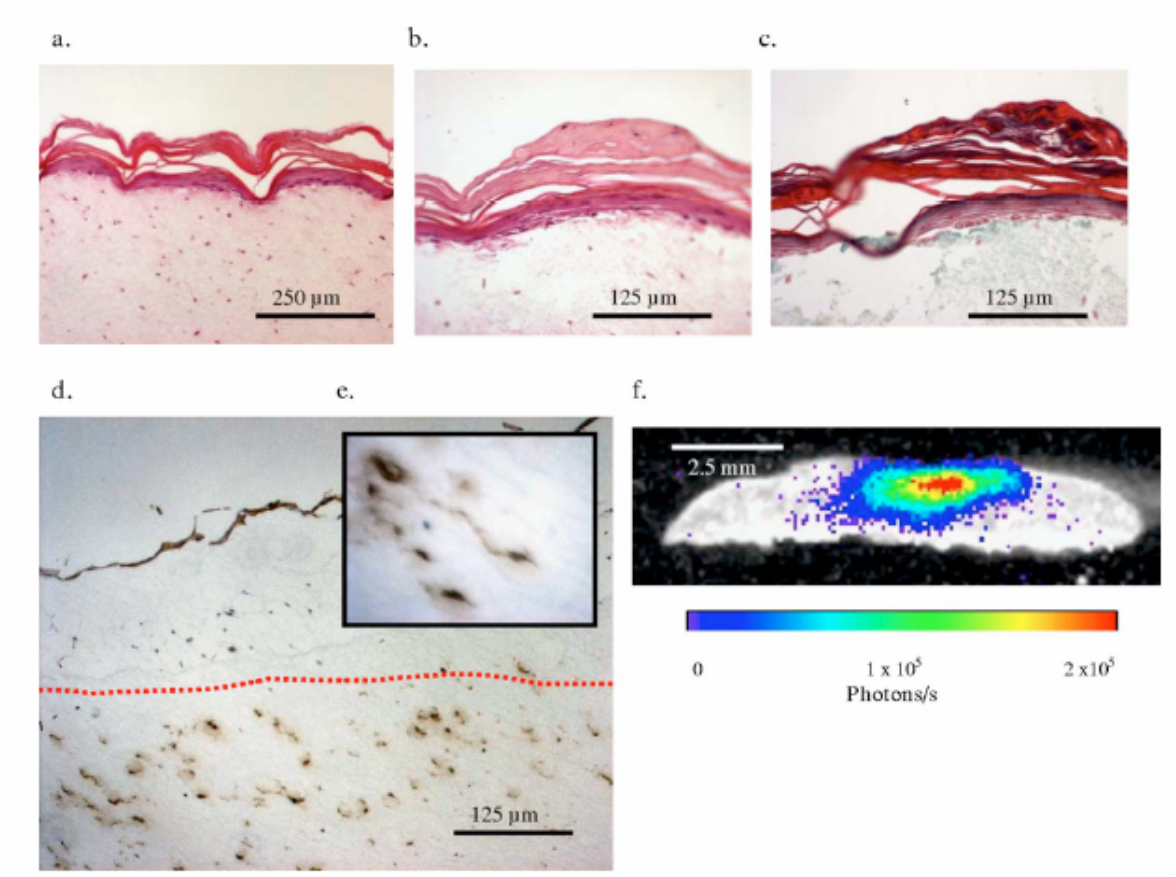

Figure 3.8. **Immunohistochemistry of raft cultures. (a)**. Hematoxylin and eosin stain of a normal raft at 10X magnification. **(b)**. Hematoxylin and eosin stain of a raft irradiated with a CO_2 laser for 1.584 W/cm^2 for 60 seconds (20X magnification, bar, 125 µm) **(c)**. Gomori trichrome (green) of the same raft in B. **(d)**. Hsp70 antibody staining of a laser irradiated raft taken at 20X magnification. **(e)**. 100X magnification of slide e. **(f)**. BL microscopy of 96 µm thick cross-section slice of laser damaged region of raft imaged with IVIS 200 (1.584 W/cm^2, 1.0 Watt, for 60 seconds).

3.5. Discussion

In this study, we demonstrated that an organotypic raft culture model equipped with a bioluminescent reporter gene, under control of a heat activated promoter (hsp70a1), can be used to monitor thermally modulated gene expression. This approach provides a model capable of non-invasively detecting subtle biochemical changes of biological processes demanding sequential analysis, as in laser-tissue damage studies. An inducible and highly characterized protein, hsp70, was tested in the context of this novel model. An adenovirus (hsp70a1-luc) equipped with the hsp70 promoter is shown to efficiently transfect differentiated raft cultures *in situ*, and permitted

hsp70 transcription to be monitored after laser radiation, [**Figure 3.7(a-b)**]. The results indicate that hsp70 expression is maximal 4-12 hours after laser radiation. These findings are consistent with previous studies on hsp70 expression [12, 13]. The results of the CO_2 laser radiated rafts reveal that a minimum radiation of 0.679 W/cm^2 was needed to activate the hsp70 response, and a maximum radiation of 2.262 W/cm^2 was associated with tissue ablation and significant cell death.

Although the utility of this model is shown in the context of a laser-tissue interaction, it is noteworthy to mention its potential utility beyond this application. This model can also be useful to study other dynamic bio-molecular relationships in skin, including aspects of wound repair. This model is quite versatile, since the skin constituents and its environment can be selected and controlled by the user. Thus, this approach can be used to create models for other tissues of interest. Also, the model can be further expanded to study other genes of interest, such as TGF-ß1 and TGF-ß3, which have been identified to a play a role in wound healing [5, 29, 30].

3.5.1 Characterizing the hsp70 response

3.5.1.1 Using BL as a surrogate marker for hsp70 mRNA and protein

After identifying that an MOI = 1 resulted in optimal transfection, the correlation between bioluminescence and hsp70 protein and mRNA levels was determined. The data shows that increasing the heat shock exposure causes increases in bioluminescent light intensity, native hsp70 protein levels, and hsp70 mRNA levels [**Figures 3.2, 3.3(d), 3.4(a-c)**]. Heat shocking the NHDFs in a water bath at 44°C for 10 minutes results in a 25-fold increase in bioluminescent intensity, and a 12-fold increase in hsp70 mRNA levels, compared to the controls. While exposing the NHDFs to 44°C for 20 and 40 minutes results in 100 and 130-fold increases in bioluminescent intensity, 4 and 8-fold increases in native hsp70 protein levels, and 200 and 500-fold increases in hsp70

mRNA expression, respectively [**Figures 3.2, 3.3(d), 3.4(a-c)**]. Plotting these bioluminescent intensities versus the hsp70 mRNA (data not shown) and native hsp70 protein levels (ELISA) [**Figure 3.3(d)**], generates correlation coefficients of (R^2 = 0.91) and (R^2 = 0.99), respectively. Thus, the data indicates that the absolute bioluminescence intensity is an accurate surrogate marker for actual hsp70 levels, as well as for relative hsp70 mRNA levels.

3.5.1.2 Temporal Features of hsp70 response

This study not only served to verify the hsp70 system was sensitive to minor temperature changes, but also revealed some significant temporal information about the hsp70 response. The most interesting temporal finding for the NHDFs is that the maximal hsp70 mRNA levels occurred 4-6 hours after heat shock, while maximal bioluminescent intensity occurred 6-12 hours after heat shock [**Figures 3.2(a), 3.4(a)**]. This 6-12 hour bioluminescent peak corresponds to the time of maximal hsp70 expression. This bioluminescent intensity peak agrees with previous literature where maximal expression was found to occur 6 to 12 hours after heat shock induction [13]. The observed decrease in hsp70 mRNA levels 8-12 hours post-heat shock may be the result of negative feedback regulation caused by increased hsp70 protein levels. This theory is corroborated by the increasing bioluminescence intensity between 8-12 hours. Moreover, the 2 hour delay between the hsp70 mRNA peak and bioluminescence intensity maximum is an indication of the time it takes to translate mRNA into nascent protein.

In previously published hsp70 studies, five zones of physiologic stress were demonstrated [12]. In this study, the real-time RT-PCR and the bioluminescent intensity data served to verify the crossing of one of these physiologic zones. O'Connell-Rodwell et al. characterized zone 3 where times/temperatures of stress resulted in delayed peaks of expression [12]. The data indicates that zone 3 was traversed as the cell's heat shock

exposure was prolonged from 44°C for 10 minutes to 44°C for 20 minutes. Crossing this boundary resulted in 4 times higher bioluminescent intensity, 20 times higher hsp70 mRNA levels, and a delayed hsp70 response [**Figure 3.2 and 3.4(a)**]. This delayed hsp70 response is clearly demonstrated using the bioluminescence data where the maximal bioluminescent intensity occurred at 4-6 hours for the 10 minute exposure, and at 12 hours for the 20 minute heat shock [**Figure 3.2**]. Adhering to the delayed hsp70 response theory, the hsp70 mRNA data demonstrated that the response to the 10 minute exposure was maximal 0-4 hours after heat shock, and the response to the 20 minute exposure peaked at 4-6 hours after heat shock [**Figure 3.4(a)**].

Overall, the results indicated that our system is sensitive to detect increases in heat shock. From the literature and previous studies, we expected the hsp70 response to behave as many other proteins do in that it would be upregulated after an initial stimulus and then decline after the stimulus had been removed [13]. When a cell is exposed to thermal stress (via heated water bath or laser radiation) a multitude of proteins denature. Protein denaturation is characterized by alterations in the secondary and tertiary structure of the molecule. The proteins loss of structure precipitates its loss of function. The presence of denatured proteins within the cell acts as a stimulus for the transcription of hsp70. Once sufficient hsp70 protein has been translated for repair, the additional hsp70 can bind the heat shock transcription factor, HSF1, which then downregulates hsp70 production. **Figure 3.2** shows that increasing the exposure time at 44°C from 20 to 40 minutes leads to an increase in hsp70 promoter activation and more bioluminescent light intensity. The NHDFs are incubated at 37°C thus when exposed to the 44°C water bath, they undergo a 7 °C temperature increase. This increase agrees with previous literature where moderate heat shock temperatures (39^{o}- 44^{o} C) were used to activate the heat shock response [31, 32]. As anticipated, increasing the duration of

heat shock exposure from 20 to 40 minutes enhanced the degree of activation of the heat shock response.

3.5.2 Transient transfections

The transient nature of adenoviral transfection precludes the transfection of cells prior to constructing skin equivalents [**Figure 3.6(a)**]. The data illustrates that a peak in bioluminescent intensity is observed 48 hours after transfection. The data reveals that the bioluminescent intensity is lower 24 hours after transfection than at 48 hours. This lower bioluminescent intensity could be due to an incubation time. In essence this could be related to the time required for the adenovirus to become familiar with the cell's transcriptional machinery. In previous adenovirus studies, Kugel identified an early transition in RNA polymerase II transcription, termed "escape commitment". Escape commitment occurs rapidly after initiation, and is characterized by sensitivity to competitor DNA [33]. This competitor DNA may be the reason for the cell's low bioluminescent intensity 24 hours post-transfection [33]. The cells may not be fully functioning as far as transgene expression goes until ~48 hours, thus explaining the maximum bioluminescent expression occurring 48 hours after transfection. From 49 to 73 hours, the bioluminescent signal decreases by 50% and by 145 hours only 17% of the initial signal remains [**Figure 3.6(a)**]. The transgene expression decreases due to cell proliferation and cell expulsion of adenoviral DNA. Since 72 hours after transfection half of the bioluminescent signal is present, this can be noted as an endpoint for adenovirus experimentation. Thus, the window for experimentation using this adenovirus ranges from 24-60 hours after transfection. This has important implications for the transfection of rafts. Since rafts take 10-12 days to fully develop, transfecting the cells before raft construction is not feasible. As a direct ramification of these findings, the rafts were transfected *in situ* after being fully developed. Of concern is the fact that

in situ transfection of intact rafts may not yield spatially homogeneous transfection. The results of the experiments conducted with the constitutively expressed Ad-CMV-luc-IRES2-eGFP, show a relatively uniform BL intensity (both radially and in cross-section) indicating that the *in situ* transfection of the rafts did not result in a gradient of transfection efficiency. Thus, *in situ* transfections are a suitable and effective method for transfecting intact rafts [**Figure 3.6(c-d)**].

3.5.3 Cell type dependent hsp70 expression

After characterizing the hsp70 response in fibroblasts, the hsp70 response was examined in the other cell populations present in skin raft cultures. MOI optimization experiments were conducted for the NHDFs, NHEKs, and NHEMs and the MOI = 1 was optimal for all cell lines (data not shown). The cells were transfected with the adenovirus (MOI= 1) and their heat shock response was observed. Interestingly, the various cell types illustrated different hsp70 response kinetics following heat shock induction [**Figure 3.5(a-b)**]. The variation between the cell lines could be due to differences in transfection efficiency or to differences in the cellular stress response. **Figures 3.5(a-b)** show that for the same MOI and heating exposure time, the NHEKs have a 10-fold increase in bioluminescent intensity while having slightly lower native hsp70 protein concentrations. The reason for this may be due to impaired adenovirus transfection. In previous studies, the receptor integrin α(V)β(3) was implicated in increased adenovirus transfection [34]. NHEKs may elicit a higher bioluminescent signal due to increased affinity to up-regulate the integrin α(V)β(3) receptor. Besides the integrin receptor, other studies have observed that hsp70 is constitutively expressed in normal skin cells, with the highest level being observed in the NHEKs [35, 36]. Thus, since the NHEKs have higher expression before induction, this increased basal activity may result in higher expression after heat shock induction.

NHEMs reacted much differently than the other cell lines. While increasing the duration of heat shock exposure, lead to an increase in bioluminescent intensity [**Figure 3.5(b)**], it resulted in decreased hsp70 protein levels for the NHEMs in contrast to the NHEKs and NHDFs [**Figure 3.5(a)**]. The flow cytometry results indicate that this may be due to significant apoptosis occurring in the NHEMs [**Figure 3.3(i)**]. Using flow cytometry, the JC-1 assay was employed to determine the cell's apoptotic activity. In **figures 3(g-i)**, the JC-1 assay data revealed that for the NHDFs and the NHEKs less than 30 % of the cells were apoptotic, regardless of the heating protocol, yet for the NHEMs > 60 % of the cells, including the unheated, negative controls, were apoptotic. These findings are not unusual, other studies on NHEMs have shown that NHEMs are notoriously difficult to culture and are prone to undergo apoptosis [37]. Due to the significant apoptotic activity of the NHEMs, they were not used in the construction of the raft cultures.

3.5.4 Efficacy and utility of organotypic raft culture model

Before laser radiation experiments were performed, transfected rafts were tested using a heated water bath. The rafts were moderately heat shocked at 44°C for 20 minutes. Bioluminescent signals indicated that the peak hsp70 expression occurred 4 hours post heat shock [**Figure 3.7(b)**]. This finding is consistent with previous cell culture studies, which also found that hsp70 expresses maximally 4 hours after exposure to heat shock [13]. The rafts exposed to moderate heat shock conditions, then decreased hsp70 expression after peak expression at 4 hours. This decreased expression was anticipated due to negative feedback provided by HSF1, and is consistent with previous findings [13].

3.5.5 Laser irradiation of raft cultures

In order to determine the powers for the laser radiation experiments, a thermocouple was utilized to determine the temperature increases at various powers (data not shown). Irradiances of 1.131 W/cm^2 for 60 seconds correlated to a maximum temperature rise of ~ 22 °C at 500 μm below the surface of the raft. This is significantly higher than the 7° C temperature rise in the water bath. However, given that protein denaturation is a rate process, it is expected that a reduction in the time of heating (60 seconds vs. 20 minutes) will permit higher tolerable temperature values while generating a similar response.

Our results show that in the raft models, increasing the laser irradiance results in increased normalized bioluminescent intensity [**Figure 3.7(b)**]. Thus, for increased irradiances an increased amount of hsp70 expression is observed. (Note: the irradiance of 2.262 W/cm^2 resulted in a significantly lower signal since greater than 70 % of the tissue was ablated.) The data also showed that when increasing the irradiance from 1.131 to 1.584 W/cm^2, a comparably bioluminescent peak is seen at 8 hours. This correlates with previous studies which indicate that under moderate heat shock conditions, a maximal hsp70 response is seen sooner after induction [13]. Since the higher irradiance would result in increased heat shock conditions, this prolonged hsp70 transcription is anticipated. The raft that is exposed to a higher irradiance would presumably undergo a more severe heat shock, resulting in more protein denaturation. This increases the amount of HSF1 that is freely available and results in increased promoter activation on the heat shock element (HSE). Another interesting finding is the raft exposed to the irradiance of 0.679 W/cm^2 experienced minimal damage, and likewise elicited minimal heat shock response. This irradiance sets the lower boundary on eliciting the heat shock response. Thus, a window for CO_2 laser radiation activation of the hsp70 response was found in this study to fall within the range of 0.679-2.262

W/cm^2 for 60 second exposures. In order to ensure that the bioluminescent intensity accurately reflected regions where hsp70 expression was most substantial, bioluminescent microscopy was compared with hsp70 antibody staining. The radiated rafts had the most substantial hsp70 antibody staining (the red line) at a depth greater than 150 μm [**Figure 3.8(d-e)**]. This region corresponded exactly to the region where the highest bioluminescence intensity (red region) was observed [**Figure 3.8(f)**]. These results confirmed our findings that our adenovirally transfected skin model is capable of accurately detecting subtle biochemical changes using BLI.

3.6. Conclusion

We present an organotypic raft model used in combination with bioluminescent imaging (BLI) techniques. The efficacy of the raft model was validated and characterized by investigating the role of heat shock protein 70 (hsp70) as a sensitive marker of thermal damage. Bioluminescent imaging indicated that peak hsp70 expression occurs 4-12 hours after exposure to thermal stress conditions. The findings suggest a minimum radiation of 0.679 W/cm^2 was needed to activate the hsp70 response, and a higher radiation of 2.262 W/cm^2 was associated with a severe reduction in hsp70 response due to tissue ablation. Real-time RT-PCR and ELISA protein assays confirmed that BLI was an accurate surrogate for actual hsp70 protein levels and hsp70 mRNA levels present in the cells. The temporal features of the real-time RT-PCR and BLI peak values were found to be useful in evaluating the crossing of physiological stress zones. Hsp70 expression was localized in the damaged tissue region using bioluminescent microscopy studies. These results indicate that quantitative BLI in engineered tissue equivalents provides a powerful model that enables longitudinal studies of gene expression.

3.7. Works cited

1. Thomsen, S., *Pathologic analysis of photothermal and photomechanical effects of laser-tissue interactions.* Photochem Photobiol, 1991. **53**(6): p. 825-35.
2. Thomsen, S., J.A. Pearce, and W.F. Cheong, *Changes in birefringence as markers of thermal damage in tissues.* IEEE Trans Biomed Eng, 1989. **36**(12): p. 1174-9.
3. Wu, N., et al., *Real-time visualization of MMP-13 promoter activity in transgenic mice.* Matrix Biol, 2002. **21**(2): p. 149-61.
4. Wu, N., E.D. Jansen, and J.M. Davidson, *Comparison of mouse matrix metalloproteinase 13 expression in free-electron laser and scalpel incisions during wound healing.* J Invest Dermatol, 2003. **121**(4): p. 926-32.
5. Capon, A. and S. Mordon, *Can thermal lasers promote skin wound healing?* Am J Clin Dermatol, 2003. **4**(1): p. 1-12.
6. Desmettre, T., C.A. Maurage, and S. Mordon, *Heat shock protein hyperexpression on chorioretinal layers after transpupillary thermotherapy.* Invest Ophthalmol Vis Sci, 2001. **42**(12): p. 2976-80.
7. Laxman, B., et al., *Noninvasive real-time imaging of apoptosis.* Proc Natl Acad Sci U S A, 2002. **99**(26): p. 16551-5.
8. Virostko, J., et al., *Factors influencing quantification of in vivo bioluminescence imaging: application to assessment of pancreatic islet transplants.* Mol Imaging, 2004. **3**(4): p. 333-42.
9. Contag, C.H. and M.H. Bachmann, *Advances in in vivo bioluminescence imaging of gene expression.* Annu Rev Biomed Eng, 2002. **4**: p. 235-60.
10. Shi, Y., et al., *CARP, a cardiac ankyrin repeat protein, is up-regulated during wound healing and induces angiogenesis in experimental granulation tissue.* Am J Pathol, 2005. **166**(1): p. 303-12.
11. Morimoto, R.I., P.E. Kroeger, and J.J. Cotto, *The transcriptional regulation of heat shock genes: a plethora of heat shock factors and regulatory conditions.* Exs, 1996. **77**: p. 139-63.
12. O'Connell-Rodwell, C.E., et al., *A genetic reporter of thermal stress defines physiologic zones over a defined temperature range.* Faseb J, 2004. **18**(2): p. 264-71.
13. Beckham, J.T., et al., *Assessment of cellular response to thermal laser injury through bioluminescence imaging of heat shock protein 70.* Photochem Photobiol, 2004. **79**(1): p. 76-85.
14. Pockley, A.G., *Heat shock proteins, inflammation, and cardiovascular disease.* Circulation, 2002. **105**(8): p. 1012-7.
15. Kao, B., et al., *Evaluation of cryogen spray cooling exposure on in vitro model human skin.* Lasers Surg Med, 2004. **34**(2): p. 146-54.
16. Kao, B., et al., *Novel model for evaluation of epidermal preservation and dermal collagen remodeling following photorejuvenation of human skin.* Lasers Surg Med, 2003. **32**(2): p. 115-9.
17. Capon, A., et al., *Laser assisted skin closure (LASC) by using a 815-nm diode-laser system accelerates and improves wound healing.* Lasers Surg Med, 2001. **28**(2): p. 168-75.
18. Davidson, J.M., *Animal models for wound repair.* Arch Dermatol Res, 1998. **290 Suppl**: p. S1-11.

19. Ross, E.V., et al., *Nonablative skin remodeling: selective dermal heating with a mid-infrared laser and contact cooling combination.* Lasers Surg Med, 2000. **26**(2): p. 186-95.
20. Bissell, M.J., H.G. Hall, and G. Parry, *How does the extracellular matrix direct gene expression?* J Theor Biol, 1982. **99**(1): p. 31-68.
21. Viehoever, A.R., et al., *Organotypic raft cultures as an effective in vitro tool for understanding Raman spectral analysis of tissue.* Photochem Photobiol, 2003. **78**(5): p. 517-24.
22. Asselineau, D., et al., *Human epidermis reconstructed by culture: is it "normal"?* J Invest Dermatol, 1986. **86**(2): p. 181-6.
23. Papadavid, E. and A. Katsambas, *Lasers for facial rejuvenation: a review.* Int J Dermatol, 2003. **42**(6): p. 480-7.
24. Ross, E.V., J.R. McKinlay, and R.R. Anderson, *Why does carbon dioxide resurfacing work? A review.* Arch Dermatol, 1999. **135**(4): p. 444-54.
25. Vogel, A. and V. Venugopalan, *Mechanisms of pulsed laser ablation of biological tissues.* Chem Rev, 2003. **103**(2): p. 577-644.
26. Hunt, C. and S. Calderwood, *Characterization and sequence of a mouse hsp70 gene and its expression in mouse cell lines.* Gene, 1990. **87**(2): p. 199-204.
27. Baggett, B., et al., *Thermostability of firefly luciferases affects efficiency of detection by in vivo bioluminescence.* Mol Imaging, 2004. **3**(4): p. 324-32.
28. Russell, R.A., et al., *Transient foamy virus vector production by adenovirus vectors.* Gene Ther, 2004. **11**(3): p. 310-6.
29. Martin, P., *Wound healing--aiming for perfect skin regeneration.* Science, 1997. **276**(5309): p. 75-81.
30. Whitby, D.J. and M.W. Ferguson, *Immunohistochemical localization of growth factors in fetal wound healing.* Dev Biol, 1991. **147**(1): p. 207-15.
31. Huang, L., N.F. Mivechi, and D. Moskophidis, *Insights into regulation and function of the major stress-induced hsp70 molecular chaperone in vivo: analysis of mice with targeted gene disruption of the hsp70.1 or hsp70.3 gene.* Mol Cell Biol, 2001. **21**(24): p. 8575-91.
32. Liu, A.Y., et al., *Transient cold shock induces the heat shock response upon recovery at 37 degrees C in human cells.* J Biol Chem, 1994. **269**(20): p. 14768-75.
33. Kugel, J.F. and J.A. Goodrich, *A kinetic model for the early steps of RNA synthesis by human RNA polymerase II.* J Biol Chem, 2000. **275**(51): p. 40483-91.
34. Pampori, N., et al., *Mechanisms and consequences of affinity modulation of integrin alpha(V)beta(3) detected with a novel patch-engineered monovalent ligand.* J Biol Chem, 1999. **274**(31): p. 21609-16.
35. Trautinger, F., et al., *Human keratinocytes in vivo and in vitro constitutively express the 72-kD heat shock protein.* J Invest Dermatol, 1993. **101**(3): p. 334-8.
36. Souil, E., et al., *Treatment with 815-nm diode laser induces long-lasting expression of 72-kDa heat shock protein in normal rat skin.* Br J Dermatol, 2001. **144**(2): p. 260-6.
37. Alanko, T., M. Rosenberg, and O. Saksela, *FGF expression allows nevus cells to survive in three-dimensional collagen gel under conditions that induce apoptosis in normal human melanocytes.* J Invest Dermatol, 1999. **113**(1): p. 111-6.

CHAPTER IV

OPTICAL IMAGING: A TOOL TO EXAMINE THERMAL DAMAGE IN LASER ABLATION

Gerald J. Wilmink[1], Susan R. Opalenik[2], Frederick R. Haselton[1], Mark Mackanos[4], Lillian Nanney[5], Christopher H. Contag[4], Jeffrey M. Davidson[2,3], E. Duco Jansen[1]

[1] Department of Biomedical Engineering, Vanderbilt University, Nashville, TN 37235

[2] Department of Pathology, Vanderbilt University, Nashville, TN 37235

[3] Department of Veterans Affairs Medical Center, Nashville, Tennessee 37212

[4] Department of Pediatrics, Microbiology & Immunology and Radiology, Stanford School of Medicine, Stanford, California, USA

[5] Departments of Plastic Surgery, Cell and Development Biology Research Laboratory, Vanderbilt School of Medicine, Nashville, Tennessee, USA 37212

This manuscript have been submitted for publication to the *Journal of Biomedical Optics* and is currently under review.

4.1. Abstract

Laser surgical ablation is achieved by selecting laser parameters that remove confined volumes of target tissue and cause minimal collateral damage. Pulsed mid-infrared wavelengths which preferentially target protein absorption bands have been shown to ablate tissue more efficiently than wavelengths targeting water absorption. However, the mechanism responsible for this finding has not been revealed. Previous investigations have used spectroscopic tools to analyze the tissue that is removed during ablation. In this report, we used optical imaging techniques to assess collateral damage after ablative surgery with a Free Electron Laser (FEL). Heat shock protein activation was used to assess tissue damage in a transgenic mouse strain, with the *hsp70* promoter driving luciferase and GFP expression. Luciferase and GFP activity were measured using bioluminescence and fluorescence imaging techniques. To examine the wavelength-dependence in the mid-IR, laser surgery was conducted on the *hsp70A1*-L2G mouse model using wavelengths: targeting protein (amide II band) absorption, 6.45 μm; targeting both protein (amide I band) and water, 6.10 μm; and targeting water's absorption peak, 2.94 μm. The magnitude of *hsp70* expression induced by the laser treatments was used as a quantitative sensitive marker of sub-lethal damage. Histological analyses were conducted to measure the depth of thermal damage. Bioluminescence data shows that for all wavelengths tested, the magnitude of *hsp70* expression was maximal 5 to 12 h after surgery, and increased using higher laser radiant exposures. Tissues treated using a wavelength of 6.45 μm had approximately 4x higher *hsp70* expression than tissues treated at 6.10 μm. Histology showed that the 2.94 μm wavelength damaged 2x and 3x deeper than the 6.45 μm and 6.10 μm, respectively. Lower radiant exposures were required for ablation with the 2.94 μm wavelength. Early indicators of wound repair showed that the 6.10 μm wavelength generated the least

amount of epidermal hyperplasia. Taken together, this report suggests that the 6.10 μm wavelength is a superior wavelength for laser ablation.

4.2. Introduction

The goal of surgical ablation is to remove a defined volume of biological tissue while causing minimal damage to the remaining tissue. Lasers are well suited for surgical ablation because they can be controlled to precisely and selectively remove tissue. Laser ablation procedures are nearly ubiquitous in the fields of dermatology, ophthalmology, and neurosurgery. To achieve surgical success the laser's operating parameters must be carefully selected. For the most part, surgical performance is governed by the selection of the laser's wavelength, radiant exposure, and pulse structure (1-3). Wavelengths that exhibit stronger tissue absorption can confine energy in smaller volumes and are considered the most efficient ablation wavelengths. Infrared (IR) wavelengths are highly absorbed by biological tissues, and as a result laser sources in the IR spectra are considered excellent ablation lasers.

The Vanderbilt Mark-III free electron laser (FEL) is a pulsed IR laser that is tunable between 2 and 10 μm. The FEL's wavelength tunability permits examination of the effects of wavelength, radiant exposure, and pulse structure on pulsed tissue ablation (1, 2). Edwards' studies with the FEL operating at 6.45 μm in wavelength demonstrated minimal collateral damage and high ablation yields in many biological tissues (4). This discovery provided the impetus for FEL related biomedical research and for the development of FEL clinical applications (1, 5-8). Although the FEL has been clinically successful, current research efforts are designed to examine the bio-molecular effects of ablation. The long-term goal of these efforts is to provide a basis for a more

rational selection of laser parameters and to the overall improvement of ablation procedures.

Given that the 6.45 μm wavelength is not the strongest absorbing wavelength in the IR spectra, its superiority over other IR wavelengths is surprising. As a result, many studies have been conducted to elucidate the mechanisms governing IR ablation (1, 2). In the mid-IR spectrum (2.94 μm to 8 μm), biological tissues absorb most strongly at the water absorption bands. Since biological tissue consists primarily of water (65-70%) which has peak absorptions at 2.94 and 6.10 μm, it would have been expected that these wavelengths would be superior ablative wavelengths compared to 6.45 μm.

Investigators have suggested that an underlying competition exists between the denaturation of proteins and the vaporization of water, and this competition is markedly influenced by the laser wavelength (9). Where laser wavelengths that directly target protein absorption disrupt the structural integrity of the tissue matrix to a larger degree, leading to less violent removals of tissue and less collateral damage (4). In contrast, wavelengths that target water absorption favor the vaporization of water, and this process triggers more violent removals of tissue and greater collateral damage. Recently, spectroscopic and electrophoretic tools were used to closely investigate the structural failure of proteins (1, 10). In contrast to these investigations, which examine the tissue droplets and plumes that are ejected during ablation (1, 10, 11), in the experiments reported in this study here we examine the bio-molecular effects that occur in cells that remain after ablation. Since the cellular response dictates the ultimate fate of the remaining tissue, it would be advantageous to assess this tissue for collateral damage.

When a cell's temperature rises 5-6 °C labile intracellular proteins begin to denature (12-14). Denatured proteins do not function properly and increase cell stress. A cellular response mechanism is triggered which activates the transcription of various

molecular chaperones; one such group is the Heat shock proteins (Hsps). Hsps are sensitive indicators of cellular stress with the most sensitive member being that of *hsp70* (14). Thermal stress causes the transcriptional activation of the 70 kDa heat shock protein gene (*hsp70*) and leads to ensuing protein production (*hsp70*). We previously demonstrated in engineered skin equivalents, that reporter gene systems which use the *hsp70A1* promoter to drive the expression of luciferase can be used as a surrogate marker for *hsp70* gene activation (13-15). In this work, we used the *hsp70A1-luc-GFP* transgene in a mouse model, hereafter referred to as *hsp70A1-L2G.*

The main goal for this report is to use the *hsp70A1-L2G* mouse model and optical imaging techniques to quantitatively and sequentially evaluate thermal damage in surgical ablation procedures. This study is novel because it provides a sensitive real-time readout of the magnitude of intracellular damage. Specifically, we examine the role that mid-IR laser wavelengths have on the degree of intracellular protein damage in mouse dermal tissue. Using the FEL at various radiant exposures, we assess the performance of wavelengths with primarily water absorption (λ = 2.94 μm), with water and protein (amide I band) absorption (λ = 6.10 μm), and with mostly protein (amide II band) absorption (λ=6.45 μm).

In the first set of experiments we use optical imaging techniques to visualize and quantify *hsp70* promoter activity in laser-treated mouse dorsum, with emphasis on investigating the effect that laser wavelength and radiant exposure have on the magnitude of *hsp70* expression. In the second set of experiments we use traditional histological methods to measure the actual depth of tissue injury for each laser treatment. The last set of experiments we use immunohistochemical methods to examine the early wound repair of laser-treated tissues.

In this report, we investigate the effects that wavelength and radiant exposure have on surgical ablation using *hsp70* expression as a surrogate marker of sub-lethal

damage. The main hypotheses are the following: 1. If in *in vitro* assays *hsp70* gene activation exhibits a dose-dependency, then in an *in vivo* animal model *hsp70* expression should increase with increasing laser radiant exposure 2. If the depth of laser light penetration depends on the wavelength dependent optical properties of tissues, then for laser wavelengths with deeper optical penetration depth (δ), the magnitude of *hsp70* expression should be higher. Using *hsp70* expression as a marker for cellular damage we sought to address the *in vivo* roles of *hsp70* in early wound repair. The specific goals of this study are: 1) examine the spatio-temporal limits of the *hsp70A1-L2G* model using optical imaging methods, 2) use model to investigate the effects that wavelength and radiant exposure have on *hsp70* expression, and 3) examine the relationship between *hsp70* expression and traditional damage markers.

4.3. Materials and Methods

4.3.1 Animal model

All experiments were conducted in accordance with guidelines specified by the Institutional Animal Care and Use Committee (IACUC) at Vanderbilt University. Transgenic mice in which the heat shock protein 70 (*hsp70*) promoter can drive the expression of luciferase and eGFP reporter genes were developed by the Contag laboratory (Stanford University). A detailed description on these *hsp70*-luc-GFP L2G transgenic mice has been detailed previously by Dr. Mackanos (Molecular Imaging, under review). Briefly, these mice have a FVB background and contain a *hsp70* cassette (FVB.*hsp70*-luc_2A-GFP). The cassette is as follows: the murine *hsp70*A1 promoter (Genbank accession number M76613) was attached to the luciferase coding sequence from the pGL3-Basic plasmid (Promega, Madison, WI) as described previously and fused, in frame, to the ORF of the enhanced green fluorescent protein

(eGFP; Clontech, Palo Alto, CA) with 54 base pairs (bp) of the FMDV 2A sequence followed by 24 bp of polylinker (13). The (eGFP) vector and luciferase (luc) vector are located downstream from the *hsp70* promoter. Whenever *hsp70* mRNA transcription occurs, these bicistronic reporters are also transcribed and translated. As a result, the GFP and luciferase gene products emit light which can be used as a surrogate marker for *hsp70* gene activity levels, as previously shown (15). Bioluminescent imaging and genotyping methods were used to screen the offspring produced by founder pairs. Founder pairs that generated the most consistent offspring were selected to produce all of the mice used in this experiment. In brief, offspring that generated the highest and most consistent baseline BL signal and luc cDNA signals were selected (data not shown). PCR analysis of the cDNA from offspring tails were conducted as previously described (15). Two days before FEL experiments, mice were anesthetized with isoflurane in a vaporizer (Ohmeda, BOC Health Care, UK). After the mice were sedated, a rectangular area of the dorsal fur was removed with a clipper, and small hairs were removed using depilatory cream. The mice were then returned to animal care for 2 days.

4.3.2 Free Electron Laser (FEL) operating parameters

The FEL was used to make four 6.5 mm square lesions on the dorsum of each mouse. Wounds were separated by 4 mm. The laser was operated at 30 Hz at one of the following wavelengths: 2.94, 6.1, or 6.45 μm. Energy was delivered in 5 μs macropulses with pulse energies of 2, 4, 6, 8, 10, 12.5, 15, 20, 22.5, and 25 +/- 0.5 mJ. At each wavelength the collimated beam was focused to a 200 μm gaussian beam radius in a 50-cm focal length CaF_2 lens resulting in radiant exposures of 1.59, 3.17, 4.76, 6.35, 7.96, 9.95, 11.94, 15.91, 17.91, and 19.89 J/cm^2. A standard knife edge method was conducted to measure the spot size of the Gaussian (TEM_{00}) laser beam at surface of

the mouse dorsum. This method was crucial to ensure that a consistent ω_r = 200 μm +/- 10 μm focal area was achieved for each experiment.

In order to ensure that mice were positioned in the focal plane at exactly a 48 cm distance from the lens, an optical positioning system was developed. This positioning system contained a 460A Series high performance integrated ball bearing linear stage and a black circular mouse holding plate (20 cm diameter). A separate model 200 platform was used to hold the energy meter, and the pulse energies were recorded using an EnergyMax 400A (Molectron, Portland OR, 97724). A visual representation of the setup was constructed using SolidWorks® software (SolidWorks, Concord MA) and is provided in **Figure 4.1(a)**. The mice were positioned on the plate in preparation for laser injury and were adjusted in the x, y, and z directions using micrometers ± 10 μm intervals.

The laser beam was delivered with a Computer Assisted Surgical Technique (CAST) system (16). In brief, the CAST system consists of a computer controlled galvanometer-driven mirror which is built into the line of the FEL and allows a user to scan the focused laser beam over the target tissue. The pattern for the lesions in this study was 6.5 mm^2. A National Instruments Labview program was used with the following parameters: 695 points, scale 0.2, and a step of 0.25. Wound were generated by making 1 pass, each pass consisting of 15 sweeps, and each sweep was separated by 460 μm. Each sweep took 1.33 seconds with a total exposure time of 20 s [**Figure 4.2(b)**]. Note: pilot studies indicated slight variations in *hsp70* promoter activity between the cephalic and caudal focal areas on the dorsum. Therefore, the anatomical locations for the laser treatment were randomized.

In order to ensure that each transgenic mouse exhibited comparable sensitivity to heat exposure, a positive control was used on each mouse. A set of custom designed brass rods with a surface area of 19.625 mm^2, c = 0.377 kj/kg K, mass of 37.4 grams,

and a length of 24 cm were heated to 70 °C in a heated water bath. Twenty four hours prior to each FEL experiment a rod was applied for 15 seconds on the posterior dorsum of each mouse [**Figure 4.1(b)**]. Mice exhibiting bioluminescent intensities ranging from 3 to 6 X 10^7 p/s were considered suitable for experimentation (data not shown).

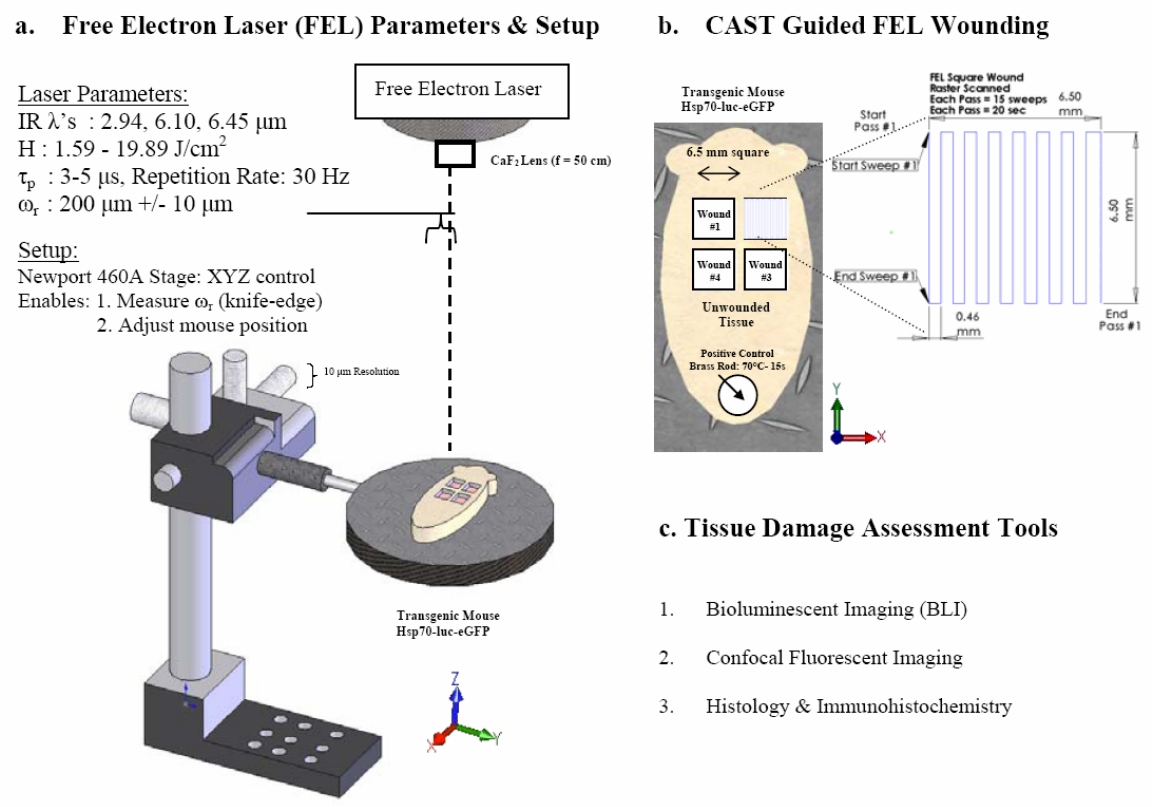

Figure 4.1. Schematic representation of experimental methodology.
(a) Free electron laser (FEL) optical positioning setup and parameters (λ: 2.94, 6.10, 6.45 µm; H: 1.59, 3.17, 4.76, 6.35, 7.96, 9.95, 11.94, 15.92, 17.91, 19.89 J/cm^2; ω_r : 200 µm +/- 10 µm; τ_p : 3-5 µs, Repetition Rate: 30 Hz. A 10 week old *hsp70A1*-L2G transgenic mouse was placed on a 20 cm diameter holding plate. The holding plate position was adjusted with a Newport 390A Series high performance linear stage (micrometers have 10µm adjustment resolution in xyz directions (Schematic constructed with SolidWorks® software).
(b) Computer Assisted Surgical Technique (CAST) Guided FEL Wounding. The CAST system was used to deliver the focused laser beam in a square 6.5 mm^2 pattern over the target mouse. Wounds were made using 1 pass, 20s/pass. Four FEL lesions were made on each mouse. Each mouse had an internal positive control made using a 70 °C brass rod applied on the dorsal skin 1 cm above the tail for 15 s. The negative control was a section of untreated dorsum.
(c) Tissue Damage Assessment Tools. 1. Bioluminescent imaging (BLI) 2. Fluorescence Imaging 3. Histology and Immunohistochemistry

4.3.3 Bioluminescent imaging (BLI)

Female *hsp70A1-L2G* mice were used for a wound healing study. After the FEL incisions were made, the mice were imaged using the Xenogen IVIS 200. Fifteen minutes before each imaging session the mice were intraperitoneally injected (27 gauge syringe) with 15 mg/ml of luciferin substrate. Based on our previous BLI studies, the half life of the bioluminescent reaction was determined to occur at approximately 37 minutes after injection (Data not provided). For bioavailability purposes, the volume of substrate injected was determined based on the mass of the mice (10 µL/gram, 20 gram mouse = 200 µL injection). Mice were imaged at 0, 2, 5, 7, 9, 12, 15, 17, 21, 24, 36, and 48 hours after the start of the FEL procedure. Bioluminescence images were integrated over 30 seconds and were imaged at a FOV A with High resolution binning.

4.3.4 Bioluminescent imaging system

Luciferase induced bioluminescent light emission activity was measured at various time points following heat shock using an IVIS 200 bioluminescent imaging system (Xenogen, Alameda, CA). Mice were placed in the imaging chamber on a heated 37 °C stage and imaged. Both photographic and bioluminescent images were acquired. Each bioluminescent image was then superimposed over its corresponding photographic image. Bioluminescent data are represented with a false color scheme representing the regions of varying light emission. Light emission from the specified regions of interest (ROIs) were quantified in units of total number of photons emitted/second (p/s) using LivingImage analysis software (v2.12,Xenogen).

To accurately measure the *hsp70* expression levels in the transgenic mice to variability factors were addressed: a) baseline variation between mice in the same group (intra-group mouse to mouse variability) b) baseline unwounded background BL expression for mice in different groups (intergroup mouse-to-mouse variability). To

account for these variances the BL intensity for each wound was and divided by the average BL intensity for the unwounded mouse dorsum in that study. This fold-induction value indicates the magnitude of *hsp70* expression generated by the laser treatment.

4.3.5 Histology

A subset of mouse skins were harvested for histological and RNA analysis. Tissues were examined for cell morphology, degree of damage, and early wound repair response. Skin samples were collected and evaluated 12, 48, and 120 h post surgery. A Olympus Vanox-T AHZ microscope equipped with a Pixera Pro 600 ES camera was used to image the slides. For the RNA processing, a dermal biopsy punch was used to extract a 4 mm diameter section of the wound (Miltex, York PA, 17402). Tissue was preserved in RNAlater and the RNA was extracted as per manufacterer's instructions (Ambion, Inc.). For standard histology, a section of the laser-treated tissue was fixed in formalin and stained using H&E and Gomori (green) stains (15). The depth of damage was evaluated using a change in tincture in the Gomori's trichrome stains and was measured using the Image Pro Plus software at a standardized magnification. The magnitude of epidermal hyperplasia was also measured from tissues evaluated at 120 h post surgery. A portion of each wound was prepared for frozen sectioning in Optical Cutting Temperature (OCT) media, flash frozen in liquid nitrogen and stored at -70 °C. These tissue sections were used for fluorescence imaging of eGFP.

4.3.6 Confocal fluorescence imaging of hsp70-eGFP

Fluorescence imaging of the second bicistronic reporter gene, eGFP, was conducted at a depth that allowed for resolution of *hsp70* expression in the z direction. Frozen tissue samples were sectioned with a microtome (10 μm thickness) and imaged using the 5X, 0.15-numerical aperture Plan-Neofluar objective lens of a Zeiss LSM510

inverted confocal microscope. Samples were excited using a 488 nm Argon laser and the *hsp70*-associated eGFP fluorescence was detected using a 505-550 nm bandpass filter. Metamorph was used quantify signals using 26 boxes, 1300 μm^2 area, each box had depth of 13 μm. Cell counts were measured using Image Pro Plus. Cell counts were measured in areas of 600 μm^2 using 60 boxes, and were preformed in triplicate. The fluorescent integrated intensity was divided by the cell number for normalization.

4.4. Results

4.4.1 Visualization of hsp70 promoter activity in laser-treated tissue

Our results indicate that laser-treated mouse dorsal skin has roughly 8 times higher bioluminescence than untreated skin. This study verifies that bioluminescent imaging techniques can be used to visualize hsp70 promoter activity in laser-treated mice. **Figure 4.2** is a sample BLI time-course study of skin treated with the FEL using a wavelength of 6.10 μm and radiant exposures of 7.96, 11.94, 15.92, and 19.89 J/cm^2. Prior to surgery, the untreated dorsal skin shows low background bioluminescent intensities, with only minor traces of signal on the skin over the spine of the mouse [**Figure 4.2(a)**]. Five hours after surgery, significant increases in BL intensities are observed for all laser treatments [**Figure 4.2(b)**]. The 19.89 and 15.92 J/cm^2 exposures show significantly higher expression than the lower exposures of 7.96 and 11.94 J/cm^2. For all wounds, the bioluminescent intensities progressively increase after surgery, and show maximum intensities 12 h post surgery [**Figure 4.2(c) and Figure 4.2(d)**]. The 19.89 J/cm^2 and 15.92 J/cm^2 treatments show false colors ranging from a blue to red color, corresponding to photon counts of 1.5×10^6 p/s and 4×10^6 p/s, respectively. In contrast, treatments using lower radiant exposures show lighter color intensities (light

green). **Figure 4.2** demonstrates that the spatio-temporal variations in *hsp70* expression can be visualized using bioluminescent imaging techniques. Furthermore, the methods can differentiate differences in *hsp70* expression within a single wound making margin detection possible. Also, the marked variation of bioluminescence intensity between laser treatments suggests that BLI techniques are sensitive enough to compare treatments among different radiant exposures.

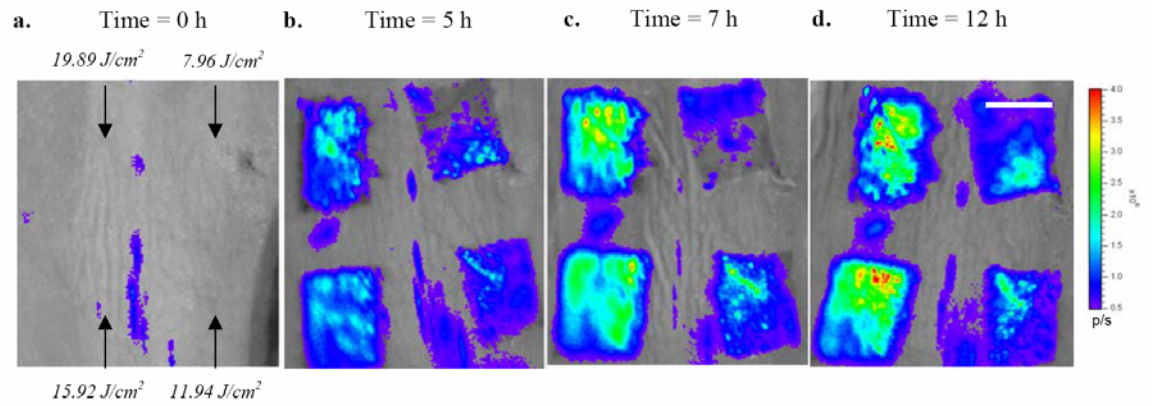

Figure 4.2. Visualization of *hsp70* promoter activity on laser-treated mouse skin
(a-d) Bioluminescent imaging time course of a FEL wounded *hsp70*-luc mouse dermis. **(a)** Time = 0 h **(b)** Time = 5 h post surgery. **(c)** Time = 7 h post surgery. **(d)** Time = 12 h post surgery. The FEL parameters used to make the wounds were the following: λ = 6.10 μm, ω_r = 200 μm, τ_p = 3-5 μs, 30 Hz, H: 7.96, 11.94, 15.92, and 19.89 J/cm^2. The pseudocolor of the plot ranges from 0.5 to 4 X 10^6 p/s, whereby high light emission regions are colored red and low light emission regions are colored violet. Spatial temporal variations in *hsp70* expression can be visualized with BLI techniques. Compared to untreated tissue, laser-treated tissue has roughly 8x higher bioluminescence intensities. *hsp70* expression is higher in the middle of each wound making wound margin detection possible. The white scale bar is 6 mm.

4.4.2 Quantification of bioluminescence

The quantitative BLI data show that the magnitude of *hsp70* expression exhibits dose-dependency and increases with increases in laser radiant exposure. To examine the wavelength-dependence in the mid-IR, laser surgery was conducted on the *hsp70A1*-L2G mouse model using the following wavelengths: targeting protein (amide II band) absorption, 6.45 μm; targeting both protein (amide I band) and water, 6.10 μm; and targeting water's absorption peak, 2.94 μm. Bioluminescent imaging techniques were used to quantify the *hsp70* fold induction levels. **Figures 4.3(a-c)** show the quantitative bioluminescence intensity plotted over time for each wavelength and radiant exposures tested. For all samples, the maximal *hsp70* expression occurred 5-12 h post surgery. A wavelength of 6.45 μm shows bi-phasic peak *hsp70* expression, with maxima occurring ~12 and 24 hours after laser treatment [**Figure 4.3(a)**]. Increases in radiant exposures from 7.96 to 19.89 J/cm^2 show *hsp70* fold-inductions of 12 to 28-fold. All laser treatments at a wavelength of 6.10 μm have peak *hsp70* expression 12 h after surgery [**Figure 4.3(b)**]. A maximum *hsp70* fold-induction of 18x is achieved using a radiant exposure of 17.91 J/cm^2. **Figure 4.3(c)** shows the *hsp70* expression kinetics at a wavelength of 2.94 μm. Compared to the other wavelengths at similar radiant exposures, the 2.94 μm treatment induced markedly more visual damage to the tissue (data not shown). Therefore, treatments using radiant exposures less than 7.96 J/cm^2 were also tested. A maximum *hsp70* fold-induction of 23x is achieved using a radiant exposure of 3.17 J/cm^2. The magnitude of *hsp70* expression increases as the radiant exposure is increased from 1.59 to 3.17 J/cm^2. Radiant exposure greater than 3.17 J/cm^2 lead to decreases in *hsp70* expression.

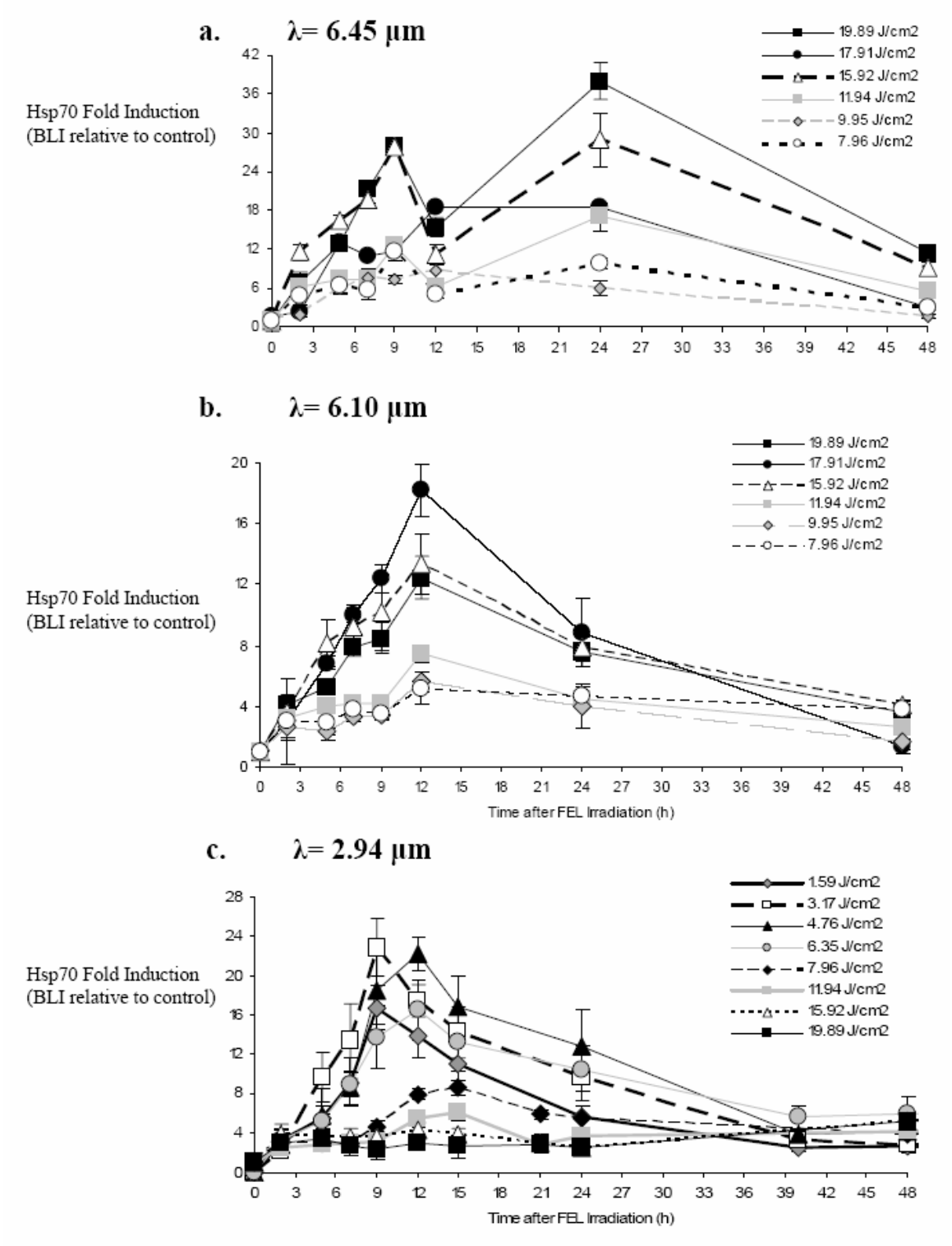
a.
λ= 6.45 µm
Hsp70 Fold Induction
(BLI relative to control)
19.89 J/cm2
17.91 J/cm2
15.92 J/cm2
11.94 J/cm2
9.95 J/cm2
7.96 J/cm2
b.
λ= 6.10 µm
Hsp70 Fold Induction
(BLI relative to control)
19.89 J/cm2
17.91 J/cm2
15.92 J/cm2
11.94 J/cm2
9.95 J/cm2
7.96 J/cm2
Time after FEL Irradiation (h)
c.
λ= 2.94 µm
Hsp70 Fold Induction
(BLI relative to control)
1.59 J/cm2
3.17 J/cm2
4.76 J/cm2
6.35 J/cm2
7.96 J/cm2
11.94 J/cm2
15.92 J/cm2
19.89 J/cm2
Time after FEL Irradiation (h)

Figure 4.3. Quantification of *hsp70* expression using bioluminescent imaging (BLI)
(a) Normalized bioluminescent intensity (BLI) indicating fold induction of *hsp70* expression for mice wounded with $FEL_{\lambda = 6.45\ \mu m}$. Peak *hsp70* expression is bi-phasic with maxima occurring 9-12 h and 24 h post surgery. *hsp70* levels are dose dependent, and a maximum *hsp70* fold induction of 28 is achieved using a radiant exposure of 19.89 J/cm^2. Sixteen wounds were made on 4 mice in the following manner: H = 7.96 J/cm^2 (n=4), 9.95 J/cm^2 (n=8), 11.94 J/cm^2 (n=4), 15.92 J/cm^2 (n=4), 17.91 J/cm^2 (n=8), and 19.89 J/cm^2 (n=4). Prior to each imaging session, 200 µL of luciferin (15 mg/ml) were injected i.p. and incubated for 15 min. Bioluminescent images were integrated over 30 seconds at a FOV A with the IVIS 200 at t = 0, 2, 5, 7, 9, 12, 15, 17, 24, and 48 h. The BLI data were normalized to the unwounded section of tissue. Values are reported as mean standard errors; error bars smaller than symbol are not shown.
(b) Normalized bioluminescent intensity (BLI) indicating fold induction of *hsp70* expression for mice wounded with $FEL_{\lambda = 6.10\ \mu m}$. Same laser parameters as (a). Peak expression occurs 12 h post surgery, with a peak fold induction of 18 using 17.91 J/cm^2.
(c) Normalized bioluminescent intensity (BLI) indicating fold induction of *hsp70* expression for mice wounded with $FEL_{\lambda = 2.94\ \mu m}$. Same laser parameters as (a), but lower radiant exposures of 1.59, 3.17, 4.76, and 6.35 J/cm^2 were also examined. A peak fold induction of 23x is achieved 9 h post surgery using 3.17 J/cm^2 and at 12 h of 23x using 4.76 J/cm^2 . Exposures exceeding 4.76 J/cm^2 lead to decreases in *hsp70* expression.

4.4.3 Using histologic studies to evaluate laser-treated tissue

Tissues are compared at the laser conditions that generated similar magnitudes of *hsp70* expression. Specifically laser parameters that show a 12-fold induction in *hsp70* expression 12 h after laser surgery, based on [**Figure 4.4(a-c)**]. The 12-fold induction value was selected because each treatment had conditions that generated this amount making it suitable for comparison. Radiant exposures of 11.94, 15.92, and 1.59 J/cm^2 were used for the wavelengths of 6.45 μm, 6.10 μm, and 2.94 μm, respectively. Cellularity and damage were visualized using a Hematoxylin and Eosin stain [**Figures 4.4(a-c)**] and a Gomori's trichrome stain [**Figures 4.4(d-f)**]. **Figures 4.4(a-c)** indicate marked differences in the histological characteristics among the 3 wavelengths. Compared to the other wavelengths, the 6.45 μm treatment shows the thickest superficial layer of coagulation (see arrow) [**Figure 4.4(a)**]. **Figures 4.4(d-f)** reveal marked differences in tissue damage patterns. Tissues treated with 6.45 μm show the deepest zones of collagen damage, and the 6.10 μm wavelength shows the shallowest depth of damage (red staining).

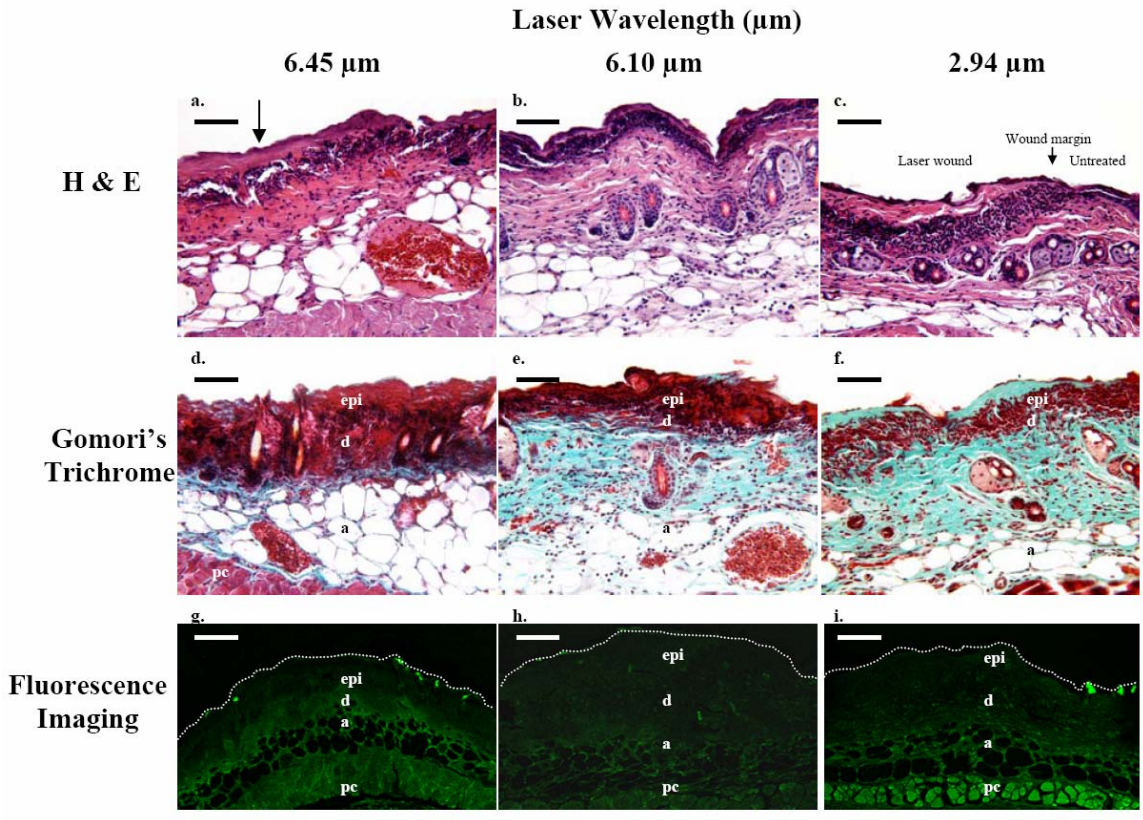

Figure 4.4. Morphological methods to measure depth of damage and Fluorescent Imaging to depths of *hsp70* expression.

(a-c) Histological slides of laser-damaged tissue evaluated 12 h post injury (Hematoxylin and Eosin Stains). For a consistent comparison, tissues showed using exposures that induced comparable (12 fold) increases in *hsp70* expression. Radiant exposures of 11.94, 15.92, and 1.59 J/cm^2 were used for the wavelengths of 6.45 µm, 6.10 µm, and 2.94 µm, respectively (scale bar = 150 µm). Tissues treated with 6.45 µm show denatured collagen at a deeper depth than tissues treated at 6.10 µm. For 6.45 µm, the 11.94 J/cm^2 sample has denatured collagen that extends as deep as in the muscle (panniculus carnosus) layer.

(d-f) Gomori's (green) trichrome stain is used to visualize the depth of damage of laser treated tissue (scale bar = 150 µm). This stain confirms the full-thickness nature of the injury at 6.45 µm and the minimal damage at 6.10 µm.

(g-h) Fluorescence imaging of *hsp70* induced GFP expression. Tissues were fixed 12 h post injury (scale bar = 75 µm). Zeiss LSM Image Browser was used to process images. For the H = 11.94 J/cm^2 the 6.45 µm tissue has damage to a depth of 150 µm where eGFP signal is not present, and modest eGPF expression is also observed in the muscle (panniculus carnosus). While at 6.10 µm much less signal is observed in deeper dermis. (epidermis = epi, dermis = d, a = adipose tissue, and pc = panniculus carnosus)

4.4.4 Depth resolving *hsp70* expression

The tissue treated with 6.45 μm has modest signal throughout as evidenced by the green color reporting higher promoter activity. To examine the spatial distribution of *hsp70* expression, the green fluorescent protein expression was measured using fluorescence microscopy. Depth resolving *hsp70* expression allowed us to develop a 3D understanding of *hsp70* expression after FEL treatments. Fluorescence images of each laser treated tissue are provided in [**Figures 4.4(g-i)**]. The highest signal appears in the reticular dermis and in the muscle (panniculus carnosus). The epidermis and papillary dermis are damaged to a depth of approximately 100 μm, as evidenced by the absence of GFP expression. This dark area of absent GFP expression correlated to the tissue damage observed in **Figure 4.4(d)**. Compared to 6.45 μm, much lower GFP expression is observed in the tissue treated with a wavelength of 6.10 μm [**Figure 4.4(h)**]. At 2.94 μm significant expression is observed in the epidermis and superficial dermis, and some in the muscle [**Figure 4.4(i)**].

To compare the laser treatments, the magnitude of reporter expression is quantified with respect to depth [**Figure 4.5**]. The recorded integrated fluorescent intensities are plotted versus tissue depth [**Figure 4.5(a)]**. For the 2.94 μm, peak emission is bi-phasic with maxima at 40 μm and 150 μm below the skin's surface (marked with *). In contrast, at 6.45 μm the expression is lowest closest to the skin's surface and increases with depth with a maximum at 150 μm below the surface. Compared to the other wavelengths, the 6.10 μm has significantly less signal at all depths. In **Figure 4.5(b)**, the cell density per 600 μm^2 region of tissue is plotted versus depth. At 6.10 μm the largest group of cells appear approximately 40 μm below the surface. In contrast, the 2.94 μm and 6.45 μm treatments show the highest cell densities approximately 100 to 150 μm below the surface. The data suggest that the 6.10 μm wavelength promotes more cellular migration to the skin surface than the other

wavelengths. Quantitative fluorescence intensities were then normalized to cell density, and these normalized fluorescence values are plotted versus depth in **Figure 4.5(c)**. The wavelengths of 2.94 and 6.45 μm show bi-phasic peaks occurring at 50 and 250 μm below the surface, while the 6.10 μm treatment has peak expression from 100 to 150 μm below the skin surface.

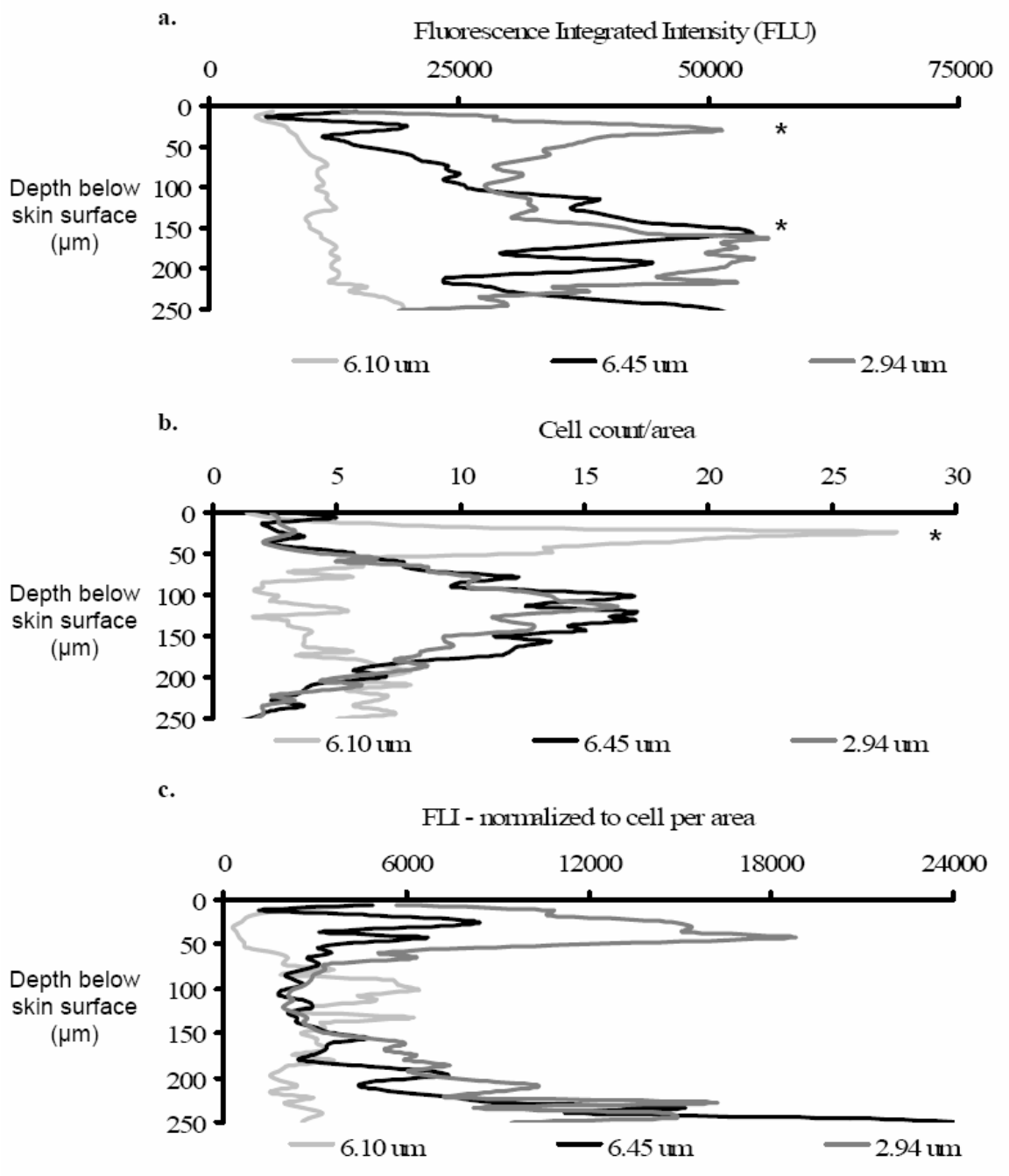
a.
Fluorescence Integrated Intensity (FLU)
0
25000
50000
75000
0
50
100
150
200
250
Depth below skin surface (µm)
*
*
6.10 um
6.45 um
2.94 um
b.
Cell count/area
0
5
10
15
20
25
30
0
50
100
150
200
250
Depth below skin surface (µm)
*
6.10 um
6.45 um
2.94 um
c.
FLI - normalized to cell per area
0
6000
12000
18000
24000
0
50
100
150
200
250
Depth below skin surface (µm)
6.10 um
6.45 um
2.94 um

Figure. 4.5. Quantification of Fluorescence Signal
(a) Fluorescent integrated intensity (FLU) versus depth of tissue (μm). Fluorescent intensity was integrated on three separate tissues over 1300 μm^2 areas at 26 positions below the surface, separated by 13 μm. Mean fluorescence intensity is plotted and the SD < 5 % (data not shown for clarity). The 2.94 μm treatment is bi-phasic with maxima at 40 μm and 150 μm below the skin's surface (Marked with *). The 6.45 μm treatment shows peak expression 150 μm below the skin surface. The 6.10 μm treatment shows lower expression at all depths.
(b) Average Cell number per area versus depth of tissue. From a serial section of tissue using a H&E stain and Image Pro Plus the cells were counted. Areas of interest were 600 μm^2 and n=10 for 3 different tissues.
(c) Normalized fluorescent intensity (FLU) versus depth of tissue. The fluorescent intensity units in **(a)** were normalized to the cell numbers in **(b)** and plotted.

4.4.5 Quantification of collateral thermal damage

For all of the wavelengths tested, the depth of damage is dose-dependant with higher laser radiant exposures showing deeper damage. To measure the magnitude of collateral thermal damage in laser treated tissues traditional histological methods were utilized. The depth of tissue damage was evaluated 12 h after laser surgery using Gomori trichrome stains, where tincture changes indicate damaged collagen. The measured depth of damage is plotted versus FEL radiant exposure (J/cm^2) [**Figure 4.6(a)**]. Interestingly, the depth of damage with 2.94 μm is 3x that at 6.10 μm, and approximately 2x that at 6.45 μm. Since 6.45 μm is the deepest penetrating wavelength, we expected it to damage the deepest. Apparently, the 2.94 μm wavelength, which has the shallowest optical penetration depth damages tissue deeper. The 6.10 μm wavelength, which is absorbed by both water and protein (amide I band) shows the least collateral tissue damage.

4.4.6 The effects of laser wavelength and radiant exposure on the magnitude of *hsp70* expression

The maximum magnitudes of *hsp70* expression were measured and are plotted versus laser radiant exposure (J/cm^2) [**Figure 4.6(b)**]. For all wavelengths tested, increases in radiant exposure led to increases in *hsp70* expression. However, at 2.94 μm a maximum *hsp70* expression of approximately 20-fold occurs with a radiant exposure of 4.76 J/cm^2 while exposures greater than 4.76 J/cm^2 show decreases in *hsp70* expression. This decrease suggests that significant damage is induced in the tissue and as a result the cells are compromised and can not report activity. At 6.45 μm, a maximum of 26-fold occurs with the 19.89 J/cm^2 exposure, and with 6.10 μm a 16-fold induction with 17.91 J/cm^2. Overall, among the wavelengths tested, a wavelength of 6.10 μm generates the lowest levels of hsp70 expression.

4.4.7 Correlation between *hsp70* expression and collateral thermal damage

For both 6.45 and 6.10 μm, the depth of damage increases linearly with the *hsp70* level. In contrast, at 2.94 μm, the *hsp70* level rapidly drops after reaching levels of approximately 22-fold. In **Figure 4.6(c)**, the *hsp70* fold-induction levels are plotted versus the measured depth of tissue damage. Since the protein absorbing wavelengths (6.10 and 6.45 μm) show a linear increase in *hsp70* expression, the data suggests that these wavelengths exhibit a similar relationship (see black line) [**Figure 4.6(c)**]. In contrast, the slope for the water absorbing wavelength of 2.94 μm reveals a markedly different trend than the protein targeting wavelengths (see gray line) [**Figure 4.6(c)**]. At low radiant exposures the depth of damage increases with increases in *hsp70* expression, but for higher radiant exposures the tissue is overly compromised and *hsp70* levels drop off.

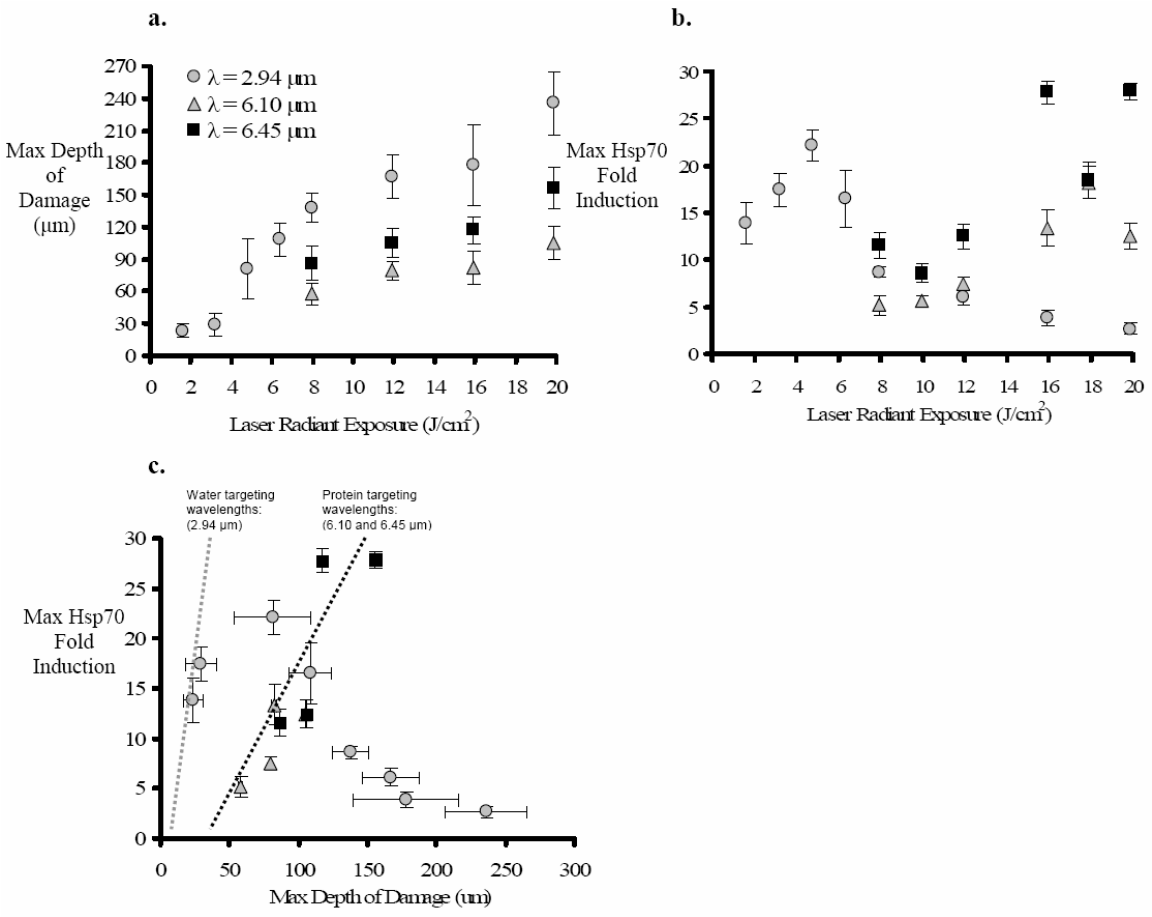

Figure 4.6. Collateral Thermal Damage

(a) Depth of Damage at 12 h plotted versus FEL exposure radiant exposure (J/cm^2). Higher FEL radiant exposures cause deeper tissue damage. The 2.94 µm treatment damages 2X deeper than 6.45 µm and 3X deeper than 6.10 µm. Depth of damage was measured using histological stains (Gomori Trichrome) on sectioned tissue. Image Pro plus was used to measure the zone of thermal damage as indicated by tincture changes. Mean and standard deviations for damage depths are shown (n=90)

(b) Peak *hsp70* expression is plotted versus laser radiant exposure (J/cm^2) for 2.94, 6.10, and 6.45 µm. For all wavelengths, higher radiant exposures result in higher *hsp70* expression levels. One marked difference between the 3 treatment wavelengths is that the 2.94 µm has maximal *hsp70* expression at 5 J/cm^2. Exposures greater than 5 J/cm^2 led to decreases in *hsp70* expression.

(c) *hsp70* Fold Induction plotted versus actual depth of tissue damage (µm). The data for 6.45 and 6.10 µm lie on the same slope (black dotted line), and the 2.94 µm data slope is shifted and steeper (gray dotted line). A linear relationship exists between measured tissue damage and *hsp70* expression levels.

4.4.8 Epidermal hyperplasia

At 120 h post surgery, tissue treated with a wavelength of 6.10 μm show the least amount of epidermal thickening. For all wavelengths tested, the degree of epidermal hyperplasia is dose-dependant and increases with increases in laser radiant exposure. In normal cutaneous repair, the epidermis thickens in relation to the magnitude of the damaging insult. Thus, pronounced thickening of the epidermis, referred to as epidermal hyperplasia, can be used as an indicator of a more robust repair response, presumably caused by a more damaging insult. Laser treated tissues using a radiant exposure of 11.94 J/cm^2 are provided for each treatment wavelength [**Figure 4.7(a-d)**]. The magnitude of the epidermal hyperplasia was measured using Image Pro Plus analysis software on Gomori trichrome stained sections (Note: untreated epidermis has mean thickness of roughly 20 μm). The tissue treated with 6.10 μm showed negligible epidermal hyperplasia as evidenced by the depth of epidermis staining pinkish/purple [**Figure 4.7(b)**]. At the same radiant exposure, both 6.45 μm and the 2.94 μm treatments show 2x more hyperplasia than the 6.10 μm treatment [**Figure 4.7(c-d)**]. The magnitude of epidermal thickening 120 h after FEL surgery is plotted versus the laser radiant exposure [**Figure 4.7(e)**]. At the lowest radiant exposure (7.96 J/cm^2) each treatment wavelength achieve similar degrees of epidermal hyperplasia (roughly 4-5x thicker). Maximal epidermal thickening of 10-fold is achieved using a wavelength of 2.94 μm and a radiant exposure of 19.89 J/cm^2. Tissues treated using the 6.10 μm wavelength show the least amount of hyperplasia. The magnitude of hyperplasia at 6.10 μm is statistically different from the other wavelengths (* = $P < 0.1$, ** = $P < 0.005$, *** = $P < 0.001$, and $n=25$).

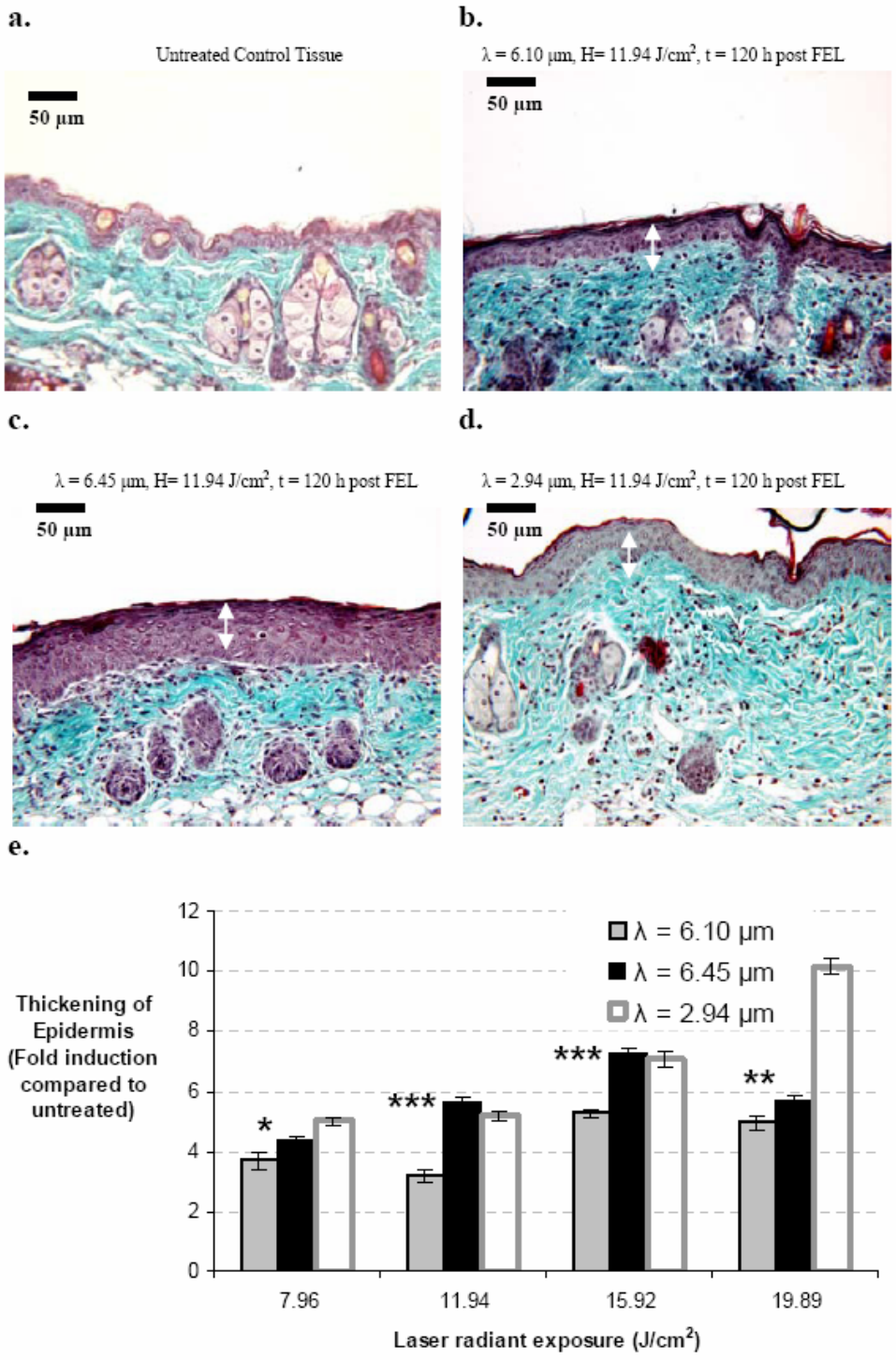
a.
Untreated Control Tissue
50 µm
b.
λ = 6.10 µm, H= 11.94 J/cm², t = 120 h post FEL
50 µm
c.
λ = 6.45 µm, H= 11.94 J/cm², t = 120 h post FEL
50 µm
d.
λ = 2.94 µm, H= 11.94 J/cm², t = 120 h post FEL
50 µm
e.
Thickening of Epidermis (Fold induction compared to untreated)
λ = 6.10 µm
λ = 6.45 µm
λ = 2.94 µm
*
***
***
**
0
2
4
6
8
10
12
7.96
11.94
15.92
19.89
Laser radiant exposure (J/cm²)

Figure 4.7. Epidermal Hyperplasia: An Early Wound Repair Response in Laser- Treated Tissues. (a-d) Sample representation of Gomori Trichrome stains of tissues evaluated 120 h post surgery (scale bar = 50 μm). (a) Untreated tissue (b) λ = 6.10 μm, (c) λ = 6.45 μm (d) λ = 2.94 μm. Note: all laser treatments used a radiant exposure of 11.94 J/cm^2 Thickened epidermis is most evident following the 6.45 μm exposure. (Arrow = thickened epidermis)
(e) The magnitude of epidermal thickening 120 h after FEL exposure is plotted versus the radiant exposure for each wavelength. (Note: untreated tissue has an average thickness of 20 μm). The magnitude of epidermal hyperplasia was measured using Gomori trichrome stained sections and Image Pro Plus analysis software. For all wavelengths tested the magnitude of epidermal hyperplasia increases with laser radiant exposure. Tissue treated with 6.10 μm shows the least epidermal hyperplasia. The mean and SEM for the magnitude of epidermis thickening were statistically compared to the 6.10 μm wavelength using a student's t-test (* = P < 0.1, ** = P< 0.005, *** = P < 0.001, and n=25).

4.5. Discussion

In this report, we examine the sublethal collateral damage in the tissue that remains after laser ablation. Tissues treated with the 6.10 μm wavelength show the lowest magnitude of hsp70 expression, the shallowest zone of damage, and the least amount of epidermal thickening; therefore, compared to 2.94 μm and 6.45 μm, the 6.10 μm wavelength is the optimum ablation wavelength. This study is novel because we use a transgenic mouse model (*hsp70A1-L2G*) to quantify cellular damage with sensitive methods. Furthermore, this study is the first time that multimodal molecular imaging techniques were used to measure thermal damage in a full animal model.

In this report, we examine the affect that mid-IR wavelengths have on cellular damage. We hypothesized that specific wavelengths of IR light that were targeted to dermal protein absorption would achieve less thermal damage than water targeting water absorption. To test the hypothesis, we tuned the FEL to water and protein absorbing wavelengths (2.94 μm, 6.10 μm, and 6.45 μm), and assessed ensuing collateral damage using optical imaging and histological methods. Compiling the data, we come to the following conclusions. First, we find that the magnitude of *hsp70*

expression is dose-dependent and increases with increasing radiant exposures. Second, *hsp70* expression is wavelength dependent. Third, the optical imaging techniques and histological data both show that a laser wavelength of 6.10 μm induces the least *hsp70* and causes the least thermal damage, and therefore is a superior ablation wavelength. Fourth, multimodal imaging of a transgenic mouse model allows for the characterization of the bio-molecular effects in surgical ablation procedures.

4.5.1 The magnitude of *hsp70* expression increases with laser radiant exposure

In our skin equivalent model we found that *hsp70* expression increased with increasing thermal exposures (14, 15). Therefore, we hypothesized that treating mouse skin with increasing laser radiant exposures would lead to increases in *hsp70* expression. As anticipated, increases in laser radiant exposure led to increases in the magnitude of *hsp70* expression [**Figure 4.3** and **Figure 4.6(b)**]. However, a wavelength of 2.94 μm using radiant exposures greater than 4.76 J/cm^2 resulted in decreases in *hsp70* expression [**Figure 4.6(b)**]. This decrease in *hsp70* expression was not expected but can be explained. First, compared to the other wavelengths tested, using radiant exposures greater than 4.76 J/cm^2, the 2.94 μm wavelength induced markedly more collateral thermal damage [**Figure 4.6(a)**]. This damage was visually apparent, where coagulation and bleeding occurred, immediately after laser surgery (data not shown). One explanation for this decrease in signal is that tissues treated with 2.94 μm may experience higher tissue temperatures than the tissues treated with the protein absorbing wavelengths (eg. 6.10 and 6.45 μm). Studies using diffusion modeling have also shown that layer-specific heating can occur generating variations in tissue temperatures achieved during ablation (20). These elevated temperatures may cause more severe photothermal damage that impairs the cell and perhaps the cellular machinery that makes the bioluminescence reaction possible. Bioluminescence requires

ATP as a cofactor, thus damage to the mitochondria (which occurs at temperatures exceeding 50 °C) may reduce the efficiency of the reaction and thereby reduce the light emissions (13, 21). Overall, the collateral thermal damage that is generated using high radiant exposures at 2.94 μm may be too severe and compromise the sensitivity of our reporter gene system. RT PCR experiments were conducted on these tissues to confirm the levels of actual *hsp70* mRNA in these tissues (data not shown). To summarize, the data suggest that *hsp70* expression increases with increasing laser radiant exposures. The data also indicate that using laser wavelengths that target water absorption may generate higher tissue temperatures and cause more thermal damage than protein targeting wavelengths.

4.5.2 The magnitude of *hsp70* expression varies with wavelength

When laser light penetrates tissue the optical energy is absorbed by target biomolecules, mostly water and the protein collagen, and is converted into heat causing photothermal effects to occur. At longer infrared wavelengths ($\lambda > 1750$ nm), absorption is dominant over scattering and application of Beer-Lambert law is appropriate to determine the spatial distribution of absorbed laser radiation (22). The depth that laser light penetrates in tissue, termed the optical penetration depth (δ), depends on the absorption coefficient (μ_a) of the tissue at a particular wavelength. Water exhibits max absorption at a wavelength of 2.94 μm (μ_a = 12000 cm^{-1}) and 6.10 μm (μ_a = 2780 cm^{-1}) (22). The most abundant protein in the dermis (collagen) exhibits peaks at 6.10 μm (amide I band) where water absorption is a sixth that of collagen, and at 6.45 μm (amide II band) where absorption is half that of collagen (22). The δ at 2.94 μm, 6.10 μm, and 6.45 μm can be approximated to be roughly 1 μm, 5 μm, and 10 μm, respectively. Based on these fundamental principles we generated the following hypotheses. First, we hypothesized that since the depth that laser light penetrates is governed by the

wavelength-dependant properties of skin, then using laser wavelengths that have deeper δ's will deposit energy in larger optical zones, affecting larger population of cells, and therefore induce higher levels of *hsp70* expression. Second, we further hypothesized that since the specific biomolecule (water vs. protein) that each wavelength targets affects the volumetric energy distribution, then wavelengths that target both water and protein (eg. 6.10 μm) should have a better energy partitioning and induce less collateral thermal damage than wavelengths preferentially targeting water (eg. 2.94 μm).

The data demonstrate that the deeper penetrating wavelength of 6.45 μm induced roughly 2x higher *hsp70* expression compared to 6.10 μm [**Figure 4.3(a-b)** and **Figure 4.6(b)**]. While at the similar exposures the shallow penetrating wavelength of 2.94 μm induced a much lower levels of *hsp70* expression than the 6.45 μm wavelength. Since the 6.45 μm has the largest δ, we expected it to induce the highest *hsp70* expression. But assuming the *hsp70* levels are merely a factor of the δ does not account for the high levels of *hsp70* expression that are observed at 2.94 μm using lower radiant exposures [**Figure 4.3(c)** and **Figure 4.6(b)**]. We anticipated that the *hsp70* expression levels at 2.94 μm to be markedly less than those of 6.45 and 6.10 μm. The preferential heating of the water layer at 2.94 μm may explain the higher *hsp70* expression levels (23). Since 2.94 μm is maximally absorbed by water, these data may suggest that wavelengths that target water induce greater damage than protein absorbing wavelengths. Also, the preferential targeting of the amide II band at 6.45 μm may induce more structural protein denaturation and explain for the higher *hsp70* levels. Based on the similar expression profiles observed at 6.45 and 6.10 μm and the differences observed at 2.94 μm, we suggest that the specific biomolecule that a laser wavelength targets greatly affects the magnitude of the *hsp70* expression.

The temporal expression kinetics of *hsp70* expression also appear to be affected by the laser treatment wavelength. Tissues treated with the 6.45 μm wavelength

exhibited biphasic peaks occurring 9-12 h and 24 h after surgery, while the tissues treated with 6.10 and 2.94 μm (both water absorbing wavelengths) had only one maxima in *hsp70* expression occurring 9-12 h after laser treatment [**Figure 4.3(b-c)**]. These data further suggests that laser wavelengths that preferentially target protein over water exhibit different response kinetics. The presence of the second peak at 6.45 μm may be due to the *hsp70* expression of another set of underlying cells which the 6.10 and 2.94 μm do not affect. The biphasic response may also indicate the presence of a more robust inflammatory response which activates *hsp70* expression.

Since BLI can not provide depth information, fluorescence techniques were used to explore *hsp70* signal in each skin layer. The fluorescent data further show that the laser wavelength not only affects the magnitude of *hsp70* expression but also the spatial distribution of the absorbed radiation in the tissue [**Figure 4.4(g-i)** and **Figure 4.5(a-c)**]. Since the 2.94 μm wavelength has the shallowest δ, we expected that its *hsp70* signal should be highest immediately below the skin's surface. As expected, maximal *hsp70* promoter activity occurred immediately below the skin's surface (depth = 40 μm) [**Figure 4.5(c)**]. In contrast, we expected that since the 6.10 μm is absorbed by both water and protein, we expected the tissue to have more efficient energy distribution and achieve more homogenous heating throughout. The data in **Figure 4.5(c)** suggests that this homogenous heating may explain the lower and more constant *hsp70* levels, evident at all depths [**Figure 4.5(c)**].

In this report, we define an expression threshold using the measured *hsp70* levels; whereby, the expression threshold is defined by the radiant exposure that causes decreases in *hsp70* expression levels. The data suggest wavelengths targeting water absorption peaks (eg. 2.94 μm) have lower thresholds than protein targeting wavelengths. Wavelengths with high water absorption (λ= 2.94 μm) appear to have a lower threshold for damage [**Figure 4.6(b)**]. In contrast, the 6.45 and 6.10 μm do not

have observable thresholds. For instance, at 2.94 μm radiant exposures exceeding 4.76 J/cm^2 lead to decreases in *hsp70* and therefore is defined as the threshold value. The protein targeting wavelengths do no exhibit thresholds at low radiant exposures.

4.5.3 Protein targeting wavelengths cause less collateral damage than wavelengths targeting water absorption

During laser ablation tissue temperatures have been reported to exceed 400 °C (24). When skin is exposed to these elevated temperatures, its molecular constituents represented by fibrillar Type I collagen (35% by volume) and water (65% by volume) begin to denature and vaporize, respectively. Collagen denaturation is a irreversible kinetic process largely governed by the temperature-time history and specimen hydration level (25). Denaturation occurs slowly at low temperatures and quickly at high temperatures, and as a general rule of thumb comparable levels of denaturation can be achieved by decreasing the magnitude of exposure time for each 5 °C increase in temperature. Collagen has been shown to denature at 60 °C using minute exposures (26). During ablation, the thermal history of skin falls within this range and therefore methods to accurately assess collagen damage are important. Traditionally, histological methods are the gold standard for measuring thermal collateral tissue damage, and are used in this report. However, other methods to examine denaturation have also been developed. One such method uses the changes in birefringence as a marker of thermal damage (27). The main limitation of this method is that is difficult to quantify the changes in birefringence. In this report, we measured damage using Gomori trichrome stains and compared these data to our optical imaging techniques. We sought to examine if a relationship existed between the traditional method and out optical imaging techniques. The data show that for all of the wavelengths tested, increases in the laser radiant exposure show increases in collateral thermal damage [**Figure 4.6(a)**]. The

deepest damage was achieved using 2.94 μm, which was roughly 2x deeper than 6.10 and 6.45 μm. The deeper damage at 2.94 μm could be due to the higher temperatures that are generated in the tissue which denature more collagen. Alternatively, the direct targeting of water at 2.94 μm may cause increased levels of tissue dehydration which also increases the rate of collagen denaturation. Comparing the protein targeting wavelengths, the data show that the 6.45 μm treatment induced more collateral damage than 6.10 μm. This finding suggests that 6.10 μm is a superior surgical ablation wavelength. Overall, the data suggest that wavelengths targeting non-specific water absorption cause more collateral damage than wavelengths targeting protein absorption.

The tissue damage measurements were compared to the *hsp70* expression levels to examine if a correlation exists between the two methods. The relationship was explored to see if the non-invasive readout of *hsp70* levels could be used as a surrogate marker for the degree of tissue injury. For all wavelength tested, a linear relationship exists between the recorded *hsp70* levels and the measured tissue damage (**Figure 4.6(c)**). However, the 6.45 μm and 6.10 μm wavelengths have similar slopes and are markedly different than the data for 2.94 μm [**Figure 4.6(c)**]. This may suggest that the 2.94 μm wavelength induces more *hsp70* for lower magnitudes of tissue damage, and therefore is a more damaging wavelength. Since a linear relationship exists for the protein targeting wavelengths this may imply that the magnitude of magnitude of *hsp70* reporter activity could be used an indicator of damage depth.

4.5.4 The 6.10 μm wavelength causes the least amount of epidermal hyperplasia

Wound repair is a complex coordinated sequence of overlapping biochemical and cellular events that result in the restoration of damaged tissue (28). Under normal conditions of wound repair, the processes that result in cutaneous healing follow a specific time course. In the early stages of re-epithelialization, keratinocytes favor

proliferation over differentiation, in order to replenish the lost material and rapidly resurface the wound site and form a barrier to keep fluid in and pathogens out. Recent wound repair studies have used the magnitude of epidermal hyperplasia as an indicator of the early wound repair response (29). Whereby, pronounced epidermal hyperplasia is a characteristic of a more robust repair process, presumably initiated by a more damaging insult. All laser treatments cause the tissue epidermis to thicken after treatment [**Figure 4.7(a-d)**]; however the magnitude of thickening increases with increasing radiant exposure [**Figure 4.7(e)**]. The most interesting finding is that the 6.10 μm wavelength shows the least thickening. The data suggest that the 6.10 μm wavelength causes the least robust repair, and based on this wound repair indicator suggest that the 6.10 μm is a superior ablation wavelength.

4.5.5 Using Hsp70 expression as a surrogate marker in laser-tissue interactions

The cellular response mechanism to thermal stress, consists in part of heat shock proteins (HSPs), and is activated immediately after exposure to elevated temperatures and increases progressively over time. The *hsp70* gene and the *hsp70* protein are the most highly induced and widely characterized HSP (19). Due to its marked induction, our lab has used *hsp70* expression as a sensitive indicator of sublethal thermal damage in laser procedures (14, 15). Using *in vitro* skin equivalents consisting of cells with the *hsp70*-luc transgene, we have previously verified that the bioluminescent light emission was linearly proportional to the actual intracellular *hsp70* levels present in the cells (15). This validation confirmed that the light emissions driven by *hsp70* promoter activity are an accurate surrogate marker for intracellular *hsp70* levels. This study is our initial attempt in examining *hsp70* expression in a full animal model (*hsp70A1-L2G)*. Therefore, molecular biology studies were conducted to validate that the light emissions correlated to actual intracellular protein levels. The RT PCR and ELISA experiments

confirmed that the *hsp70* promoter activity is indeed an accurate surrogate marker in the mouse model.

4.5.6 Advantages of using multimodal optical imaging techniques

The two principal optical imaging techniques used in this study are bioluminescence and fluorescence imaging. Bioluminescence techniques measure the light emission of a chemical reaction using luciferase, and fluorescence methods use a laser source to excite a fluorescent protein, in this case GFP, and measure the emitted light from a shifted wavelength. Fundamentally, both methods measure emitted light from a living source. However, each method activates the light emission differently, and it is in this intrinsic difference that plays to the inherent advantages and limitations of each method. Therefore, models that use multimodal imaging techniques can ascertain a greater wealth of biological information than those using a single imaging modality.

The main advantage of bioluminescence is that it can detect very low levels of background free light from deep tissue sources. In fact, studies show that as few as 200 cells can be detected at a depth of 2 cm in an *in vivo* mouse model (17). Mouse dermis is roughly 300 μm so for this study bioluminescence techniques are well suited to measure the emission of light from the entire laser treated tissue zone. However, since BLI images are two dimensional and lack depth information, fluorescent methods were used to probe for *hsp70* promoter activity in respect to depth. Nevertheless, the above properties make BLI well suited for the visual representation, characterization, and quantification of reporter gene expression over time. The sample time course BLI data demonstrated that laser treated wounds had roughly 8x higher bioluminescence than unwounded tissue [**Figure 4.2(a-d)**]. The center of the laser treated wounds show higher *hsp70* expression than the wound margins [**Figure 4.2(c-d)**]. This suggests that BLI can detect differences in *hsp70* expression within a single wound. Although the

spatial resolution of BLI is reported to be approximately 3-5 mm, the graphic displays in **Figure 4.2(d)** suggest that this method can discern variations in gene expression within a 7 mm square wound (18). In summary, the visual representations using BLI techniques show that laser treated tissue has significantly higher signal than untreated background tissue. The data also demonstrate that BLI techniques can detect variations in *hsp70* activity within the margins of a single wound and can be used to detect variations amongst different laser treatments on a single mouse.

The advantages and limitations of fluorescence imaging (FLI) are a direct result of using a laser source to excite the reporter gene. Since GFP emission does not require a chemical reaction, a live tissue is not a requisite for FLI. As a result, FLI can be measured post mortem on fixed tissues. Herein, laser-treated tissues were sectioned and the cross sectional *hsp70* promoter activity was measured in the regions of laser-treated mouse skin [**Figure 4.4(g-f)** and **Figure 4.5(a-c)**]. The advantage of fluorescence is that it has roughly 2x higher spatial resolution than bioluminescence methods. However, the significant auto-fluorescent background of skin makes quantification difficult. To circumvent this issue we used a laser scanning microscope, an inverted confocal scope, and bandpass filters to reduce the non-specific fluorescence light measured from the tissues.

4.6. Conclusion

In summary, we demonstrated that multimodal imaging techniques and a transgenic mouse model (*hsp70*-L2G) can aid in the assessment of the bio-effects in surgical ablation procedures. The bioluminescence data suggest that the magnitude of *hsp70* expression is dose-dependent and is wavelength-dependent. Specifically, the 6.10 μm wavelength induced the least *hsp70* expression. The histological data also

showed that the 6.10 μm wavelength caused the least collateral thermal damage after surgical ablation. The wound repair data showed that the 6.10 μm induced the lowest amount of epidermal hyperplasia. Taken together, our data show that the mid-IR wavelength of 6.10 μm is the superior surgical ablation wavelength.

Previous studies have used optical imaging techniques to visualize the promoter activity of genes involved in cutaneous wound repair (30-32). The present report suggests that this *hsp70* transgenic model in combination with the other wound healing mice in our lab can serve as useful tools to investigate laser-tissue interactions. These models can now be harnessed to improve laser surgical procedures. These methods can also be used to examine a host of aesthetic laser procedures, such as in skin resurfacing procedures. The model may also serve as a useful tool in the optimization of preconditioning protocols which require the careful manipulation of *hsp70* expression.

4.7. Works cited

1. Mackanos, M.A., Kozub, J.A., Hachey, D.L., Joos, K.M., Ellis, D.L., and Jansen, E.D. 2005. The effect of free-electron laser pulse structure on mid-infrared soft-tissue ablation: biological effects. *Phys Med Biol* 50:1885-1899.
2. Mackanos, M.A., Kozub, J.A., and Jansen, E.D. 2005. The effect of free-electron laser pulse structure on mid-infrared soft-tissue ablation: ablation metrics. *Phys Med Biol* 50:1871-1883.
3. Hutson, M.S. 2004. Advances in the Physical Understanding of Laser Surgery at 6.45 microns. In *International Free Electron Laser Conference*. Trieste, Italy.
4. Edwards, G., Logan, R., Copeland, M., Reinisch, L., Davidson, J., Johnson, B., Maciunas, R., Mendenhall, M., Ossoff, R., Tribble, J., et al. 1994. Tissue ablation by a free-electron laser tuned to the amide II band. *Nature* 371:416-419.
5. Joos, K.M., Shah, R.J., Robinson, R.D., and Shen, J.H. 2006. Optic nerve sheath fenestration with endoscopic accessory instruments versus the free electron laser (FEL). *Lasers Surg Med* 38:846-851.
6. Mawn, L.A., Shen, J.H., Jordan, D.R., and Joos, K.M. 2004. Development of an orbital endoscope for use with the free electron laser. *Ophthal Plast Reconstr Surg* 20:150-157.
7. Joos, K.M., Mawn, L.A., Shen, J.H., and Casagrande, V.A. 2003. Chronic and acute analysis of optic nerve sheath fenestration with the free electron laser in monkeys. *Lasers Surg Med* 32:32-41.

8. Joos, K.M., Shen, J.H., Shetlar, D.J., and Casagrande, V.A. 2000. Optic nerve sheath fenestration with a novel wavelength produced by the free electron laser (FEL). *Lasers Surg Med* 27:191-205.
9. Edwards, G.S., and Hutson, M.S. 2003. Advantage of the Mark-III FEL for biophysical research and biomedical applicationsPresented at the `XIV Russian Synchrotron Radiation Conference SR2002', held at Novosibirsk, Russia, on 15-19 July 2002.doi:10.1107/S0909049503007970. *Journal of Synchrotron Radiation* 10:354-357.
10. Xiao, Y., Guo, M., Parker, K., and Hutson, M.S. 2006. Wavelength-dependent collagen fragmentation during mid-IR laser ablation. *Biophys J* 91:1424-1432.
11. Kahle, G., Stadter, H., Seiler, T., and Wollensak, J. 1992. Gas chromatographic and mass spectroscopic analysis of excimer and erbium: yttrium aluminum garnet laser-ablated human cornea. *Invest Ophthalmol Vis Sci* 33:2180-2184.
12. Morimoto, R.I., Kroeger, P.E., and Cotto, J.J. 1996. The transcriptional regulation of heat shock genes: a plethora of heat shock factors and regulatory conditions. *Exs* 77:139-163.
13. O'Connell-Rodwell, C.E., Shriver, D., Simanovskii, D.M., McClure, C., Cao, Y.A., Zhang, W., Bachmann, M.H., Beckham, J.T., Jansen, E.D., Palanker, D., et al. 2004. A genetic reporter of thermal stress defines physiologic zones over a defined temperature range. *Faseb J* 18:264-271.
14. Beckham, J.T., Mackanos, M.A., Crooke, C., Takahashi, T., O'Connell-Rodwell, C., Contag, C.H., and Jansen, E.D. 2004. Assessment of cellular response to thermal laser injury through bioluminescence imaging of heat shock protein 70. *Photochem Photobiol* 79:76-85.
15. Wilmink, G.J., Opalenik, S.R., Beckham, J.T., Davidson, J.M., and Jansen, E.D. 2006. Assessing laser-tissue damage with bioluminescent imaging. *Journal of Biomedical Optics* 11:041114.
16. Reinisch, L., Mendenhall, M., Charous, S., and Ossoff, R.H. 1994. Computer-assisted surgical techniques using the Vanderbilt Free Electron Laser. *Laryngoscope* 104:1323-1329.
17. Troy, T., Jekic-McMullen, D., Sambucetti, L., and Rice, B. 2004. Quantitative comparison of the sensitivity of detection of fluorescent and bioluminescent reporters in animal models. *Mol Imaging* 3:9-23.
18. Massoud, T.F., and Gambhir, S.S. 2003. Molecular imaging in living subjects: seeing fundamental biological processes in a new light. *Genes Dev* 17:545-580.
19. Pockley, A.G. 2002. Heat shock proteins, inflammation, and cardiovascular disease. *Circulation* 105:1012-1017.
20. Hutson, M.S., Hauger, S.A., and Edwards, G. 2002. Thermal diffusion and chemical kinetics in laminar biomaterial due to heating by a free-electron laser. *Physical Review E* 65:061906.
21. Tsong, T.Y., and Su, Z.D. 1999. Biological effects of electric shock and heat denaturation and oxidation of molecules, membranes, and cellular functions. *Ann N Y Acad Sci* 888:211-232.
22. Vogel, A., and Venugopalan, V. 2003. Mechanisms of pulsed laser ablation of biological tissues. *Chem Rev* 103:577-644.
23. Hutson, M.S., Hauger, S.A., and Edwards, G. 2002. Thermal diffusion and chemical kinetics in laminar biomaterial due to heating by a free-electron laser. *Phys Rev E Stat Nonlin Soft Matter Phys* 65:061906.
24. Harris, D.M., Fried, D., Reinisch, L., Bell, T., Schachter, D., From, L., and Burkart, J. 1999. Eyelid resurfacing. *Lasers Surg Med* 25:107-122.

25. Wright, N.T., and Humphrey, J.D. 2002. Denaturation of collagen via heating: an irreversible rate process. *Annu Rev Biomed Eng* 4:109-128.
26. Allain, J.C., Le Lous, M., Cohen, S., Bazin, S., and Maroteaux, P. 1980. Isometric tensions developed during the hydrothermal swelling of rat skin. *Connect Tissue Res* 7:127-133.
27. Thomsen, S., Pearce, J.A., and Cheong, W.F. 1989. Changes in birefringence as markers of thermal damage in tissues. *IEEE Trans Biomed Eng* 36:1174-1179.
28. Davidson, J.M., and Benn, S.I. 1996. Biochemical and molecular regulation of angiogenesis and wound repair. *In: Cellular and Molecular Pathogenesis, A.E. Sirica (ed), Raven Press, New York*:79-108.
29. Florin, L., Knebel, J., Zigrino, P., Vonderstrass, B., Mauch, C., Schorpp-Kistner, M., Szabowski, A., and Angel, P. 2006. Delayed wound healing and epidermal hyperproliferation in mice lacking JunB in the skin. *J Invest Dermatol* 126:902-911.
30. Wu, N., Opalenik, S., Liu, J., Jansen, E.D., Giro, M.G., and Davidson, J.M. 2002. Real-time visualization of MMP-13 promoter activity in transgenic mice. *Matrix Biol* 21:149-161.
31. Wu, N., Jansen, E.D., and Davidson, J.M. 2003. Comparison of mouse matrix metalloproteinase 13 expression in free-electron laser and scalpel incisions during wound healing. *J Invest Dermatol* 121:926-932.
32. Izzo, A.D., Mackanos, M.A., Beckham, J.T., and Jansen, E.D. 2001. In vivo optical imaging of expression of vascular endothelial growth factor following laser incision in skin. *Lasers Surg Med* 29:343-350.

CHAPTER V

MOLECULAR IMAGING-ASSISTED OPTIMIZATION OF HSP70 EXPRESSION DURING LASER PRECONDITIONING FOR WOUND REPAIR ENHANCEMENT

Gerald J. Wilmink[1], Susan R. Opalenik[2], Lillian B. Nanney[3], Anita Mahadevan-Jansen[1], Jeffrey M. Davidson[2,4], E. Duco Jansen[1]

[1]Department of Biomedical Engineering, Vanderbilt University, Nashville, TN 37235

[2]Department of Pathology, Vanderbilt University, Nashville, Tennessee 37212

[3]Department of Plastic Surgery, Cell & Developmental Biology, Vanderbilt School of Medicine, Nashville, Tennessee, USA 37212

[4]Department of Veterans Affairs Medical Center, Nashville, Tennessee 37212

This manuscript have been submitted for publication to the *Journal of Investigative Dermatology* and is currently under review.

5.1. Abstract

Patients at risk for impaired healing may benefit from prophylactic measures aimed at improving wound repair. Several photonic devices claim to enhance repair by thermal and photochemical mechanisms. We hypothesized that laser-mediated preconditioning would enhance surgical wound healing that was correlated with hsp70 expression. Using a pulsed diode laser (λ = 1.86 μm, τ_p =2 ms, 50 Hz, H = 7.64 mJ/cm^2) the skin of transgenic mice that contain an hsp70 promoter driven luciferase were preconditioned 12 hours before surgical incisions were made. Laser protocols were optimized *in vitro* and *in vivo* using temperature, blood flow, and hsp70-mediated bioluminescence measurements as benchmarks. Biomechanical properties and histological parameters of wound healing were evaluated for up to 14 days. Bioluminescent imaging studies *in vivo* indicated that an optimized laser protocol increased hsp70 expression by 15-fold. Under these conditions laser preconditioned incisions were two times stronger than control wounds. Our data suggest that mild laser-induced heat shock acting in correlation with an expression of hsp70 may be a useful therapeutic intervention prior to surgery.

5.2. Introduction

Several sublethal stimuli such as hyperthermia [1], desiccation, ATP depletion [2], and ischemia [3] can induce a sublethal stress response. The cellular response mechanism to thermal stress consists in part of heat shock proteins (HSPs). The expression of these molecular chaperones is activated immediately after exposure to elevated temperatures and reaches a maximum several hours later. HSPs are found in all organisms and comprise a large family of cytoplasmic proteins ranging from 20 to 120 kilodaltons. These molecular chaperones play an integral role in maintaining intracellular homeostasis by assisting in protein folding and by mediating processes which protect the cell from further injury [1].

The *hsp70* gene and hsp70 protein are the most highly induced targets of heat shock and the best characterized HSP [4, 5]. Due to its marked induction, *hsp70* expression is commonly used as a sensitive indicator of thermal damage to cells [4, 6]. The kinetics of *hsp70* upregulation are directly related to the hyperthermic regimen, dependent on both temperature and exposure time, and hsp70 is induced by temperature increases of $\geq$ 5-6 ^{o}C [1, 4, 7]. Although the kinetics of *hsp70* expression vary depending on the organism, tissue, and cell type some general trends are evident [8]. First, the magnitude of hsp70 expression increases in response to elevated thermal stress until a thermal threshold is reached, followed by a subsequent decrease. Secondly, peak hsp70 expression is bi-phasic, with maxima occurring between 8-12 hours and then approximately 24 hours after thermal stress [9, 10]. Third, severe levels of thermal stress may delay hsp70 expression as cellular machinery used to produce hsp70 is damaged.

There is evidence that pre-treating cells or tissue with an initial mild thermal elevation elicits a stress response that can serve to protect the tissue from subsequent

lethal stresses [11-13]. This process of pretreating tissue is commonly referred to as 'preconditioning.' Preconditioned cells exhibit greater survivability than untreated cells when exposed to subsequent stresses [14]. Preconditioning is believed to be due to increased production of HSPs, as first described by Ritossa in 1962 [15]. Since increased hsp70 expression is induced by stressors such as heat, it is hypothesized that its increased expression conveys increased cellular protection [13]. After an initial thermal stress, Hsp70 stabilizes the cell by tending to the recently denatured proteins and by preventing the production of misfolded proteins [16]. Hsp70 also functions at key regulatory points in the control of apoptosis, thereby inhibiting cell death and promoting cell survival [14, 17-19].

Tissue preconditioning protocols have been effectively incorporated into surgical procedures [20], the recovery of thermally injured tissues [21-23], protection to ischemia reperfusion injury [24-26], and even for cancer therapies [27, 28]. We hypothesized that a device with the ability to supply precise dosimetry and real-time, non-invasive optimization of hsp70 expression would yield the best of preconditioning protocols. We have demonstrated that the cellular response to thermal stress can be serially monitored as expression of the *luciferase* (*luc)* transgene under control of the *hsp70A1* promoter [7, 29]. The *hsp70A1-luc* system has been used to assess the extent of sublethal cellular damage in the context of a laser-tissue interaction [4, 29], and to better understand *hsp70* expression kinetics [29].

The main goal for the present study is to use a mouse model (*hsp70A1-luc)* and thermal and optical imaging methods to develop and optimize a laser preconditioning protocol in skin. The specific goals of this study were to a) characterize the kinetics (magnitude, timing) of hsp70 expression *in vitro* and *in vivo*, b) select laser parameters that induce optimal hsp70 levels while causing minimal collateral damage, and c) demonstrate the effectiveness of the protocols to enhance cutaneous wound repair.

5.3. Materials and Methods

5.3.1 Animal model

Experiments were conducted in accordance with guidelines specified by the Institutional Animal Care and Use Committee (IACUC) at Vanderbilt University. Transgenic mice in which the heat shock protein 70 (hsp70) promoter drives the luciferase and eGFP reporter genes were a generous donation from Dr. Chris Contag at Stanford University. A detailed description on the *hsp70A1-luc*-GFP L2G transgenic mouse has been detailed previously by Dr. Mark Mackanos. Briefly, the transgenic mice are of a FVB background and contain a hsp70 cassette (FVB.*hsp70A1-luc*_2A-GFP). The cassette is as follows: the murine hsp70A1 promoter (Genbank accession number M76613) was attached to the luciferase coding sequence from the pGL3-Basic plasmid (Promega, Madison, WI) as described previously and fused, in frame, to the ORF of the enhanced green fluorescent protein (eGFP; Clontech, Palo Alto, CA) with 54 base pairs (bp) of the FMDV 2A sequence followed by 24 bp of polylinker [7]. The cDNA for (eGFP) and luciferase (luc) vector are located downstream from the hsp70 promoter. Therefore, whenever the transcriptional factors are present which induce hsp70 mRNA transcription, these bicistronic reporters are transcribed and translated. Resultantly, the GFP and luciferase gene products emit light which can be used as a surrogate marker for hsp70 gene activity levels, as previously shown [29]. Note, preliminary experiments were conducted on diabetic mice. Diabetes was chemically induced with streptozotocin (STZ), using a single dose at 175 mg/kg. Blood glucose was measured with a glucometer, and mice with glucose levels ≥ 350 mg/dl were classified “diabetic.”

5.3.2 In vitro cell culture experiments

Dermal fibroblasts were isolated from the *hsp70A1-luc*-eGFP mouse and immortalized with the hTERT gene for *in vitro* experiments. Two day old mice were euthanized and their dermis was excised and digested in 0.2% collaganase (type III) in DMEM containing 10% fetal bovine serum at 37 °C overnight in culture incubator. Cells were subsequently centrifuged at 1000xg for 5 minutes, plated in DMEM (10% fetal bovine serum and pen/strep) and incubated overnight. Media was replaced after 72 hrs, and the cells were replenished with media every 2-3 days until confluent.

On day 1, immortalized mouse dermal fibroblasts (MDF) were plated in six well (9.62 cm^2) tissue culture plates with 10^5 cells per well in 2 ml of culture medium (Costar, Fisher Scientific, Sewanee, Georgia). On day 3 the culture plates were sealed with parafilm and then heat shocked by floating them in a water bath at 43, 44, or 45 °C for varying exposure times (0 to 120 min). Heat shocked cells were placed back in a 37°C, 5% CO_2 incubator (Forma Scientific) for defined time periods before analysis.

5.3.3 Bioluminescent imaging & cell viability assays for mouse dermal fibroblasts

Cells (control and heat shocked) were imaged for bioluminescent intensity as previously described [29]. In brief, D-luciferin potassium salt (Biosynth AG, Switzerland) is diluted in ddH_2O to a concentration of 2.25 mg/ml. Before each imaging session, 150 µL of substrate was added to each well. After delivery of the substrate, the cells were incubated for 5 min before each imaging session to ensure for maximal bioavailability of substrate. Luciferase-induced bioluminescent light emission was measured 12 h after heat using an IVIS 100 bioluminescent imaging system (Xenogen, Alameda, CA) and light emission was quantified using Living Image analysis software(v2.12, Xenogen).

Light emission was measured from each well and was quantified as a photon flux in units of total number of photons emitted/second.

In order to provide information to supplement the BLI data, cell viability assays using sensitive fluorometric methods were performed. Forty eight hours after thermal stress, 300 µl of CellTiter-Blue Cell Viability Assay was added to each well and incubated for 2 hours (G808B, protocol, TB317, Promega, Madison, WI) and analyzed using a Bio-Tek Synergy HT fluorescent plate reader. Fluorescent values for each sample were normalized to controls and expressed as a percent viability.

5.3.4 Damage determination

The Arrhenius integral is a rate process for characterizing tissue damage, such as coagulation or birefringence loss, as a function of temperature and time at that temperature. Thermal damage is exponentially dependent on temperature and linearly dependent on time of exposure [8]. The equation for the integral is:

$$\Omega = \ln\left(\frac{C_0}{C(t)}\right) = \int_0^{t_p} A\exp(-E_a / RT)dt \qquad (1)$$

where Ω is the tissue damage, A is the frequency factor - i.e. damage rate (1/sec), E_a is the activation energy in [J/mole], T is the temperature of exposure [^{o}K], R is the gas constant at 8.32 [J/mol K], and the integral is over the time of the heat exposure. The Arrhenius integral takes into account temperature-time history of the sample to predict tissue damage based on the damage threshold. The threshold for tissue damage is usually determined by pathological analysis and is a ratio of the concentration of native (undamaged) tissue before irradiation exposure (C_0) to the concentration of native tissue at the end of the exposure time (C_T). Beckham reported using NIH 3T3 cells equipped with hsp70-luc reporter gene that the Arrhenius relationship holds for biological

responses [8]. Similar to Beckham, in our experiments the maximum hsp70 level determined by bioluminescence was selected as the endpoint of damage. Under isothermal conditions, the Arrhenius relationship shows a linear increase in damage with exposure time increases. By fitting the experimental data to the integral, the relationship becomes linear. After setting Ω = 1, the equation then becomes:

$$\ln (t) = E_a/RT - \ln (A) \quad (2)$$

Plotting the data using ln (t) <seconds> versus 1/T <Kelvin> will provide a slope (E_a) and y-intercept (-ln A) from which the activation energy and frequency factor and were derived, respectively.

5.3.5 Laser preconditioning experiments in vivo

Two days before laser experiments, mice were anesthetized with isoflurane in an isoflurane vaporizer (V-10 Series, VetEquip Inc, Pleasanton, CA) and a rectangular area of the dorsal fur was removed with a clipper. The remaining hair remnants above the surface were removed using depilatory cream and the skin was thoroughly cleansed with water to remove residual cream. The mice were then returned to animal care for 2 days.

The preconditioning of tissues was accomplished with a Aculight Renoir diode laser (Renoir; Aculight, Bothel, WA). Laser light was coupled into a 600 μm diameter multimode silica fiber for transmission and delivery.

5.3.6 Two laser preconditioning protocols

Arrhenius plots indicated that sufficient tissue preconditioning can be achieved either by using short exposures (seconds) at high temperatures (50-60 °C) or by using longer exposures (minutes) at lower temperatures (40-50 °C) [14, 47]. In the literature, various thermal protocols have been used to maximally induce hsp70 expression, as shown in Table 1. We elected to investigate laser preconditioning protocols using two differing

thermal regimens. One experimental condition used a low-temperature long-duration protocol (T_LE_L) and the second experimental condition tested a high-temperature short-duration protocol (T_HE_S). The laser parameters used for the T_HE_S protocol were λ = 1.85 μm, repetition rate 50 Hz, τ_p = 2 ms, beam diameter 5 mm, H = 9.17 mJ/cm^2. The optimized preconditioning T_LE_L parameters: λ = 1.85 μm, repetition rate 50 Hz, τ_p = 2 ms, beam diameter 5 mm, H = 7.64 mJ/cm^2. The laser parameters used for a positive control were λ = 1.85 μm, repetition rate 50 Hz, τ_p = 2 ms, beam diameter 5 mm, H = 30 mJ/cm^2. The positive control induced tissue whitening and was used as an indicator of irreversible tissue damage.

5.3.7 Optimizing laser preconditioning protocols

Laser preconditioning protocols (temperature and exposure time) were optimized using thermal infrared, bioluminescent, and laser perfusion Doppler imaging methods. Tissue temperatures were measured in real time during laser preconditioning treatments using an infrared (IR) camera (A20 series, FLIR Systems, Portland, OR). The camera is sensitive to temperature changes ± 0.1 °C. ThermaCAM researcher 2.8 SR-3 software was used to analyze the data.

5.3.8 Bioluminescent imaging of living mice

After mice were preconditioned with the laser, the *hsp70*-induced luciferase bioluminescence was measured at various time points following heat shock using an IVIS 200 BLI system (Xenogen, Alameda, CA). Fifteen minutes before each imaging session the mice were anaesthetized with isoflurane and injected (27 gauge syringe) with 15 mg/ml of luciferin substrate i.p.. using a dose of 10 μl/gram body weight. Mice were imaged at 0, 3, 6, 9, 12, 15, and 24 hours after the start of the laser treatment. Mice were placed in the imaging chamber on a 37 °C stage, and bioluminescent images

were acquired using a integration time of 2 minutes. Bioluminescent data were represented with a false color scheme representing the regions of varying light emission, and quantified using LivingImage analysis software (v2.12,Xenogen). Light emissions from specified regions of interest (ROIs) were quantified as a photon flux in units of total number of photons emitted/second/ROI (p/s/ROI). To account for mouse-to-mouse variability, measured BLI values for each wound were normalized to the BLI value of the unwounded but shaved dorsum. This normalization was conducted at each time point. The normalization procedure yielded a fold induction number which is indicative of the relative magnitude of *hsp70* expression in each wound compared to normal, untreated tissue.

In order to ensure each transgenic mouse exhibited comparable sensitivity to heat exposure, the Aculight laser was used on each mouse to induce a positive control lesion using a fluence of 30 mJ/cm^2 for 20 seconds. This lesion was positioned 1/2 cm anterior to the tail on the dorsum of each mouse. Animals that showed greater than 20% deviation from the mean in response to this control tissue were excluded from the studies. An IR camera was used to measure the temperature that this treatment induced, and this temperature was shown to be reach of peak temperature of 65 °C for the 20 second heating interval.

5.3.9 Laser Doppler perfusion imaging

Dynamic blood flow on the mice dorsum was mapped with a high resolution PIM-2 Laser Doppler perfusion imager (Perimed Inc., North Royalton, OH). The parameter settings during the measurement were: scanning area, 20 x 20 mm; high resolution scanning; distance between the scanner head and wound, 17.8 cm. The measurement of the image and perfusion value was carried out by the LDIwin2.6 software package (Perimed AB, Sweden). The extent of blood perfusion for each sample was normalized to an

untreated control region. Normalized perfusion values were collected at 10 min, 3 days, and 10 day intervals after laser treatment.

5.3.10 Laser preconditioning to improve wound repair

Twelve hours after laser preconditioning, four full thickness longitudinal incisions, separated by 1.5 cm and each 1.0 cm in length, were made on the dorsum of each mouse. The four lesions consisted of 2 laser preconditioned areas and 2 untreated control areas. The anterior preconditioned wounds were compared to anterior control regions of tissue, and vice versa. This was done to reduce the bias due to the anatomical position of each wound. Wounds were closed with 7.5 mm clips, and the clips were removed on day 5. Immediately after wounding with the surgical scalpel, bioluminescence images of the mice were taken as previously described [10]. The BLI images served to verify that the laser preconditioning protocol induced hsp70 expression at the surgical wound site.

5.3.11 Tensile strength measurement

To compare the difference in wound healing between scalpel incisions (control) and laser preconditioned scalpel incisions, we measured maximum loads and tensile strengths of full-thickness wound skin from transgenic mice (n=9) at days 7, 10, and 14 after injury. Tensiometry was performed on skin incisions using the Instron 5542 tensiometer (Instron, Canton, MA) within 3 h after tissue harvest [61]. All tensiometry was performed in a blinded fashion. A small portion of incision was placed in 4% paraformaldehyde and then embedded in paraffin, and the sections subsequently used for histologic and immunohistochemical analysis.

5.3.12 Histologic parameters of wound healing

In order to evaluate cellular structure, damage, and collagen deposition a subset of the test animals were euthanized to provide mouse skin for histological and immunohistochemical analysis. Skin samples were collected 12, 48, 72, 120, and 240 h after wounding. Standard histological processing of formalin-fixed, paraffin-embedded samples included H&E and Gomori's trichrome as previously described [8, 10]. An Olympus Vanox-T AHZ microscope equipped with a Pixera Pro 600 ES camera was used to image the slides.

5.3.13 Immunohistochemistry

An immunohistochemical study was conducted on tissue sections to evaluate the effects that laser preconditioning protocols have on wound repair. Paraffin sections (7 μm) of mouse back skin were analyzed by immunological methods. Macrophages expressing the F4/80 surface marker were immunostained with a rat monoclonal antisera. Cell Proliferation was evaluated using a Ki-67 antigen. Apoptotic cells were selectively highlighted within tissue samples by immunostaining for cleaved caspase-3. Apoptotic cells with fragmented DNA were also visualized with DeadEnd Colorimetric TUNEL System. Immunohistochemistry was performed using the following antibodies: F4/80 (Cl:A3-1, F4/80; Serotec, Inc., Raleigh, NC), Ki67 (VP-RM04, Vector Laboratories, Burlingame, CA), DeadEnd Calorimetric TUNEL System (G3250, Promega Corporation, Madison, WI), and Caspase-3 (9PIG748, Promega, Madison, WI). The Dako Envision+ HRP/DAB+ System (DakoCytomation) was used to produce localized, visible staining. The slides were lightly counterstained with Mayer's hematoxylin, dehydrated and coverslipped. Olympus Vanox-T AHZ microscope (Olympus America, PA), Olympus Plan Opo Primary Objectives (10x, and 20x), and Image Pro Plus software (Media Cybernetics, Bethesda, MD) were used to image the slides.

5.4. Results

5.4.1. *In vitro* hsp70 expression kinetics

Figure 5.1(a) displays hsp70 expression kinetics for mouse dermal fibroblasts (MDF) exposed to thermal stress protocols at 43, 44, or 45 °C for 10, 20, 30, 40, 80, or 120 min. A maximal hsp70 expression, 18-fold greater than in the control cell cultures, occurred when MDF were maintained at 43 °C for 80 min. At higher temperatures maximal hsp70 expression was blunted and it only reached 8-fold at 44 °C for 30 min and a 6-fold at 45 °C after 20 min. In the groups exposed to the briefest thermal stress (10 min exposure), hsp70 expression was linearly proportional with temperature.

5.4.2. *In vitro* cell viability studies in mouse dermal fibroblasts

Levels of hsp70 expression were markedly affected by cell viability as shown in [**Figure 5.1(b)**]. At the lowest level of thermal stress (43 °C) cells maintained viability for the longest period (80 min) before showing a sharp decline, while cells that were exposed to incrementally higher thermal stress conditions at 44°C or 45°C showed precipitous declines after much briefer exposures of 20-40 min. Interestingly, cell viability data for MDFs exposed to very transient (10 min) thermal stresses at 44 or 45 °C showed enhanced numbers of viable cells compared to controls, suggesting that transient high temperature exposures may enhance cell proliferation.

5.4.3. Arrhenius damage analysis

Empirical models, such as the Arrhenius damage model, use mathematical expressions to describe damage processes and can aid in the optimization of preconditioning protocols. The hsp70-luc data and the cell viability data were used to investigate the Arrhenius relationship. Using equation (1): ln (t) = E_a/RT – ln (A), the data were plotted with ln (t) <seconds> versus 1/T <Kelvin>. From these plots, the slope and the y-intercept were used to calculate the activation energy (E_a) and the frequency factor (A) values. Where E_a is the energy barrier that molecules must surmount to denature, and A is the measure of the molecular collision frequency. Using the cell viability data, we measured the threshold of damage, with Ω = 1 denoting a cell viability of 1/e or 37%, as previously described [35]. The data are plotted in **Figure 5.1(c)**, and the resultant A and E_A values of 2.4 X 10^{74} s^{-1} and 4.7 X 10^5 J/mol are provided in **Figure 5.1(d)**. The data are consistent with published values in the literature (see **Table 5.2**), and confirms that using cell viability as an endpoint for damage adheres to the Arrhenius relationship [35-37]. The second way we assessed the Arrhenius relationship was using the maximum Hsp70 fold induction determined using BLI as an endpoint [8]. Although, the resultant E_A and A values of 2.4 X 10^{45} s^{-1} and 3.0 X 10^5 J/mol (Figure 1c and 1d) vary from the data generated with the cell viability method, a linear correlation still exists between E_a and ln (A). Since the data adhere to the linear regression, E_a = 2642 ln (A) + 17200, with less than a 1 percent margin in error, this confirms that the Arrhenius parameters are consistent with published values [38]. More importantly, it confirms that the methods used can be used to model and predict damage and can improve our preconditioning methods.

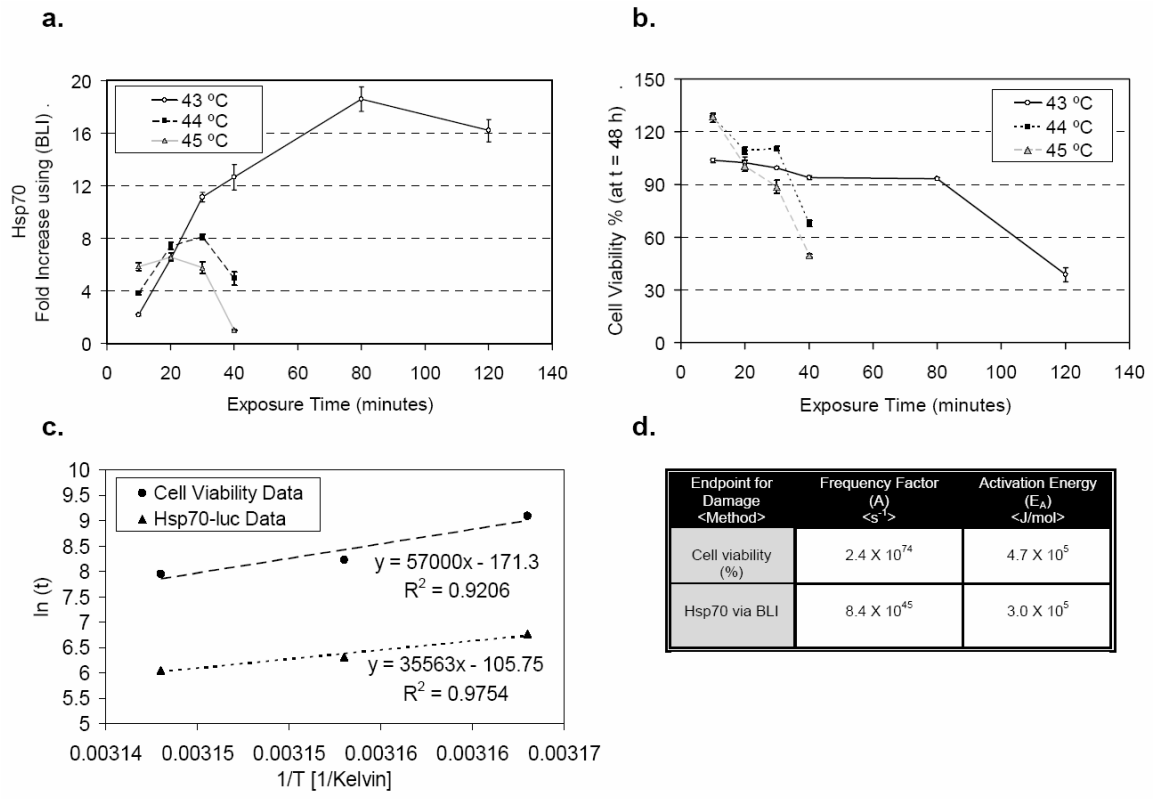

Endpoint for Damage <Method>	Frequency Factor (A) $<s^{-1}>$	Activation Energy (E_A) <J/mol>
Cell viability (%)	2.4×10^{74}	4.7×10^{5}
Hsp70 via BLI	8.4×10^{45}	3.0×10^{5}

Figure 5.1. ***In Vitro*** **Thermal Stress Protocols in Mouse Dermal Fibroblasts**
(a) Bioluminescent intensity data (BLI) indicative of hsp70 expression were acquired 12 h after variable time exposures at 3 different temperatures. Quantification of hsp70 expression was achieved by normalizing the sample average BLI to unheated control average BLI. Each time point represents six cell culture samples. **(b)** Viability measurements were made using a TiterBlue Assay at 48 h after thermal stress. Quantification of viability percentages (%) were calculated by normalizing the fluorescent value of each sample to unheated controls. **(c)** Arrhenius damage plots, data were plotted using the equation: ln (t) = E_a/RT – ln with ln (t) <seconds> versus 1/T <Kelvin>. From these plots, the slope and the y-intercept were used to calculate the activation energy (E_a) and frequency factor (A). **(d)** Arrhenius damage parameters.

5.4.4. Temperature calibrations for laser preconditioning protocols *in vivo*

We selected a laser source to test the effect of thermal preconditioning *in vivo*. Tissue temperatures were measured with an infrared camera. **Figure 5.2** presents the tissue temperatures induced during laser treatment for two laser preconditioning protocols and a positive control protocol (H = 30 mJ/cm^2 for 30 s). The T_HE_S protocol (high fluence, short exposure) generated tissue temperatures ranging between 48 and 50 °C while the T_LE_L protocol (low fluence, low exposure) generated tissue temperatures between 43 and 44 °C.

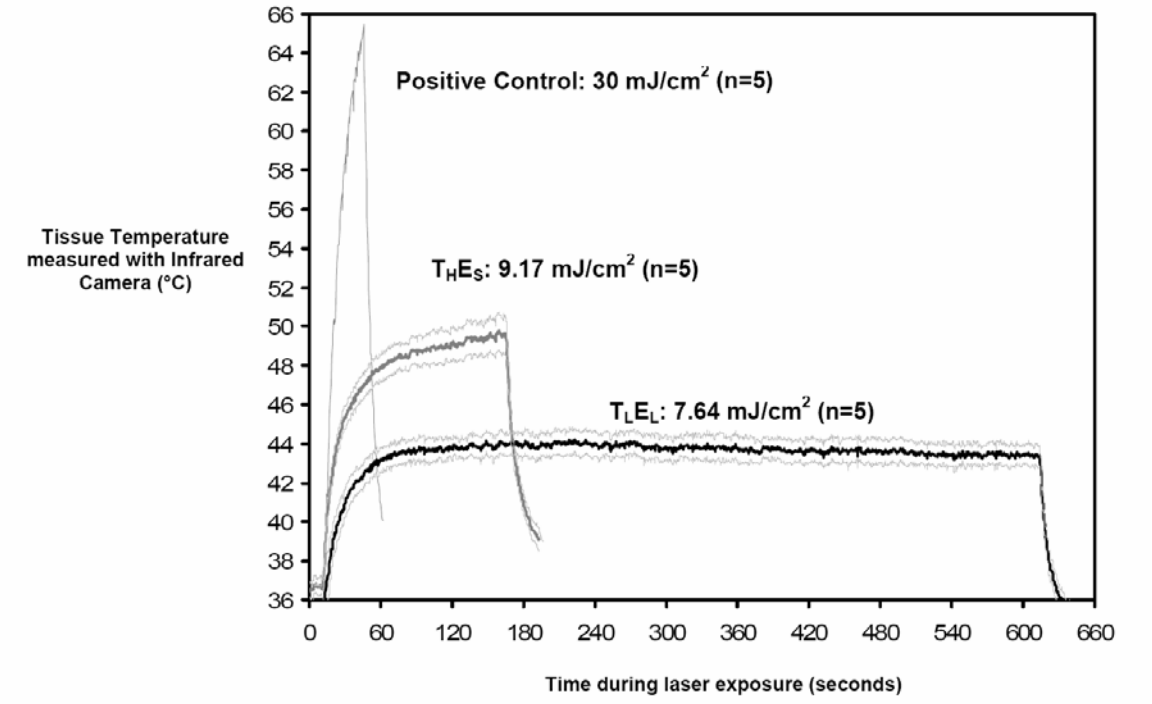

Figure 5.2. Assessment of Mouse Skin Temperature During Development of Laser Preconditioning Protocols. A thermal infrared imaging (IR) camera was used to measure real time mouse skin tissue temperatures induced by the high temperature short exposure (T_HE_S) and the low temperature long exposure (T_LE_L), and positive control laser protocols are shown. Values represent the mean temperature (n=5).

5.4.5. Visualization of *in vivo* hsp70 promoter activity within laser treated skin

Skin equivalents lack many cell populations needed for tissue repair, thus we utilized the *hsp70A1-luc* mouse model to assess the effects of thermal preconditioning *in vivo* [4, 7, 29-32]. Bioluminescent imaging methods were conducted to verify that hsp70 promoter activity could be visualized on laser-treated mouse dorsum. **Figure 5.3(a)** presents a sample bioluminescent image of the dorsal surface of a transgenic mouse 12 h after laser preconditioning protocol (H = 7.64 mJ/cm^2). Bioluminescent emission (false colors) resulting from four laser treatments, using exposure durations of 5, 10, 15, and 20 minutes are visible on the dorsum of the mouse. The 20 min exposures evoked greater light emissions as compared to shorter exposures.

5.4.6. Laser preconditioning increases blood flow

Since local hyperthermia has been demonstrated to increase blood flow [33], we sought to examine if laser preconditioning protocols increased blood flow to the treated regions. Blood perfusion was measured 10 min, 3 d, and 10 d after laser preconditioning treatments using laser Doppler imaging. The highest perfusion rates, 6-fold greater than control skin, were measured at 10 days following a 20 min exposure [**Figure 5.3(b)**]. The 10 min laser exposure induced the highest flow that was 3.71-fold greater than controls. This level persisted for 10 days, while the 20 minute laser exposure showed a progressive increase in blood flow.

5.4.7. Optimization of *in vivo* hsp70 promoter activity within laser treated skin

Various exposure conditions were tested for each laser protocol to determine the relationship between exposure duration and hsp70 expression levels. In the T_HE_S protocol (9.17 mJ/cm^2), exposure durations of 60, 90, 120, and 150 s were tested. Maximal hsp70 expression occurred 9 to 15 h after laser exposure [**Figure 5.3(c)**]. Laser

pre-treatments produced maximal hsp70 levels that were 11.65-fold greater than controls at an exposure duration of 150 s. The 120 second exposure induced 4 times less hsp70 than the 150 s exposure ($p < 0.05$).

The T_LE_L protocol ($H = 7.64$ mJ/cm^2) at exposure durations of 5, 10, 15, and 20 min produced markedly different profiles compared to the T_HE_S protocol. Hsp70 expression increased linearly with increasing durations of exposure, and a maximum level of hsp70 of a 17-fold induction was achieved after a 20 min exposure [**Figure 5.3(d)**].

Figures 5.3(e-f) depict the hsp70 fold induction levels as a function of exposure time. In the T_HE_S protocol the hsp70 levels increased exponentially with laser exposure time, while the hsp70 levels increased linearly with laser exposure time in the T_LE_L protocol. These optimization data suggest that the T_LE_L protocol may provide a more consistent and reliable induction of hsp70 levels.

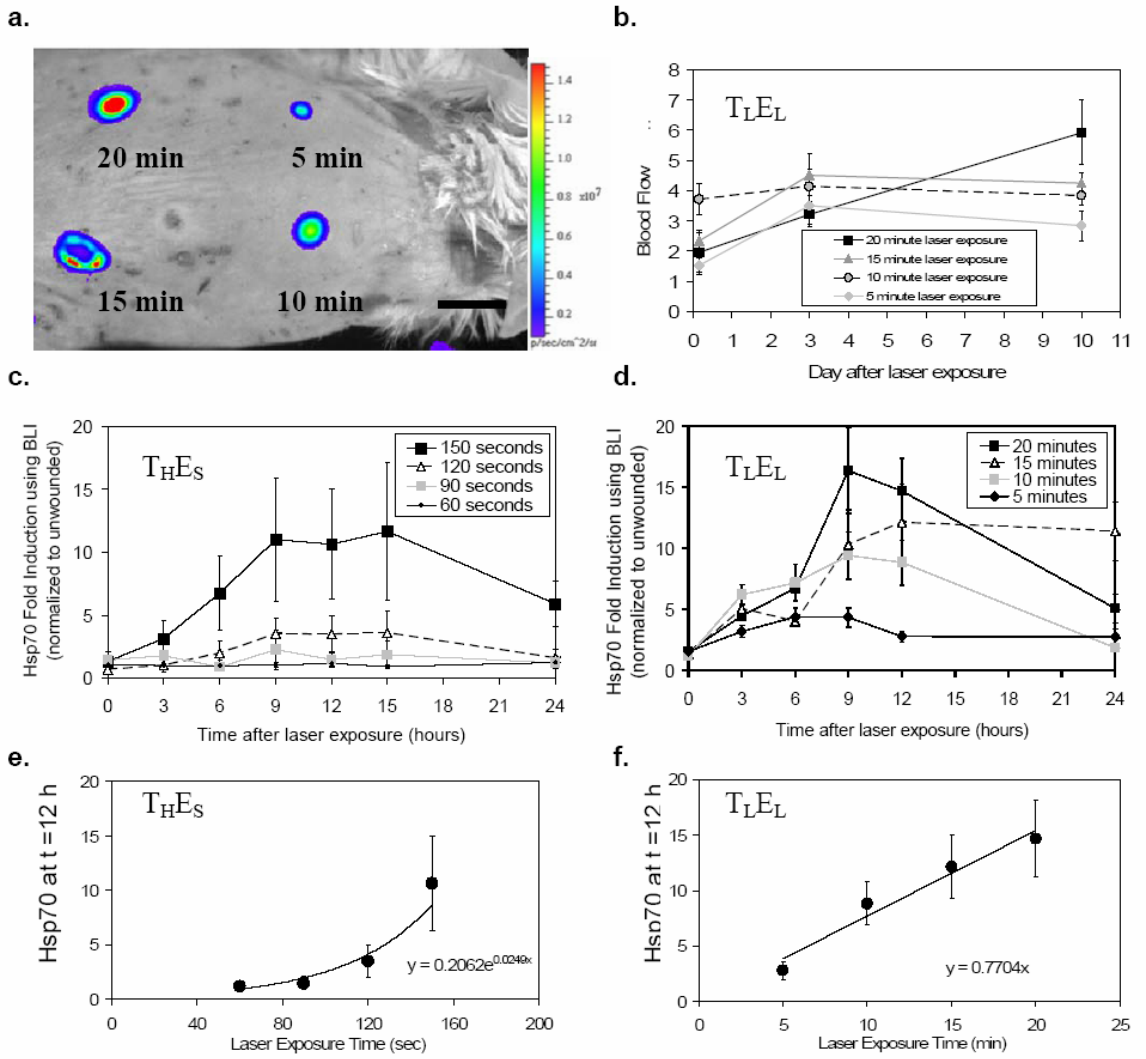

Figure 5.3. ***In vivo*** **Visualization and Quantification of hsp70 promoter activity in laser treated areas. (a)** Sample bioluminescent image 12 h after laser preconditioning **(b)** Normalized mean blood perfusion measurements versus time for various laser exposures using the T_LE_L laser protocol (n=4). **(c)** hsp70 levels plotted versus time after laser exposure for the T_HE_S laser protocol. **(d)** hsp70 levels plotted versus time after laser exposure for the T_LE_L laser protocol. **(e)** Maximum hsp70 fold induction for T_HE_S protocol and **(f)** T_LE_L protocol (R^2 = 0.96). Values represent the mean and standard deviation for hsp70 fold induction (n=5).

5.4.8. Histologic studies to evaluate preconditioning protocols

Immunohistologic studies were conducted in preconditioned mouse skin to evaluate histological damage, cellular proliferation, and apoptosis. **Figures 5.4(a-d)** and **5.4(e-h)** reveal marked differences in the histological characteristics among the 4 treatment groups at 12 h and 3 d. Control tissue is illustrated in **Figure 5.4(a,e)** show healthy intact mouse skin. The lethal laser protocol (positive control; **Figure 5.4(b,f)** produced tissue damage to a depth of 150 μm. Tissue treated with the T_LE_L preconditioning protocol showed minor damage only to the stratum corneum [**Figure 5.4(c and g)**]. In contrast, the T_HE_S protocol induced mild damage as evidenced by epidermal hyperplasia and a modest inflammatory infiltrate in the papillary dermis [**Figure 5.4(d)**]. **Figures 5.4(e-h)** also reveal marked differences in histological characteristics among the four treatment groups. The most noticeable difference 3 d post-treatment was the degree of epidermal hyperplasia. The thickness of the epidermis hyperplasia was plotted versus time for each treatment group [**Figure 5.4(i)**]. The data show that the T_LE_L protocol induced less epidermal hyperplasia than the T_HE_S protocol. Pronounced epidermal hyperplasia, a characteristic of the intermediate phase of wound repair, suggesting that the T_LE_L protocol produced less epidermal injury than the T_HE_S protocol [34].

The extent of cellular proliferation was examined using a Ki67 immunodetection [**Figures 5.5(a-d)**], and apoptosis was evaluated with a TUNEL stain in tissues from the T_LE_L protocol [**Figures 5.5(e-f)**]. There was substantial proliferation in the basal cells and in the bulge region around the hair follicle in the preconditioned tissues [**Figure 5.5(a) and 5(c)**]. While the control tissue (untreated) showed few basal cells actively replicating or proliferating [**Figure 5.5(b) and 5.5(d)**]. Laser preconditioned tissues did not show apoptotic activity [**Figure 5.5(e,f)**]. Caspase-3 antibody stains were also conducted and also show minimal evidence of apoptosis (data not shown).

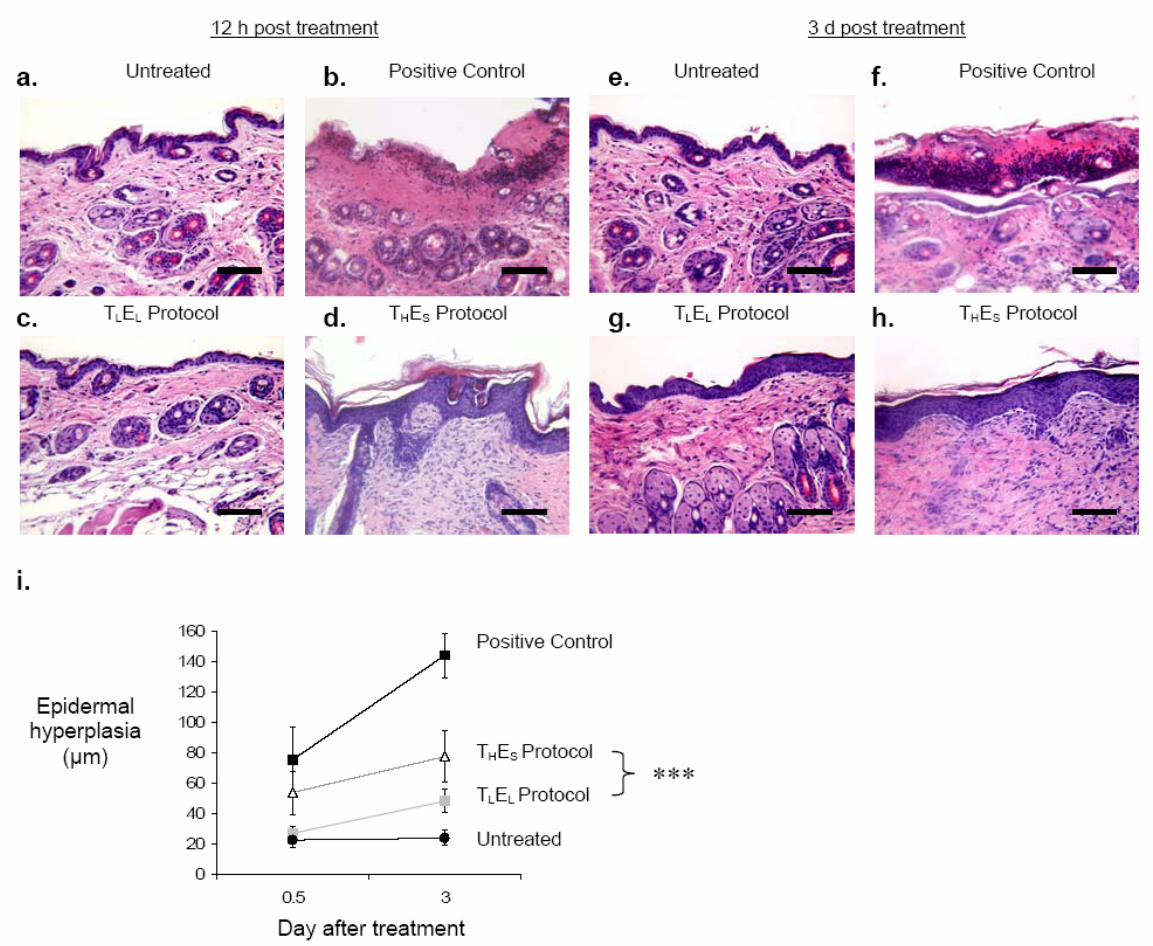

Figure 5.4. Immunohistochemical Evaluation of Preconditioning Protocols on intact mouse skin. (a-d) H & E stains 12 h post treatment (bar = 100 μm) **(a)** Untreated control tissue shows a healthy epidermis and hair follicles. **(b)** Positive control using lethal laser protocol shows ablation of the epidermis and coagulation in the upper dermis. **(c)** T_LE_L preconditioning protocol shows only minor superficial damage restricted to the stratum corneum. **(d)** T_HE_S protocol induces mild damage that stimulates an epidermal hyperplasia and inflammatory influx into the upper dermis. **(e-h)** H & E stains 72 h post treatment **(e)** Untreated control tissue shows a healthy epidermis. **(f)** Positive control using lethal laser protocol epidermal ablation and coagulation on the upper dermis. **(g)** T_LE_L preconditioning protocol shows only minor epidermal hyperplasia. **(h)** T_HE_S protocol induces mild damage that stimulates significant epidermal hyperplasia. **(i)** Epidermal hyperplasia plotted versus time for each laser treatment. Mean and standard deviations for depth of hyperplasia were statistically compared with a student's t-test (******* = $P < 0.001$)

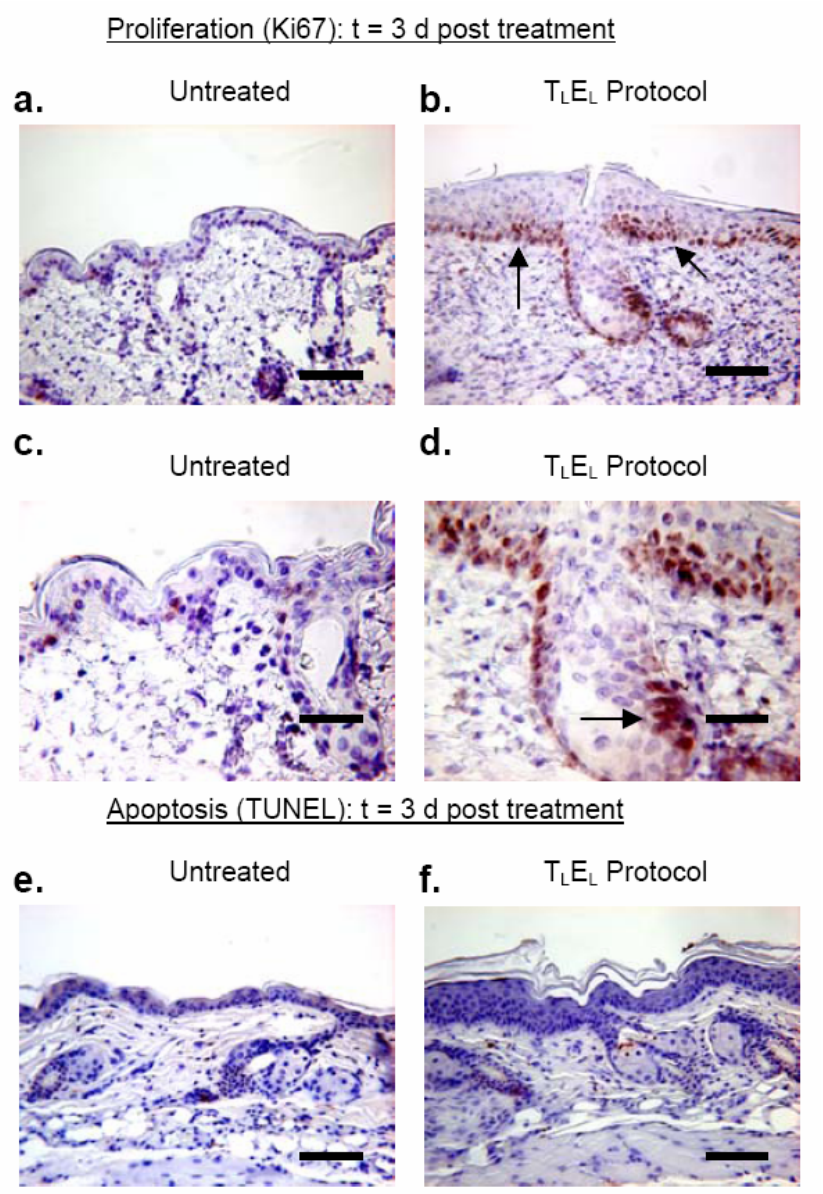

Figure 5.5. Immunohistochemical Studies to Evaluate Preconditioning Protocols.
(a-d) Cellular proliferation using a Ki67 immunomarker 3 d after laser induced thermal stress. **(a)** Control (non-wounded) areas of skin show minimal steady state levels of epidermal proliferation (bar = 100 μm) **(b)** Laser treated (T_LE_L) tissue shows many basal cells actively replicating or proliferating (marked by arrow) (bar = 100 μm) **(c-d)** Ki67 immunostain (bar = 50 μm). **(c)** Control (non-wounded) areas of skin show minimal proliferation. **(d)** Laser treated (T_LE_L) tissue shows transient amplifying cells emerging from the bulge region (marked by arrow). **(e-f)** Apoptotic profiles are visualized with a TUNEL stain at day 3. **(e)** Laser treated (T_LE_L). **(f)** Control skin samples with no visible apoptotic figures.

5.4.9. Laser preconditioning protocols can manipulate hsp70 expression

We investigated the effects of the T_LE_L laser preconditioning protocol on full thickness scalpel incisions. **Figure 5.6(a)** presents a sample bioluminescent image of hsp70 promoter activity on a mouse with two preconditioned wounds (Right) and two control scalpel incisions (Left). The laser preconditioned wounds showed much higher hsp70 promoter activity. **Figure 5.6(b)** shows the quantitative bioluminescent intensity for each wound 12 h after preconditioning. Laser preconditioned areas had average inductions of 10.75 ± 3.03 while the control areas had averages of 1.72 ± 0.15. A paired one-tailed student t-test indicated that the thermally preconditioned wounds had statistically significantly higher levels of hsp70 promoter activity ($p < 0.01$).

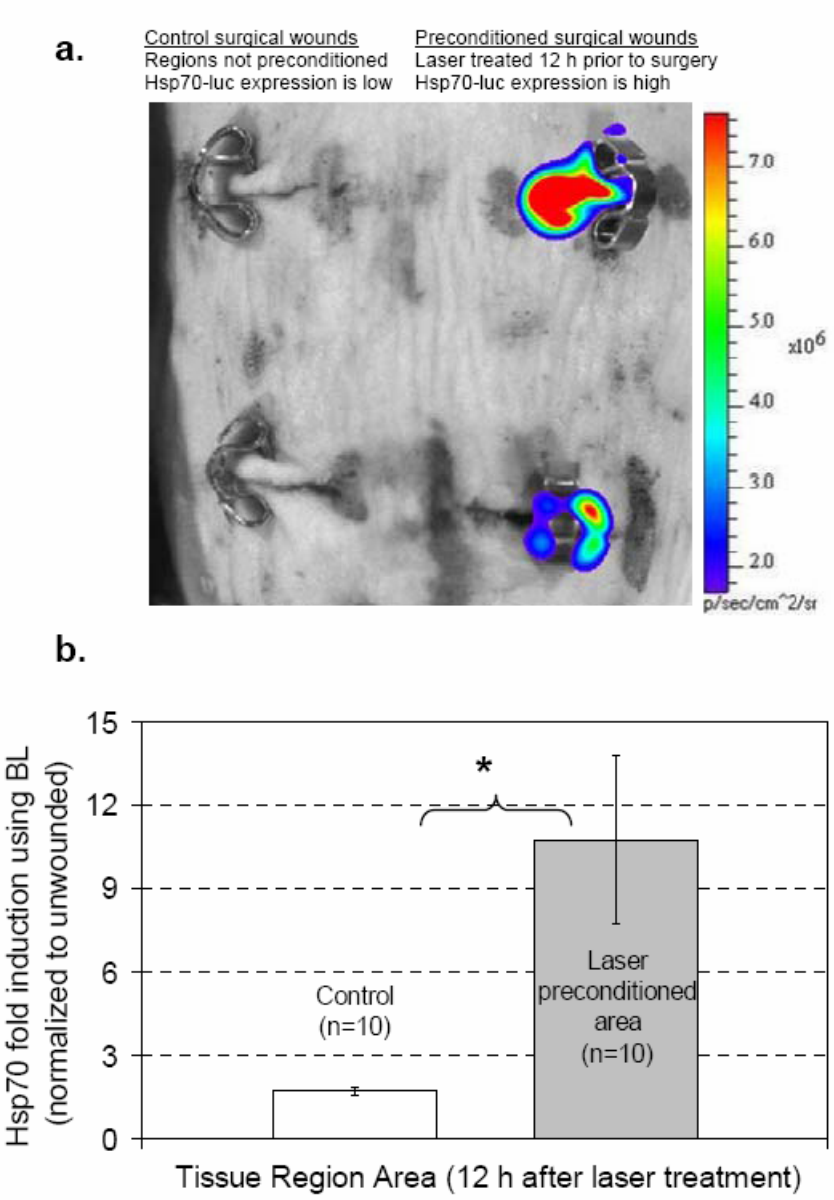

Figure 5.6. Laser Manipulation of hsp70 Expression Before Surgical Wounding. (a) Sample bioluminescent representation of control wounds (left) and laser pretreated surgical wounds (right) using the T_LE_L laser protocol at 12 h post surgery. **(b)** hsp70 Fold Inductions on control and laser pretreated wounds. Ten regions were imaged for each condition and the mean hsp70-fold induction was normalized to non-wounded control area of skin. The mean and standard deviations for hsp70 fold induction were statistically compared using a student t-test (n=10, * = P <0.01).

5.4.10. Histologic characterization of incisional healing following laser preconditioning

To evaluate the affect that laser preconditioning (T_LE_L) has on early wound repair, qualitative patterns of collagen deposition were assessed after scalpel incision. In sections stained with Gomori trichrome, wounds that were not preconditioned show pale green staining in the adjacent tissue that is indicative of a wide degree of disruption to the collagen deposition patterns in the dermis immediately adjacent to the incisional site [**Figure 5.7(a)**]. Wounds preconditioned with the T_LE_L laser protocol show intense green staining indicative of normal non-disrupted collagen deposited patterns [**Figure 5.7(b)**]. Additional differences were evident between the non-preconditioned and preconditioned wounds within the surface epithelium [**Figure 5.7(c-d)**]. Preconditioned wounds showed significantly less epidermal hyperplasia (31.9 ± 1.7 μm) than control wounds (75.2 ± 6.2 μm) [**Figure 5.7(e)**] ($p<0.001$). Granulation tissue in the preconditioned incisional wound beds also had a higher cell density (~19 cells/1000 μm^2) compared to control wounds (~10 cells/1000 μm^2) [**Figure 5.7(f)**] ($p<0.001$).

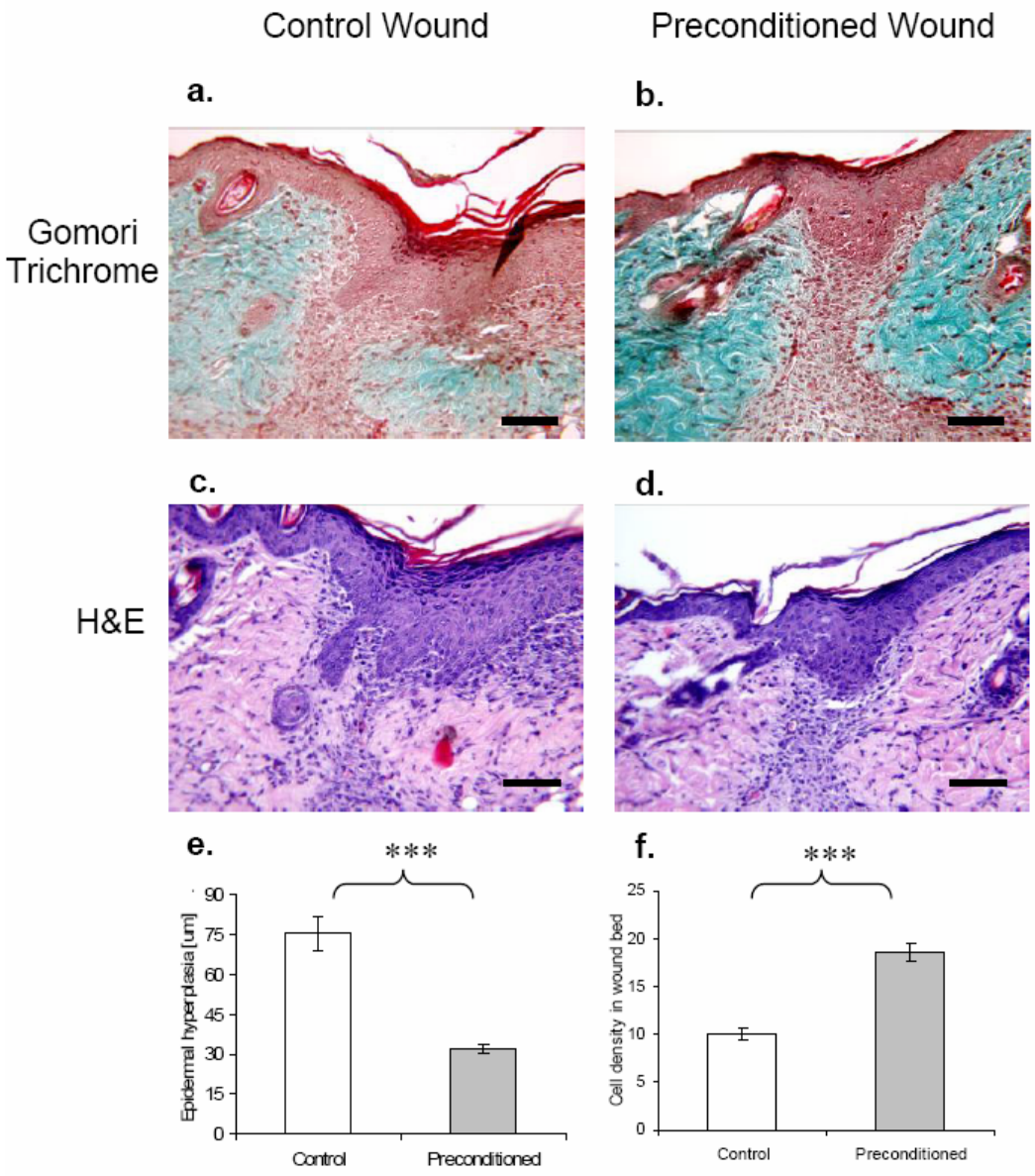

Figure 5.7. Collagen Deposition and Cellularity in Surgical Preconditioned Wounds
(a-b) Gomori trichrome staining 5 d post-incision **(a)** Control wounds reveal major disruption and only pale staining adjacent to the incisional track of non-preconditioned incisions. **(b)** Preconditioned wounds show normal intense green patterns of collagen in the adjacent dermis. **(c-d)** Hemotoxlyin and Eosin staining 5 d post-surgery **(c)** The surgical wound without preconditioning shows epidermal hyperplasia adjacent to the wound margin and a minimal cellular density in the granulation tissue within the wound bed. **(d)** A laser preconditioned surgical wound shows normal adjacent epidermis but a comparatively more robust granulation tissue within the wound bed (bar = 100 μm). **(e)** Plot of epidermal hyperplasia over the incision and in immediate adjacent epidermis. Preconditioned surgical wounds have significantly less epidermal hyperplasia than controls, an indicator of enhanced repair. **(f)** Plot of cell density within each wound bed per 1000 μm^2. The mean and standard deviations were statistically compared using a student's t-test (******* $p < 0.001$ and $n=20$).

5.4.11. Laser preconditioning improves wound repair

To compare the difference in wound healing between untreated and laser preconditioned scalpel incisions in normal and diabetic mice, we measured the maximum load and tensile strength of full-thickness wound skin from mice (n=9) at days 7 and 10 after injury [**Figure 5.8(a)**]. The average percent (%) increase in maximum load is plotted versus day post surgery. In the normal mice, preconditioned incisions were 60 % stronger than controls 7 days post surgery and 40 % stronger than controls at day 10. Preconditioned incisions in diabetic mice were unhealed by day 7, but were 10 % stronger by day 10. In **Figure 5.8(b)** the average percent increase (%) in tensile stress is plotted versus day post surgery. Preconditioned incisional wounds were 70% (58 ± 13%, Mean ± SD) stronger than controls 7 days post surgery, and 50% stronger than controls at day 10. Preconditioned incisions in diabetic mice were 10 % stronger by day 10. Mean scores for the maximum load and tensile stress were statistically significant compared using a paired student's t-test (*** $p < 0.01$, ** $p < 0.05$, and $n = 9$).

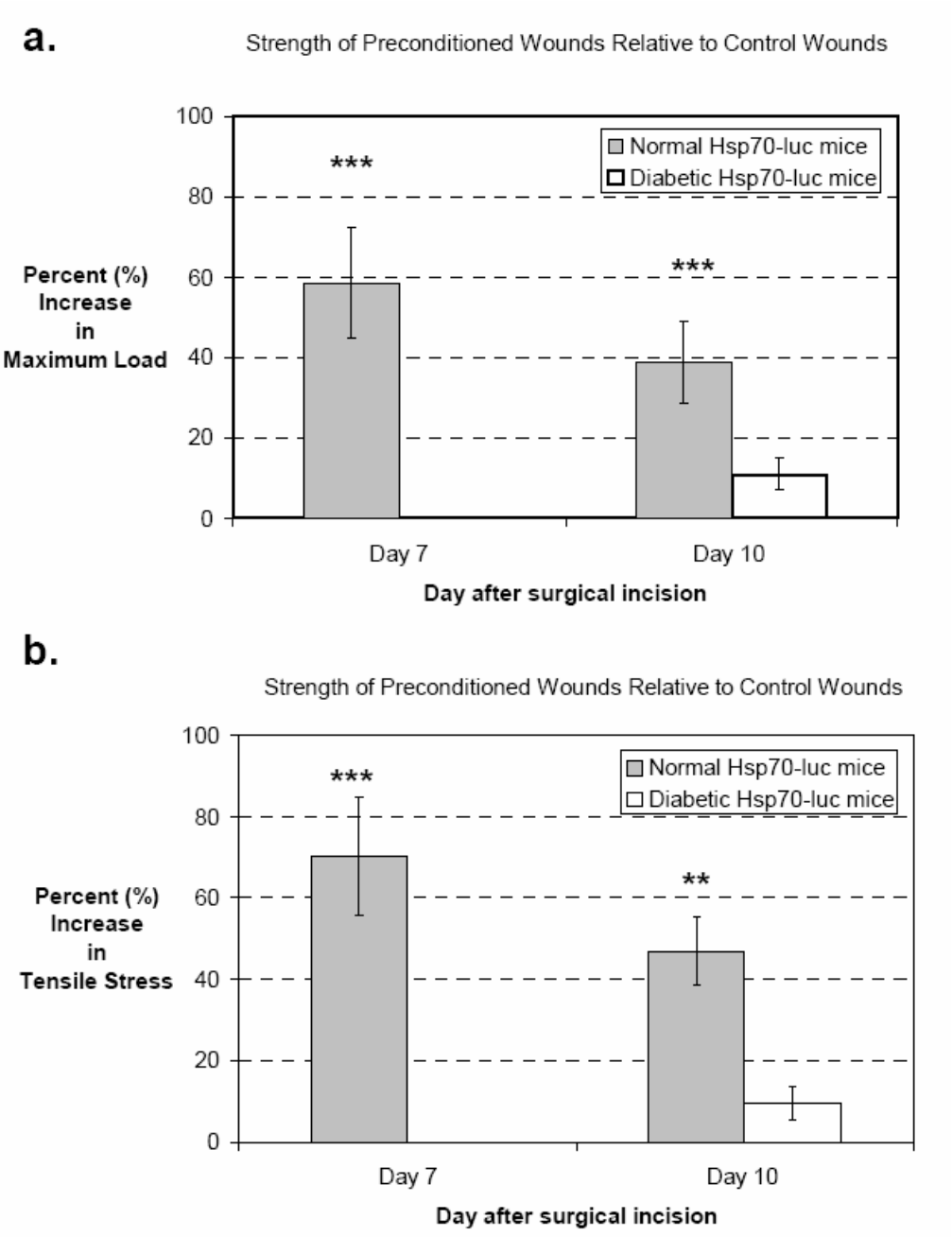

Figure 5.8. Laser Preconditioning Protocol Enhancements to Wound Repair. Tensiometer data for full-thickness wounds from transgenic mice (n=9) and diabetic mice (n=6) at days 7 and 10 after injury. (a) Average percent (%) increase in maximum load is plotted versus day post surgery (b) Average percent increase (%) in tensile stress is plotted versus day post surgery. The preconditioned incision wounds were ~60% (58 ± 13%, Mean ± SD) stronger than controls 7 days post surgery, and ~35% stronger than controls at day 10. Preconditioned surgical wounds on diabetic mice achieved only a 10 % increase in wound strength at day 10. Diabetic wounds were not healed enough for tensiometry at day 7. The mean and standard deviation for the max load and tensile stress were statistically compared using a paired student's t-test (*** $p < 0.01$, ** $p < 0.05$, and $n = 9$).

Table 5.1. Thermal preconditioning protocols to maximally induce Hsp70 Expression

Low-Temperature Long Duration (T_LE_L)				High-Temperature Short Duration (T_HE_S)			
Model:Type	Temperature (°C)	Exposure time (min)	Citation	Model:Type	Temperature (°C)	Exposure time (min)	Citation
Animal: mouse	41 °C	15 min	(Pespeni, Hodnett et al. 2005)	Cell: BAEC	48 °C	2 min	(Rylander, Diller et al. 2005)
Animal: rat	42-42.5 °C	15 min	(Leger, Smith et al. 2000)	Animal: Rat	50°C	3 sec	(Souil, Capon et al. 2001)
Cell: rat cardiac	42 °C	30-60 min	(Vigh, Literati et al. 1997)	Cell: NIH-3T3	50 °C	35 sec	(O'Connell-Rodwell, Shriver et al. 2004)
Cell: NHDF	43 °C	20-40 min	(Wilmink, Opalenik et al. 2006)	Cell: BAEC	50 °C	1 min	(Rylander, Diller et al. 2005)
Cell: BAEC	44 °C	22 min	(Rylander, Diller et al. 2005)	Cell: RPE	55 °C	3 sec	(Dinh, Zhao et al. 2001)
Tissue: (RAFT)	44 °C	20 min	(Wilmink, Opalenik et al. 2006)	Cell: NHEK	55 °C	4 sec	(Bowman, Schuschereba et al. 1997)
Cell: NIH-3T3	44 °C	40 min	(Beckham, Mackanos et al. 2004)	Cell: NHEK	58 °C	1 sec	(Dinh, Zhao et al. 2001)

Table 5.2. Comparison of Arrhenius Damage Parameters versus published values

Biological Level	Sample	Endpoint for Damage (Method)	Frequency factor (A) $\langle s^{-1} \rangle$	Activation Energy (E_A) <J/mol>	Citation
Tissue	Artery	Visible whitening	5.6×10^{53}	4.3×10^{5}	(Agah, Pearce et al. 1994)
Tissue	Cartilage	Cell viability (%)	1.2×10^{70}	4.5×10^{5}	(Diaz, Nelson et al. 2003)
Cell	MDF	Cell Viability (%)	2.4×10^{74}	4.7×10^{5}	Figure 5.1.
Cell	BAEC	Cell Viability (%)	4.1×10^{58}	4.1×10^{5}	(Rylander, Diller et al. 2005)
Macromolecule (Protein)	25% albumin	Denaturation/whitening	3.2×10^{56}	3.8×10^{5}	(McNally 1999)
Macromolecule (Protein)	60% albumin	Denaturation/whitening	3.5×10^{57}	3.9×10^{5}	(McNally 1999)
Gene	MDF	Hsp70 via BLI	8.4×10^{45}	3.0×10^{5}	Figure 5.1.
Gene	NIH 3T3	Hsp70 via BLI	7.0×10^{282}	1.7×10^{6}	(Beckham, Mackanos et al. 2004)

5.5. Discussion

In this report we developed a laser preconditioning protocol that enhances cutaneous wound repair in a murine model. The laser protocol was optimized using temperature, hsp70 expression, blood perfusion, and immunohistochemical measurements as benchmarks. The methods and mouse model (*hsp70A1-luc)* used in the design of this protocol have broader implications since they provide the framework that is required to systematically design therapeutic protocols for a clinical setting.

Tissue preconditioning has been shown to induce tissue alterations that confer protection to subsequent damage. Thermal preconditioning appears to act, at least in part, by means of elevated heat shock proteins. Thermal preconditioning has had a favorable impact on surgical intervention [20, 35], recovery of thermally injured tissues [21-23], protection to ischemia reperfusion injury [24-26], and in cancer therapies [27, 28]. Thermal preconditioning is reported to provide numerous effects on cells and tissues: (1) Increased resistance and survivability when exposed to subsequent lethal thermal stresses [14]; (2) Cross-protection to subsequent different stressors (ie. mechanical stress in surgical intervention) [36]; (3) Increased protective responses upon exposure to subsequent stresses: increased cell migration and proliferation, reduced inflammation, and reduced apoptosis [17, 18, 37, 38]; and (4) Improved cutaneous wound repair [39].

Physical and pharmacological techniques are the main methods used to upregulate HSP expression and precondition tissues. Recent pharmacological agents, Bimoclomal (Cytrx Corp, San Diego) and Geldanamycin, show clinical promise but due to their non-specific actions and multiplicity of biochemical effects, are still considered inferior to traditional physical methods [39, 40]. Whole body hyperthermia, using a heated pad or water bath, is the classic physical preconditioning method. Since this

method elevates HSP expression in all tissues a frequent complication associated with this approach is excessive tissue dehydration [41]. Work by Harder et al circumvented these complications by using a heated blanket to locally induce HSP expression in restricted skin, and this technique improved skin flap survival in pigs [42]. Heated blankets are attractive because they are simple and inexpensive, but they rely on the diffusion of heat and require lengthy preconditioning sessions which are not conducive to the time constraints of a clinical setting. Non-contact physical methods, such as focused ultrasound, radiofrequency, and microwave sources, also show promise since they can induce rapid and focused HSP induction in deep tissues [43, 44]. However, in applications targeting superficial skin, lasers are ideal since they also allow for rapid and focused induction without effecting deeper tissues [45].

In this study a pulsed infrared (IR) diode laser was used to precondition tissues. The use of lasers for this purpose is advantageous for several reasons. First, lasers can heat tissue volumetrically, rather than depending on heat diffusion from contact to a heating element. Second, the operating parameters of the laser (λ, τ_p, H, repetition rate) can be selected to achieve the desired depth to which light is absorbed and hence tissue is heated. This allows for precise control over the spatial distribution of thermal induction and accurate dosimetry. For the work reported the output laser wavelength was fixed at 1.85 μm. At this wavelength the optical penetration depth in water (the main chromophore in soft tissue) is roughly 600 μm [46]. However, since the laser is tunable from 1.85-1.88 μm, which corresponds to a steep part of the water absorption curve, this tunability permits precise control over the depth of tissue heating. Since mouse skin is 200-300 μm thick, this laser could effectively heat the entire dermis allowing for the restricted induction of hsp70 expression. Third, the laser light can be coupled into a fiber optic cable, facilitating delivery to internal tissues, thus the findings could be extended to endoscopic surgery. This characteristic is particularly attractive and makes the

described system amenable to various clinical situations, such as in the area of cardiac research [24-26].

Criteria for Developing Effective Preconditioning Protocols

We postulated that a successful laser preconditioning protocol designed to enhance the repair of surgical wounds must achieve the following criteria: 1) elevate tissue temperature for prescribed exposure duration, 2) induce hsp70 levels in the tissue, 3) cause minimal irreversible tissue damage and cell death, 4) increase blood flow to the surgical site, and 5) increase tissue strength.

Many *in vitro* and *in vivo* studies have investigated hsp70 expression kinetics at various stress temperatures and exposure durations. After reviewing the literature, it appears that two general thermal regimens exist; one using high temperatures for a short duration and the other using lower temperatures for a longer exposure duration [14, 47], summarized in **Table 5.1**. Based on these data we developed and tested two separate laser preconditioning protocols from each thermal regimen; a low-temperature long-duration protocol (T_LE_L) and a high-temperature short-duration protocol (T_HE_S). The tissue temperatures generated by each protocol were measured in real-time using an IR camera, and these measurements proved to be critical in the optimization of each protocol. In a clinical setting, temperature measurements may not be possible, and instead temperatures could be predicted before protocol inception using thermal modeling [27].

In an effort to better understand the magnitude and timing of hsp70 induction, our group has developed *hsp70A1-luc* reporter gene constructs, and we have incorporated this construct in cells and tissue equivalents [4, 7, 8]. Using the same reporter gene construct affords us with the ability to accurately extrapolate information from cells to tissues. We previously investigated the hsp70 kinetics in human skin cells (eg.

fibroblasts, keratinocytes, melanocytes) and found that the peak expression occurred 8-12 h after heat shock. These studies also showed that magnitude of hsp70 expression increased with increased exposure temperatures [8]. In order to compare our results, and considering that hsp70 expression kinetics are tissue specific, we investigated the hsp70 expression kinetics of dermal fibroblasts derived from the *hsp70A1-luc* transgenic mouse. Mouse dermal fibroblasts were selected for the *in vitro* studies because they are the chief dermal cell and are critical to wound repair. In this report, we found that in the mouse fibroblasts, hsp70 expression was maximal using a temperature of 43°C and decreased using exposure temperatures of 44°C. In contrast, in our previous study the human fibroblasts showed higher hsp70 expression at 44°C as compared to 43 °C [8]. Apparently, human fibroblasts can withstand higher thermal stress than mouse dermal fibroblasts, as the viability of murine fibroblasts is decreased with thermal regimens of 44°C for over 30 minutes. Although the stress response differences between human and mouse fibroblasts are subtle this information is critical for developing accurate human clinical protocols.

After determining the laser parameters which generate optimal temperatures for both thermal protocols, the next step was determining the exposure duration which would achieve maximal hsp70 expression. Maximal hsp70 expression was assessed with a transgenic mouse that is equipped with a bioluminescent reporter gene (luciferase), under control of a heat activated promoter (*hsp70a1*). This novel full system model affords us with a high throughput platform that allows us to test the affect that different laser parameters have on hsp70 expression. For the T_LE_L laser preconditioning protocol, hsp70 levels increased linearly with increasing laser exposure duration. Surprisingly, linear increases were not shown using the T_HE_S laser protocol. The data show that peak hsp70 levels of 11.65 are induced with the 150 s exposure and shorter 120 s exposures only achieved 4-fold induction. The large disparity in hsp70 levels

between exposure durations suggested that the T_HE_S laser protocol was more difficult to tailor for specific hsp70 levels. In summary, for the T_LE_L laser preconditioning protocol any exposure between 10-20 minutes induces sufficient hsp70 levels (~10 fold); while, for the T_HE_S protocol exposures greater than 120 seconds were required to fulfill the hsp70 requirement. In future studies, the hsp70 expression kinetics will be examined using empirical models. Empirical models use mathematical expressions to describe the kinetics of a particular system, and one such expression is the Arrhenius relationship. The Arrhenius relationship predicts that tissue injury is linearly proportional to the time of exposure and exponentially dependent on temperature [48]. The Arrhenius relationship assumes a biophysical process and recently was demonstrated to be useful in examining hsp70 expression kinetics [4]. The underlying principle that governs the Arrhenius model may be useful in optimizing proper combinations of temperature and time. An Arrhenius analysis was conducted for our *in vitro* experiments and is provided in **Figure 5.1** and compared to published values in **Table 5.2**. Herein, we sought to measure the Arrhenius parameters, as previously described in [8, 35] using both cell viability and Hsp70 expression as endpoints of damage. The values that we measured using both methods are provided in **Figure 5.1(d**) and are compared to published values in the literature in **Table 5.2**. For the temperatures tested, the values are comparable to other cell experiments using similar methods (**Table 5.2**). The different values that were generated for A and E_a appears to be alarming and demonstrate an inconsistency in the data. But the differences in values can be accounted for due to use of different methods (cell viability vs. Hsp70-luc expression) to measure the damage. Wright examined the relationship between Arrhenius parameters and found that published values in the literature are linearly correlated. In fact, he found that slightly different regression lines exist for proteins compared to tissues. For proteins he found that using literature values that E_a = 2610 ln (A) + 26200 and for cells that E_a = 2642 ln (A) + 17200 [38]. The data

we generated in this study agree with these linear regression lines and are consistent with the data seen in the literature [38]. More importantly, it confirms that the methods used can be used to predict damage and to improve our preconditioning methods.

Arrhenius damage values depend greatly on the biological level investigated (eg. tissue, cell, gene activity), the endpoint method, and the sensitivity of the damage endpoint method (eg. cell viability measured using fluoremetric techniques versus ethidium bromide). For instance, a method which uses the visual measurement of tissue whitening is less sensitive than a method which extracts the cells and uses methods to assess cell viability [49]. Our *in vivo* laser preconditioning data shows that using T = 43-44 °C we saw linear increases in Hsp70 expression in proportion to exposure time [**Figure 5.3(f)**], while the higher temperature protocol did not have linear increases [**Figure 5.3(e)**]. It appears that Arrhenius relationships are valid at lower temperatures but are difficult to model for higher temperatures where the temperature is not constant (isothermal conditions no longer apply).

For maximum effectiveness, laser preconditioning protocols must induce hsp70 expression while causing minimal irreversible tissue damage and cell death. All of the exposure times tested using the T_LE_L laser preconditioning protocol exhibited sufficient hsp70 levels while inducing minimal cellular damage. In contrast, the T_HE_S protocol only had sufficient hsp70 levels using a 150 second exposures, and this exposure duration induced unwanted tissue damage and epidermal hyperplasia. Therefore, the T_LE_L laser preconditioning protocol was determined to be superior and was selected for use in the surgical wound repair experiments. Irreversible thermal tissue damage is observed macroscopically as tissue whitening. This occurs when extracellular matrix proteins are coagulated causing visible light to be scattered and subsequently reflected, and the phenomenon is reported to occur after exposure to 65°C for 35 s [49]. In this study, the laser delivered positive control was selected to generate temperatures that whitened the

mouse skin. The positive control served as a useful indicator for irreversible thermal damage and was used to compare the ensuing tissue effects in the preconditioned regions of tissues.

Cell death can occur in a regulated way through apoptotic mechanisms or in an abrupt way by means of necrosis. It has been reported that severe injury causes immediate cell death, while cells that experience moderate damage take days to succumb to the insult [26]. The *in vitro* experiments in this report demonstrated that ten minute exposures at higher temperatures (44°C) induced cell proliferation, and this is indicated by cell viability values being greater than 100%. The T_LE_L laser preconditioning protocol, which also generates a T= 44°C for a 10 minute duration induced sufficient cellular proliferation. Apoptosis stains also confirmed that the T_LE_L protocol caused only slight increases in apoptosis activity. Although we use hsp70 expression in this study as a benchmark indicator of the preconditioning effect, various other investigations have indicated that elevated hsp70 expression plays a role in blocking stress induced apoptosis. Hsp70 blocks apoptosis by antagonizing apoptosis inducing factor [50], preventing the recruitment of procaspase-9 [51], and by preventing the activation of stress kinases [38]. Moreover, since the T_LE_L protocol does not preferentially activate only heat shock protein (HSP) genes, other non-HSP genes may also be responsible for the survival advantage observed. Most of these non-HSP genes function either in signal transduction or in cell growth pathways. For instance, the MAP kinase pathway plays a central role in signal transduction pathways and it may contribute to the increased survivability of pretreated cells [47]. Since MAP kinases phosphorylate HSF-1, and sufficient levels of HSF-1 are required for maximal hsp70 transcription, their stimulated activity is coupled to hsp70 expression. The phosphatases DUSP1 and DUSP2 are also activated by thermal stress, and may contribute to the observed survival advantage [52, 53]. It has been hypothesized that subsequent expression of DUSP phosphatases allow

the MAP kinase pathway to “reset” thus rendering the cells responsive to subsequent stressors after an initial thermal stress [53]. Even though the mechanism is not elucidated in this report, the expected correlation between elevated hsp70 expression and reduced apoptosis is observed.

Local hyperthermia can increase the blood flow to treated regions, and this immediate increase in blood flow that is observed after the T_LE_L laser preconditioning treatment may aid in the delivery of cells and growth factors to pretreated surgical sites [33]. Other studies indicate that the increased blood flow observed in preconditioned tissues may be due to increases in iNOS [54]. The increased delivery of macrophages may correlate with increased wound debridement and enhanced cutaneous repair. The increased supply of various growth factors and cytokines, such as bFGF, VEGF, TGF-β [55-57], may also function to enhance the repair of a preconditioned wound. It has been reported that the bFGF gene is upregulated during thermal exposures, and VEGF and TGF-β levels are upregulated after thermal exposures [55-57]. Since these genes are important in active wound repair they may also contribute to the survival advantage observed in laser preconditioned tissues.

In this study, the T_LE_L laser preconditioning protocol was demonstrated to improve the strength of wound repair in normal wounds. Preconditioned wound beds showed higher cell densities than control wound, and this increase in cells may confer a more concerted and robust repair process. The exact role that hsp70 plays in preconditioning is still not entirely clear, and preconditioning may in fact be dependent or at least co-dependent on increased blood flow, increased presence of growth factors, and the reduced apoptotic activity. Ongoing investigations in our lab show that the affect of preconditioning is dramatically reduced in hsp70 null cells [58]. The methods used in this report will be tested on our hsp70 knockout mouse, and this work will provide definitive evidence of the role that hsp70 plays in preconditioning.

In summary, in this report a laser preconditioning protocol was optimized using thermal infrared and optical imaging measurements as benchmarks. Two laser protocols were investigated a low-temperature long-duration protocol (T_LE_L) and a high-temperature short-duration protocol (T_HE_S). Both protocols were capable of achieving sufficient hsp70 expression levels, but the T_HE_S laser protocol required a 150 second exposure duration. This exposure duration induced significantly more epidermal hyperplasia than suitable exposures using the T_LE_L protocol, and therefore T_LE_L protocol was found to be superior for laser preconditioning. The T_LE_L laser protocol induced minimal histological damage, demonstrated a positive impact on cellular proliferation while causing minimal apoptosis. The T_LE_L laser preconditioning protocol was useful in stimulating wound repair by enhancing cell migration into the wound bed, and resulted in increased wound tensile strength. We speculate that this method can be used to improve repair in a chronic wound, like those in diabetic patients. In normal conditions of wound repair, the processes that result in cutaneous healing follow a specific time course, but conditions created in diabetes impair the normal sequence of wound repair [59]. In normal wound repair, hsp70 is rapidly induced but in the chronic wound setting, hsp70 is decreased [60]. This developed laser preconditioning protocol may be useful in inducing hsp70 expression and may improve diabetic wound repair.

5.6. Works cited

1. Morimoto, R.I., P.E. Kroeger, and J.J. Cotto, *The transcriptional regulation of heat shock genes: a plethora of heat shock factors and regulatory conditions.* Exs, 1996. **77**: p. 139-63.
2. Kabakov, A.E. and V.L. Gabai, *Heat shock proteins and cytoprotection : ATP-deprived mammalian cells*. 1997, New York: Springer. 237 p.
3. Richard, V., N. Kaeffer, and C. Thuillez, *Delayed protection of the ischemic heart--from pathophysiology to therapeutic applications.* Fundam Clin Pharmacol, 1996. **10**(5): p. 409-15.
4. Beckham, J.T., et al., *Assessment of cellular response to thermal laser injury through bioluminescence imaging of heat shock protein 70.* Photochem Photobiol, 2004. **79**(1): p. 76-85.
5. Pockley, A.G., *Heat shock proteins, inflammation, and cardiovascular disease.* Circulation, 2002. **105**(8): p. 1012-7.
6. Desmettre, T., C.A. Maurage, and S. Mordon, *Heat shock protein hyperexpression on chorioretinal layers after transpupillary thermotherapy.* Invest Ophthalmol Vis Sci, 2001. **42**(12): p. 2976-80.
7. O'Connell-Rodwell, C.E., et al., *A genetic reporter of thermal stress defines physiologic zones over a defined temperature range.* Faseb J, 2004. **18**(2): p. 264-71.
8. Wilmink, G.J., et al., *Assessing laser-tissue damage with bioluminescent imaging.* J Biomed Opt, 2006. **11**(4): p. 041114.
9. Diller, K.R., *Stress protein expression kinetics.* Annu Rev Biomed Eng, 2006. **8**: p. 403-24.
10. Wilmink, G.J., et al. *Wavelength-dependent dynamics of heat shock protein 70 expression in free electron laser wounds*. in *Thermal Treatment of Tissue: Energy Delivery and Assessment IV*. 2007. San Jose, CA: Proceedings of SPIE.
11. Li, Y., et al., *Retinal preconditioning and the induction of heat-shock protein 27.* Invest Ophthalmol Vis Sci, 2003. **44**(3): p. 1299-304.
12. Kim, J.M., et al., *Effect of thermal preconditioning before excimer laser photoablation.* J Korean Med Sci, 2004. **19**(3): p. 437-46.
13. Topping, A., et al., *Successful reduction in skin damage resulting from exposure to the normal-mode ruby laser in an animal model.* British Journal of Plastic Surgery, 2001. **54**(2): p. 144-150.
14. Bowman, P.D., et al., *Survival of human epidermal keratinocytes after short-duration high temperature: synthesis of HSP70 and IL-8.* Am J Physiol, 1997. **272**(6 Pt 1): p. C1988-94.
15. Ritossa, F., *A new puffing pattern induced by temperature shock and DNP in Drosopholia.* Experiantia, 1962. **15**: p. 571-3.
16. Wynn, R.M., et al., *Molecular chaperones: heat-shock proteins, foldases, and matchmakers.* J Lab Clin Med, 1994. **124**(1): p. 31-6.
17. Samali, A. and T.G. Cotter, *Heat shock proteins increase resistance to apoptosis.* Exp Cell Res, 1996. **223**(1): p. 163-70.
18. Mosser, D.D., et al., *Role of the human heat shock protein hsp70 in protection against stress-induced apoptosis.* Mol Cell Biol, 1997. **17**(9): p. 5317-27.
19. Jaattela, M., et al., *Major heat shock protein hsp70 protects tumor cells from tumor necrosis factor cytotoxicity.* Embo J, 1992. **11**(10): p. 3507-12.
20. Snoeckx, L.H., et al., *Heat shock proteins and cardiovascular pathophysiology.* Physiol Rev, 2001. **81**(4): p. 1461-97.

21. Seppa, L., A.L. Hanninen, and M. Makarow, *Upregulation of the Hsp104 chaperone at physiological temperature during recovery from thermal insult.* Mol Microbiol, 2004. **52**(1): p. 217-25.
22. Baskaran, H., et al., *Poloxamer-188 improves capillary blood flow and tissue viability in a cutaneous burn wound.* J Surg Res, 2001. **101**(1): p. 56-61.
23. Merchant, F.A., et al., *Poloxamer 188 enhances functional recovery of lethally heat-shocked fibroblasts.* J Surg Res, 1998. **74**(2): p. 131-40.
24. Currie, R.W., et al., *Heat-shock response is associated with enhanced postischemic ventricular recovery.* Circ Res, 1988. **63**(3): p. 543-9.
25. Gowda, A., et al., *Cardioprotection by local heating: improved myocardial salvage after ischemia and reperfusion.* Ann Thorac Surg, 1998. **65**(5): p. 1241-7.
26. Rylander, M.N., et al., *Correlation of HSP70 expression and cell viability following thermal stimulation of bovine aortic endothelial cells.* J Biomech Eng, 2005. **127**(5): p. 751-7.
27. Rylander, M.N., et al., *Optimizing heat shock protein expression induced by prostate cancer laser therapy through predictive computational models.* J Biomed Opt, 2006. **11**(4): p. 041113.
28. Wang, M.H., M.E. Grossmann, and C.Y. Young, *Forced expression of heat-shock protein 70 increases the secretion of Hsp70 and provides protection against tumour growth.* Br J Cancer, 2004. **90**(4): p. 926-31.
29. Wilmink, G.J., et al., *Assessing laser-tissue damage with bioluminescent imaging.* Journal of Biomedical Optics, 2006. **11**(4): p. 041114.
30. Contag, C.H., et al., *Visualizing gene expression in living mammals using a bioluminescent reporter.* Photochem Photobiol, 1997. **66**(4): p. 523-31.
31. Contag, P.R., et al., *Bioluminescent indicators in living mammals.* Nat Med, 1998. **4**(2): p. 245-7.
32. Contag, C.H. and M.H. Bachmann, *Advances in in vivo bioluminescence imaging of gene expression.* Annu Rev Biomed Eng, 2002. **4**: p. 235-60.
33. Song, C.W., *Effect of local hyperthermia on blood flow and microenvironment: a review.* Cancer Res, 1984. **44**(10 Suppl): p. 4721s-4730s.
34. Florin, L., et al., *Delayed wound healing and epidermal hyperproliferation in mice lacking JunB in the skin.* J Invest Dermatol, 2006. **126**(4): p. 902-11.
35. Lepore, D.A., et al., *Role of priming stresses and Hsp70 in protection from ischemia-reperfusion injury in cardiac and skeletal muscle.* Cell Stress Chaperones, 2001. **6**(2): p. 93-6.
36. Parsell, D.A. and S. Lindquist, *The function of heat-shock proteins in stress tolerance: degradation and reactivation of damaged proteins.* Annu Rev Genet, 1993. **27**: p. 437-96.
37. Garrido, C., et al., *Heat shock proteins: endogenous modulators of apoptotic cell death.* Biochem Biophys Res Commun, 2001. **286**(3): p. 433-42.
38. Gabai, V.L., et al., *Hsp70 prevents activation of stress kinases. A novel pathway of cellular thermotolerance.* J Biol Chem, 1997. **272**(29): p. 18033-7.
39. Vigh, L., et al., *Bimoclomol: a nontoxic, hydroxylamine derivative with stress protein-inducing activity and cytoprotective effects.* Nat Med, 1997. **3**(10): p. 1150-4.
40. Kiang, J.G., et al., *Geldanamycin treatment inhibits hemorrhage-induced increases in KLF6 and iNOS expression in unresuscitated mouse organs: role of inducible HSP70.* J Appl Physiol, 2004. **97**(2): p. 564-9.
41. Pespeni, M., M. Hodnett, and J.F. Pittet, *In vivo stress preconditioning.* Methods, 2005. **35**(2): p. 158-64.

42. Harder, Y., et al., *Improved skin flap survival after local heat preconditioning in pigs.* J Surg Res, 2004. **119**(1): p. 100-5.
43. Walters, T.J., et al., *HSP70 expression in the CNS in response to exercise and heat stress in rats.* J Appl Physiol, 1998. **84**(4): p. 1269-77.
44. Madio, D.P., et al., *On the feasibility of MRI-guided focused ultrasound for local induction of gene expression.* J Magn Reson Imaging, 1998. **8**(1): p. 101-4.
45. Souil, E., et al., *Treatment with 815-nm diode laser induces long-lasting expression of 72-kDa heat shock protein in normal rat skin.* Br J Dermatol, 2001. **144**(2): p. 260-6.
46. Hale, G.Q., MR, *Optical constants of water in 200nm to 200 um wavelength region.* Applied Optics, 1973. **12**(3): p. 555-563.
47. Dinh, H.K., et al., *Gene expression profiling of the response to thermal injury in human cells.* Physiol Genomics, 2001. **7**(1): p. 3-13.
48. Moritz, A.a.F.H., *Studies of thermal injury in the conduction of heat to and through skin and the temperatures attained therein.* American Journal Pathology, 1947. **23**: p. 531-549.
49. Vogel, A. and V. Venugopalan, *Mechanisms of pulsed laser ablation of biological tissues.* Chem Rev, 2003. **103**(2): p. 577-644.
50. Ravagnan, L., et al., *Heat-shock protein 70 antagonizes apoptosis-inducing factor.* Nat Cell Biol, 2001. **3**(9): p. 839-43.
51. Beere, H.M., et al., *Heat-shock protein 70 inhibits apoptosis by preventing recruitment of procaspase-9 to the Apaf-1 apoptosome.* Nat Cell Biol, 2000. **2**(8): p. 469-75.
52. Keyse, S.M. and E.A. Emslie, *Oxidative stress and heat shock induce a human gene encoding a protein-tyrosine phosphatase.* Nature, 1992. **359**(6396): p. 644-7.
53. Ishibashi, T., et al., *A novel dual specificity phosphatase induced by serum stimulation and heat shock.* J Biol Chem, 1994. **269**(47): p. 29897-902.
54. Contaldo, C., et al., *The influence of local and systemic preconditioning on oxygenation, metabolism and survival in critically ischaemic skin flaps in pigs.* J Plast Reconstr Aesthet Surg, 2007.
55. Erdos, G., et al., *Heat-induced bFGF gene expression in the absence of heat shock element correlates with enhanced AP-1 binding activity.* J Cell Physiol, 1995. **164**(2): p. 404-13.
56. Kanamori, S., et al., *Induction of vascular endothelial growth factor (VEGF) by hyperthermia and/or an angiogenesis inhibitor.* Int J Hyperthermia, 1999. **15**(4): p. 267-78.
57. Flanders, K.C., et al., *Hyperthermia induces expression of transforming growth factor-beta s in rat cardiac cells in vitro and in vivo.* J Clin Invest, 1993. **92**(1): p. 404-10.
58. Beckham, J.T. and G. Wilmink, *2007 ASLMS abstracts - disclosure and FDA status.* Lasers in Surgery and Medicine, 2007. **39**(S19): p. 87-100.
59. Braddock, M., C.J. Campbell, and D. Zuder, *Current therapies for wound healing: electrical stimulation, biological therapeutics, and the potential for gene therapy.* Int J Dermatol, 1999. **38**(11): p. 808-17.
60. McMurtry, A.L., et al., *Expression of HSP70 in healing wounds of diabetic and nondiabetic mice.* J Surg Res, 1999. **86**(1): p. 36-41.
61. Benn, S.I., et al., *Particle-mediated gene transfer with transforming growth factor-beta1 cDNAs enhances wound repair in rat skin.* J Clin Invest, 1996. **98**(12): p. 2894-902.

CHAPTER VI

CONCLUSIONS AND FUTURE WORK

Gerald Joseph Wilmink

Department of Biomedical Engineering

Vanderbilt University

Nashville, Tennessee 37235

6.1 Project summary

Lasers have proven to be useful tools in medical procedures. Efficient laser procedures treat a defined volume of target tissue and generate minimal damage to the surrounding tissue regions. Unwanted damage to the surrounding tissue can greatly impair the tissue's repair response and in turn can reduce the effectiveness of a laser procedure [1]. In an effort to improve the outcome achieved in laser procedures, many investigations have been conducted to better understand the photothermal mechanisms that govern laser-tissue interactions. However, most of these research efforts have not examined the damage that occurs directly to the cells, and rather have emphasized on the damage that is generated in the extracellular matrix (ECM). It is advantageous to focus on the intracellular photothermal effects because they are activated by lower temperatures than the extracellular effects, and also because they are occurring upstream to events occurring in adjacent tissue [2].

The general goal for this research project was to examine in real time the cellular processes that are associated with laser-tissue damage. Ten years ago, a project like this could not have been conducted because the imaging tools to explore intracellular damage processes were not available. However, during this post-genomic era, many advances have occurred that have opened the door for novel molecular imaging strategies. Molecular imaging techniques use genomic manipulation and sensitive imaging devices to examine biological processes in living subjects. The bulk of this project was conducted using bioluminescent imaging (BLI), a sensitive optical imaging modality. BLI strategies use optically active reporter genes to signal the activity of biological processes. In this project, we used a thermo-responsive promoter sequence, heat shock protein 70 (hsp70A1), as an indicator for intracellular thermal effects. The hsp70A1 promoter was an ideal target sequence for this project because it is a temperature-responsive gene that is activated by temperature increases of only 5-6 °C

[2, 3]. The hsp70 promoter sequence acts like an “on-off” switch for the transcription of two reporter genes, chemiluminescent luciferase (*luc*) and enhanced green fluorescent protein (*eGFP*). The use of the *hsp70-luc-eGFP* reporter system was significant because it gave us the unique opportunity to accurately track and quantify the cell’s response to thermal stress in laser-tissue interactions. The *hsp70-luc-eGFP* transgene was incorporated into every cell, skin model, and mouse that was used in this report. Using cells equipped with this sensitive reporter gene system, laser-tissue damage was examined in the context of aesthetic, surgical, and therapeutic procedures. The data in this report demonstrated that quantitative BLI in skin equivalents was a useful method for assessing damage that was associated with aesthetic resurfacing procedures. This report also showed that the transgenic mouse strain (*hsp70A1-luc-eGFP*) was a valuable tool for evaluating collateral tissue damage in laser ablation procedures, and the mouse was also shown to be a valuable means for developing laser preconditioning protocols.

6.2 Chapter highlights

In order to provide a fruitful discussion on the impact of this research, below I offer a summary of the highlights from each chapter. The goal for chapter II was to provide the framework, nomenclature, and background required for understanding laser-tissue interactions. Since the interplay between lasers and tissue is what ultimately gives rise to photothermal effects, sections in this chapter were dedicated to both lasers and tissue. With skin being the principal target tissue in this report, the first section of this chapter was dedicated to the anatomy and properties of skin. Then the fundamental principles and mechanisms that govern laser energy transport were outlined. A subsequent section was devoted to the heat shock protein family, and in particular hsp70. The concept of using hsp70 expression as both a biomarker and for therapeutic

objectives was then discussed. The chapter concluded with a section on molecular imaging strategies, and how they can be used as tools to examine biological processes.

In chapter III a reproducible skin model was developed and tested using a clinically relevant laser skin resurfacing (LSR) protocol. Using the skin model, sublethal laser damage was measured after LSR in a non-invasive and sequential manner. The adenovirus, which carried the *hsp70-luc* transgene, was effective at transfecting all human skin cells and was effective for *in situ* transfections of skin equivalents. The proof-of-principle *in vitro* experiments verified that increased thermal exposures resulted in increased luciferase expression. The experiments using traditional biochemical assays showed that luciferase expression as an accurate surrogate marker for actual hsp70 mRNA and protein levels. For all skin cells tested, the BLI data indicated that the magnitude of hsp70 expression increased with increases in thermal exposure durations and was maximal 8-12 h after thermal stress. Interestingly, the hsp70 expression kinetics were markedly different for each cell type, suggesting that hsp70 expression is cell-type dependent. The significance and impact of this finding will be discussed in section 6.3.3. Overall, this study demonstrated that quantitative BLI in skin equivalents provides a powerful model to examine damage in aesthetic LSR procedures.

In Chapter IV collateral tissue damage associated with laser ablation was examined in the *hsp70-luc-eGFP* mouse strain. The Free Electron Laser (FEL) was tuned to commonly used surgical ablation wavelengths (2.94 μm, 6.1 μm, and 6.45 μm), and the resultant tissue damage was compared. The hsp70 expression kinetics (spatially and temporally) varied markedly with the laser operating parameters (wavelength and radiant exposure). For all wavelengths tested, increases in radiant exposure resulted in increases in the magnitude of *hsp70* expression. Compared to the other wavelengths tested, 6.10 μm had lower hsp70 levels, generated less collateral damage, and caused less epidermal thickening. Therefore, this report confirmed that 6.10 μm was a superior

ablation wavelength in skin and should be used for laser surgical ablation procedures. The finding that 6.10 μm is superior at ablating skin is significant, and the implications of this result are addressed in great detail in section 6.3.3.

Chapter V reported on the development of a laser preconditioning protocol. The preconditioning protocol enhanced the repair of surgical wounds in a murine model. In a broader sense, this report confirmed that eliciting mild stress responses can serve to protect tissue from subsequent stresses. The laser preconditioning that used long exposures (minutes) and lower temperatures (43-44°C) was shown to be more effective than the protocol that used shorter exposures (seconds) and higher temperatures (48-50°C). The optimized laser protocol used a pulsed diode laser with the following operating parameters: λ = 1.85 μm, τ_p =2 ms, 50 Hz, H = 7.64 mJ/cm^2, t = 10 m exposure. The optimized laser preconditioning protocol induced hsp70 expression by 15-fold, increased blood flow by 4-fold, and increased the strength of surgical wounds by 2-fold. Overall, this report confirmed that mild laser-induced heat shock acting through an expression of hsp70 shows promise as a preconditioning therapeutic intervention prior to surgery.

6.3 Impact of research

6.3.1 Duty and benefits of measuring impact of medical research

The goal of medical research is to improve the lives of patients through the advancement of medical practices. Every year in the United States billions of dollars are spent to support medical research. Since medical research monies come from tax payers, government agencies, and charitable foundations, it is a researcher's duty to justify that these dollars are making a difference in the lives of people. Besides being a duty, the careful reporting of research impact also has many benefits. Research reports

can be used to give funding institutions a more meaningful view of their return on investment or they can be used to provide our society with the explicit benefits of a specific project. Reporting on the impact of a research project is also beneficial to the scientist because the report can serve as a compass to guide future research efforts.

6.3.2 Biomedical Engineering: basic science and translational medical research

To accurately assess the impact of a particular research project, the specific findings of a project must be examined with respect to the field in which it was conducted. This research project was conducted in the field of biomedical engineering. Biomedical engineering (BME) is a discipline that advances knowledge in engineering, biology and medicine, and uses that science to drive the development of therapeutics and devices to improve human health [4]. BME research is conducted at both the basic science and clinical/medical levels. Basic research experiments in BME are designed to gain a fundamental understanding of living systems through the application of engineering techniques. The function of basic scientific research is to answer questions about the mechanisms of specific biological processes and to develop and test the effectiveness of potential treatments using non-human models. Once compelling evidence is obtained, researchers then strive to move the findings into human clinical trials. In contrast, clinical research studies seek to directly improve medical practice by developing diagnostic and therapeutic devices and processes. Overall, basic science research and clinical research are not only both valuable to BME research but they are also interconnected.

6.3.3 Direct impact of this basic science research

The basic science research conducted in this study has directly enriched the following disciplines and/or research communities: the cell stress and chaperone,

biomedical optics, and dermatology. The cell stress and chaperone research community conducts mechanistic and phenomenological studies to better understand the cellular stress response and the mechanism of chaperone activity. Recently this community has placed added emphasis on studies that use and apply chaperone activity for therapeutic purposes in clinical applications [5]. To efficiently bridge from the cellular to the organism level, chaperone activity must be examined at various biological levels using a variety of model systems. In this project, we examined the stress response of cells in culture, in skin equivalents, and in animal models. The one consistent finding that was demonstrated in all cell types and skin models was that the magnitude of *hsp70* expression was in direct relation to the imposed hyperthermic regimen (exposure duration and temperature). However, quite surprisingly, the *hsp70* expression kinetics varied markedly for different cell types and for different model systems. From a fundamental standpoint this finding is quite interesting because it suggests two things: first, each cell type has its own specific response to thermal stress; and second, a cell's stress response depends on its surroundings and the response changes when placed in tissue equivalents and/or in full biological systems. In regards to the individualized stress responses, cells may have evolved different cellular stress responses for survival purposes. The main implication of these findings will prove to be critical in the optimization of preconditioning protocols. Since a protocol needs to effectively precondition many different cell types during one clinical session, the varying responses between cell types need to be considered and optimized. The difference between the mRNA and protein expression kinetics was another finding that may be critical for optimizing the preconditioning protocols. Hsp70 protein expression was maximal 8 to 12 h after the initial thermal stress while hsp70 mRNA expression was maximal 4 to 6 h after stress. Based on the central dogma of molecular biology, it is known that cell transcribes mRNA before translating a protein. However, considering that a piece of

mRNA is translated into a protein in only a deci-second, it seems unusual that there is such a marked disparity in the occurrence of their peaks. The central question that this finding begs, yet still remains unanswered is why does maximum expression take so long to occur (~8 to 12 h) after thermal stress. Are there other chaperone proteins that are activated before hsp70 proteins respond to the thermal stress? If so, what proteins are they? Also, hsp70 functions to refold denatured proteins, but what protein refolds hsp70?

The goal of biomedical optics research is to use optics technology for therapeutic and diagnostic medical applications. At a fundamental level, this project was of interest for the biomedical optics community because it provided an opportunity to explore the dynamic relationship between biological responses and the physical principles that activate them [6]. Under the biomedical optics umbrella, this research contributed primarily to the fields of laser-tissue interaction (LTI) and molecular imaging. The goal of LTI research is to investigate the photo-biological mechanisms that govern the interaction of light in biological tissue. Traditional research efforts have used thermal models and empirical studies to examine the thermal effects of laser radiation. In this study, we used the hsp70-luc-eGFP reporter gene system to gauge and quantify the cell's response to thermal stress. This novel development is significant because it gives the LTI community a powerful tool to detect and quantify thermal stress at a cellular level. These reporter genes systems provided us with the means to report and publish large quantities of thermal bio-effects data. This bio-effects data also has broader implications because it can be compared to the damage values predicted using theoretical thermal models. These types of comparisons will help refine and improve our current thermal models, and in turn will advance the way we think about photothermal interactions. These reporter gene tools were particularly instrumental in determining that a wavelength of 6.10 μm was the most efficient for ablating skin. This finding is

important because it can be used as criteria in the design and development of new cost effective benchtop lasers. Alternative benchtop lasers, such as the tunable 6 μm wavelength ZPG-OPO system, are greatly needed because the FEL, despite its clinical utility, is very expensive to operate [7]. Therefore studies like this which examine the effect of specific laser operating parameters are helpful for developing more affordable laser sources.

This research also contributed to the field of molecular imaging. Molecular imaging research combines clinical and preclinical imaging modalities with molecular and cellular biology to improve the understanding of biological events in living systems [8]. Molecular imaging tools are commonly used to assess the efficacy of therapeutic interventions. Recent initiatives by the NIH and FDA have placed extra emphasis on the advancement of preclinical small-animal imaging, and as a result basic science research in this area is critical [9]. This research demonstrated that bioluminescent imaging (BLI) techniques are effective tools for quantifying gene expression in a non-invasive manner. In a general sense, these research findings also helped in further defining and establishing bioluminescent imaging as the only suitable and affordable preclinical imaging modality that can be used to measure gene expression.

The final field that this work contributed to is dermatology. Dermatology research is interested in all aspects of cutaneous biology and skin disease, and the wound repair community is interested in research that seeks to advance wound repair [10]. In this research we developed a novel laser preconditioning protocol which we optimized using molecular imaging techniques. In terms of basic science research, the methodology used to develop this preconditioning protocol is useful for this community. Many wound repair investigations focus solely at a tissue, cellular or molecular level. In this study we not only examined biomarkers of wound repair at all biological levels, we also used this information to develop more meaningful protocols. Beyond the impact that this work has

at a basic science level, the clinical potential of this preconditioning method will be discussed in section 6.3.6.

6.3.4 Tallying outputs: the common scientific measuring stick

Internal evaluations at universities and annual research reports require a scientist to quantify their research activity using numerical outputs. The most common productivity outputs include the number of papers published, impact factors of the publishing journals, and the number of scientific conferences at which the research is presented. Using this traditional view of assessment, the research described in this report provided the resources to publish three manuscripts in high impact factor journals, publish three scientific proceedings, and was presented at ten scientific conferences. These quantifiable outputs are important but the actual impact of these efforts must be more closely scrutinized. Many research project summaries focus on the outputs of their research because it is easier to analyze. However, the problem with reporting on research in this light is that it doesn't take into the consideration the original fundamental goal of BME research, which is to improve patient health care. Therefore, in the section below I will attempt to look beyond specific research outputs and will rather document the broader outcomes of this project.

6.3.5 A framework and model to examine outcomes

The proper framework is required to qualify the actual impact of a specific research project. The fundamental notion of focusing on outcomes instead of outputs was first described by the United Way of America in 1996 [11]. This research model is useful for a scientist because it helps them determine if their research has potential to achieve long-term outcomes. This medical research model essentially divides research into four aspects: inputs, activities, outputs, and outcomes. Research inputs are defined

as the grants, scientists, and technologies used in the research. Activities are defined as the specific projects that are conducted, and the outputs are the scientific publications and presentations generated from the research. The outcomes category consists of initial, intermediate, and long-term outcomes. The initial outcome is characterized by a clinical decision maker becoming aware of a new medical technique. The intermediate outcome is defined as the time period when the research is implemented in clinical practice. The long-term outcome describes when a new medical technique leads to the improvement in patient well-being.

After reviewing the research conducted in this report, the finding that merits the most impact is the development of the laser preconditioning protocol. The preconditioning protocol was shown to enhance wound repair and has potential to greatly impact our health care system. Applying the United Way model to this specific project, it is clear that a pulsed IR diode laser and the multimodal imaging techniques were the inputs used to develop this novel technique. Various research experiments were conducted as activities to optimize this laser preconditioning protocol. The research output culminated with the publication of the article in the Journal of Investigative Dermatology. This scientific publication is the initial outcome of this research and it serves to increase the awareness of this novel method to the dermatology community. However, in order for this technique to have intermediate and long-term outcomes which actually improve patient care, the method must be implemented in human clinical trials.

6.3.6 The next step: moving basic science findings into the clinical

Since the described laser preconditioning method has been optimized and developed in a mouse model, the next logical step is to design a clinical trial that implements this new technique on human subjects. A clinical trial is an organized

testing of a treatment to assess its safety, efficacy, benefits and cost in human subjects. The initial step in conducting a clinical trial is the submission of a clinical proposal, and since this treatment involves the use of a pulsed IR diode laser, our group will also have to obtain an investigational device exemption (IDE) approval from the FDA. The next step will be to discuss this idea with dermatologists and surgeons who are also interested in improving wound repair. Then using campus and hospital resources, subjects who are going to undergo elective surgery should be recruited. Then, Phase I trials will be conducted. The goal for phase I testing will be to replicate the success we saw in the mouse model by determining the optimal laser parameters that enhance wound repair in human subjects. In Phase I trials we will test the laser preconditioning protocol in a small group of people (n= 20-80) [12]. The safety and the side effects of the protocol will be evaluated, and this phase should take roughly ~1-2 years. For Phase II testing we will test the protocol on a larger cohort (n= 100-300). The main goal for this phase will be to determine the safety and efficacy of the laser preconditioning procedure. Then for Phase III we will give the protocol to ~1000-3000 subjects. The aim for this phase will be to confirm the effectiveness of protocol, monitor side effects, and compare the safety and clinical effectiveness of the laser method to standard untreated incisional wounds. The final post-market phase, phase IV, will be conducted to provide additional information in regards to the efficacy and safety of the laser preconditioning method. Overall, laser preconditioning has potential to provide various long-term outcomes, including the improved treatment of chronic wounds and the enhanced repair of elective surgeries.

6.4 Future Work

The exciting work presented in this dissertation has set the ground work for a variety of future research opportunities. The basic science and clinical research studies described below are currently underway or will be underway in the near future.

Both the adenovirus (Adv) and the raft model discussed in Chapter III can be used in future studies. The Adv-*hsp70-luc* is particularly valuable because it can be used to transiently transfect skin cells that were not yet tested. For instance, Langerhans cells (LCs), a common dendritic cell in the skin may be an attractive candidate. LCs are interesting for the following reasons: first, they are one of the initial cells that is in contact with pathogens at the skin's surface; second, they play critical roles in initiating adaptive immune responses; and last, they participate in regulating contact hypersensitivity [13]. Examining the *hsp70* expression kinetics of LCs may help in further optimizing laser preconditioning protocols. Also, an Adv using the promoter sequence of other genes of interest could be developed and used in a similar manner. Specifically, adenoviruses could be developed using the promoters for Hsp90, Hsp40, and TGF-β1. For the most part, the adenoviral system was an effective tool for transducing cells. However, the main drawback of adenoviral transfection methods is that the transgene remains episomal and does not integrate into the host genome. This limitation causes the expression of transgenes delivered with an adenoviral system to be transient and therefore decrease over time due to dilution of viral DNA by cell division. Transient tranfected cells also have a small window for experimentation which limits the time available for experimentation. It may therefore be advantageous to develop other viral systems, such as retroviral or lentiviral systems. The principal advantage in using lentiviral systems is that they can be used to stably transfect actively dividing, neuronal, growth arrested, and contact inhibited cells. Stable transfections are possible with lentiviral systems because the transgene is imported into the nuclei of cell by cis-acting

elements and once integrated into host genome confers stable transfection. The main limitation of lentiviral systems is that their concentrated titer is much lower than those produced with adenoviral systems, 10^7 TU/ml compared to 10^{11} pfu/ml [14]. This lower viral content would require larger volumes of virus for comparable transfection efficiency.

The skin equivalent model developed in Chapter III is useful because it can be used to study any dynamic bio-molecular relationship in skin. For instance, the raft model could be used in other laser-tissue interactions, such as in surgical laser ablation or other types of laser procedures. The raft model can also be used to examine skin pathogenesis, to understand viral pathogenesis of HPV, or even to improve optical diagnostic methods, such as in Raman Spectroscopy [15, 16]. Rafts are attractive models to researchers because the cells used in the model and its environment can be selected and controlled by the user. This customizable feature opens the door for efforts to make the raft models more sophisticated. For instance, if a researcher were interested in emulating wound repair, inflammatory and endothelial cells could be added to the raft. With these cells present, wound repair could be achieved, and valuable biological insights may be gained with this model. Although the raft protocol is quite straightforward, making reproducible rafts takes a great deal of time and skill. In lieu of making rafts, living bi-layered skin substitutes such as Apligraf® (Organogenesis, Inc.) and Dermagraft® (Advanced Biohealing, Inc.) can now be purchased. One commercially available product is the Algimatrix skin equivalent made by Gibco [17]. Algimatrix uses a basement membrane which consists of laminin I, collagen IV, entactin, and heparin sulfate proteoglycan. Algimatrix skin equivalents may be a cheaper and more efficient model for future skin experiments.

In Chapter IV we used the hsp70-luc-GFP mouse model to assess the damage associated with laser surgical ablation procedures. Since this model can be used to sensitively quantify tissue damage it may be a useful tool for improving laser

skin resurfacing (LSR) procedures. Every year approximately 250,000 patients in the United States undergo elective LSR procedures to remove scars or to treat wrinkles. Traditional LSR lasers, such as the Sharplan 1060 CO_2, are effective at contracting cutaneous tissue but have significant complications (eg. prolonged recovery time, persistent erythema) [18]. In the interest of developing a more efficient LSR laser source, Ellis et. al. used the FEL to demonstrate that wavelengths that target tissue proteins contract tissue more efficiently than current LSR sources [19]. Specifically, Ellis et.al. found that two IR energy bands, 7.2-7.4 μm (C-H bend) and 7.6-7.7 μm (amide III band), provided increased contraction relative to the traditional CO_2 laser [19]. It may be worthwhile to use the hsp70-luc mouse model to closely examine the effectiveness of 7 μm wavelengths on cutaneous contraction. These studies may serve as the initial steppingstone in the development of more efficient LSR laser sources using radiation with 7 μm wavelengths.

On a similar note, the mouse model could also be used to examine fractional resurfacing, a recently developed LSR method that has been shown to be particularly useful for plastic surgery. Fractional resurfacing is a new concept of cutaneous remodeling whereby laser-induced zones of microthermal injury are surrounded by normal untreated tissue [20]. Most of the major laser manufacturers have developed lasers that achieve fractional resurfacing. For instance, Sciton's Profractional, Reliant's Fraxel, and Palomar's 1550 [20-23]. It would be very interesting test these lasers side-by-side using our hsp70-luc model.

Besides laser surgery, the effects of other surgical devices can be examined using the mouse model. For instance, Johnson & Johnson has developed an Ultrasonic harmonic scalpel device which has been shown to effectively cut tissue, but the mechanism by which the device works is currently unknown. The only information known about this ultrasonic device is that it uses a blade vibrating at ultrasonic

frequencies to cut tissue and form hemostatic seals, and during this process it has been shown to generate temperatures ranging from 50 to 100 ^{o}C. Tools such as the hsp70-luc mouse model may help elucidate the mechanism that this device uses which may in turn lead to the improvement of the device's performance.

Although the fluorescence imaging techniques were only modestly exploited in this study, future work could be done to harness the power of the second reporter gene (*eGFP*). One specific application would be to conduct confocal fluorescent imaging in real time on laser-treated mice. With the help of Sam Wells, the director of the Vanderbilt FLI facility, hsp70 expression kinetics could be depth resolved on live animals. Examining the spatial features of hsp70 expression may help in optimizing our laser preconditioning protocols and may also enrich thermal therapies, which are typically employed in conjunction with radiation treatments [24, 25]. Since HSP expression control has not been incorporated into therapy design, a better understanding of HSP expression may open the door for improved model design and therapy.

In a set of experiments discussed in Chapter V, we used the mouse model as a source for creating new cell lines (eg. mouse dermal fibroblasts). Using cells derived from the mouse model was intriguing because these cells did not require a transfection because they contain the *hsp70-luc-eGFP* transgene. It may be fruitful in the future to extract other cells types from this mouse model. For instance, LC cells, which activate immune responses, may be an interesting candidate.

The laser preconditioning protocol enhanced wound repair in normal Hsp70-luc-eGFP mice, but had only modest success in diabetic mice. Future studies need to be conducted to examine this disparity, and the protocols may need to be adjusted for maximal usefulness in the diabetic mouse model. Wound repair should also be

investigated using more sophisticated and clinical relevant wounds, such as in excisional wounds. The mechanism that the laser preconditioning protocol uses could also be explored. The recently acquired hsp70 knock-out mouse will be particularly useful in these pursuits. Repeating the laser preconditioning experiments on the hsp70 knock-out mouse will verify in a definitive manner whether hsp70 plays a critical role in the enhanced wound repair seen after preconditioning. Other techniques, such as RNA interference, microarrays, laser capture microdissection, 2D gel electrophoresis, and laser Doppler perfusion, may also be useful tools in elucidating this mechanism. In this work blood flow was measured using laser Doppler perfusion imaging. However, more sensitive blood flow measurements should be explored, potentially using the Vevo 770^{TM} high-resolution imaging system (VisualSonics Inc, Ontario, CA) which is housed in the Vanderbilt Small Animal Imaging Center. Efforts were made using this device but the thickness of the required topical gel made it difficult to register and position the probe over specific wounded areas. Refining these imaging methods may be useful for obtaining more sensitive blood flow measurements.

The developed laser preconditioning protocol could also be implemented before various different types of procedures. For instance, preconditioning could be used to prepare tissues before LSR procedures or even before surgical ablation procedures. Based on the data in this report, I would anticipate that preconditioning may reduce the collateral damage induced in the treated tissues. On the flip side, it also may be of interesting to use the laser treatment method as a post-treatment measure. For instance, the laser preconditioning protocol could be delivered on a pre-existing chronic wound. Since this scenario is more common than the incidence of elective surgery, this method should be pursued to improve wound repair and in particular diabetic wound repair. In fact, recent preliminary studies have shown that using a laser to treat existing wounds does show promise.

6.5 Research considerations

6.5.1 Protection of research subjects

The protection of research subjects and the societal impact of this research were considered throughout the course of these studies. No human subjects were used in this research. As this research project was directed towards the development of *in vitro* and *in vivo* imaging modalities, animal experimentation was necessary. The proper and ethical use of animals in scientific research was ensured in all experimentation. All lab personnel completed the Animal Research Training Program sponsored by the Institutional Animal Care and Use Committee, as required by Vanderbilt University. All experiments were conducted in accordance with National Institutes of Health regulations for the ethical use of animals in research and were pre-approved by the Vanderbilt Institutional Animal Care and Use Committee. Appropriate training on general lab safety and standard chemical, biological, and radiation safety was required for personnel involved in this study in compliance with institutional guidelines.

6.5.2 Societal implications

Lasers are valuable medical tools and methods that can improve laser procedures are important to develop. Optical imaging tools can effectively be used on animal models, and the optimized laser parameters can then more easily be translated for human use. Improved laser protocols will result in better laser skin resurfacing, more efficient laser surgical ablation, and more efficient laser preconditioning protocols. Specifically, the laser treatment of diabetic ulcers may be an important therapeutic measure that may be used in the future to treat diabetic wounds and thereby increase their quality of life and life expectancy.

6.6 Works cited

1. Bryant, G.L., et al., *Histologic study of oral mucosa wound healing: a comparison of a 6.0- to 6.8-micrometer pulsed laser and a carbon dioxide laser.* Laryngoscope, 1998. **108**(1 Pt 1): p. 13-7.
2. Morimoto, R.I., P.E. Kroeger, and J.J. Cotto, *The transcriptional regulation of heat shock genes: a plethora of heat shock factors and regulatory conditions.* Exs, 1996. **77**: p. 139-63.
3. Kregel, K.C., *Heat shock proteins: modifying factors in physiological stress responses and acquired thermotolerance.* J Appl Physiol, 2002. **92**(5): p. 2177-86.
4. Foundation, T.W., *Biomedical Engineering*. 2007, The Whitaker Foundation.
5. Neuman, H., *Cell Stress Society International*. 2007, Alliance Communications Group.
6. Phillips, R. and S. Quake, *The Biological Frontier of Physics*, in *Physics Today*. 2006. p. 38-43.
7. Mackanos, M.A., et al., *Mid infrared optical parametric oscillator (OPO) as a viable alternative to tissue ablation with the free electron laser (FEL).* Lasers Surg Med, 2007. **39**(3): p. 230-6.
8. Contag, C.H. and M.H. Bachmann, *Advances in in vivo bioluminescence imaging of gene expression.* Annu Rev Biomed Eng, 2002. **4**: p. 235-60.
9. Fischer, A., *Report finds new emphasis on preclinical imaging*, in *Biophotonics International*. 2007. p. 24-25.
10. Bergstresser, P., *Journal of Investigative Dermatology*. 2007, Nature Publishing Group.
11. America, U.W.o., *Measuring Practical Outcome*. 1996, United Way of America.
12. Medicine, N.L.o., *ClinicalTrials.gov*. 2007, U.S. National Institutes of Health.
13. Kaplan, D.H., et al., *Epidermal langerhans cell-deficient mice develop enhanced contact hypersensitivity.* Immunity, 2005. **23**(6): p. 611-20.
14. Corporation, I., *ViraPower Lentiviral Expression Systems*. 2005, Invitrogen Corporation: Carlsbad, CA. p. 1-12.
15. Chow, L.T. and T.R. Broker, *In vitro experimental systems for HPV: epithelial raft cultures for investigations of viral reproduction and pathogenesis and for genetic analyses of viral proteins and regulatory sequences.* Clin Dermatol, 1997. **15**(2): p. 217-27.
16. Viehoever, A.R., et al., *Organotypic raft cultures as an effective in vitro tool for understanding Raman spectral analysis of tissue.* Photochem Photobiol, 2003. **78**(5): p. 517-24.
17. Perkel, J., *Taking Cell Culture to a new dimension*, in *QUEST*. 2007. p. 22.
18. Perez, M.I., D.E. Bank, and D. Silvers, *Skin resurfacing of the face with the Erbium:YAG laser.* Dermatol Surg, 1998. **24**(6): p. 653-8; discussion 658-9.
19. Ellis, D.L., et al., *Free electron laser infrared wavelength specificity for cutaneous contraction.* Lasers Surg Med, 1999. **25**(1): p. 1-7.
20. Kono, T., et al., *Prospective direct comparison study of fractional resurfacing using different fluences and densities for skin rejuvenation in Asians.* Lasers Surg Med, 2007. **39**(4): p. 311-4.
21. Collawn, S.S., *Fraxel skin resurfacing.* Ann Plast Surg, 2007. **58**(3): p. 237-40.
22. Buis, J. and J.M. Mazer, *[Fractional photo-thermolysis by laser Fraxel as an adjuvant for facial surgical rejuvenation].* Ann Chir Plast Esthet, 2007. **52**(3): p. 222-33.

23. Chiu, R.J. and R.W. Kridel, *Fractionated photothermolysis: the Fraxel 1550-nm glass fiber laser treatment.* Facial Plast Surg Clin North Am, 2007. **15**(2): p. 229-37, vii.
24. Rylander, M.N., et al., *Heat shock protein expression and injury optimization for laser therapy design.* Lasers Surg Med, 2007. **39**(9): p. 731-46.
25. Rylander, M.N., et al., *Optimizing heat shock protein expression induced by prostate cancer laser therapy through predictive computational models.* J Biomed Opt, 2006. **11**(4): p. 041113.